CONSTRUCTING SCATTERING AMPLITUDES FROM THEIR FORMAL PROPERTIES

A DISSERTATION
SUBMITTED TO THE DEPARTMENT OF PHYSICS
AND THE COMMITTEE ON GRADUATE STUDIES
OF STANFORD UNIVERSITY
IN PARTIAL FULFILLMENT OF THE REQUIREMENTS
FOR THE DEGREE OF
DOCTOR OF PHILOSOPHY

Andrew McLeod
August 2017

This dissertation is online at: http://purl.stanford.edu/bv314fr9257

Includes supplemental files:

1. Ancillary files to Chapter 1 *(Chapter_1_ancillary.tar.gz)*
2. Ancillary files to Chapter 2 *(Chapter_2_ancillary.tar.gz)*
3. Ancillary files to Chapter 3 *(Chapter_3_ancillary.tar.gz)*
4. Ancillary files to Chapter 4 *(Chapter_4_ancillary.tar.gz)*

I certify that I have read this dissertation and that, in my opinion, it is fully adequate in scope and quality as a dissertation for the degree of Doctor of Philosophy.

Lance Dixon, Primary Adviser

I certify that I have read this dissertation and that, in my opinion, it is fully adequate in scope and quality as a dissertation for the degree of Doctor of Philosophy.

Peter Graham

I certify that I have read this dissertation and that, in my opinion, it is fully adequate in scope and quality as a dissertation for the degree of Doctor of Philosophy.

Renata Kallosh

Approved for the Stanford University Committee on Graduate Studies.

Patricia J. Gumport, Vice Provost for Graduate Education

This signature page was generated electronically upon submission of this dissertation in electronic format. An original signed hard copy of the signature page is on file in University Archives.

Abstract

Scattering amplitudes in quantum field theory encode the probability of configurations of incoming and outgoing particles scattering into each other, as well as particle masses and decay rates. Traditionally they have been calculated using Feynman diagrams, but this method generally proves too computationally intensive to allow for the calculation of higher-loop contributions, which are relevant for making predictions in particle physics experiments and to our understanding of quantum field theory itself. As a step in the direction of filling this computational gap, this dissertation presents an improved bootstrap method for computing scattering amplitudes in the planar limit of maximally supersymmetric Yang-Mills theory. This method does away with Feynman diagrams altogether, and instead uses knowledge of the symmetries and analytic properties of scattering amplitudes, in conjunction with an understanding of the mathematical form these amplitudes take in general and special kinematics, to uniquely determine them at high loop orders. In particular, it makes use of the fact that amplitudes in this theory are expressible in terms of generalized polylogarithms for seven and fewer particles. The first part of this dissertation focuses on six-particle kinematics, where previously-unappreciated algebraic constraints on these amplitudes are described that restrict both their double derivatives and their double discontinuities. Alongside previously-understood constraints, these properties are used to uniquely determine all six-particle amplitudes in this theory through five loops. These explicit results are then used to provide analytic and numerical evidence for a recently-conjectured positivity property these amplitudes are thought to have in certain kinematic regions. In the second part of this dissertation, it is shown that these methods straightforwardly generalize to seven-particle kinematics, where they

in fact prove to be even more restrictive than in six-particle kinematics. In particular, a smaller set of constraints is shown to be sufficient to determine specific seven-point amplitudes at three and four loops, up to integration constants. While the results presented in this thesis are confined to the planar limit of maximally supersymmetric Yang-Mills theory, these bootstrap methods are expected to prove useful even in theories without supersymmetry.

If the fool would persist in his folly he would become wise.

– William Blake, *The Marriage of Heaven and Hell*

What hath night to do with sleep?

– John Milton, *Paradise Lost*

Acknowledgments

It would seem that Alexander Pope's observation that "a little learning is a dangerous thing" only grows more perspicacious as academia continues to specialize. If I am to prove the counterexample (as indeed I aspire to), it will be chiefly due to the excellent direction and support I have received from my mentors and collaborators throughout my graduate school career.

First and foremost, I am indebted and grateful to my advisor Lance Dixon, whose inexhaustible energy and drive to understand the hidden structures underlying scattering amplitudes has engendered my own fascination with these objects. In addition to freely (and patiently) sharing his expertise in the areas of physics and mathematics represented in this thesis (not to mention the work it builds on), Lance has shown me what it means to strive for excellence in all aspects of research.

I am also grateful to a host of other collaborators, each of whom has enriched this first stage of my research journey and without whose insight I would have a much narrower understanding of the field. I would especially like to thank Georgios Papathanasiou, Simon Caron-Huot, Einan Gardi, Matt von Hippel, Jaroslav Trnka, Marcus Spradlin, James Drummond, Claude Duhr, and John Joseph Carrasco in this regard. In addition, I have benefitted from many indelible discussions with my fellow graduate students in the field of scattering amplitudes, most notably Enrico Hermann, Chia-Hsien Shen, James Stankowicz, and Julio Martinez.

My time at Stanford has been made immensely enjoyable by the community I have come into contact with here, not just within the Physics Department and at SLAC but also throughout campus. I would particularly like to thank Savas Dimopoulos and Peter Graham for taking me in as a first year graduate student and initiating me into

the world of high-energy theory through explorations into what might lie beyond the Standard Model. Naturally, I have also learned a great deal of physics (and perhaps even more non-physics) from the multitude of Stanford graduate students I have had the pleasure of interacting with over the course of my studies—a group simply too large to enumerate. I trust these people all know who they are, and can only hope I have positively impacted their Stanford experience as much as they have mine.

Finally, many thanks go to my parents and my brother, without whose continual support it would not have been possible—and without whose encouragement I would not have had the confidence—to pursue my interests wherever they have led.

Contents

List of Tables

List of Figures

Introduction

Scattering amplitudes have long been of interest as one of the basic observables one can calculate in quantum field theory. These quantities encode not only the probability of specific configurations of incoming and outgoing particles scattering into each other, but also the masses and decay rates of the particles in a given theory. Of special interest are amplitudes in $SU(N)$ gauge theories (alternately called Yang-Mills theories), due to the fact that we know that the real world is well-described by the Standard Model, an $SU(3) \times SU(2) \times U(1)$ gauge theory, at energies currently accessible to particle accelerator experiments. However, despite this practical interest and the efforts of multiple generations of physicists, theoretical uncertainties for some of the predictions at the currently-operating Large Hadron Collider (LHC) remain at the $\sim 10\%$ level, making them comparable to the corresponding experimental uncertainties.

While part of the difficulty in making predictions at the LHC can be attributed to the large number of interacting particles in the Standard Model and the fact that the $SU(3)$ part of its gauge group is confined at low energies, another fundamental limitation arises because of how we traditionally compute even the simplest amplitudes in quantum field theory. This is in terms of Feynman diagrams, a procedure wherein one pictorially expands an amplitude as all possible ways the incoming particles can interact to become the outgoing ones, and sums over the contribution coming from each diagram. An example of this type of expansion is seen in Figure 1, where the first few Feynman diagrams for the scattering of two distinguishable quarks in a $U(1)$ gauge theory are shown. When the particles in a quantum field theory interact

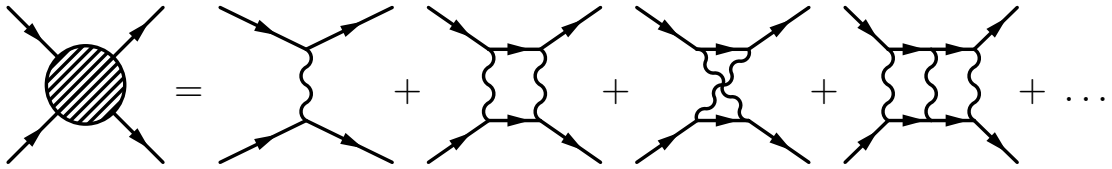

Figure 1: The Feynman diagram expansion in for the scattering of distinguishable quarks in $U(1)$ gauge theory. The straight lines represent quarks with a given spin, and the wavy lines represent photons.

weakly, the contributions made by diagrams with a large number of internal particles are suppressed relative to diagrams with fewer interaction vertices. This allows amplitudes to be approximated by truncating this expansion at a certain loop order, which is to say by throwing away all Feynman diagrams whose internal lines trace out more than this number of loops.

Fortuitously (if one is interested in the weakly-coupled regime), it is the Feynman diagrams with the fewest number of loops that are easiest to compute—for example, the first term in the expansion in Figure 1 can be straightforwardly determined to be

$$ig^2 q_1 q_2 \frac{\bar{u}(p_1')\gamma^\mu u(p_1)\ \bar{u}(p_2')\gamma_\mu u(p_2)}{(p_1 - p_1')^2},$$

where p_i, p_i', and q_i correspond to the incoming momentum, outgoing momentum, and $U(1)$ charge of the i^{th} quark, and g is the coupling constant associated with each interaction vertex. The products of gamma matrices with incoming and outgoing spinors encode the helicity structure of the scattering process. Even in the absence of loops, however, the number of diagrams one can write down increases factorially with the number of scattering particles. For this reason, it wasn't until 1985 that the tree-level contribution was calculated for two incoming gluons scattering into four outgoing ones (an amplitude relevant for making predictions at particle colliders like the LHC) by Parke and Taylor [1]. While their original result spanned eight pages, these authors were quickly able to simplify and generalize this expression to any number of outgoing particles for the maximum helicity-violating (MHV) part of the all-gluon amplitude, in which two gluons have negative helicity while all other helicities are positive [2].

Their final result for the cross section—that is, the square of the amplitude, in which guise scattering amplitudes enter observable predictions—takes the compact form

$$\left|\mathcal{A}_n(p_1^-, p_2^-, p_3^+, \ldots, p_n^+)\right|^2 \propto \sum_{\sigma \in S_n} \frac{(p_1 \cdot p_2)^4}{(p_{\sigma_1} \cdot p_{\sigma_2})(p_{\sigma_2} \cdot p_{\sigma_3}) \cdots (p_{\sigma_n} \cdot p_{\sigma_1})}$$

where all colors and polarizations have been summed over, and we have dropped the kinematic-independent prefactor; the remaining sum is taken over all permutations of the momenta of the scattering particles. As this result resums an arbitrarily large number of Feynman diagrams for large values of n, this prediction provided one of the first indications that scattering amplitudes themselves aren't as complicated as the Feynman diagram techniques normally used to compute them.

The situation becomes more complicated when one wants to compute Feynman diagrams involving loops, because one must integrate over all possible intermediate states of the particles in each loop. This can already prove a challenge at two loops, and while great progress has been made recently on four-particle scattering, basically none of the amplitudes relevant to five- or higher-particle scattering processes at the LHC are currently known at this order. This signifies a strong need for new computational techniques and ways of reformulating the quantities under study. One such reframing of the problem is realized by the unitarity method, which takes advantage of the fact that the probabilities assigned to all possible outgoing configurations of scattered particles must sum to one [3]. This translates to the S-matrix requirement that $S^\dagger S = 1$, or—if we separate out the contribution coming from interacting particles by writing $S = 1 + iT$—that $2\text{Im}T = T^\dagger T$. When expanded perturbatively in the coupling, this relates the imaginary part of an amplitude—corresponding to its discontinuity across some set of branch cuts—to lower-loop amplitudes. As the branch cuts of amplitudes are associated with internal particles going on shell (being assigned their physical mass), this relation identifies diagrams that have some of their internal particles put on shell with products of lower-loop amplitudes that are sown together by these on-shell particles. This makes it possible to express amplitudes (up to rational terms, which don't have associated branch cuts) in terms of these lower-loop building blocks by considering unitarity cuts in all momentum channels.

The method of generalized unitarity takes this one step further, by considering the residues of diagrams with even more internal particles put on shell [4]. Using such cuts, one can construct the full integrand associated with an amplitude—that is, the rational function of the internal and external momenta sitting inside the integration symbol—at any loop order. This information can in turn be used to identify the amplitude itself (again, up to rational terms) when it can be expanded in terms of a basis of known integrals. However, the study of integrands themselves has also proven fruitful in recent years, and has given rise to efficient computational tools [5, 6, 7], unexpected relations between gauge theory and gravity [8, 9, 10], and novel ways of thinking about what scattering amplitudes compute [11, 12, 13, 14]. Although a general method for carrying out the integration over these integrands is still wanting, this growing command over the integrands entering field theory calculations has given rise to an increased understanding of the amplitudes we are ultimately interested in.

With the use of these and other such methods, the last three decades have seen an eruption of progress in our ability to calculate scattering amplitudes. These advancements, moreover, have continually borne out the observation that scattering amplitudes, even at high loop orders, are endowed with a mathematical simplicity that is not at all apparent from their Feynman diagram expansion. This is exceptionally true in highly supersymmetric theories, in which particles of different spin are related to each other. For this reason, it is in these theories that many of the most striking advances have been made.

The theory this thesis will focus on is the maximally supersymmetric gauge theory in four dimensions, $\mathcal{N} = 4$ super-Yang-Mills (SYM) theory [15, 16] (if we were to add more supersymmetry, we would get a theory of gravity). In particular, we consider this theory at the origin of the moduli space, where no scalars have been given vacuum expectation values and all gauge bosons are correspondingly massless. Consequently, the only two parameters that enter this theory are the coupling constant and the number of colors N in the gauge group, and its particle content is given by unbroken massless supermultiplets each involving two spin-1 gluons, eight spin-$\frac{1}{2}$ gluinos, and six complex scalars related by the action of the supersymmetry generators. Amplitudes with different particle content are related by supersymmetry

and R-symmetry Ward identities, and in this theory these identities are rich enough to completely determine amplitudes involving particles other than gluons in terms of purely gluonic amplitudes for eight or fewer scattering particles [17]. Correspondingly, we will concern ourselves exclusively with all-gluon amplitudes. In addition to maximal supersymmetry, this theory enjoys a conformal symmetry that is not spoiled by quantum corrections. These symmetries combine to form a superconformal group, described by the graded Lie algebra $su(2,2|4)$, which includes 30 bosonic generators and 32 fermionic generators (which change the helicity of the object they act on).

While it is known that this theory can't describe the real world, its highly constrained mathematical structure makes it a natural arena for the development of novel computational techniques that can hopefully be generalized to the Standard Model. It is known, for instance, that the same types of iterated integrals appear in the amplitudes of both of these theories. For amplitudes involving a sufficiently small number of particles, all current calculations have shown it is enough to consider the space of multiple polylogarithms, defined recursively by

$$\mathrm{G}(a_1,\ldots,a_n;z)=\int_0^z\frac{dt}{t-a_1}G(a_2,\ldots,a_n;t),\qquad \mathrm{G}(\underbrace{0,\ldots,0}_{n};z)=\frac{\log^n z}{n!}\,.$$

This space of functions includes the natural logarithm $\log z = G(0;z)$ as well as the classical polylogarithms $\mathrm{Li}_n(z)=\mathrm{G}(0,\ldots,0,1;z)$, and comes equipped with a notion of 'transcendental weight' corresponding to the number of integrations appearing in the construction of a given multiple polylogarithm. (In the case of products of functions, transcendental weight is additive.) The utility of this measure is that the L-loop contribution to every amplitude in $\mathcal{N}=4$ SYM is believed to have uniform transcendental weight $2L$. This is not true of non-supersymmetric gauge theories, where amplitudes generically have mixed transcendental weight and can receive contributions from elliptic integrals when the matter content of the theory includes particles with different masses (elliptic functions are also expected to appear in higher-point amplitudes in $\mathcal{N}=4$ SYM). However, $\mathcal{N}=4$ SYM amplitudes appear as part of the leading transcendental piece of the polylogarithmic component of non-supersymmetric amplitudes, so there is at least a minimal sense in which our increasing understanding

of these amplitudes already gives us a glimpse into the Standard Model.

The computations presented in this thesis make use of further simplifications that occur when the number of colors N becomes large. This has the effect of suppressing contributions coming from non-planar Feynman diagrams—those whose internal lines cross when projected onto a plane—because their associated color factors give rise to fewer factors of N than their planar analogues. In this limit, $\mathcal{N} = 4$ SYM becomes integrable and has a finite radius of convergence [18], indicating that it should be exactly solvable. Amplitudes in this limit moreover become dual to light-like polygonal (super-)Wilson loops [19, 20, 21, 22, 23, 24, 25], endowing them with a dual superconformal symmetry that combines with the ordinary superconformal symmetry to form an infinite-dimensional Yangian symmetry [19, 26, 27, 28, 29, 30].

This large amount of additional symmetry strongly constrains the form amplitudes can take in the planar limit—in fact, up to additive constants it fixes the four- and five-particle amplitudes to be nothing more than the exponentiated one-loop contribution dressed with certain anomalous dimensions, as conjectured by Bern, Dixon, and Smirnov [31]. The success of this 'BDS ansatz' is now understood from the dual (Wilson loop) perspective, where it solves the inhomogeneous part of an anomalous dual conformal Ward identity associated with ultraviolet divergences that appear at the cusps of polygonal Wilson loops [20, 21, 22, 23]. Since the amplitude/Wilson loop duality maps the infrared of one theory to the ultraviolet of the other, and because these Wilson loops receive no other divergent contributions, the solution to this Ward identity accounts for all infrared-divergent contributions on the amplitudes side of the duality for any number of particles.

The fact that these infrared divergences exponentiate is not surprising, since this exponentiation is a general property of gauge theories—what is surprising is that the finite part of the amplitude exponentiates as well for fewer than six particles. However, this can be seen to follow from the fact that the solution to the anomalous Ward identity governing these Wilson loops is unique for four- and five-particle kinematics, thus determining the finite as well as the divergent pieces of these amplitudes. Once six or more particles are involved, it becomes possible to construct ratios of kinematic invariants that respect the dual conformal symmetry of the amplitude.

These dual conformal invariants are annihilated by the (nonanomalous part of the) Ward identity, implying that any solution to this Ward identity can be shifted by an arbitrary function that depends only on these variables. The upshot is that the n-particle amplitude in planar $\mathcal{N} = 4$ SYM is known up to a finite function of dual conformal invariants, which can appear first in six-particle kinematics—all of which is completely obscured by the Feynman diagram expansion of these amplitudes. It is this set of finite, dual conformally invariant functions that the present thesis will concern itself with.

The first efforts to compute six- and seven-particle corrections to the the BDS ansatz focussed on the 'remainder function' R_n, which encodes the MHV part of the amplitude, and the 'ratio functions' $\mathcal{P}_n^{\mathrm{N}^k\mathrm{MHV}}$, which encode the helicity configuration with $2 + k$ negative helicity gluons [32, 33, 34, 35, 36, 37, 38, 39, 40, 41]. The first of these quantities is defined in terms of the n-particle MHV amplitude $\mathcal{A}_n^{\mathrm{MHV}}$ and the corresponding BDS ansatz $\mathcal{A}_n^{\mathrm{BDS}}$ by

$$\mathcal{A}_n^{\mathrm{MHV}} \;=\; \mathcal{A}_n^{\mathrm{BDS}} \,\times\, \exp(R_n)\,,$$

while the second is given by the ratio of each other helicity component of the amplitude to the MHV part of the amplitude,

$$\mathcal{P}_n^{\mathrm{N}^k\mathrm{MHV}} = \frac{\mathcal{A}_n^{\mathrm{N}^k\mathrm{MHV}}}{\mathcal{A}_n^{\mathrm{MHV}}}\,.$$

In addition to being infrared finite, these functions inherit a broad set of formal properties from the amplitude, including

- symmetries under permutations of particle indices,
- simple spacetime parity transformations,
- branch cuts only in physical channels,
- derivatives constrained by the action of the dual superconformal generators,
- universal collinear and multiparticle factorization properties,

- and restricted behavior in special kinematics, such as the multi-Regge limit and the near-collinear region.

This set of properties, combined with the observation that all known six- and seven-particle amplitudes in this theory are expressible in terms of multiple polylogarithms with specific kinematic arguments, makes possible a bootstrap approach to computing the remainder and ratio functions [32, 33, 34].

The strategy adopted by the 'Hexagon' and 'Heptagon' bootstrap programs is to first build the full space of multiple polylogarithms that can appear in the remainder and ratio functions at a given loop order, and then impose known properties of these functions on a general ansatz in this space. The verb 'build' is appropriate here, because while it proves easy (at least for six- and seven-particle amplitudes) to write down all multiple polylogarithms that depend on the right set of kinematic invariants, this naïve approach leads to a far larger space of functions than is needed—in particular, the vast majority of functions in this space will have unphysical branch cuts. A more nuanced approach can be adopted by taking advantage of the Hopf algebra structure these polylogarithms respect [42, 43]. In particular, they are endowed with a coproduct Δ that breaks down each function into tensor products of functions of lower transcendental weight. This map preserves the total weight, and its action on a function of weight w can be split into components as

$$\Delta = \sum_{p+q=w} \Delta_{p,q}.$$

where $\Delta_{p,q}$ maps the space of weight $p+q$ polylogarithms to a tensor space of weight p polylogarithms times weight q polylogarithms. Each of these coproduct components contains the same information, up to powers of π. This provides a natural algebraic structure within which functions with some desirable physical properties can be constructed. That is, instead of using the coproduct to analyze a known polylogarithm, one can use it to 'build' a function, or rather its coproduct, out of a general tensor space of lower-weight polylogarithms. For instance, we can define a function F of

weight w by its action under $\Delta_{w-1,1}$ as

$$\Delta_{w-1,1}F \equiv \sum_{\{s_i\}} F^{s_i} \otimes \log s_i$$

for some set of weight $w-1$ functions F^{s_i} (the superscript denotes the logarithm each of these functions is paired with, not a power), and some set of 'symbol letters' s_i that for us will be algebraic combinations of kinematic invariants. Only logarithms appear in the second entry because they constitute a basis of polylogarithms of unit transcendental weight. If the functions in this tensor product are chosen to satisfy some desirable algebraic or analytic property, they can endow the constructed function with these properties as well. For instance, the monodromy operator (which computes the discontinuity picked up by encircling a point) only acts on the first entry of the coproduct, meaning that the function F will only have the branch cuts it inherits from the functions F^{s_i}. Similarly, derivatives only act on the second entry of the coproduct, so the derivative of F will be given by

$$dF = \sum_{\{s_i\}} F^{s_i} \; d\log s_i \; ,$$

implying that the above coproduct-level definition is equivalent to specifying the derivatives of the function F. This means that we also need to specify an integration base point to complete the definition of our function F. To ensure that this integration can be carried out, we must also impose some 'integrability constraints' on the combination of functions appearing in our coproduct-ersatz of F, since an arbitrary linear combination of functions in this tensor space will not correspond to the coproduct of a genuine function. This is equivalent to requiring that partial derivatives acting on F commute.

This technique for bootstrapping multiple polylogarithms with special properties was first proposed by Dixon, Drummond, von Hippel, and Pennington [34], and—as the results presented in this thesis will hopefully demonstrate—has proven a fruitful one. As it will play a central role in the computations presented throughout the rest of this work, a worked example of this bootstrap procedure is provided in Appendix D,

where the space of two-dimensional functions appearing in a certain kinematic limit of six-particle scattering is explicitly constructed through weight 3. Carrying out this construction in general six-particle kinematics gives rise to the space of Hexagon functions, which are defined to be multiple polylogarithms such that that (i) only a specific set of nine arguments enter the logs appearing in weight one entries of their coproduct, and that (ii) have discontinuities in only physical channels. Heptagon functions, the analogous functions in seven-particle kinematics, can be similarly defined in terms of a different set of forty-two allowed arguments. With a basis of either set of functions at weight $2L$, it is straightforward—if sometimes computationally burdensome—to impose symmetry, parity, and proper behavior under the action of the dual superconformal generators on a general ansatz. However, these constraints by themselves are not generally sufficient to determine the ratio or remainder functions, so knowledge of kinematic limits must be used to impose further conditions on this ansatz.

One limit of interest in this respect is the collinear limit, in which two or more scattering gluons become collinear. In the strict collinear limit, gauge theory amplitudes are expected to factorize into lower-point amplitudes times splitting functions. This translates to a vanishing condition on loop-level corrections to the six-particle BDS ansatz, since the BDS ansatz for fewer particles is exact. On the other hand, the condition that the functional dependence of the seven-particle amplitude reduces to that of Hexagon functions in all collinear limits turns out to be extremely restrictive, as we will see in Part II of this thesis. In planar $\mathcal{N} = 4$, a great deal is also understood about the near-collinear limit from the amplitude/Wilson loop duality [44, 45, 46, 47]. In particular, the amplitude can be expanded as a power series around the collinear limit for finite coupling, using an operator product expansion that describes the limit in which two of the lines in the Wilson loops dual to amplitudes become collinear [48, 49, 50, 51, 52, 53, 54, 55, 56, 57]. This provides a source of boundary data and consistency checks, through any order one is intrepid enough to compute this operator product expansion to.

A second limit that can provide boundary data or consistency checks is the multi-Regge limit, in which the scattering particles are strongly ordered in rapidity. Here

the amplitude can be transformed into Fourier-Mellin space, where it is determined by a BFKL eigenvalue and impact factor, both of which can be computed perturbatively [58, 59, 60, 61, 62, 37]. Notably, the amplitude exponentiates in Fourier-Mellin space, such that the terms that appear in this limit with two or more powers of large logs are predicted by the multi-Regge limit of lower-loop amplitudes.

In Part I of this thesis, these and new constraints are used to uniquely determine the six-particle scattering amplitude in planar $\mathcal{N} = 4$ at four and five loops. First, Chapter 1 presents an extended set of constraints following from the action of the dual superconformal generators on these amplitudes (in the guise of the $\bar{Q}$ equation [63, 64]), which are used in combination with the other constraints outlined above to compute the NMHV ratio function at four loops. This complements a previous computation of the four loop remainder function using similar methods [35], thus completing the calculation of the four-loop amplitude. This chapter was published, in a slightly modified form, with Lance Dixon and Matt von Hippel [38].

In Chapter 2, an entirely new class of constraints is shown to follow from the work of Steinmann [65, 66, 67], who showed that the discontinuities of discontinuities of amplitudes are required to vanish when these discontinuities are taken in channels that partially overlap. These constraints do not apply directly to the remainder and ratio functions, but can be made transparent by bootstrapping instead a set of functions normalized by a 'BDS-like' ansatz in which all dependence on three-particle kinematic invariants has been removed (see Appendix F). These new functions are related to the original remainder and ratio functions by a simple exponentiated factor, but live in the subspace of the Hexagon function space where these double discontinuities vanish. Since this property can be built into functions at the level of the coproduct, it gives rise to a drastically smaller space of functions that need be constructed. This new restriction is then used in combination with only general constraints on the form the amplitude can take to compute the full six-particle amplitude at five loops. In other words, it is shown that knowledge of just the symmetries and analytic properties of the amplitude, in combination with an understanding of the form these amplitudes must take in either the near-collinear or multi-Regge limit, is sufficient to determine the amplitude through five loops—no external boundary data is needed as input. This

chapter was published, in a slightly modified form, with Simon Caron-Huot, Lance Dixon, and Matt von Hippel [68].

Chapter 3 goes on to give one answer to the question: what can we do with these amplitudes now that they've been computed? It does this by making contact with some of the structure seen at the level of the Amplituhedron formulation of planar $\mathcal{N} = 4$ integrands [13]. Namely, the Amplituhedron construction provides a kinematic region where the integrands of these amplitudes are positive, and where it has been further conjectured that the amplitude itself may be uniformly positive [69]. (Note that this does not follow from the positivity of the integrand, because generic integration contours—and in particular, the usual Minkowski contour—do not manifestly preserve positivity.) This chapter presents analytic and numerical evidence in support of this conjecture through five loops, and in fact makes the stronger observation that both the ratio function and BDS-like normalized MHV amplitude appear to grow monotonically in certain kinematical regions. This points to a surprising property of the contour of integration (which is not yet understood), and the potential existence of another formulation of the theory that would make this currently unexplained property manifest. This chapter was published, in a slightly modified form, with Lance Dixon, Matt von Hippel, and Jaroslav Trnka [70].

Part II turns to the kinematics of seven-particle scattering, and Chapter 4 uses the same types of bootstrap techniques considered in six-particle kinematics to uniquely determine the symbols of the four-loop MHV amplitude and three-loop NMHV amplitude. (The symbol can be thought of as just the maximally iterated coproduct, which lives in a $2L$-fold tensor space of weight one logarithms.) Moreover, it is shown that these objects are even more constrained than their six-particle counterparts, insofar as only constraints on the form of the amplitude in general and collinear kinematics are needed to uniquely determine these objects (in six-particle kinematics the mathematical form of either the near-collinear limit or the multi-Regge limit was needed to seed higher-loop constraints from lower-loop predictions). This chapter was published, in a slightly modified form, with Lance Dixon, James Drummond, Thomas Harrington, Georgios Papathanasiou, and Markus Spradlin [71].

Part I

Six-Particle Kinematics

Chapter 1

The Ratio Function at Four Loops

1.1 Introduction

Over the past few decades, the hidden simplicity of $\mathcal{N} = 4$ super-Yang-Mills (SYM) theory [15, 16] has been steadily revealed. The theory is conformally invariant for any value of the coupling [72, 73, 74]. In the planar limit of a large number of colors, further simplifications take place: the perturbative expansion has a finite radius of convergence, and the theory becomes integrable [18]. Related to integrability, the theory is endowed with a dual superconformal symmetry [26, 27, 28, 19, 29], and scattering amplitudes are dual to polygonal Wilson loops with light-like edges [19, 20, 21, 22, 23, 24, 25]. These features make it an ideal setting for exploring general properties of gauge theory amplitudes, especially for large numbers of external legs and high loop orders. The infrared divergences of scattering amplitudes in planar $\mathcal{N} = 4$ SYM are captured by the BDS ansatz [31]. When amplitudes are divided by this ansatz, the ratio is not only infrared-finite, but its components are functions only of dual conformally invariant cross ratios [75, 76]. This restricted set of kinematic variables simplifies dramatically the problem of determining the amplitudes. In particular, scattering amplitudes with four or five external particles are uniquely determined, up to constants, because there are no nontrivial cross ratios in these cases.

In the six-point case, the subject of this paper, only three functions are needed

to specify the scattering amplitudes. Each function depends on three independent cross ratios, which we call u, v and w. The first such function, the *remainder function*, $R_6(u, v, w)$, is defined to be the maximally-helicity-violating (MHV) all-gluon amplitude divided by the BDS ansatz [75, 76]. MHV amplitudes involving particles other than gluons are related to this function by the $\mathcal{N} = 4$ superalgebra, and can be combined with the all-gluon amplitude to form an MHV super-amplitude [77, 78, 79, 80]. Other helicity configurations, such as the next-to-MHV (NMHV) amplitude, are specified as *ratio functions*, which are defined by dividing the super-amplitude for the chosen helicity configuration by the MHV super-amplitude [29]. The NMHV ratio function can be further decomposed into two independent functions, V and $\tilde{V}$, which multiply dual superconformal R-invariants — five-brackets of supersymmetric versions of momentum twistors [81, 82]. For the six-point amplitude, the next-to-next-to-MHV amplitude is related to the MHV amplitude by parity. Therefore, R_6, V and $\tilde{V}$ are the only functions that can appear in this amplitude.

In principle, these functions could be determined at L loops by direct integration of the loop integrand. There are various approaches to computing the multi-loop integrand, see for example refs. [7, 83, 84, 11, 85, 86, 13, 14]. However, integrating such representations of the integrand is nontrivial. The *hexagon function bootstrap* [32, 33, 34, 35, 36, 37] sidesteps this problem by constructing ansätze for the functions in the space spanned by iterated integrals [87] with *(transcendental) weight* $2L$. The assumption that the functions lie in this space was originally inspired by the compact analytic form found for the two-loop remainder function [42], following earlier work [88, 89]. It can also be argued for from various "dLog" representations of the loop integrand [11, 85, 86]. Indeed, there is evidence that iterated-integral representations should exist for all scattering amplitudes with fewer than ten particles [11]. Familiar examples of iterated integrals include logarithms, polylogarithms, Riemann ζ values, and multiple polylogarithms [90, 91], where the weight is given by the number of integrations. By requiring that an ansatz spanning this space of functions has the appropriate analytic properties and functional dependence, and by further matching it to known physical limits of six particle scattering, the six-point remainder and NMHV ratio functions have been uniquely determined, through four

loops [35] and three loops [37], respectively. A similar *heptagon function* bootstrap, based on cluster variables [39, 40] has yielded the (symbol of the) seven-point remainder function — with remarkably little input from physical limits [41]. The main purpose of this article is to extend the hexagon function bootstrap to the NMHV six-point amplitude at four loops.

Hexagon functions are defined by two conditions [34]:

1. Their derivatives with respect to the cross ratios can be expanded in terms of just nine hexagon functions of one lower weight, $n-1$. Equivalently, there are nine different $\{n-1,1\}$ elements of the coproduct [92, 43], corresponding to nine letters in the symbol [93, 94, 95, 96] of the function. We also refer to these functions as *final entries* (of the symbol).

2. Their branch cuts are only in u, v and w, and not in any of the other six symbol letters [46].

The first condition can be used to construct hexagon functions iteratively in the weight. The branch-cut condition is imposed iteratively as well, although at each order most of it is automatically obeyed, given that the first derivative obeys it by construction. The branch-cut condition massively prunes the space of iterated integrals. For example, at weight eight — the weight we will primarily be concerned with in this paper — a representation of the space of iterated integrals in terms of multiple polylogarithms without imposing the branch-cut condition [34] leads to 1,675,553 such functions, whereas there are only 6,916 hexagon functions. (Recently a more economical multiple-polylogarithm representation has been found which requires only 500,217 functions at weight eight [97].)

In this paper, we use the hexagon function bootstrap to determine the four-loop NMHV ratio function, starting from an ansatz of weight-eight hexagon functions for each V and $\tilde{V}$. Due to the combination of R-invariants multiplying these functions and their permutations in the ratio function, a number of discrete symmetry constraints can be applied from the outset. Some of the discrete symmetries are subsets of the S_3 group of permutations of u, v, and w. There is also a "parity" which leaves u, v, w alone but flips the sign of a square root needed to define certain symbol letters y_i;

parity takes $y_i \leftrightarrow 1/y_i$. The function $V(u, v, w)$ must be parity-even and symmetric in the exchange $u \leftrightarrow w$, while $\tilde{V}(u, v, w)$ is parity-odd and antisymmetric under the same exchange.

A particularly powerful constraint comes from dual superconformal symmetry, which leads to a "$\bar{Q}$" differential equation [63, 64]. The consequences of this equation for the first derivatives of six-point amplitudes were explored in refs. [64, 98]. It has also been studied recently in the context of the operator product expansion [99, 100]. Here we will be interested in its global implications. For the MHV remainder function, it implies that only six of the nine final entries are allowed. This information was used in the hexagon function bootstrap for this function at four loops, although it still left over 100 free parameters [35]. In the initial construction of the NMHV ratio function at three loops [37], a seven-final-entry condition [64, 98] was imposed on both V and $\tilde{V}$. After the fact, it was found empirically that a function related to V had only five final entries, but the connection to the $\bar{Q}$ equation was not yet clear [37]. Subsequently, we have understood that the five-final-entry condition can be derived from the $\bar{Q}$ equation, but also that this equation has much more powerful consequences [98]. The five-final-entry condition is a restriction on just one permutation of the parity-even part of the ratio function; the full power of the $\bar{Q}$ equation comes from how it relates different permutations to each other, and also how it relates the parity-even and parity-odd functions. Imposing the more general restrictions at the outset, along with the discrete symmetry requirements, we find only a 34-parameter family of solutions at four loops. (The five-final-entry condition, plus a seven-final-entry condition on $\tilde{V}$, together with the same discrete symmetry constraints, would have left 808 parameters at four loops.)

To this 34-parameter ansatz we apply the same physical constraints used at three loops [37]. In the collinear limit, in which two external legs of the amplitude become parallel, the six-point amplitude must reduce to a splitting function times a five point amplitude. Because the five-point ratio function is trivial, loop corrections to the six-point ratio function must vanish in this limit. This constraint fixes all but five of the 34 parameters. Furthermore, while the hexagon functions are free of unphysical singularities, some of the R-invariants have spurious poles. Therefore, any linear

combination of V and $\tilde{V}$ that multiplies an R-invariant that has a spurious pole must vanish as that pole is approached. Previously, this condition provided a useful constraint [33, 37]. Now, however, the combination of the $\bar{Q}$ and collinear constraints is so powerful that no additional parameters are fixed by the spurious-pole constraint (at least through four loops).

To fix the five remaining parameters at four loops, we turn to the multi-Regge limit. There has been considerable study of the remainder function in this limit [58, 59, 101, 102, 103, 104, 32, 60, 105, 106, 107, 35, 108, 62, 109]. In the NMHV case, a factorization was proposed at the leading-logarithmic level by Lipatov, Prygarin and Schnitzer [61], and later extended to all orders [62, 37]. The quantities entering the multi-Regge factorization — the BFKL eigenvalue and the impact factor — can either be determined order-by-order [37], or all at once using integrability and a continuation from the near-collinear limit [62] (see also ref. [109]). The three-loop ratio function suffices to determine the multi-Regge limit to next-to-leading-logarithmic (NLL) accuracy. Matching the five-parameter ansatz at four loops to the NLL result, we fix all five parameters remaining in the ansatz.

Once we have uniquely determined the solution, we can check it against further boundary data. It predicts the next-to-next-to-leading-logarithmic (NNLL) terms in the multi-Regge limit, and even the $\mathrm{N^3LL}$ impact factor. All of these results agree with previous predictions [35, 37, 62]. Many further checks come from the operator product expansion (OPE) controlling the near-collinear limit [44, 45, 46, 47], by virtue of the representation of the (super)amplitude as a light-like polygonal Wilson (super)loop. The Wilson loop OPE can be calculated nonperturbatively in the coupling, using technology first developed by Basso, Sever and Vieira (BSV), wherein the expansion is carried out in the number of flux tube excitations [48, 49, 50, 51]. This expansion corresponds to the number of powers of $\sqrt{w}$ in the series expansion around the collinear limit $w \to 0$, $u + v \to 1$. More recently, this flux-tube approach has been extended to all helicity configurations [52, 53, 54, 55, 56, 57]. Previously, we used some of this information in the construction of the three-loop ratio function. With the additional $\bar{Q}$ constraints imposed, the OPE comparison becomes purely a cross-check, at least through four loops. We have compared the series expansion of

our results to both the single and double flux-tube excitation OPE predictions, and all are in agreement.[1]

Another interesting limit is that of multi-particle factorization, where the six-point amplitude splits into two four-point amplitudes connected by a single-particle exchange (at tree level). In this limit, two cross ratios get large at the same rate: $u, w \to \infty$ with u/w and v fixed. At three loops, it was found that the behavior of the even part of the ratio function in this limit was extremely simple, and could be expressed just in terms of a polynomial in one kinematic combination, $\ln(uw/v)$, with constant (ζ-valued) coefficients. We find that this pattern persists at four loops.

In order to gain some insight into the structure of the NMHV amplitude, we explore the analytic and numerical features of V and $\tilde{V}$ through four loops in a number of kinematic regions. We give (relatively) compact formulas for V and $\tilde{V}$ on particular lines through the space of cross ratios where they simplify. We obtain numerical values and plot them on these lines, and on various two-dimensional surfaces. From the finite radius of convergence of the perturbative expansion of planar $\mathcal{N} = 4$ SYM, we expect the ratios of perturbative coefficients at successive loop orders to eventually approach the same negative constant. However, the rate at which this happens can depend on the location within the space of cross ratios. In many limits, there are logarithmic divergences, where the power of the logarithm increases with the loop order. Sufficiently close to these limits, the generic asymptotic behavior does not hold. However, we observe that away from these singular regions, the ratios between successive loop orders do become increasingly flat as the loop order increases.

Another aspect of this work is to improve our knowledge of the space of hexagon functions at higher weight, not only to help with the four-loop construction performed in this article, but also as a platform for going to higher loops in the future. We have constructed a basis for this space now through weight eight, whereas previously only a weight-five basis had been constructed [34]. The weight-six part of the basis allows us to write the three-loop quantities $R_6^{(3)}$, $V^{(3)}$ and $\tilde{V}^{(3)}$ as single functions, whereas previously we had to describe them for generic (u, v, w) in terms of their first derivatives, or equivalently their $\{5, 1\}$ coproduct elements. Similarly, we can

[1] We thank Andrei Belitsky for assistance with this comparison.

express the four-loop quantities for generic (u, v, w) in terms of the weight-eight basis, although the expressions do start to become rather lengthy.

The structure of this paper is as follows. In section 1.2 we describe the setup and give an overview of the constraints we impose. We also outline the iterative construction of a basis of hexagon functions. In section 1.3 we discuss the constraints coming from the $\bar{Q}$ equation, which does the bulk of the work in fixing parameters. In section 1.4 we discuss the multi-Regge constraint, which fixes the final five parameters in our four-loop ansatz. In section 1.5 we analyze the near-collinear limit and compare it to the OPE predictions. In section 1.6 we study the multi-particle factorization limit. In section 1.7 we study the quantitative behavior of the result on various lines and surfaces in the space of cross ratios. Finally, in section 1.8 we conclude and provide our outlook for the future. There are four appendices. Appendix A gives more details on the construction of a hexagon function basis. Appendix B gives the three-loop quantities $R_6^{(3)}$, $V^{(3)}$ and $\tilde{V}^{(3)}$ in terms of the weight-six basis, while appendix C gives parts of the expressions of the corresponding four-loop quantities in terms of the weight-eight basis. Finally, appendix D describes the basis of functions of (u, v) to which the hexagon functions collapse on the surface $w = 1$. This function space is useful for implementing the spurious-pole constraint.

Many of the analytic results in this paper are too lengthy to present in the manuscript. Instead we attach them as computer-readable ancillary files, which are also available on the webpage [110]. The files describe: functional integrability constraints, the ratio function and remainder function through four loops in terms of the weight-eight basis, a coproduct-based definition of the basis, expansions of the ratio function in the near-collinear limit and in the multi-Regge limit, multiple polylog representations in other "bulk" regions, harmonic polylog representations on particular lines, a basis of functions for the surface $w = 1$ through weight seven, and the ratio function and remainder function on $w = 1$ through three loops in terms of this basis.

1.2 Setup and overview of constraints

1.2.1 Decomposition of ratio function in terms of R-invariants

As in past work at one, two, and three loops [29, 111, 33, 37], we describe the six-point amplitude using an on-shell superspace [77, 78, 79, 80]. We package the on-shell states of the theory into a superfield Φ depending on Grassmann variables η^A, $A = 1, 2, 3, 4$, transforming in the fundamental representation of $SU(4)$:

$$\Phi \;=\; G^+ + \eta^A \Gamma_A + \tfrac{1}{2!}\eta^A\eta^B S_{AB} + \tfrac{1}{3!}\eta^A\eta^B\eta^C \epsilon_{ABCD}\overline{\Gamma}^D + \tfrac{1}{4!}\eta^A\eta^B\eta^C\eta^D\epsilon_{ABCD}G^-. \quad (1.1)$$

Here G^+, Γ_A, $S_{AB} = \frac{1}{2}\epsilon_{ABCD}\overline{S}^{CD}$, $\overline{\Gamma}^A$, and G^- are the positive-helicity gluon, gluino, scalar, anti-gluino, and negative-helicity gluon states, respectively.

The superamplitude $\mathcal{A}(\Phi_1, \Phi_2, \ldots, \Phi_n)$ contains all the information about the component helicity amplitudes, which can be extracted as particular terms in the expansion in the Grassmann variables. The superamplitude can be factored into the product of the MHV superamplitude and the ratio function $\mathcal{P}$ [29],

$$\mathcal{A} \;=\; \mathcal{A}_{\rm MHV} \times \mathcal{P}\,. \quad (1.2)$$

The ratio function is infrared finite. Expanding it in the η variables for six-particle scattering yields three terms,

$$\mathcal{P} \;=\; 1 + \mathcal{P}_{\rm NMHV} + \mathcal{P}_{\overline{\rm MHV}}\,. \quad (1.3)$$

Because $\mathcal{A}_{\rm MHV} \times \mathcal{P}_{\overline{\rm MHV}}$ is just the parity conjugate of the MHV superamplitude $\mathcal{A}_{\rm MHV}$, the only quantity not determined by the MHV expression is $\mathcal{P}_{\rm NMHV}$, which we compute.

We represent the kinematic variables in terms of dual coordinates (x_i, θ_i). (For a full discussion see e.g. ref. [112].) The momenta $k_i^{\alpha\dot\alpha} = k_i^\mu \sigma_\mu^{\alpha\dot\alpha}$ and supermomenta $q_i^{\alpha A}$ are expressed in terms of the dual coordinates as,

$$k_i^{\alpha\dot\alpha} = \lambda_i^\alpha \tilde\lambda_i^{\dot\alpha} = x_i^{\alpha\dot\alpha} - x_{i+1}^{\alpha\dot\alpha}, \qquad q_i^{\alpha A} = \lambda_i^\alpha \eta_i^A = \theta_i^{\alpha A} - \theta_{i+1}^{\alpha A}\,. \quad (1.4)$$

The dual coordinates appear in the amplitude either through the three dual conformal cross ratios, or (in the R-invariants) through the momentum supertwistors.

The three cross ratios are given by,

$$u = u_1 = \frac{x_{13}^2\, x_{46}^2}{x_{14}^2\, x_{36}^2}\,, \qquad v = u_2 = \frac{x_{24}^2\, x_{51}^2}{x_{25}^2\, x_{41}^2}\,, \qquad w = u_3 = \frac{x_{35}^2\, x_{62}^2}{x_{36}^2\, x_{52}^2}\,, \tag{1.5}$$

where $x_{ij}^2 \equiv (x_i^\mu - x_j^\mu)^2$. The momentum supertwistors [81, 82] are

$$\mathcal{Z}_i = (Z_i \,|\, \chi_i), \qquad Z_i^{R=\alpha,\dot\alpha} = (\lambda_i^\alpha, x_i^{\beta\dot\alpha}\lambda_{i\beta}), \qquad \chi_i^A = \theta_i^{\alpha A}\lambda_{i\alpha}\,. \tag{1.6}$$

The momentum twistors Z_i transform linearly under dual conformal symmetry, so that the four-bracket $\langle abcd\rangle \equiv \epsilon_{RSTU} Z_a^R Z_b^S Z_c^T Z_d^U$ is a dual conformal invariant (although it is not invariant under projective transformations of the Z_i). To construct dual superconformal invariants we can package the four-brackets, along with the χ_i, into five-brackets of momentum supertwistors called R-invariants as follows:

$$(f) \;\equiv\; [abcde] \;=\; \frac{\delta^4(\chi_a\langle bcde\rangle + \text{cyclic})}{\langle abcd\rangle\langle bcde\rangle\langle cdea\rangle\langle deab\rangle\langle eabc\rangle}\,. \tag{1.7}$$

Here the six external lines are labeled $\{a, b, c, d, e, f\}$, and we use shorthand notation to represent the five-bracket of $\mathcal{Z}_a, \mathcal{Z}_b, \mathcal{Z}_c, \mathcal{Z}_d$, and $\mathcal{Z}_e$ by the remaining leg f.

For higher-point amplitudes these R-invariants obey many identities; however, here it is sufficient to only consider one [29]:

$$(1) - (2) + (3) - (4) + (5) - (6) \;=\; 0. \tag{1.8}$$

Using this identity the tree-level ratio function can be represented in two equivalent ways:

$$\mathcal{P}^{(0)}_{\text{NMHV}} \;=\; (2) + (4) + (6) \;=\; (1) + (3) + (5). \tag{1.9}$$

At loop level, the R-invariants are dressed by two functions of the cross ratios: a

parity-even function $V(u,v,w)$ and a parity-odd function $\tilde{V}(y_u,y_v,y_w)$ [29, 33]:

$$\begin{aligned}\mathcal{P}_{\rm NMHV} \;=\; \frac{1}{2}\Big[&[(1)+(4)]V(u,v,w)+[(2)+(5)]V(v,w,u)+[(3)+(6)]V(w,u,v)\\ &+[(1)-(4)]\tilde{V}(y_u,y_v,y_w)-[(2)-(5)]\tilde{V}(y_v,y_w,y_u)+[(3)-(6)]\tilde{V}(y_w,y_u,y_v)\Big]\,.\end{aligned} \tag{1.10}$$

The y_i are dual conformally invariant parity-odd variables; indeed the definition of parity is the inversion $y_i \leftrightarrow 1/y_i$. The y_i variables can be defined in terms of (u,v,w) as follows:

$$y_u = \frac{u-z_+}{u-z_-}\,, \qquad y_v = \frac{v-z_+}{v-z_-}\,, \qquad y_w = \frac{w-z_+}{w-z_-}\,, \tag{1.11}$$

where

$$z_\pm = \frac{1}{2}\Big[-1+u+v+w \pm \sqrt{\Delta}\Big]\,, \qquad \Delta = (1-u-v-w)^2 - 4uvw\,. \tag{1.12}$$

So alternatively, parity can be defined as $\sqrt{\Delta} \leftrightarrow -\sqrt{\Delta}$, while leaving (u,v,w) invariant. Each point (u,v,w) corresponds to two points in the y_i variables, (y_u,y_v,y_w) and $(1/y_u,1/y_v,1/y_w)$. Parity-even functions have the same values at both y_i points, whereas the values of parity-odd functions flip sign between the two y_i points.

1.2.2 V, $\tilde{V}$, E, $\tilde{E}$ and U

The functions $V(u,v,w)$ and $\tilde{V}(y_u,y_v,y_w)$ can be expanded perturbatively. At tree level, the function $V(u,v,w)$ is equal to unity, while $\tilde{V}(y_u,y_v,y_w)$ vanishes. Their full loop expansions are

$$V \;=\; 1+\sum_{L=1}^{\infty} a^L V^{(L)}\,, \tag{1.13}$$

$$\tilde{V} \;=\; \sum_{L=2}^{\infty} a^L \tilde{V}^{(L)}\,, \tag{1.14}$$

where $a = g^2_{\rm YM}N_c/(8\pi^2)$ is our loop expansion parameter, in terms of the Yang-Mills coupling constant $g_{\rm YM}$ and the number of colors N_c. (The one-loop quantity $\tilde{V}^{(1)}$

vanishes because there is no parity-odd weight-two hexagon function.)

It is convenient to introduce some other functions E and $\tilde{E}$, which are closely related to V and $\tilde{V}$, but defined more directly in terms of the NMHV amplitude, rather than its ratio to the MHV amplitude. The $\bar{Q}$ equation will be simplest when expressed in terms of these functions. First recall that the MHV amplitude can be expressed in terms of two quantities, the BDS ansatz [31] and the remainder function R_6 [75, 76]:

$$\mathcal{A}_{\rm MHV} \;=\; \mathcal{A}_{\rm BDS} \,\times\, \exp(R_6)\,. \tag{1.15}$$

Therefore if we divide the NMHV superamplitude by the BDS ansatz $\mathcal{A}_{\rm BDS}$, rather than by the MHV amplitude, that ratio will have the same expansion (1.10), but with $V \to V\exp(R_6)$ and $\tilde{V} \to \tilde{V}\exp(R_6)$. In fact, we are going to divide the NMHV amplitude by a slightly-different, "BDS-like" function. Such a quantity has already been considered in the analysis of the strong-coupling behavior of amplitudes [113], as well as in the study of the multi-particle factorization limit of the NMHV amplitude [37].

Before describing the BDS-like ansatz, we recall that the BDS ansatz can be written as [31],

$$\frac{\mathcal{A}_n^{\rm BDS}}{\mathcal{A}_n^{\rm MHV\,(0)}} \;=\; \exp\left[\sum_{L=1}^{\infty} a^L \left(f^{(L)}(\epsilon)\frac{1}{2}M_n^{1-\rm loop}(L\epsilon) + C^{(L)}\right)\right], \tag{1.16}$$

where $\mathcal{A}_n^{\rm MHV\,(0)}$ is the MHV tree-level super-amplitude, and

$$f^{(L)}(\epsilon) \equiv f_0^{(L)} + \epsilon\, f_1^{(L)} + \epsilon^2\, f_2^{(L)}\,. \tag{1.17}$$

Two of the constants,

$$f_0^{(L)} \;=\; \frac{1}{4}\,\gamma_K^{(L)}\,, \qquad f_1^{(L)} \;=\; \frac{L}{2}\,\mathcal{G}_0^{(L)}\,, \tag{1.18}$$

are given in terms of the cusp anomalous dimension γ_K and the "collinear" anomalous dimension $\mathcal{G}_0$, while $f_2^{(L)}$ and $C^{(L)}$ are other (zeta-valued) constants. We won't need the specific values of any of these constants except for the cusp anomalous dimension.

This quantity is known to all orders [114]; its expansion to four loops is given by

$$\gamma_K(a) = \sum_{L=1}^{\infty} a^L \, \gamma_K^{(L)} = 4a - 4\zeta_2 \, a^2 + 22\zeta_4 \, a^3 - 4\left(\frac{219}{8}\zeta_6 + (\zeta_3)^2\right)a^4 + \mathcal{O}(a^5) \, . \quad (1.19)$$

The function $M_n^{1-\text{loop}}(L\epsilon)$ is the one-loop amplitude, normalized by the tree amplitude $\mathcal{A}_n^{\text{MHV}\,(0)}$, and evaluated in dimensional regularization with $D = 4 - 2\epsilon$, but letting $\epsilon \to L\epsilon$.

The normalized six-point one-loop amplitude is given by [3]

$$\begin{aligned} M_6^{1-\text{loop}}(\epsilon) \;\; = \;\; & \sum_{i=1}^{6}\Bigg[\frac{1}{4}\ln^2\Big(\frac{-s_{i,i+1,i+2}}{-s_{i+1,i+2,i+3}}\Big) - \frac{1}{\epsilon^2}(-s_{i,i+1})^{-\epsilon} \\ & \qquad - \ln\Big(\frac{-s_{i,i+1}}{-s_{i,i+1,i+2}}\Big)\ln\Big(\frac{-s_{i+1,i+2}}{-s_{i,i+1,i+2}}\Big)\Bigg] \\ & - \text{Li}_2(1-u) - \text{Li}_2(1-v) - \text{Li}_2(1-w) + 6\,\zeta_2 \, , \end{aligned} \quad (1.20)$$

where $s_{i,i+1} = (k_i + k_{i+1})^2$ and $s_{i,i+1,i+2} = (k_i + k_{i+1} + k_{i+2})^2$. Notice that $M_6^{1-\text{loop}}$ has non-trivial dependence on the three-particle momentum invariants $s_{i,i+1,i+2}$, both explicitly and implicitly through the three cross ratios. However, this dependence can be removed by shifting $M_6^{1-\text{loop}}$ by a particular totally symmetric function of the cross ratios,

$$Y(u,v,w) \;\equiv\; \text{Li}_2(1-u) + \text{Li}_2(1-v) + \text{Li}_2(1-w) + \frac{1}{2}\Big(\ln^2 u + \ln^2 v + \ln^2 w\Big) \, . \quad (1.21)$$

We let

$$\begin{aligned} \hat{M}_6(\epsilon) \;\; &= \;\; M_6^{1-\text{loop}} + Y(u,v,w) \\ &= \;\; \sum_{i=1}^{6}\Bigg[-\frac{1}{\epsilon^2}\Big(1 - \epsilon\ln(-s_{i,i+1})\Big) - \ln(-s_{i,i+1})\ln(-s_{i+1,i+2}) \\ & \qquad\qquad + \frac{1}{2}\ln(-s_{i,i+1})\ln(-s_{i+3,i+4}) + \zeta_2\Bigg] \, , \end{aligned} \quad (1.22)$$

which contains only the two-particle invariants $s_{i,i+1}$.

Then we can define the BDS-like function by

$$\frac{\mathcal{A}_6^{\text{BDS}-\text{like}}}{\mathcal{A}_6^{\text{MHV (0)}}} = \exp\left[\sum_{L=1}^{\infty} a^L \left(f^{(L)}(\epsilon)\frac{1}{2}\hat{M}_6(L\epsilon) + C^{(L)}\right)\right]. \tag{1.23}$$

Using eq. (1.22), it is related to the BDS ansatz by

$$\mathcal{A}_6^{\text{BDS}-\text{like}} = \mathcal{A}_6^{\text{BDS}} \exp\left[\frac{\gamma_K}{8} Y(u,v,w)\right]. \tag{1.24}$$

Finally, we normalize the NMHV superamplitude by the BDS-like ansatz, and define new functions $E(u,v,w)$ and $\tilde{E}(u,v,w)$ as the coefficients of the R-invariants:

$$\begin{aligned}\frac{\mathcal{A}_{\text{NMHV}}}{\mathcal{A}_6^{\text{BDS}-\text{like}}} = \frac{1}{2}\Big[&[(1)+(4)]E(u,v,w) + [(2)+(5)]E(v,w,u) + [(3)+(6)]E(w,u,v) \\ &+ [(1)-(4)]\tilde{E}(y_u,y_v,y_w) - [(2)-(5)]\tilde{E}(y_v,y_w,y_u) + [(3)-(6)]\tilde{E}(y_w,y_u,y_v)\Big].\end{aligned} \tag{1.25}$$

The relations between the new expansion coefficients, E and $\tilde{E}$, and the old ones, V and $\tilde{V}$, are:

$$E(u,v,w) = V(u,v,w)\exp\left[R_6(u,v,w) - \frac{\gamma_K}{8}Y(u,v,w)\right], \tag{1.26}$$

$$\tilde{E}(u,v,w) = \tilde{V}(u,v,w)\exp\left[R_6(u,v,w) - \frac{\gamma_K}{8}Y(u,v,w)\right]. \tag{1.27}$$

As long as the remainder function R_6 is known to the same loop order, it is straightforward to pass back and forth between $(E,\tilde{E})$ and $(V,\tilde{V})$. The consequences of the $\bar{Q}$ equations, which hold globally in (u,v,w), are simplest to describe in terms of E and $\tilde{E}$. On the other hand, the boundary data is often described in terms of V and $\tilde{V}$.

One exception is the limit of multi-particle factorization, in which the perturbative simplicity of E, or rather its logarithm U, was first noticed. We define

$$U(u,v,w) = \ln E(u,v,w), \qquad E(u,v,w) = \exp\Big[U(u,v,w)\Big]. \tag{1.28}$$

In section 1.6 we will see that this function has the same simple behavior at four loops that it has through three loops [37].

1.2.3 Hexagon functions

In order to construct the NMHV amplitude at four loops, we build on the observation that through three loops $V^{(L)}$ and $\tilde{V}^{(L)}$ have been found to belong to the space of hexagon functions of weight $2L$ [37]. A hexagon function is defined to be any function whose symbol is constructed from letters drawn from the set

$$\mathcal{S}_u = \{u, v, w, 1-u, 1-v, 1-w, y_u, y_v, y_w\}\,, \tag{1.29}$$

and which has only physical branch cuts [34]. The latter condition implies that hexagon functions can only have discontinuities when either u, v, or w approaches zero or infinity. This condition can be enforced at the level of the symbol by only allowing the variables u, v, and w to appear in the first entry of the symbol. Hexagon functions in which none of the variables y_u, y_v, or y_w appear can be factored into functions whose symbols have letters drawn from $\{u, 1-u\}$, or $\{v, 1-v\}$, or $\{w, 1-w\}$. Such functions can be expressed as (products of) harmonic polylogarithms (HPLs) of a single variable [115]. Functions whose symbols contain y_u, y_v, or y_w are more complex. They can be defined iteratively in terms of lower-weight hexagon functions by means of their derivatives. They can also be represented in terms of multiple polylogarithms in particular regions. In ref. [34], the space of hexagon functions was explored through weight six and a basis of irreducible hexagon functions through weight five was introduced. Irreducible hexagon functions are those that cannot be written as products of lower-weight hexagon functions.

The derivatives of a weight-n hexagon function F are given by [34]

$$\begin{aligned}\left.\frac{\partial F}{\partial u}\right|_{v,w} = \frac{F^u}{u} - \frac{F^{1-u}}{1-u} + \frac{1-u-v-w}{u\sqrt{\Delta}}F^{y_u} \\ + \frac{1-u-v+w}{(1-u)\sqrt{\Delta}}F^{y_v} + \frac{1-u+v-w}{(1-u)\sqrt{\Delta}}F^{y_w}\,,\end{aligned} \tag{1.30}$$

$$\sqrt{\Delta}y_u\frac{\partial F}{\partial y_u}\bigg|_{y_v,y_w} = (1-u)(1-v-w)F^u - u(1-v)F^v - u(1-w)F^w - u(1-v-w)F^{1-u} + uvF^{1-v} + uwF^{1-w} + \sqrt{\Delta}F^{y_u}\,, \quad (1.31)$$

as well as the cyclic permutations of these formulae under $u \to v \to w \to u$, $y_u \to 1/y_v \to y_w \to 1/y_u$. Each of the rational prefactors in eq. (A.2) is $[\partial(\ln x)/\partial u]|_{v,w}$ for some $x \in \mathcal{S}_u$, while in eq. (A.3) the corresponding rational prefactor is $[\partial(\ln x)/\partial y_u]|_{y_v,y_w}$. The F^x for $x \in \mathcal{S}_u$ denote nine weight-$(n-1)$ hexagon functions. These functions are also referred to as elements of the $\{n-1,1\}$ coproduct component of F [43]:

$$\Delta_{n-1,1}(F) \equiv \sum_{i=1}^{3}\Big[F^{u_i}\otimes\ln u_i + F^{1-u_i}\otimes\ln(1-u_i) + F^{y_i}\otimes\ln y_i\Big]\,. \quad (1.32)$$

The $\{n-1,1\}$ coproduct component specifies all the first derivatives of F. Hence it completely specifies F, up to an additive constant.

To fix the additive constant, we will typically require that basis functions vanish at the point $(u,v,w) = (1,1,1)$. Physical constraints are imposed elsewhere, so we need to transfer information about the value of functions at other points to the point $(1,1,1)$. We can transfer the information along special lines that cut through the (u,v,w) space. For example, the line $(1,v,v)$ connects $(1,1,1)$ to $(1,0,0)$. The latter point corresponds to a soft limit (a special case of two collinear limits), where there are physical constraints. On the line $(1,v,v)$, all hexagon functions collapse to HPLs in the single variable v. The standard notation for such functions is $H_{\vec{w}}(v)$, where $\vec{w} = w_1, w_2, \ldots, w_n$ is a list of n elements (at weight n), all of which are either 0 or 1. We can use shuffle identities to always choose $w_n = 1$ for $n > 1$, and it is convenient to have the argument be $1-v$ so that the function is regular at $v = 1$. Furthermore we use a compressed notation in which $(m-1)$ 0's followed by a 1 is written as m. Thus we define $H^v_{3,1,1} = H_{0,0,1,1,1}(1-v)$, and so forth. The function $\mathrm{Li}_2(1-v)$ entering the definition of $Y(u,v,w)$ is H^v_2 in this notation.

Equation (A.2) and its cyclic permutations form the cornerstone for the construction of a basis of hexagon functions, iteratively in the weight. Suppose one knows all hexagon functions at weight $(n-1)$. One can define a candidate set of weight n

hexagon functions by introducing arbitrary linear combinations of the weight $(n-1)$ functions for each of the $\{n-1,1\}$ coproduct elements F^x, $x \in \mathcal{S}_u$. This construction is naturally graded by parity. That is, if F is parity-even, then the six coproducts F^{u_i} and F^{1-u_i} are parity-even and should be drawn from the parity-even subspace at weight $(n-1)$, while the three coproducts F^{y_i} are parity-odd. If F is parity-odd, the reverse is true.

Not all combinations of $\{n-1,1\}$ coproduct elements F^x correspond to actual functions. First of all, they should obey the functional integrability conditions,

$$\frac{\partial^2 F}{\partial u_i \partial u_j} = \frac{\partial^2 F}{\partial u_j \partial u_i}\,, \qquad i \neq j. \tag{1.33}$$

These conditions can be recast as linear constraints on the $\{n-2,1,1\}$ coproduct elements of F, namely $F^{y,x}$, where $F^{y,x}$ is defined as the y coproduct element for F^x, i.e.

$$\Delta_{n-2,1}(F^x) \equiv \sum_{i=1}^{3} \Big[F^{u_i,x} \otimes \ln u_i + F^{1-u_i,x} \otimes \ln(1-u_i) + F^{y_i,x} \otimes \ln y_i \Big]\,. \tag{1.34}$$

In fact, the functional integrability conditions (1.33) only involve the antisymmetric combination $F^{[x,y]} \equiv F^{x,y} - F^{y,x}$. The constraints are given by:

$$\begin{aligned}
F^{[u_i,u_j]} &= -F^{[y_i,y_j]}\,,\\
F^{[1-u_i,1-u_j]} &= F^{[y_i,y_j]} + F^{[y_j,y_k]} + F^{[y_k,y_i]}\,,\\
F^{[u_i,1-u_j]} &= -F^{[y_k,y_i]}\,,\\
F^{[u_i,y_i]} &= 0\,,\\
F^{[u_i,y_j]} &= F^{[u_j,y_i]}\,,\\
F^{[1-u_i,y_i]} &= F^{[1-u_j,y_j]} - F^{[u_j,y_k]} + F^{[u_k,y_i]}\,,\\
F^{[1-u_i,y_j]} &= -F^{[u_k,y_j]}\,,
\end{aligned} \tag{1.35}$$

for all $i \neq j \neq k \in \{1,2,3\}$. There are a total of 12 independent parity-even relations (if F is even) and 14 parity-odd ones. We list them all explicitly in an ancillary file.

One can solve the system of linear equations (1.35) to obtain a set of functions

F, which is almost the set of hexagon functions at weight n. There is one more branch-cut condition that has to be satisfied [34]: The derivative $\partial_u F$ in eq. (A.2) has a $1/(1-u)$ singularity as $u \to 1$, which will lead to a $\ln(1-u)$ branch-cut unless we require,

$$\left[F^{1-u} + F^{y_v} - F^{y_w}\right]\Big|_{u\to 1} \;=\; 0. \tag{1.36}$$

Although this condition appears to be a strong one, holding for any v and w, for $u = 1$ the combination $F^{1-u} + F^{y_v} - F^{y_w}$ turns out to be independent of v and w, once the integrability conditions (1.35) are satisfied. This constancy can be verified using the basis of functions described in appendix D. Thus eq. (1.36) only fixes weight $(n-1)$ (zeta-valued) constants in F^{1-u}, if F is parity-even. The constants can be fixed in the corner of the $u = 1$ plane where v and w both vanish, namely the Euclidean multi-Regge kinematics (EMRK), which is also known as the soft limit [34]. This limit can also be reached by taking $y_u \to 1$ with y_v and y_w fixed. In this limit, $\Delta = 0$ and the parity-odd functions F^{y_i} vanish, so the condition (1.36) and its permutations reduce to the three conditions

$$F^{1-u_i}|_{u_i\to 1,\; u_j,u_k\to 0} \;=\; F^{1-u_i}(y_i = 1, y_j, y_k) \;=\; 0, \qquad i \neq j \neq k, \tag{1.37}$$

for even F. If F is parity-odd, then eq. (1.36) involves the constant part of the parity-even functions F^{y_v} and F^{y_w}. However, such constant terms are forbidden by the requirement that F vanishes when $y_i \to 1$, independently of y_j and y_k. This is equivalent to the conditions,

$$F^{y_j}(y_i = 1, y_j, y_k) \;=\; 0, \qquad i \neq j \neq k, \tag{1.38}$$

for odd F.

The combined solution to eqs. (1.35), (1.37) and (1.38), for otherwise arbitrary hexagon functions as $\{n-1, 1\}$ coproduct elements, generates the space of weight-n hexagon functions F, apart from a few constants. These constants are the linear combinations of the independent multiple zeta values (MZVs) at weight n. Most of the weight-n functions are reducible, i.e. they are products of lower-weight hexagon

functions. In order to identify the irreducible subspace, one can generate the vector space of reducible hexagon functions, and remove them from the complete space of solutions. This procedure was carried out in ref. [34], and a basis of hexagon functions was constructed through weight five.

1.2.4 A basis at weight six, seven and eight

Our calculation of the four-loop ratio function was facilitated by extending this basis of hexagon functions to weight six and seven. We also constructed a weight-eight basis, but only after obtaining the four-loop result. The extension of the basis beyond weight five was not strictly necessary; indeed, the four-loop remainder function was determined without such a basis [35]. In this case, the weight-five basis was used repeatedly to generate all of the $\{5,1,1,1\}$ elements of the coproduct of a generic (parity-even) weight-eight function. From these functions all of the $\{6,1,1\}$ coproduct elements were constructed, then all of the $\{7,1\}$ coproduct elements, and finally all of the weight-eight functions. The integrability and branch-cut conditions were imposed at each step, but there was no attempt to construct a basis beyond weight five. However, the present approach provides a more direct route to the weight-eight four-loop ratio function. It will also be a platform for going to five loops in the future, starting with the $\{8,1,1\}$ coproduct elements. (Or one could extend the basis to weight nine and work with the $\{9,1\}$ coproduct elements.)

The basis at weight six also allows us to present results for R_6, V and $\tilde{V}$ at three loops that are significantly more compact than previous representations in terms of the $\{5,1\}$ coproducts (see appendix B). Similarly, the weight-eight basis lets us write each of the four-loop functions as a single weight-eight function, although of course the four-loop results are not as compact as the three-loop ones. In ancillary files, we provide $R_6^{(L)}$, $V^{(L)}$ and $\tilde{V}^{(L)}$ for $L = 3, 4$. We also provide a coproduct description of the hexagon function basis at weight six, seven and eight; this basis is described further in appendix A.

There is a certain arbitrariness in defining a basis of irreducible functions; in principle, one can make an arbitrary linear transformation on the basis, and one can

add any linear combination of reducible functions to any candidate basis function. However, in the course of constructing the higher-weight basis functions, we found that some care in the construction leads to much simpler representations for physical quantities such as $R_6^{(3)}$, $V^{(3)}$, and $\tilde{V}^{(3)}$. One can generate a "random" basis by asking MAPLE or MATHEMATICA to provide a null space "orthogonal" to the reducible function space. However, when $R_6^{(3)}$, $V^{(3)}$, or $\tilde{V}^{(3)}$ are expressed in terms of such a basis, the rational numbers multiplying the basis functions in the expressions for these quantities have quite large numerators and denominators, with sometimes as many as 13 digits. A better way to select the basis for irreducible hexagon functions at weight n is to require that their weight $\{n-1,1\}$ coproduct elements collectively contain exactly one of the weight $(n-1)$ basis elements, and with unit coefficient. One cannot require this for all weight n irreducible functions; there are too many of them, compared with the number of weight $(n-1)$ ones. We start by imposing this criterion on the y_i coproduct entries, and preferentially for the functions with the most y_i entries in their symbol, as these typically have the most complicated coproducts. When we run out of weight $(n-1)$ irreducible functions, we impose the criterion using products of logarithms and weight $(n-2)$ irreducible functions instead. It is usually possible to further reduce the number of terms appearing in the coproducts of the basis functions by adding suitable linear combinations of reducible functions to them. Finally, as in ref. [34], we constructed our basis functions so that they form orbits under the permutation group S_3 acting on the variables u, v, and w, either singlets, three-cycles or six-cycles.

The basis we have constructed in this way through weight eight leads to quite parsimonious rational number coefficients when R_6, V, and $\tilde{V}$ (or their coproduct elements) are expanded in terms of the basis functions. For instance, the rational numbers multiplying the weight-six irreducible functions in $R_6^{(3)}$, $V^{(3)}$, and $\tilde{V}^{(3)}$ have denominators that are all powers of 2, up to an occasional factor of 3. The largest denominator is 128, while the largest numerator is 149. (The coefficients in front of the pure-HPL terms don't boast the same level of simplicity, but this is unsurprising since the above prescription for choosing irreducible hexagon functions only constrains each function up to the addition of reducible functions.) We also constructed a set

of weight-five basis functions without the degeneracy of the basis defined in ref. [34], by organizing the S_3 orbits differently. Even so, converting $R_6^{(3)}$, $V^{(3)}$, and $\tilde{V}^{(3)}$ to the weight-five basis of ref. [34] (which was selected with slightly different criteria in mind) only gives rise to slightly more complicated rational-number coefficients. So we will continue to use the weight-five basis of ref. [34].

Using the basis through weight six, we give the results for the three-loop functions $R_6^{(3)}$, $V^{(3)}$, and $\tilde{V}^{(3)}$ in eqs. (B.1), (B.3) and (B.5) of appendix B and in an ancillary file. Continuing the construction to weight eight, we give a similar representation for the four-loop functions $R_6^{(4)}$, $V^{(4)}$, and $\tilde{V}^{(4)}$ in appendix C. In this case, we only give the terms containing the irreducible weight-eight basis functions in the text; the remaining terms, which are products of lower-weight functions, are very lengthy and can be found in the same ancillary file.

1.2.5 Overview of the constraints

Our goal is to find a unique pair of functions $E(u,v,w)$ and $\tilde{E}(u,v,w)$ at four loops. We begin with an ansatz for the $\{7,1\}$ coproduct of a generic weight 8 hexagon function. There are 5153 such functions with even parity, which are candidates for $E^{(4)}$, and 1763 with odd parity, which are candidates for $\tilde{E}^{(4)}$. We then apply a succession of constraints to our ansatz in order to arrive at a unique result.

We largely follow the methodology of ref. [37], with some refinements. In particular, we apply the following constraints:

- **Symmetry:** Under the exchange of u and w, E is symmetric, while $\tilde{E}$ is antisymmetric:

$$E(w,v,u) \;=\; E(u,v,w), \qquad \tilde{E}(y_w,y_v,y_u) \;=\; -\tilde{E}(y_u,y_v,y_w). \tag{1.39}$$

- $\bar{Q}$ **Equation:** Caron-Huot and He predicted [64, 98] that the final entries of the hexagon functions that make up $V(u,v,w)$ should belong to a seven-element set. At lower loop orders, two of us observed [37] that the function $U(u,v,w)$ has final entries from a more constrained five-element set. This relation can

now be derived from the $\bar{Q}$ equation, but there are a host of other relations, which we describe further below. Together they are very powerful and do the bulk of the work in reducing the number of parameters in the ansatz, at four loops as well as at lower loops.

- **Collinear Vanishing:** In the collinear limit, the six-point ratio function should approach the five-point ratio function, multiplied by some splitting function. Because the only non-vanishing components of the five-point super-amplitude are MHV and NMHV, which are related by parity, and because there are no dual conformally invariant cross ratios at five points, the five-point ratio function is trivial; it vanishes at loop level. As such, the loop level six-point ratio function must vanish in the collinear limit. We take this limit by sending $w \to 0$ and $v \to 1-u$. In this limit, all of the R-invariants vanish except for (1) and (6), which become equal. Taking into account that parity-odd functions such as $\tilde{V}$ always vanish in this limit, we have the constraint,

$$[V(u,v,w) + V(w,u,v)]_{w\to 0,\ v\to 1-u} \ = \ 0. \tag{1.40}$$

- **Spurious Pole Vanishing:** Physical states give rise to poles in scattering amplitudes when the sums of color-adjacent momenta vanish, when $(k_i + k_{i+1} + \ldots + k_{j-1})^2 \equiv x_{ij}^2 = 0$. These sums come from four-brackets of the form $\langle i-1, i, j-1, j\rangle$. Poles of any other form, in particular poles arising from other four-brackets, should not appear. Individual R-invariants have such spurious poles, so these must cancel between R-invariants at tree level. At loop level, the corresponding condition is that the relevant combination of V and $\tilde{V}$ must vanish on any spurious pole. As it happens, examining one of these spurious poles is sufficient to guarantee vanishing on the others, by Bose symmetry of the super-amplitude. If we choose to fix behavior on the pole $\langle 2456\rangle \to 0$, we need to cancel potential poles from R-invariants (1) and (3) with equal and opposite residues. This leads to the condition,

$$[V(u,v,w) - V(w,u,v) + \tilde{V}(y_u,y_v,y_w) - \tilde{V}(y_w,y_u,y_v)]_{\langle 2456\rangle\to 0} \ = \ 0. \tag{1.41}$$

where the $\langle 2456 \rangle \to 0$ limit can be implemented by taking $w \to 1$ with u and v held fixed; more precisely,

$$\begin{aligned} w &\to 1\,, & y_u &\to (1-w)\frac{u(1-v)}{(u-v)^2}\,, \\ y_v &\to \frac{1}{(1-w)}\frac{(u-v)^2}{v(1-u)}\,, & y_w &\to \frac{1-u}{1-v}\,. \end{aligned} \tag{1.42}$$

We have used a basis of irreducible two-variable functions, discussed in appendix D, to impose this constraint.

- **Multi-Regge Limit:** The multi-Regge limit is a generalization of the Regge limit for $2 \to n$ scattering, where the outgoing particles are strongly ordered in rapidity. We build on our three-loop results, using our generalization of the work of Lipatov, Prygarin, and Schnitzer [61] to subleading logarithmic order. We also compare our results to a recent all-orders proposal [62].

- **Near-Collinear Limit:** As at three loops, we employ the pentagon decomposition of the NMHV Wilson loop OPE developed by Basso, Sever, and Vieira [49]. Their calculation uses integrability to compute the OPE nonperturbatively in the coupling, in an expansion in the number of flux-tube excitations, corresponding to powers of $\sqrt{w}$ in the near-collinear limit. Actually, our new understanding of the $\bar{Q}$ equation is such a powerful constraint that our ansatz is completely fixed before comparing with the OPE constraints, so the OPE results serve as a pure cross check of our assumptions (and theirs). We perform these checks at the first order of the OPE, corresponding to one state propagating across the Wilson loop [49], and then at second order (two flux excitations) [50] using explicit results of Belitsky [53, 54, 116]. In an ancillary file, we provide limits of V and $\tilde{V}$ to third order, making possible comparisons to the OPE terms involving three flux-tube excitations (we leave these checks to the intrepid reader).

In addition to these constraints, we should point out a residual freedom in our definition of $\tilde{V}$, first noticed in ref. [37]. If we add an arbitrary cyclicly symmetric

function $\tilde{f}$ to $\tilde{V}$, we find that it vanishes in the full ratio function:

$$\begin{aligned} & \frac{1}{2}\Big[[(1)-(4)]\tilde{f}(u,v,w) - [(2)-(5)]\tilde{f}(u,v,w) + [(3)-(6)]\tilde{f}(u,v,w)\Big] \\ = \; & \frac{1}{2}\Big[[(1)+(3)+(5)] - [(2)+(4)+(6)]\Big]\; \tilde{f}(u,v,w) \\ = \; & 0, \end{aligned} \tag{1.43}$$

and thus remains unfixed by any physically meaningful limits.

This "gauge freedom" was used in ref. [37] to set the sum of the cyclic permutations of $\tilde{V}$ to zero, essentially as an arbitrary choice of gauge. We make the same choice here. However, when presenting numerical results we usually present "gauge invariant" quantities: Instead of $\tilde{V}$, we use the difference of two cyclic permutations, such as $\tilde{V}(v,w,u) - \tilde{V}(w,u,v)$. Any cyclicly-symmetric contribution vanishes in such linear combinations, while the physical information is still preserved. Whenever $\tilde{V}$ appears in physical limits, it does so in these linear combinations.

1.3 $\bar{Q}$ Equation

In refs. [63, 64], an equation was presented describing the action of the dual superconformal generator $\bar{Q}$ on a generic amplitude. In terms of the dual Grassmann variables χ_i and momentum twistors Z_i, the dual superconformal generator for an n-point amplitude is a first-order differential operator,

$$\bar{Q}^A_a \;=\; (S^A_\alpha, \bar{Q}^A_{\dot{\alpha}}) \;=\; \sum_{i=1}^{n} \chi_i^A \frac{\partial}{\partial Z_i^a}\,. \tag{1.44}$$

The reason it does not annihilate the amplitude is because of a collinear anomaly, and so its action on an L-loop N^{k}MHV amplitude can be expressed in terms of the integral over an $(L-1)$-loop N^{k+1}MHV amplitude with one more external leg. For the NMHV six-point amplitude we need the N^{2}MHV seven-point amplitude, but by parity this amplitude is equivalent to the NMHV amplitude. The $\bar{Q}$ equation for the

NMHV six-point amplitude takes the form [63, 64],

$$\bar{Q}\mathcal{R}_{6,1} \;=\; \frac{\gamma_K}{8}\int d^{2|3}\mathcal{Z}_7\Big[\mathcal{R}_{7,2} - \mathcal{R}_{6,1}\mathcal{R}^{\rm tree}_{7,1}\Big] \;+\; \text{cyclic}, \tag{1.45}$$

where

$$\mathcal{R}_{6,1} \;=\; \frac{\mathcal{A}_{\rm NMHV}}{\mathcal{A}_6^{\rm BDS}}\,. \tag{1.46}$$

Similarly, $\mathcal{R}_{7,2}$ is the BDS-normalized N^{2}MHV 7-point amplitude, and $\mathcal{R}^{\rm tree}_{7,1}$ is the ratio of NMHV to MHV 7-point tree super-amplitudes. The integration is over a super-momentum-twistor $\mathcal{Z}_7$ along a collinear limit corresponding to one edge of the hexagon. The "+ cyclic" terms correspond to the other edges.

An analysis of the leading singularities of $\mathcal{R}_{7,2}$ [98] shows that there are only four linearly independent residues from the edge shown,

$$(1)\,\bar{Q}\ln\frac{\langle 5612\rangle}{\langle 5614\rangle}\,,\qquad (2)\,\bar{Q}\ln\frac{\langle 5612\rangle}{\langle 5614\rangle}\,,\qquad (4)\,\bar{Q}\ln\frac{\langle 5612\rangle}{\langle 5614\rangle}\,,\qquad (5)\,\bar{Q}\ln\frac{\langle 5612\rangle}{\langle 5614\rangle}\,, \tag{1.47}$$

where $(1),(2),(4),(5)$ are the R-invariants (f) defined in eq. (1.7). However, integration of the seven-point tree amplitude in the second, collinear subtraction term in eq. (1.45) would seem to give more possible residues. Using eq. (3.7) of ref. [64], one finds a term [98]

$$\int d^{2|3}\mathcal{Z}_7\mathcal{R}^{\rm tree}_{7,1} \;=\; \ln\frac{\langle 6134\rangle\langle 6523\rangle}{\langle 6123\rangle\langle 6534\rangle}\,\bar{Q}\ln\frac{\langle 5612\rangle}{\langle 5613\rangle}\,. \tag{1.48}$$

The unwanted $\langle 5613\rangle$ term can be removed by considering the action of $\bar{Q}$ on $\hat{\mathcal{R}}_{6,1}$ rather than $\mathcal{R}_{6,1}$, where

$$\hat{\mathcal{R}}_{6,1} \;=\; \frac{\mathcal{A}_{\rm NMHV}}{\mathcal{A}_6^{\rm BDS-like}} \;=\; \mathcal{R}_{6,1}\times\exp\left[-\frac{\gamma_K}{8}Y(u,v,w)\right]. \tag{1.49}$$

Here $\hat{\mathcal{R}}_{6,1}$ is the quantity expanded in terms of E and $\tilde{E}$ in eq. (1.25). The extra factor of $\exp[-\frac{\gamma_K}{8}Y]$ in $\hat{\mathcal{R}}_{6,1}$ leads to an additional contribution from the action of $\bar{Q}$ on Y.

Note from eq. (3.89) that

$$\partial_u Y \;=\; \frac{\ln u}{u(1-u)} \;=\; \ln u\;\partial_u \ln\!\left(\frac{u}{1-u}\right). \tag{1.50}$$

Using the cyclic symmetry of Y and rewriting u, v, w in terms of momentum-twistors, we have for $\bar{Q}Y$ (as for any first-order differential operator acting on Y),

$$\bar{Q}\,Y \;=\; \ln\frac{\langle 3456\rangle\langle 6123\rangle}{\langle 6134\rangle\langle 5623\rangle}\;\bar{Q}\ln\frac{\langle 6123\rangle\langle 3456\rangle}{\langle 5613\rangle\langle 2346\rangle} \;+(2\text{ cyclic})\,. \tag{1.51}$$

From this form, it is apparent that in $\bar{Q}\hat{\mathcal{R}}_{6,1}$ the $\bar{Q}\ln\langle 5613\rangle$ term cancels between the $\bar{Q}Y$ contribution and eq. (1.48).

As a result, the residues in $\bar{Q}\hat{\mathcal{R}}_{6,1}$ are given by eq. (1.47) plus cyclic permutations. Taking into account the identity [64]

$$(6)\;\bar{Q}\ln\frac{\langle 1234\rangle}{\langle 1235\rangle} \;=\; 0, \tag{1.52}$$

and all of its permutations, and completing the momentum twistors into the projectively invariant variables in $\mathcal{S}_u$ in eq. (1.29), one finds that eq. (1.47) is equivalent to the following set of final entries [98]:

$$\begin{gathered}(1)\,d\ln(uw/v)\,,\\ (1)\,d\ln\!\left(\frac{(1-w)u}{y_v\,w(1-u)}\right),\\ \Big[(2)+(5)+(3)+(6)\Big]d\ln\!\left(\frac{v}{1-v}\right)+(1)\,d\ln\!\left(\frac{w}{y_u\,(1-w)}\right)+(4)\,d\ln\!\left(\frac{u}{y_w\,(1-u)}\right),\end{gathered} \tag{1.53}$$

plus cyclic rotations, for a total of $3\times 6 = 18$ linear combinations. This number should be compared with a naive count of $6\times 9 = 54$ possible R-invariants times final entries, or $5\times 9 = 45$ independent functions if we take into account the tree identity (1.8).

Next we impose the $\bar{Q}$ relations (1.53) as constraints on the $\{n-1,1\}$ coproducts of the functions E and $\tilde{E}$ defined by eq. (1.25). We do this in the cyclic-vanishing

gauge for $\tilde{E}$:

$$\tilde{E}(u,v,w) + \tilde{E}(v,w,u) + \tilde{E}(w,u,v) \;=\; 0. \tag{1.54}$$

We can rewrite the derivatives of this condition in terms of the $\{n-1,1\}$ coproducts of $\tilde{E}$:

$$\begin{aligned}
\tilde{E}^u(u,v,w) + \tilde{E}^u(v,w,u) + \tilde{E}^u(w,u,v) &= 0, &(1.55)\\
\tilde{E}^{1-u}(u,v,w) + \tilde{E}^{1-u}(v,w,u) + \tilde{E}^{1-u}(w,u,v) &= 0, &(1.56)\\
\tilde{E}^{y_u}(u,v,w) + \tilde{E}^{y_u}(v,w,u) + \tilde{E}^{y_u}(w,u,v) &= 0, &(1.57)
\end{aligned}$$

as well as the cyclic images of these equations.

Then the $\bar{Q}$ relations that involve parity-even functions (except the first, which we group here for convenience) are

$$\begin{aligned}
E^{y_u}(u,v,w) &= E^{y_w}(u,v,w), &(1.58)\\
E^{1-v}(u,v,w) &= 0, &(1.59)\\
E^{1-u}(u,v,w) &= -E^u(u,v,w) - E^v(u,v,w), &(1.60)\\
E^{1-u}(u,v,w) + E^{1-w}(u,v,w) &= E^{1-v}(v,w,u) + E^{1-u}(v,w,u), &(1.61)\\
3\,[\tilde{E}^{y_u}(u,v,w) - \tilde{E}^{y_v}(u,v,w)] &= 2\,E^{1-w}(u,v,w) - E^{1-w}(w,u,v), &(1.62)
\end{aligned}$$

while the remaining ones, which involve parity-odd functions, are

$$\begin{aligned}
3\,[\tilde{E}^u(w,u,v) + \tilde{E}^{1-u}(w,u,v)] &= \tilde{E}^v(u,v,w) + \tilde{E}^w(v,w,u)\\
&\quad - \tilde{E}^v(w,u,v) - \tilde{E}^w(w,u,v), &(1.63)\\
3\,\tilde{E}^{1-u}(u,v,w) &= \tilde{E}^v(u,v,w) + \tilde{E}^w(u,v,w) - \tilde{E}^v(v,w,u)\\
&\quad - \tilde{E}^w(v,w,u) - E^{y_u}(u,v,w) + E^{y_v}(u,v,w), &(1.64)\\
2\,[E^{y_u}(u,v,w) - E^{y_v}(u,v,w)] &= 3\,[\tilde{E}^w(v,w,u) - \tilde{E}^u(w,u,v)]\\
&\quad + \tilde{E}^v(v,w,u) - \tilde{E}^v(w,u,v). &(1.65)
\end{aligned}$$

All permutations of these equations are implied. The first three of the above equations do not mix different permutations of E. They are equivalent to the five-final-entry conditions found for $U = \ln E$ [37]. These relations are also manifest from the form (1.53).

We have used the symmetry relations (1.39) in writing these equations. Using this symmetry, the arguments of E and $\tilde{E}$ can be restricted to (u, v, w), (v, w, u), (w, u, v). At the outset there are nine final entries, for a total of $2 \times 3 \times 9 = 54$ independent functions (not counting how they are related to each other by permutations). Altogether there are 18 independent even relations and 18 odd relations (including the cyclic vanishing conditions) which leads to 9 linearly independent even functions and 9 odd ones. This agrees with the 18 linear combinations of final entries described in eq. (1.53).

In practice, we use the $\bar{Q}$ relations to write all of the other $\{n-1, 1\}$ coproducts in terms of just six functions: $E^u(u, v, w)$, $E^v(u, v, w)$ (symmetric in $(u \leftrightarrow w)$), $E^{y_v}(u, v, w)$ (symmetric in $(u \leftrightarrow w)$), $\tilde{E}^u(u, v, w)$, $\tilde{E}^v(u, v, w)$ (antisymmetric in $(u \leftrightarrow w)$), and $\tilde{E}^{y_v}(u, v, w)$ (antisymmetric in $(u \leftrightarrow w)$). For these six functions, we insert the most general linear combination of weight $(2L-1)$ hexagon functions with the right symmetry. Then we use the $\bar{Q}$ relations to generate the rest of the $\{n-1, 1\}$ coproducts of E and $\tilde{E}$, and also as further constraints on the ansatz. At the same time, we impose the functional integrability constraints (1.35), as well as the branch-cut conditions (1.37) and (1.38). Solving all these equations simultaneously leads to the remaining number of parameters in the line labelled "$\bar{Q}$ equation" in table 1.1.

We never need to construct the full space of weight $2L$ functions directly. The number of initial parameters is dictated by the number of weight $(2L-1)$ functions. At four loops, there are 1,801 parity-even weight 7 functions, and 474 parity-odd weight 7 functions. We start with 4,550 unknown parameters, from E^u (1,801), E^v (996), E^{y_v} (272), $\tilde{E}^u$ (474), $\tilde{E}^v$ (202) and $\tilde{E}^{y_v}$ (805). This is just twice the total number of weight 7 functions. One implementation of the combined equations gives 28,569 equations for the 4,550 parameters — obviously with a great deal of redundancy. This linear system can be solved by MAPLE in under an hour on a single processor, in terms of just 30 remaining parameters. (There are four more parameters, corresponding to

Constraint	$L=1$	$L=2$		$L=3$		$L=4$	
	even	even	odd	even	odd	even	odd
0. Integrable functions	10	82	6	639	122	5153	1763
1. (Anti)symmetry in u and w	7	50	2	363	49	2797	786
2. Cyclic vanishing of $\tilde{V}$	7	50	2	363	39	2797	583
3. $\bar{Q}$ equation	2	5		12		34	
4. Collinear vanishing	0	0		1		5	
5. Spurious-pole vanishing	0	0		1		5	
6. LL multi-Regge kinematics	0	0		0		1	
7. NLL multi-Regge kinematics	0	0		0		0	

Table 1.1: Remaining parameters in the ansätze for $V^{(L)}$ and $\tilde{V}^{(L)}$ after each constraint is applied, at each loop order. Here we use the full $\bar{Q}$ equation, which together with symmetry and functional integrability fixes almost all of the parameters at the outset.

the weight 8 constants ζ_8, $\zeta_3\zeta_5$, $\zeta_2(\zeta_3)^2$ and $\zeta_{5,3}$. These parameters are invisible at the level of the $\{7,1\}$ coproducts, but they are fixed in the next step by the collinear vanishing condition.)

The collinear vanishing condition (1.40) is simple to implement and it fixes all of the remaining parameters at one and two loops. At three and four loops it leaves only one and five parameters, respectively.

It might seem counterintuitive at first sight that the combination of the $\bar{Q}$ and collinear constraints could fix all of the parameters through two loops, because each constraint appears to be homogeneous, i.e. the right-hand side of the constraint is zero. A homogeneous constraint should always allow for at least one free parameter, from rescaling any solution by an overall multiplicative constant. The catch, of course, is that the $\bar{Q}$ constraint is on E and $\tilde{E}$, while the collinear constraint is on V and $\tilde{V}$, and these are related to each other inhomogeneously, by a known additive function

at a given loop order. In other words, in terms of E and $\tilde{E}$, the collinear vanishing constraint is inhomogeneous.

Next we examine the spurious-pole condition (1.41). It depends on two variables, u and v. We impose it by making use of the function space described in appendix D, for which we have a basis through weight seven. At four loops, in order to use the weight-seven basis, we first take the derivative of eq. (1.41) with respect to u, using eq. (D.3) to write it in terms of the $\{7,1\}$ coproduct components. (The condition is antisymmetric in $(u \leftrightarrow v)$, so it is sufficient to inspect the u derivative.) However, we find that the full $\bar{Q}$ relations seem to almost completely subsume the spurious-pole condition. That is, when we impose the spurious-pole condition after the collinear vanishing condition, *no* additional parameters are fixed by it, at least through four loops.

In order to see how much the $\bar{Q}$ relations cover the spurious-pole condition, we also tried imposing this condition *before* the collinear vanishing condition. In this case, a few parameters can be fixed, exclusively those that multiply very simple functions in the parity-even part E, of the form

$$c \ln^k(uw/v) \tag{1.66}$$

for odd values of k. Here c is a weight-$(2L-k)$ zeta-value that gives the correct total weight to the function (1.66), namely $2L$ at L loops. It is easy to see that functions of the form (1.66) cannot be fixed by $\bar{Q}$ for either even or odd k. The only $\bar{Q}$ relation to which these functions contribute at all is eq. (1.60), and they cancel trivially between the two terms on the right-hand side, E^u and E^v. For even values of k, the functions (1.66) are still unfixed by the $\bar{Q}$ relations, but they drop out of the spurious-pole condition (1.41), simply because $\ln^k(uw/v) - \ln^k(vw/u) \to 0$ as $w \to 1$.

At three and four loops, we need to impose constraints from the multi-Regge limit to fix the final few parameters. That is the subject of the next section.

Before we appreciated the full power of the $\bar{Q}$ relations, we carried out a similar analysis, but only imposing the five final-entry condition on U and a seven final-entry condition on $\tilde{V}$. In order to impose the latter condition at four loops, we needed

to leave the cyclic-vanishing gauge for $\tilde{V}$. This introduced a number of unphysical, gauge parameters. In table 1.2 we tabulate the remaining parameters at different loop orders under these conditions. It is remarkable how much more power there is in the full $\bar{Q}$ relations, namely the ones that relate $\{n-1,1\}$ coproducts of E and $\tilde{E}$ with different permutations. Whereas in table 1.1 there are only 34 parameters left after imposing the $\bar{Q}$ constraint, at the same level in table 1.2, after imposing the 7 final-entry condition on $\tilde{V}$ there are still $487+321=808$ physical parameters!

It is clear that this kind of massive parameter reduction at the outset will make it much more feasible to go to higher loops. It also drastically reduces the amount of boundary data required. In table 1.2 we see that at four loops we needed to use the NNLL multi-Regge information. (Information at this accuracy is available [35, 37] without relying on integrability-based predictions [62].) We also needed to use the $\mathcal{O}(T^1)$ terms in the OPE limit to fix the final two parameters. In contrast, in table 1.1 all parameters are fixed without any use of the OPE limit, and only the NLL approximation for multi-Regge-kinematics.

1.4 Multi-Regge kinematics

In order to fix the last few parameters at four loops, we analyze the limit of multi-Regge kinematics (MRK) for the NMHV amplitude, following closely ref. [37]. The multi-Regge limit in this context refers to $2\to 4$ scattering, with the four outgoing particles strongly ordered in rapidity. In particular, it involves the all-gluon amplitude, with helicities

$$3^+6^+ \to 2^+4^-5^+1^+\,, \tag{1.67}$$

where the cross ratios become

$$u_1\to 1\,,\qquad u_2,u_3\to 0\,, \tag{1.68}$$

with the ratios

$$\frac{u_2}{1-u_1}\equiv\frac{1}{(1+w)\,(1+w^*)}\quad\text{and}\quad\frac{u_3}{1-u_1}\equiv\frac{ww^*}{(1+w)\,(1+w^*)} \tag{1.69}$$

Constraint	$L=1$	$L=2$		$L=3$		$L=4$	
	even	even	odd	even	odd	even	odd
0. Integrable functions	10	82	6	639	122	5153	1763
1. (Anti)symmetry in u and w	7	50	2	363	$39+10$	2797	$583+203$
2. 5 even final-entry conditions	3	14	2	78	$39+10$	487	$583+203$
3. 7 odd final-entry conditions	3	14	1	78	$21+3$	487	$321+64$
4. Collinear vanishing	0	2	1	28	$21+3$	284	$321+64$
5. $\mathcal{O}(T^1)$ 6134 OPE	0	0	1	0	$21+3$	110	$321+64$
6. NNLL multi-Regge kinematics	0	0	0	0	$3+3$	0	$219+64$
7. Spurious-pole vanishing	0	0		$0+3$		$2+64$	
8. $\mathcal{O}(T^1)$ 1111 OPE	0	0		$0+3$		$0+64$	
9. $\mathcal{O}(T^{1,2})$ 1114 OPE	0	0		$0+3$		$0+64$	

Table 1.2: Remaining parameters in the ansätze for $V^{(L)}$ and $\tilde{V}^{(L)}$ after each constraint is applied, at each loop order. In this version we do not use the full $\bar{Q}$ equation, but only the 5 (7) final-entry condition in the parity even (odd) sector. The first six constraints do not mix the parity-even and parity-odd function spaces, so we can count the number of even and odd parameters separately until we reach the spurious-pole constraint. The 7 final-entry condition can only be satisfied if we abandon the cyclic-vanishing condition, which leaves some unphysical "gauge" parameters. We split the number of odd parameters into "physical + gauge"; only the former number is relevant.

held fixed. Here we use (u_1, u_2, u_3) instead of (u, v, w) for the cross ratios, to avoid confusion with the traditional MRK variable w.

In ref. [37] two of us extended the NMHV leading-logarithmic MRK ansatz of Lipatov, Prygarin, and Schnitzer [61] along the lines of the MHV MRK factorization

described by Fadin and Lipatov [60]. We proposed the following ansatz:

$$\begin{aligned}\mathcal{P}_{\text{NMHV}} \times e^{R_6+i\pi\delta}|_{\text{MRK}} = \; & \cos\pi\omega_{ab} \\ & -i\frac{a}{2}\sum_{n=-\infty}^{\infty}(-1)^n\left(\frac{w}{w^*}\right)^{\frac{n}{2}}\int_{-\infty}^{+\infty}\frac{d\nu}{(i\nu+\frac{n}{2})^2}|w|^{2i\nu}\,\Phi_{\text{Reg}}^{\text{NMHV}}(\nu,n) \\ & \qquad\times\left(-\frac{1}{1-u_1}\frac{|1+w|^2}{|w|}\right)^{\omega(\nu,n)},\end{aligned} \tag{1.70}$$

where

$$\begin{aligned}\omega_{ab} &= \frac{1}{8}\,\gamma_K(a)\,\log|w|^2\,, \\ \delta &= \frac{1}{8}\,\gamma_K(a)\,\log\frac{|w|^2}{|1+w|^4}\,,\end{aligned} \tag{1.71}$$

and $\gamma_K(a)$ is the cusp anomalous dimension, given in eq. (1.19). Here $\omega(\nu,n)$ is known as the BFKL eigenvalue, and is the same for MHV and NMHV, while $\Phi_{\text{Reg}}^{\text{NMHV}}(\nu,n)$ is the NMHV impact factor. Both may be expanded perturbatively in a:

$$\begin{aligned}\omega(\nu,n) &= -a\left(E_{\nu,n}+a\,E_{\nu,n}^{(1)}+a^2\,E_{\nu,n}^{(2)}+\mathcal{O}(a^3)\right)\,, \\ \Phi_{\text{Reg}}^{\text{NMHV}}(\nu,n) &= 1+a\,\Phi_{\text{Reg}}^{\text{NMHV},(1)}(\nu,n)+a^2\,\Phi_{\text{Reg}}^{\text{NMHV},(2)}(\nu,n) \\ &\qquad +a^3\,\Phi_{\text{Reg}}^{\text{NMHV},(3)}(\nu,n)+\mathcal{O}(a^4)\,.\end{aligned} \tag{1.72}$$

By expanding eq. (1.70) in a and performing the summation and integration, we are left with functions of w and w^* that we can compare to the MRK limit of the ratio function.

The configuration (1.67) corresponds to the $(\chi_4)^4$ component of the ratio function. Taking the MRK limit of this component, the R-invariants reduce to functions of w^*:

$$(1)\to\frac{1}{1+w^*}\,,\qquad (5)\to\frac{w^*}{1+w^*}\,,\qquad (6)\to 1, \tag{1.73}$$

while the other R-invariants vanish.

Parity symmetry of the ratio function leads, in this limit, to a symmetry under $(w,w^*)\to(1/w,1/w^*)$. Taking advantage of this symmetry, we break up the ratio

function as follows:

$$\begin{aligned}\mathcal{P}^{(L)}_{\rm MRK} &= 2\pi i \sum_{r=0}^{L-1} \ln^r(1-u_1)\Bigg\{ \frac{1}{1+w^*}\Big[p_r^{(L)}(w,w^*) + 2\pi i\, q_r^{(L)}(w,w^*)\Big] \\ &\qquad + \frac{w^*}{1+w^*}\Big[p_r^{(L)}(w,w^*) + 2\pi i\, q_r^{(L)}(w,w^*)\Big]\Big|_{(w,w^*)\to(1/w,1/w^*)}\Bigg\} \\ &\quad + \mathcal{O}(1-u_1)\,. \end{aligned} \tag{1.74}$$

Here the $p_r^{(L)}(w,w^*)$ and $q_r^{(L)}(w,w^*)$ are composed of functions known as single-valued harmonic polylogarithms (SVHPLs) [117, 105]. In general, $p_r^{(L)}$ and $q_{r-1}^{(L)}$ are closely related to each other. They are determined by the BFKL eigenvalue and impact factor evaluated to the same subleading order in a. Essentially, $q_{r-1}^{(L)}$ is generated by taking the log of (-1) out of the last factor of eq. (1.70) instead of a $\ln(1-u_1)$. For this reason, $q_{L-1}^{(L)}$ vanishes, and we will refer to both $p_{L-1}^{(L)}$ and $q_{L-2}^{(L)}$ as leading-log (LL), $p_{L-2}^{(L)}$ and $q_{L-3}^{(L)}$ as next-to-leading-log (NLL), and so on.

The relations between $p_r^{(L)}$ and $q_{r-1}^{(L)}$ that we quote below involve the coefficients appearing in the MRK expansion of the remainder function,

$$[R_6]^{(L)}_{\rm MRK} = 2\pi i \sum_{r=0}^{L-1} \ln^r(1-u_1)\Big[g_r^{(L)}(w,w^*) + 2\pi i\, h_r^{(L)}(w,w^*)\Big]\,, \tag{1.75}$$

which can be found through four loops in refs. [105, 35]. They also involve the lower-loop $p_r^{(L)}$ functions, given in ref. [37].

After imposing collinear vanishing, we fix the five remaining parameters in our four-loop ansatz by matching to the functions $p_r^{(4)}$ and $q_r^{(4)}$. Four of the five parameters are fixed merely by matching to the LL expressions $p_3^{(4)}$ and $q_2^{(4)}$. We remark that when we perform the same analysis at three loops, there is a single undetermined parameter at this stage, which is fixed by the LL coefficient $p_2^{(3)}$.

At four loops, the one parameter remaining after LL matching is fixed by matching to the NLL coefficients $p_2^{(4)}$ and $q_1^{(4)}$. The NLL BFKL eigenvalue and NMHV impact factor needed to compute these functions were already fixed at lower loops. The four-loop coefficient functions through NLL are presented below. We express them in terms of functions $L^{\pm}_{\vec{w}}$ defined in ref. [105], which are combinations of SVHPLs having

definite symmetry properties under complex conjugation ($w \leftrightarrow w^*$) and inversion ($w \leftrightarrow 1/w$, $w^* \leftrightarrow 1/w^*$):

$$q_3^{(4)} = 0\,, \tag{1.76}$$

$$\begin{aligned} p_3^{(4)} = \frac{1}{768}\Big[&-120\,L_4^- + 192\,L_{2,1,1}^- - 4\,(L_0^- - 20\,L_1^+)\,L_3^+ + 96\,L_1^+\,L_{2,1}^- \\ &+ 8\,(L_2^-)^2 + 8\,(L_0^-)^2\,L_2^- - 5\,(L_0^-)^3\,L_1^+ - 10\,(L_0^-)^2\,(L_1^+)^2 \\ &- 8\,L_0^-\,(L_1^+)^3 - 16\,(L_1^+)^4 + 96\,\zeta_3\,L_1^+\Big]\,, \end{aligned} \tag{1.77}$$

$$q_2^{(4)} = \frac{3}{2}\,p_3^{(4)} - \frac{1}{2}L_1^+\,p_2^{(3)} - g_1^{(2)}\,p_1^{(2)} - g_2^{(3)}\,p_0^{(1)}\,, \tag{1.78}$$

$$\begin{aligned} p_2^{(4)} = \frac{1}{64}\Big\{&-87\,L_5^+ + 14\,L_{4,1}^- + 32\,L_{3,1,1}^+ + 8\,L_{2,2,1}^+ - 96\,L_{2,1,1,1}^- \\ &- \frac{1}{2}\,(11\,L_0^- + 46\,L_1^+)\,L_4^- - (L_0^- - 4\,L_1^+)\,L_{3,1}^+ + 12\,L_0^-\,L_{2,1,1}^- \\ &+ \Big[12\,(L_0^-)^2 - 11\,L_0^-\,L_1^+ + 20\,(L_1^+)^2\Big]\,L_3^+ - \frac{12}{5}\,(L_1^+)^5 \\ &+ 2\,\Big[(L_0^-)^2 - 2\,L_0^-\,L_1^+ + 12\,(L_1^+)^2\Big]\,L_{2,1}^- - \frac{13}{240}\,(L_0^-)^5 \\ &+ \Big[\frac{5}{24}\,(L_0^-)^3 + \frac{13}{4}\,(L_0^-)^2\,L_1^+ - L_0^-\,(L_1^+)^2 + 4\,(L_1^+)^3\Big]\,L_2^- \\ &- \frac{11}{8}\,(L_0^-)^4\,L_1^+ + \frac{5}{4}\,(L_0^-)^3\,(L_1^+)^2 - \frac{7}{3}\,(L_0^-)^2\,(L_1^+)^3 - 2\,L_0^-\,(L_1^+)^4 \\ &- \zeta_2\,\Big[48\,L_3^+ + 48\,L_{2,1}^- + 24\,L_1^+\,L_2^- - 3\,(L_0^-)^3 - 6\,(L_0^-)^2\,L_1^+ - 16\,(L_1^+)^3\Big] \\ &+ \zeta_3\,\Big[2\,L_2^- + (L_0^-)^2 + 28\,L_0^-\,L_1^+ + 8\,(L_1^+)^2\Big] - 102\,\zeta_5 - 48\,\zeta_2\,\zeta_3\Big\}, \end{aligned} \tag{1.79}$$

$$q_1^{(4)} = p_2^{(4)} - \frac{1}{2}L_1^+\Big[p_1^{(3)} - \zeta_2\,p_1^{(2)}\Big] - g_1^{(2)}\,p_0^{(2)} - g_0^{(2)}\,p_1^{(2)} - g_1^{(3)}\,p_0^{(1)}\,. \tag{1.80}$$

Once the final five parameters are fixed, we can obtain the NNLL and N^{3}LL coefficients $p_1^{(4)}$, $q_0^{(4)}$ and $p_0^{(4)}$ with no ambiguity. We obtain:

$$\begin{aligned} p_1^{(4)} = \frac{1}{64}\Big\{&96\,L_6^- + 58\,L_{5,1}^+ + 16\,L_{4,2}^+ - 12\,L_{4,1,1}^- - 24\,L_{3,1,1,1}^+ + 240\,L_{2,1,1,1,1}^- \\ &- \frac{1}{2}\,(3\,L_0^- + 450\,L_1^+)\,L_5^+ - (9\,L_0^- - 22\,L_1^+)\,L_{4,1}^- \\ &+ 4\,(L_0^- + 5\,L_1^+)\,L_{3,1,1}^+ + 16\,L_1^+\,L_{2,2,1}^+ - 12\,(L_0^- + 6\,L_1^+)\,L_{2,1,1,1}^- \end{aligned}$$

$$
\begin{aligned}
&- \left[13\,(L_0^-)^2 + 25\,L_0^-\,L_1^+ + 16\,(L_1^+)^2\right] L_4^- \\
&- \left[5\,(L_0^-)^2 - 18\,L_0^-\,L_1^+ - 8\,(L_1^+)^2\right] L_{3,1}^+ \\
&- 4\left[2\,(L_0^-)^2 - 3\,L_0^-\,L_1^+ + 12\,(L_1^+)^2\right] L_{2,1,1}^- \\
&+ \left[\frac{3}{8}\,(L_0^-)^3 + \frac{67}{2}\,(L_0^-)^2\,L_1^+ - 12\,L_0^-\,(L_1^+)^2 + \frac{71}{3}\,(L_1^+)^3\right] L_3^+ \\
&+ \left[2\,(L_0^-)^3 - (L_0^-)^2\,L_1^+ + 5\,L_0^-\,(L_1^+)^2 + 14\,(L_1^+)^3\right] L_{2,1}^- \\
&- 7\,(L_3^+)^2 - 4\,(L_{2,1}^-)^2 + 8\,L_{2,1,1}^-\,L_2^- - \frac{1}{4}\left[(L_0^-)^2 + 12\,(L_1^+)^2\right](L_2^-)^2 \\
&- \Big[4\,L_0^-\,L_3^+ - \frac{13}{8}\,(L_0^-)^4 - \frac{25}{6}\,(L_0^-)^3\,L_1^+ + \frac{1}{2}\,(L_0^-)^2\,(L_1^+)^2 \\
&\qquad\qquad + L_0^-\,(L_1^+)^3 - 8\,(L_1^+)^4\Big] L_2^- \\
&- \frac{37}{720}\,(L_0^-)^6 - \frac{1}{48}\,(L_0^-)^5\,L_1^+ - \frac{97}{24}\,(L_0^-)^4\,(L_1^+)^2 + 2\,(L_0^-)^3\,(L_1^+)^3 \\
&- \frac{13}{3}\,(L_0^-)^2\,(L_1^+)^4 - L_0^-\,(L_1^+)^5 - \frac{22}{15}\,(L_1^+)^6 \\
&+ \zeta_2\Big[180\,L_4^- - 8\,L_{3,1}^+ - 144\,L_{2,1,1}^- - 4\,(L_0^- - 6\,L_1^+)\,L_{2,1}^- - 4\,(L_2^-)^2 \\
&\qquad\qquad - 4\left[8\,(L_0^-)^2 + 3\,L_0^-\,L_1^+ - 12\,(L_1^+)^2\right] L_2^- \\
&\qquad\qquad - 44\,(L_0^- - L_1^+)\,L_3^+ + \frac{1}{6}\,(L_0^-)^4 + 16\,(L_0^-)^3\,L_1^+ \\
&\qquad\qquad - 26\,(L_0^-)^2\,(L_1^+)^2 - 58\,L_0^-\,(L_1^+)^3 + 108\,(L_1^+)^4\Big] \\
&+ \zeta_3\Big[22\,L_3^+ - 4\,L_{2,1}^- + 4\,(6\,L_0^- - L_1^+)\,L_2^- - \frac{5}{3}\,(L_0^-)^3 + 3\,(L_0^-)^2\,L_1^+ \\
&\qquad\qquad + 35\,L_0^-\,(L_1^+)^2 - 10\,(L_1^+)^3\Big] \\
&+ \zeta_4\left[216\,L_2^- + 108\,(L_0^- - 2\,L_1^+)\,L_1^+\right] \\
&- \zeta_5\,(21\,L_0^- + 54\,L_1^+) - 4\,\zeta_2\,\zeta_3\,(3\,L_0^- - 10\,L_1^+)\Big\}, \qquad (1.81)
\end{aligned}
$$

$$
q_0^{(4)} \;=\; \frac{1}{2}\,p_1^{(4)} - \frac{1}{2}L_1^+\left[p_0^{(3)} - \zeta_2\,p_0^{(2)} + \frac{11}{2}\,\zeta_4\,p_0^{(1)}\right] + \pi^2\left[p_3^{(4)} - g_1^{(2)}p_1^{(2)} - 2\,g_2^{(3)}p_0^{(1)}\right]
$$

$$
\begin{aligned}
&- \pi^2\, L_1^+ \left[p_2^{(3)} - 2\, g_1^{(2)} p_0^{(1)}\right] + \frac{\pi^2}{2}\,(L_1^+)^2\, p_1^{(2)} - \zeta_2\,(L_1^+)^3\, p_0^{(1)} \\
&- g_0^{(2)} p_0^{(2)} - g_0^{(3)} p_0^{(1)}\,, \qquad (1.82)
\end{aligned}
$$

and

$$
\begin{aligned}
p_0^{(4)} \;=\; \frac{1}{64}\Big\{ & 1718\, L_7^+ - 96\, L_{6,1}^- - 42\, L_{5,1,1}^+ - 72\, L_{4,2,1}^+ + 12\, L_{4,1,1,1}^- \\
& - 8\, L_{3,1,1,1,1}^+ - 48\, L_{2,2,1,1,1}^+ - 16\, L_{2,1,2,1,1}^+ - 240\, L_{2,1,1,1,1,1}^- \\
& + 2\,(43\, L_0^- + 24\, L_1^+)\, L_6^- + \frac{1}{2}\,(3\, L_0^- + 122\, L_1^+)\, L_{5,1}^+ \\
& + (17\, L_0^- - 6\, L_1^+)\, L_{4,1,1}^- - 4\,(L_0^- + 3\, L_1^+)\, L_{3,1,1,1}^+ \\
& + 12\,(3\, L_0^- + 10\, L_1^+)\, L_{2,1,1,1,1}^- + 16\, L_1^+\, L_{4,2}^+ \\
& - \frac{1}{4}\left[849\,(L_0^-)^2 - 132\, L_0^-\, L_1^+ + 552\,(L_1^+)^2\right] L_5^+ \\
& + \left[13\,(L_0^-)^2 - 19\, L_0^-\, L_1^+ + 8\,(L_1^+)^2\right] L_{4,1}^- \\
& - \left[3\,(L_0^-)^2 + 16\, L_0^-\, L_1^+ + 12\,(L_1^+)^2\right] L_{3,1,1}^+ \\
& + 2\left[3\,(L_0^-)^2 + 4\,(L_1^+)^2\right] L_{2,2,1}^+ - 24\, L_{3,3,1}^+ \\
& + 8\left[(L_0^-)^2 - 4\, L_0^-\, L_1^+ + 3\,(L_1^+)^2\right] L_{2,1,1,1}^- \\
& + 4\, L_0^-\, L_{2,1}^-\, L_3^+ + 2\,(3\, L_0^-\, L_{3,1}^+ + 4\, L_1^+\, L_{2,1,1}^-)\, L_2^- \\
& + \frac{1}{16}\Big[128\, L_{2,1}^- - 163\,(L_0^-)^3 - 118\,(L_0^-)^2\, L_1^+ \\
& \qquad - 332\, L_0^-\,(L_1^+)^2 - 56\,(L_1^+)^3\Big] L_4^- \\
& - \frac{1}{8}\left[3\,(L_0^-)^3 + 52\,(L_0^-)^2\, L_1^+ - 80\, L_0^-\,(L_1^+)^2 - 24\,(L_1^+)^3\right] L_{3,1}^+ \\
& - \frac{1}{6}\left[23\,(L_0^-)^3 + 18\,(L_0^-)^2\, L_1^+ + 18\, L_0^-\,(L_1^+)^2 + 132\,(L_1^+)^3\right] L_{2,1,1}^- \\
& + \frac{1}{48}\Big[1041\,(L_0^-)^4 - 312\,(L_0^-)^3 L_1^+ + 996\,(L_0^-)^2 (L_1^+)^2 \\
& \qquad + 16\, L_0^- (L_1^+)^3 + 496\,(L_1^+)^4\Big] L_3^+ \\
& - \frac{1}{8}\Big[13\,(L_0^-)^4 - 38\,(L_0^-)^3\, L_1^+ - 16\,(L_0^-)^2\,(L_1^+)^2 \\
& \qquad - 80\, L_0^-\,(L_1^+)^3 + 16\,(L_1^+)^4\Big] L_{2,1}^-
\end{aligned}
$$

$$
\begin{aligned}
&- \frac{1}{2}\left[3\,(L_0^-)^2\,L_1^+ + 4\,(L_1^+)^3\right](L_2^-)^2 + \frac{1}{3}\,L_0^-\,(L_1^+)^6 \\
&- \frac{1}{8}\Bigg[64\,L_{4,1}^- + 16\,L_0^-\,L_1^+\,L_3^+ - 8\,(L_0^-)^4\,L_1^+ - \frac{43}{5}\,(L_0^-)^5 \\
&\qquad\qquad - 24\,(L_1^+)^5 - \frac{97}{3}\,(L_0^-)^3\,(L_1^+)^2 + 10\,(L_0^-)^2\,(L_1^+)^3 \\
&\qquad\qquad - 4\,L_0^-\,(L_1^+)^4\Bigg]\,L_2^- + \frac{83}{2016}\,(L_0^-)^7 \\
&- \frac{1691}{720}\,(L_0^-)^6\,L_1^+ + \frac{223}{240}\,(L_0^-)^5\,(L_1^+)^2 - \frac{32}{105}\,(L_1^+)^7 \\
&- \frac{109}{36}\,(L_0^-)^4\,(L_1^+)^3 - \frac{1}{2}\,(L_0^-)^3\,(L_1^+)^4 - \frac{44}{15}\,(L_0^-)^2\,(L_1^+)^5 \\
&+ \zeta_2\Bigg[542\,L_5^+ - 84\,L_{4,1}^- - 72\,L_{3,1,1}^+ - 16\,L_{2,2,1}^+ \\
&\qquad\qquad + (65\,L_0^- + 42\,L_1^+)\,L_4^- + 432\,L_{2,1,1,1}^- \\
&\qquad\qquad + 4\,(2\,L_0^- + 5\,L_1^+)\,L_{3,1}^+ - 4\,(11\,L_0^- + 54\,L_1^+)\,L_{2,1,1}^- \\
&\qquad\qquad - \left[81\,(L_0^-)^2 - 212\,L_0^-\,L_1^+ + 436\,(L_1^+)^2\right]L_3^+ \\
&\qquad\qquad + 4\left[5\,(L_0^-)^2 - 6\,L_0^-\,L_1^+ - 6\,(L_1^+)^2\right]L_{2,1}^- \\
&\qquad\qquad - \Bigg[192\,L_3^+ + \frac{49}{6}\,(L_0^-)^3 - 24\,(L_0^-)^2\,L_1^+ \\
&\qquad\qquad\qquad + 19\,L_0^-\,(L_1^+)^2 - 62\,(L_1^+)^3\Bigg]\,L_2^- \\
&\qquad\qquad + \frac{131}{12}\,(L_0^-)^4\,L_1^+ - 33\,(L_0^-)^3\,(L_1^+)^2 - \frac{43}{40}\,(L_0^-)^5 \\
&\qquad\qquad + \frac{176}{3}\,(L_0^-)^2\,(L_1^+)^3 - 34\,L_0^-\,(L_1^+)^4 + \frac{344}{5}\,(L_1^+)^5\Bigg] \\
&+ \zeta_3\Bigg[4\,L_4^- - 26\,L_{3,1}^+ + 4\,L_{2,1,1}^- - (47\,L_0^- - 70\,L_1^+)\,L_3^+ \\
&\qquad\qquad - \frac{34}{3}\,(L_1^+)^4 + 4\,(2\,L_0^- + L_1^+)\,L_{2,1}^- + 3\,L_0^-\,(L_1^+)^3 \\
&\qquad\qquad + \frac{1}{4}\left[7\,(L_0^-)^2 + 124\,L_1^+\,L_0^- - 12\,(L_1^+)^2\right]L_2^- \\
&\qquad\qquad - \frac{3}{8}\,(L_0^-)^4 + \frac{119}{12}\,(L_0^-)^3\,L_1^+ - \frac{21}{2}\,(L_0^-)^2\,(L_1^+)^2\Bigg] \\
&+ \zeta_4\Big[804\,L_3^+ + 504\,L_{2,1}^- + 14\,(7\,L_0^- - 18\,L_1^+)\,L_2^- - 23\,(L_0^-)^3
\end{aligned}
$$

$$
\begin{aligned}
&\qquad - 130\,(L_0^-)^2\,L_1^+ + 108\,L_0^-\,(L_1^+)^2 - 384\,(L_1^+)^3\Big] \\
&+ \frac{1}{2}\,\zeta_5\Big[16\,L_2^- - 125\,(L_0^-)^2 - 84\,L_0^-\,L_1^+ + 224\,(L_1^+)^2\Big] \\
&+ 4\,\zeta_2\,\zeta_3\Big[L_2^- - 21\,L_0^-\,L_1^+ - 6\,(L_1^+)^2\Big] \\
&- 438\,\zeta_6\,(L_0^- - 2\,L_1^+) - 2\,(\zeta_3)^2\,(13\,L_0^- + 30\,L_1^+) \\
&- 720\,\zeta_7 + 504\,\zeta_3\,\zeta_4 + 396\,\zeta_2\,\zeta_5\Big\}\,. \qquad (1.83)
\end{aligned}
$$

In addition to presenting these functions here in the main text, we also include them, alongside their lower-loop analogues, in computer-readable format in an ancillary file.

These functions are also predicted by the recent all-orders proposal [62] for the BFKL eigenvalue and impact factor. In particular, the NNNLL NMHV impact factor $\Phi_{\rm Reg}^{\rm NMHV,(3)}(\nu,n)$ enters the computation of $p_0^{(4)}$. It can be extracted from the MHV impact factor (computed through NNNLL in ref. [35]) and the relation [62]

$$
\Phi_{\rm Reg}^{\rm NMHV}(\nu,n) = \Phi_{\rm Reg}^{\rm MHV}(\nu,n) \times \frac{\nu - \frac{in}{2}}{\nu + \frac{in}{2}}\,\frac{x(u+\frac{in}{2})}{x(u-\frac{in}{2})}\,, \qquad (1.84)
$$

where

$$
x(u) = \frac{1}{2}\Big[u + \sqrt{u^2 - 2a}\Big] \qquad (1.85)
$$

is the Zhukovsky variable. The rapidity u entering this formula is related to the variable ν by an integral expression [62]; its expansion to the relevant order in our notation is

$$
\begin{aligned}
u \;=\; & \nu - \frac{i}{2}\,a\,V + \frac{i}{8}\,a^2\,V\,(N^2 + 4\,\zeta_2) \\
& - \frac{i}{32}\,a^3\Big\{V\,\Big[3\,N^2\,V^2 + \frac{5}{4}\,N^4 - 2\,\zeta_2\,(4\,V^2 - N^2) + 88\,\zeta_4\Big] \\
& \qquad - 8\,\zeta_3\,\Big[-i\partial_\nu E_{\nu,n}\Big]\Big\} + \mathcal{O}(a^4), \qquad (1.86)
\end{aligned}
$$

where $V = i\nu/(\nu^2 + n^2/4)$, $N = n/(\nu^2 + n^2/4)$, and $E_{\nu,n}$ is the LL BFKL eigenvalue,

$$E_{\nu,n} = \psi\left(1 + i\nu + \frac{|n|}{2}\right) + \psi\left(1 - i\nu + \frac{|n|}{2}\right) - 2\psi(1) - \frac{N}{2}\,. \tag{1.87}$$

Expanding eq. (1.84) to $\mathcal{O}(a^3)$, we see that the relation between the NMHV and MHV impact factors becomes non-rational in ν and n at NNNLL, due to the ψ function appearing in eq. (1.86) for u, via eq. (1.87).

When we compute $p_1^{(4)}$, $q_0^{(4)}$ and $p_0^{(4)}$ from the master formula (1.70), using eq. (1.84) for $\Phi_{\text{Reg}}^{\text{NMHV}}$, we find precise agreement with the above values extracted from our unique solution. Given the complexity of eqs. (1.81), (1.82) and (1.83), this is already a rather stringent cross-check.

1.5 Near-collinear limit

By examining the near-collinear limit of the ratio function, we can make contact with the Pentagon OPE approach of Basso, Sever, and Vieira, allowing for a rich array of further cross-checks. The duality between amplitudes and Wilson loops relates NMHV amplitudes to Wilson loops with states inserted on the boundary, with different choices of states corresponding to different NMHV components [118, 119]. Through four loops, we have compared our limits with BSV's calculation of the $\chi_6\chi_1\chi_3\chi_4$ and $(\chi_1)^4$ components of the super-Wilson loop [49], as well as Belitsky's computation of the $\chi_1^3\chi_4$ component [54] and $\chi_1^2\chi_4^2$ component [53, 116].

To approach the $w \to 0$ collinear limit, we convert from the cross ratios (u, v, w)

to the variables $(F, S, T) \equiv (e^{i\phi}, e^{\sigma}, e^{-\tau})$ used by BSV in ref. [48]:

$$\begin{aligned} u &= \frac{F}{F + FS^2 + ST + F^2ST + FT^2}\,, \\ v &= \frac{FS^2}{(1+T^2)(F + FS^2 + ST + F^2ST + FT^2)}\,, \\ w &= \frac{T^2}{1+T^2}\,, \\ y_u &= \frac{F + ST + FT^2}{F(1 + FST + T^2)}\,, \\ y_v &= \frac{FS + T}{F(S + FT)}\,, \\ y_w &= \frac{(S + FT)(1 + FST + T^2)}{(FS + T)(F + ST + FT^2)}\,. \end{aligned} \tag{1.88}$$

In these variables, the collinear limit corresponds to $\tau \to \infty$, or $T \to 0$.

BSV investigate the $(\chi_1)^4$ component of the NMHV amplitude by inserting a gluonic state on the bottom cusp of the Wilson loop. Up to first order in T, the R-invariants in this component become

$$\begin{aligned} &(1) \to 0, \quad (2) \to \frac{FT}{S(1+S^2)} + \mathcal{O}\left(T^2\right), \quad (3) \to 1 - FST + \mathcal{O}\left(T^2\right), \\ &(4) \to 1 - \frac{FT}{S} + \mathcal{O}\left(T^2\right), \quad (5) \to \frac{FS^3T}{1+S^2} + \mathcal{O}\left(T^2\right), \quad (6) \to 0 + \mathcal{O}(T^4)\,. \end{aligned} \tag{1.89}$$

As in ref. [37], we find that the ratio function in this limit can be expressed as:

$$\begin{aligned} \mathcal{P}^{(1111)} \;=\; \frac{1}{2}\Bigg\{ & V(u,v,w) + V(w,u,v) - \tilde{V}(u,v,w) + \tilde{V}(w,u,v) \\ & + FT\left[-\frac{1-S^2}{S}V(u,v,w) + \frac{1+S^4}{S(1+S^2)}V(v,w,u)\right]\Bigg\} \;+\; \mathcal{O}(T^2)\,. \end{aligned} \tag{1.90}$$

We match this expression to BSV's computation of the OPE in this channel [49]. At order T^1 only a single flux-tube excitation contributes; its contribution includes an integration over the excitation's rapidity u and also involves its anomalous dimension (or energy) $\gamma(u)$, its momentum $p(u)$, a measure factor $\mu(u)$, and the NMHV dressing

functions h and $\bar{h}$. Of these, h and $\bar{h}$ can be given in closed form as

$$h(u) = \frac{2x^+(u)x^-(u)}{a}\,, \qquad \bar{h}(u) = \frac{1}{h(u)}\,, \tag{1.91}$$

where

$$x^{\pm}(u) = x(u \pm \tfrac{i}{2}) \tag{1.92}$$

is given in terms of the Zhukovsky variable defined in eq. (1.85), while $\gamma(u)$, $p(u)$, and $\mu(u)$ have perturbative expansions described in refs. [120, 48].

All together, the contribution of one gluonic excitation to the OPE is then

$$\begin{aligned}\mathcal{P}^{(1111)} = 1 &+ TF \int_{-\infty}^{\infty} \frac{du}{2\pi}\mu(u)(h(u)-1)e^{ip(u)\sigma-\gamma(u)\tau} \\ &+ \frac{T}{F}\int_{-\infty}^{\infty}\frac{du}{2\pi}\mu(u)(\bar{h}(u)-1)e^{ip(u)\sigma-\gamma(u)\tau}\,.\end{aligned} \tag{1.93}$$

Following ref. [37], we compute this integral as a sum of residues at $u = -im/2$ for positive integers m. Truncating the series in m to a few hundred terms, we obtain an expansion in terms of $S = e^{\sigma}$, which we can then match to the expansion of an ansatz of HPLs in S^2. (Other methods for performing these sums are described in ref. [121, 122].) This expression in terms of HPLs can be compared with the $\mathcal{O}(T)$ expansion of the ratio function. The expansion of the transcendental functions V and $\tilde{V}$ is computed, as in ref. [37], from the differential equations method [34].

The $\chi_6\chi_1\chi_3\chi_4$ component has a simpler OPE at order T^1. All of the R-invariants vanish except for (2) and (5), which collapse to

$$(2) \;=\; (5) \;=\; \frac{1}{\langle 6134\rangle} \;=\; \frac{e^{-\tau}}{2\cosh\sigma}\,. \tag{1.94}$$

Thus only the term multiplying $V(v,w,u)$ survives. This means that through

$\mathcal{O}(T)$ this component is remarkably simple, and is given by the following expression:

$$\begin{aligned}\mathcal{W}^{(6134)} &= \frac{e^{-\tau}}{2\cosh\sigma}\sum_{L=0}^{\infty}\left(\frac{a}{2}\right)^L\sum_{n=0}^{L}\tau^n F_n^{(L)}(\sigma) + \mathcal{O}(e^{-2\tau}) \\ &= \frac{T}{2\cosh\sigma}\times V(v,w,u)|_{\mathcal{O}(T^0)} + \mathcal{O}(T^2)\,,\end{aligned} \tag{1.95}$$

where the $F_n^{(L)}$ are given explicitly through three loops in appendix F of ref. [49] and through six loops in ref. [121, 122].

To check the $\mathcal{O}(T^2)$ terms in the OPE, which receive contributions from two flux-tube excitations, we were assisted by Andrei Belitsky, who checked the $\chi_1^3\chi_4$ component in this limit using our expansions of the V and $\tilde{V}$ functions [54]. For this component, R-invariants (1) and (4) vanish, while the behavior of the remaining components was detailed in ref. [54]. In our variables, they behave as follows through $\mathcal{O}(T^2)$:

$$\begin{aligned}(2)+(5) &= T\,\frac{1-S^2}{1+S^2}F^{1/2} - T^2\left(\frac{S-2S^3-S^5}{(1+S^2)^2}F^{3/2} + \frac{2S+4S^3}{(1+S^2)^2}F^{-1/2}\right) + \mathcal{O}(T^3)\,, \\ (3)+(6) &= (2)-(5) = (3)-(6) = TF^{1/2} - T^2SF^{3/2} + \mathcal{O}(T^3)\,.\end{aligned} \tag{1.96}$$

Belitsky has also checked the $\chi_1^2\chi_4^2$ component at $\mathcal{O}(T^2)$ through four loops [53, 116].

While the relevant expansions of V and $\tilde{V}$ in the near-collinear limit are too lengthy to include in the text, in an ancillary file we include expressions for V and $\tilde{V}$, as well as their cyclic permutations, expanded through $\mathcal{O}(T^3)$.

1.6 Multi-particle factorization

In the limit that a three-particle momentum invariant goes on shell, the six-particle amplitude factorizes into a product of two four-particle amplitudes. For MHV amplitudes in supersymmetric theories this factorization is trivial, since at least one of the two resulting four-particle amplitudes is not MHV and thus the product vanishes. In the case of NMHV amplitudes, though, this factorization is nontrivial in

some channels. For the limit $K^2 = s_{345} \to 0$, where $K = k_3 + k_4 + k_5$, it behaves as follows [123]:

$$A_6^{\rm NMHV}(k_i) \stackrel{s_{345}\to 0}{\longrightarrow} A_4(k_6, k_1, k_2, K)\, \frac{F_6(K^2, s_{i,i+1})}{K^2}\, A_4(-K, k_3, k_4, k_5)\,, \tag{1.97}$$

where F_6 is the factorization function.

In terms of the cross-ratios, this limit corresponds to letting $u, w \to \infty$, with u/w and v held fixed. For the R-invariants, this entails picking out the pole as $s_{345} \to 0$. Only R-invariants (1) and (4) have poles in this limit, and their coefficients are equal. From eq. (1.10), we see that the factorization limit of the ratio function can be explored by considering the limit of $V(u, v, w)$ as $u, w \to \infty$.

We examined this limit through three loops in ref. [37]. We found that the function U defined in eq. (1.28), rather than V, has a particularly simple limiting behavior. In particular, in the factorization limit U becomes a polynomial in $\ln(uw/v)$, with zeta-valued coefficients. We have applied the same method as in ref. [37] to take the limit of $U^{(4)}$, by iteratively working out the limiting behavior of its relevant coproducts, and fixing constants of integration using the line $(u, 1, u)$ (see section 1.7.2). We find that this simplicity of U continues to be manifest at four loops, and the factorization limit of $U^{(4)}$ is given by:

$$\begin{aligned} U^{(4)}(u, v, w)|_{u,w\to\infty} = {} & \frac{1}{4}\zeta_4 \ln^4(uw/v) - (4\zeta_5 + 3\zeta_2\zeta_3) \ln^3(uw/v) \\ & + \left(\frac{3769}{32}\zeta_6 + \frac{21}{4}\zeta_3^2\right) \ln^2(uw/v) \\ & - \left(\frac{785}{8}\zeta_7 + \frac{641}{4}\zeta_3\zeta_4 + \frac{191}{2}\zeta_2\zeta_5\right) \ln(uw/v) \\ & + \frac{133}{4}\zeta_2\zeta_3^2 + \frac{289}{4}\zeta_3\zeta_5 + \frac{62629}{64}\zeta_8\,. \end{aligned} \tag{1.98}$$

Note that the terms alternate strictly in sign from one power of $\ln(uw/v)$ to the next. At a given power of $\ln(uw/v)$, they also alternate strictly from one loop order to the next. The four loop limit (1.98), as well as the analogous results from one to three loops [37], are in perfect agreement with a prediction based on integrability [124].

Extracting the factorization function F_6 from this expression requires subtracting

off the four-point amplitudes $A_4(k_6, k_1, k_2, K)$ and $A_4(-K, k_3, k_4, k_5)$, and adding back in the BDS-like ansatz that was subtracted off when defining U. Altogether, this results in the following formula for F_6 in terms of U and quantities defined above in eqs. (1.22) and (1.23), as previously presented in ref. [37]:

$$\begin{aligned}[\ln F_6]^{(L)} &= \frac{\gamma_K^{(L)}}{8\epsilon^2 L^2}\left(1 + 2\,\epsilon\,L\,\frac{\mathcal{G}_0^{(L)}}{\gamma_K^{(L)}}\right)\left[\left(\frac{(-s_{12})(-s_{34})}{(-s_{56})}\right)^{-L\epsilon} + \left(\frac{(-s_{45})(-s_{61})}{(-s_{23})}\right)^{-L\epsilon}\right] \\ &\quad - \frac{\gamma_K^{(L)}}{8}\left[\frac{1}{2}\ln^2\left(\frac{(-s_{12})(-s_{34})}{(-s_{56})}\Big/\frac{(-s_{45})(-s_{61})}{(-s_{23})}\right) + 6\,\zeta_2\right] \\ &\quad + U^{(L)}(u, v, w)|_{u,w\to\infty} + \frac{f_2^{(L)}}{L^2} + C^{(L)} + \mathcal{O}(\epsilon). \end{aligned} \tag{1.99}$$

The limiting behavior of U should also control the multi-particle factorization behavior of higher-point N^{k}MHV amplitudes [37]. It would be interesting to check this behavior once such amplitudes become available (or use this information as an aid in their construction).

1.7 Quantitative behavior

In this section, we explore the ratio function quantitatively, plotting V and $\tilde{V}$ on a variety of lines and planes through the space of cross ratios. We stay on the Euclidean branch in the positive octant, $u, v, w > 0$, for which all the hexagon functions are real. On certain lines, these functions collapse to sums of well-known functions, such as HPLs. For another line, the diagonal line where $u = v = w$, we have series representations. For faces of the unit cube, we have constructed the function space in a manner analogous to the full hexagon function construction — see appendix D for the case where $w = 1$. We have used these constructions to obtain representations in terms of multiple polylogarithms whose arguments are the cross ratios. We can then use the program GiNaC [125, 126] to evaluate the functions numerically. There are two other "bulk" regions where we have representations in terms of multiple polylogarithms using the y_i variables. These regions, called Regions I and II in ref. [34], are inside the unit cube and also have $\Delta(u, v, w) > 0$. Although we won't

plot the functions in these bulk regions in this paper, we provide the multiple polylog representations in ancillary files.

1.7.1 The point $(1, 1, 1)$

The first place we inspect the values of V and $\tilde{V}$ is the point where all the cross ratios are equal to one: $(u, v, w) = (1, 1, 1)$. This point is our reference point for defining the constants of integration for all the irreducible hexagon functions: We define them all to vanish there (except for $\Omega^{(2)}$ which was previously defined as a particular integral). Also, the point $(1, 1, 1)$ is on the $\Delta = 0$ surface, so all parity-odd hexagon functions (including $\tilde{V}$) vanish there:

$$\tilde{V}^{(L)}(1, 1, 1) = 0 \qquad \text{for all } L. \tag{1.100}$$

However, V is nonzero at this point. The constant value of V can be fixed via the collinear limits, or even the soft limits, which correspond to the point $(1, 0, 0)$, for example. Then we fix V along the line $(1, v, v)$, using the fact that it can be expressed here in terms of HPLs of the form $H_{\vec{w}}(v)$ with $w_i \in \{0, 1\}$, as discussed in section 1.2.3. Setting $v = 1$, we find that

$$V^{(4)}(1, 1, 1) = 3\,\zeta_2\,\zeta_3^2 - 15\,\zeta_3\,\zeta_5 + \frac{5051}{12}\,\zeta_8 - 3\,\zeta_{5,3}\,. \tag{1.101}$$

This value can be compared to previous results at lower loops:

$$\begin{aligned} V^{(1)}(1, 1, 1) &= -\zeta_2\,, \\ V^{(2)}(1, 1, 1) &= 9\,\zeta_4\,, \\ V^{(3)}(1, 1, 1) &= -\frac{243}{4}\,\zeta_6\,. \end{aligned} \tag{1.102}$$

Interestingly, odd zeta values first appear in $V(1, 1, 1)$ at four loops. (A $(\zeta_3)^2$ term appears at three loops in $R_6^{(3)}(1, 1, 1)$ and $E^{(3)}(1, 1, 1)$, but it cancels in the ratio function.)

1.7.2 The lines $(u, u, 1)$ and $(u, 1, u)$

When two of the cross ratios are equal and the remaining one is equal to unity, the hexagon functions collapse to HPLs. On these lines, $\Delta = 0$, so the parity-odd functions vanish. For the parity-even functions, E is simpler to express on these lines than V, so we present it instead. Because it is symmetric in exchange of its first and third arguments, it suffices to give it on the lines $(u, u, 1)$ and $(u, 1, u)$. We use the notation introduced in ref. [35], in which we expand all products of HPLs using the shuffle algebra in order to linearize the expression in terms of HPLs. We then encode the HPL weight vectors $\vec{w}$, which consist entirely of 0's and 1's, as binary numbers, but written as a subscript in decimal. We track the length of the original weight vector with a superscript. For example,

$$H^u_1 H^u_{2,1} = H^u_1 H^u_{0,1,1} = 3H^u_{0,1,1,1} + H^u_{1,0,1,1} \to 3h^{[4]}_7 + h^{[4]}_{11}\,. \tag{1.103}$$

In this notation, the parity-even functions are

$$E^{(1)}(u,u,1) = -\zeta_2\,, \tag{1.104}$$

$$E^{(2)}(u,u,1) = \frac{1}{2}\Big[h^{[4]}_5 + h^{[4]}_{13} - 3(h^{[4]}_7 + h^{[4]}_{15})\Big] - \zeta_2\Big[h^{[2]}_1 + h^{[2]}_3\Big] + \frac{13}{2}\zeta_4\,, \tag{1.105}$$

$$\begin{aligned} E^{(3)}(u,u,1) = {} & h^{[6]}_{21} + h^{[6]}_{53} - 4(h^{[6]}_{23} + h^{[6]}_{55}) - 5(h^{[6]}_{27} + h^{[6]}_{59}) \\ & - 4(h^{[6]}_{29} + h^{[6]}_{61}) + 10(h^{[6]}_{31} + h^{[6]}_{63}) \\ & - \frac{1}{2}\zeta_2\Big[5(h^{[4]}_5 + h^{[4]}_{13}) - 19(h^{[4]}_7 + h^{[4]}_{15})\Big] \\ & + \frac{21}{2}\zeta_4\Big[h^{[2]}_1 + h^{[2]}_3\Big] - \frac{235}{6}\zeta_6 + \zeta_3^2\,, \end{aligned} \tag{1.106}$$

$$\begin{aligned} E^{(4)}(u,u,1) = {} & \frac{1}{8}\Big[- 18(h^{[8]}_{65} + h^{[8]}_{193}) - 18(h^{[8]}_{67} + h^{[8]}_{195}) - 18(h^{[8]}_{69} + h^{[8]}_{197}) \\ & - 2(h^{[8]}_{71} + h^{[8]}_{199}) - 18(h^{[8]}_{73} + h^{[8]}_{201}) - 10(h^{[8]}_{75} + h^{[8]}_{203}) \\ & - 10(h^{[8]}_{77} + h^{[8]}_{205}) + 14(h^{[8]}_{79} + h^{[8]}_{207}) - 21(h^{[8]}_{81} + h^{[8]}_{209}) \\ & - 13(h^{[8]}_{83} + h^{[8]}_{211}) + 21(h^{[8]}_{85} + h^{[8]}_{213}) - 107(h^{[8]}_{87} + h^{[8]}_{215}) \\ & - 25(h^{[8]}_{89} + h^{[8]}_{217}) - 161(h^{[8]}_{91} + h^{[8]}_{219}) - 127(h^{[8]}_{93} + h^{[8]}_{221}) \\ & + 225(h^{[8]}_{95} + h^{[8]}_{223}) - 24(h^{[8]}_{97} + h^{[8]}_{225}) - 8(h^{[8]}_{99} + h^{[8]}_{227}) \end{aligned}$$

$$
\begin{aligned}
&- 16(h^{[8]}_{101} + h^{[8]}_{229}) + 16(h^{[8]}_{103} + h^{[8]}_{231}) - 28(h^{[8]}_{105} + h^{[8]}_{233}) \\
&- 156(h^{[8]}_{107} + h^{[8]}_{235}) - 164(h^{[8]}_{109} + h^{[8]}_{237}) + 348(h^{[8]}_{111} + h^{[8]}_{239}) \\
&+ h^{[8]}_{113} + h^{[8]}_{241} + 25(h^{[8]}_{115} + h^{[8]}_{243}) - 101(h^{[8]}_{117} + h^{[8]}_{245}) \\
&+ 411(h^{[8]}_{119} + h^{[8]}_{247}) + 41(h^{[8]}_{121} + h^{[8]}_{249}) + 393(h^{[8]}_{123} + h^{[8]}_{251}) \\
&+ 267(h^{[8]}_{125} + h^{[8]}_{253}) - 525(h^{[8]}_{127} + h^{[8]}_{255})\Big] \\
&+ \frac{1}{2}\zeta_2\Big[2(h^{[6]}_{17} + h^{[6]}_{49}) + 2(h^{[6]}_{19} + h^{[6]}_{51}) - 17(h^{[6]}_{21} + h^{[6]}_{53}) \\
&\quad + 61(h^{[6]}_{23} + h^{[6]}_{55}) + 2(h^{[6]}_{25} + h^{[6]}_{57}) + 80(h^{[6]}_{27} + h^{[6]}_{59}) \\
&\quad + 61(h^{[6]}_{29} + h^{[6]}_{61}) - 143(h^{[6]}_{31} + h^{[6]}_{63})\Big] \\
&+ \frac{1}{4}\zeta_4\Big[115(h^{[4]}_{5} + h^{[4]}_{13}) - 429(h^{[4]}_{7} + h^{[4]}_{15})\Big] \\
&+ \frac{3}{2}(5\zeta_5 - 2\zeta_2\zeta_3)\,(h^{[3]}_{3} + h^{[3]}_{7}) \qquad (1.107) \\
&- 70\zeta_6(h^{[2]}_{1} + h^{[2]}_{3}) + \frac{1}{2}\zeta_2\zeta_3^2 - \frac{35}{2}\zeta_3\zeta_5 + \frac{36271}{144}\zeta_8 - \frac{3}{2}\zeta_{5,3}\,,
\end{aligned}
$$

$$
E^{(1)}(u,1,u) = -2h^{[2]}_{3} - \zeta_2\,, \qquad (1.108)
$$

$$
\begin{aligned}
E^{(2)}(u,1,u) &= \frac{1}{2}\Big[h^{[4]}_{5} - 3h^{[4]}_{7} + 2h^{[4]}_{9} - 2h^{[4]}_{11} - h^{[4]}_{13} + 15h^{[4]}_{15}\Big] \\
&\quad -\zeta_2\Big[h^{[2]}_{1} - 5h^{[2]}_{3}\Big] + \frac{13}{2}\zeta_4\,, \qquad (1.109)
\end{aligned}
$$

$$
\begin{aligned}
E^{(3)}(u,1,u) &= h^{[6]}_{21} - 4h^{[6]}_{23} - 5h^{[6]}_{27} - 4h^{[6]}_{29} + 10h^{[6]}_{31} - 3h^{[6]}_{33} - 2h^{[6]}_{35} - 2h^{[6]}_{37} \\
&\quad - 3h^{[6]}_{39} - 2h^{[6]}_{41} - 8h^{[6]}_{43} - 8h^{[6]}_{45} + 8h^{[6]}_{47} - 2h^{[6]}_{49} - 3h^{[6]}_{51} \\
&\quad - 7h^{[6]}_{53} + 9h^{[6]}_{55} - 3h^{[6]}_{57} + 8h^{[6]}_{59} + 4h^{[6]}_{61} - 40h^{[6]}_{63} \\
&\quad - \frac{\zeta_2}{2}\Big[5h^{[4]}_{5} - 19h^{[4]}_{7} + 2h^{[4]}_{9} - 22h^{[4]}_{11} - 17h^{[4]}_{13} + 55h^{[4]}_{15}\Big] \\
&\quad + \frac{\zeta_4}{2}\Big[21h^{[2]}_{1} - 83h^{[2]}_{3}\Big] - \frac{235}{6}\zeta_6 + \zeta_3^2\,, \qquad (1.110)
\end{aligned}
$$

and

$$
\begin{aligned}
E^{(4)}(u,1,u) &= \frac{1}{8}\Big[- 18h^{[8]}_{65} - 18h^{[8]}_{67} - 18h^{[8]}_{69} - 2h^{[8]}_{71} - 18h^{[8]}_{73} - 10h^{[8]}_{75} \\
&\quad - 10h^{[8]}_{77} + 14h^{[8]}_{79} - 21h^{[8]}_{81} - 13h^{[8]}_{83} + 21h^{[8]}_{85} - 107h^{[8]}_{87} \\
&\quad - 25h^{[8]}_{89} - 161h^{[8]}_{91} - 127h^{[8]}_{93} + 225h^{[8]}_{95} - 24h^{[8]}_{97} - 8h^{[8]}_{99}
\end{aligned}
$$

$$
\begin{aligned}
&- 16h^{[8]}_{101} + 16h^{[8]}_{103} - 28h^{[8]}_{105} - 156h^{[8]}_{107} - 164h^{[8]}_{109} \\
&+ 348h^{[8]}_{111} + h^{[8]}_{113} + 25h^{[8]}_{115} - 101h^{[8]}_{117} + 411h^{[8]}_{119} \\
&+ 41h^{[8]}_{121} + 393h^{[8]}_{123} + 267h^{[8]}_{125} - 525h^{[8]}_{127} + 120h^{[8]}_{129} \\
&+ 96h^{[8]}_{131} + 88h^{[8]}_{133} + 96h^{[8]}_{135} + 88h^{[8]}_{137} + 96h^{[8]}_{139} \\
&+ 88h^{[8]}_{141} + 80h^{[8]}_{143} + 88h^{[8]}_{145} + 96h^{[8]}_{147} + 92h^{[8]}_{149} \\
&+ 84h^{[8]}_{151} + 88h^{[8]}_{153} + 80h^{[8]}_{155} + 76h^{[8]}_{157} + 100h^{[8]}_{159} \\
&+ 78h^{[8]}_{161} + 102h^{[8]}_{163} + 86h^{[8]}_{165} + 110h^{[8]}_{167} + 74h^{[8]}_{169} \\
&- 62h^{[8]}_{171} - 78h^{[8]}_{173} + 458h^{[8]}_{175} + 106h^{[8]}_{177} + 130h^{[8]}_{179} \\
&- 42h^{[8]}_{181} + 654h^{[8]}_{183} + 150h^{[8]}_{185} + 686h^{[8]}_{187} + 514h^{[8]}_{189} \\
&- 390h^{[8]}_{191} + 114h^{[8]}_{193} + 122h^{[8]}_{195} + 114h^{[8]}_{197} + 106h^{[8]}_{199} \\
&+ 114h^{[8]}_{201} + 106h^{[8]}_{203} + 98h^{[8]}_{205} + 122h^{[8]}_{207} + 135h^{[8]}_{209} \\
&+ 151h^{[8]}_{211} + 17h^{[8]}_{213} + 553h^{[8]}_{215} + 179h^{[8]}_{217} + 715h^{[8]}_{219} \\
&+ 581h^{[8]}_{221} - 475h^{[8]}_{223} + 126h^{[8]}_{225} + 118h^{[8]}_{227} + 114h^{[8]}_{229} \\
&+ 138h^{[8]}_{231} + 162h^{[8]}_{233} + 538h^{[8]}_{235} + 534h^{[8]}_{237} - 546h^{[8]}_{239} \\
&+ 95h^{[8]}_{241} + 119h^{[8]}_{243} + 365h^{[8]}_{245} - 579h^{[8]}_{247} + 79h^{[8]}_{249} \\
&- 513h^{[8]}_{251} - 267h^{[8]}_{253} + 2205h^{[8]}_{255}\Big] \\
&+ \frac{\zeta_2}{2}\Big[2h^{[6]}_{17} + 2h^{[6]}_{19} - 17h^{[6]}_{21} + 61h^{[6]}_{23} + 2h^{[6]}_{25} + 80h^{[6]}_{27} \\
&+ 61h^{[6]}_{29} - 143h^{[6]}_{31} + 4h^{[6]}_{33} - 2h^{[6]}_{35} - 2h^{[6]}_{37} + 4h^{[6]}_{39} \\
&+ 84h^{[6]}_{43} + 84h^{[6]}_{45} - 180h^{[6]}_{47} - 2h^{[6]}_{49} + 4h^{[6]}_{51} + 65h^{[6]}_{53} \\
&- 199h^{[6]}_{55} + 4h^{[6]}_{57} - 182h^{[6]}_{59} - 121h^{[6]}_{61} + 383h^{[6]}_{63}\Big] \\
&+ \frac{\zeta_4}{4}\Big[115h^{[4]}_{5} - 429h^{[4]}_{7} + 20h^{[4]}_{9} - 524h^{[4]}_{11} - 409h^{[4]}_{13} + 1077h^{[4]}_{15}\Big] \\
&+ \frac{1}{2}\left(15\zeta_5 - 6\zeta_2\zeta_3\right)\Big[h^{[3]}_{3} + h^{[3]}_{5} - 3h^{[3]}_{7}\Big] - \frac{10}{3}\zeta_6\Big[21h^{[2]}_{1} - 79h^{[2]}_{3}\Big] \\
&- 2\zeta_3^2 h^{[2]}_{3} + \frac{1}{2}\zeta_2\zeta_3^2 - \frac{35}{2}\zeta_3\zeta_5 + \frac{36271}{144}\zeta_8 - \frac{3}{2}\zeta_{5,3}\,. \qquad (1.111)
\end{aligned}
$$

We provide an ancillary file containing these formulae, as well as the analogous ones for the remainder function.

The subscripts on the $h_i^{[m]}$ in these formulae are always odd, which means that the HPL weight vectors always end in 1. This restriction enforces the condition that no branch cuts start at $u = 1$. On the line $(u, u, 1)$, one can also see that there is a pairing of terms of the form $h_i^{[m]} + h_{i+2^{m-1}}^{[m]}$. This pairing is due to the coproduct relation $E^u + E^{1-u} + E^v + E^{1-v} = 0$, which holds globally as a consequence of eqs. (1.59) and (1.60). On the line $(u, u, 1)$, it implies that the u derivative has the form, $dE(u, u, 1)/du = 2\,E^u(u, u, 1)/[u(1-u)]$, which in turn implies the pairing of HPLs of the form $H_{0,\vec{w}} + H_{1,\vec{w}}$, or equivalently $h_i^{[m]} + h_{i+2^{m-1}}^{[m]}$.

We plot the behavior of V on the lines $(u, u, 1)$ and $(u, 1, u)$ in figures 1.1 and 1.2, respectively. In both cases we plot the functions at each loop order, normalized so that they are all equal to unity at the point $(u, v, w) = (1, 1, 1)$. While these functions appear to have similar behavior at each loop order away from $u = 0$, they do have dramatically varying $u \to 0$ limits, including oscillations at very small u. In this limit, the curves in figure 1.2 approach the negatives of the corresponding curves in figure 1.1. That is, $V(u, 1, u) \approx -V(u, u, 1)$ as $u \to 0$, which is a consequence of the collinear vanishing constraint (1.40) if we also let $u \to 0$, $v \to 1$ in that relation.

1.7.3 The lines $(u, 1, 1)$ and $(1, v, 1)$

The hexagon functions also collapse to the same class of HPLs on the lines where two of the three cross ratios are equal to one. These lines are not on the $\Delta = 0$ surface, so the parity-odd parts of the NMHV amplitude or ratio function do not automatically vanish. However, on the line $(1, v, 1)$, $\tilde{E}$ (or $\tilde{V}$) vanishes due to its antisymmetry under $u \leftrightarrow w$. This vanishing also means that $\tilde{E}(u, 1, 1)$ is a physical quantity, because it is equal to $\tilde{E}(u, 1, 1) - \tilde{E}(1, u, 1)$, which is a gauge-invariant difference of cyclic permutations. Again, we preferentially present E and $\tilde{E}$, rather than V and $\tilde{V}$, because they have somewhat simpler expressions. Using the $u \leftrightarrow w$ (anti-)symmetry, the functions we need to present are:

$$\begin{aligned} E^{(1)}(u, 1, 1) &= -\frac{1}{2} h_3^{[2]} - \zeta_2\,, \\ E^{(2)}(u, 1, 1) &= \frac{1}{4}\Big[h_5^{[4]} + h_9^{[4]} + h_{11}^{[4]} + h_{13}^{[4]} + 3h_{15}^{[4]}\Big] \end{aligned} \tag{1.112}$$

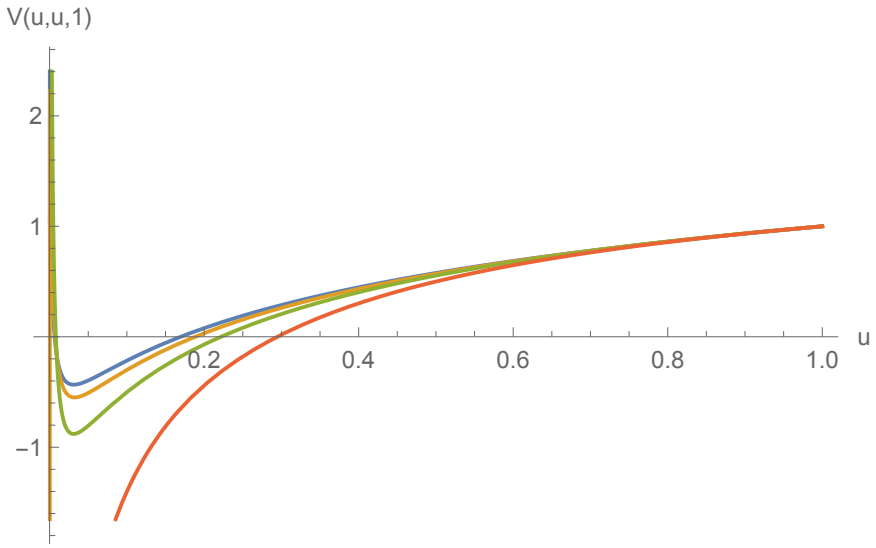

Figure 1.1: $V^{(1)}(u,u,1)$, $V^{(2)}(u,u,1)$, $V^{(3)}(u,u,1)$, and $V^{(4)}(u,u,1)$ normalized to one at $(1,1,1)$. One loop is in red, two loops is in green, three loops is in yellow, and four loops is in blue.

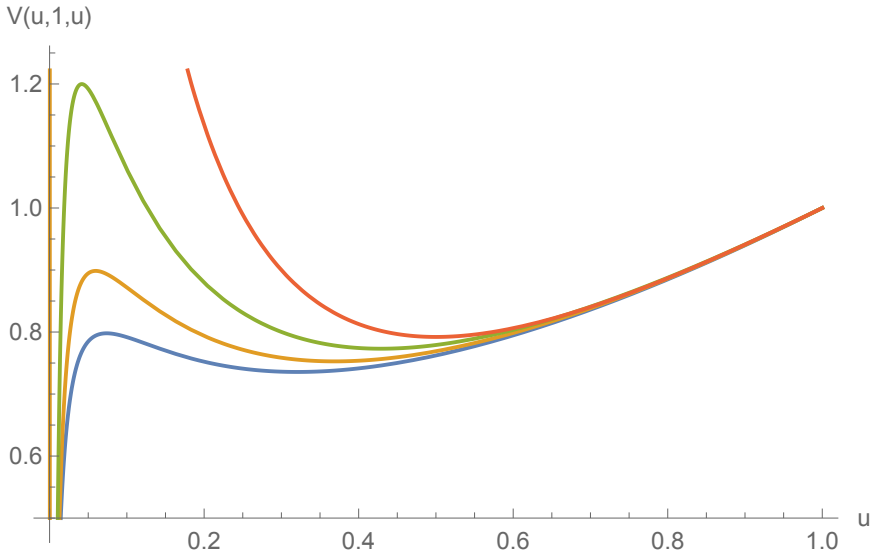

Figure 1.2: $V^{(1)}(u,1,u)$, $V^{(2)}(u,1,u)$, $V^{(3)}(u,1,u)$, and $V^{(4)}(u,1,u)$ normalized to one at $(1,1,1)$. One loop is in red, two loops is in green, three loops is in yellow, and four loops is in blue.

$$
\begin{aligned}
&- \frac{1}{2}\zeta_2\Big[h_1^{[2]} - 2h_3^{[2]}\Big] + \frac{13}{2}\zeta_4\,, \qquad (1.113)\\
E^{(3)}(u,1,1) \;=\; &-\frac{1}{8}\Big[-4h_{21}^{[6]} + h_{23}^{[6]} + h_{29}^{[6]} + 6h_{33}^{[6]} + 6h_{35}^{[6]} + 5h_{37}^{[6]} + 6h_{39}^{[6]}\\
&\quad + 5h_{41}^{[6]} + 5h_{43}^{[6]} + 5h_{45}^{[6]} + 6h_{47}^{[6]} + 6h_{49}^{[6]} + 6h_{51}^{[6]}\\
&\quad + 6h_{53}^{[6]} + 6h_{55}^{[6]} + 6h_{57}^{[6]} + 6h_{59}^{[6]} + 6h_{61}^{[6]} + 15h_{63}^{[6]}\Big]\\
&- \frac{1}{4}\zeta_2\Big[5h_5^{[4]} - h_7^{[4]} + h_9^{[4]} + h_{11}^{[4]} + 9h_{15}^{[4]}\Big]\\
&+ \frac{1}{4}\zeta_4\Big[21h_1^{[2]} - 34h_3^{[2]}\Big] - \frac{235}{6}\zeta_6 + \zeta_3^2\,, \qquad (1.114)\\
E^{(4)}(u,1,1) \;=\; &\frac{1}{16}\Big[-18h_{65}^{[8]} - 18h_{67}^{[8]} - 18h_{69}^{[8]} - 14h_{71}^{[8]} - 18h_{73}^{[8]} - 18h_{75}^{[8]}\\
&\quad - 14h_{77}^{[8]} - 10h_{79}^{[8]} - 24h_{81}^{[8]} - 24h_{83}^{[8]} + 5h_{85}^{[8]} - 20h_{87}^{[8]}\\
&\quad - 20h_{89}^{[8]} - 20h_{91}^{[8]} - 18h_{97}^{[8]} - 16h_{93}^{[8]} - 5h_{95}^{[8]} - 18h_{99}^{[8]}\\
&\quad - 18h_{101}^{[8]} - 14h_{103}^{[8]} - 24h_{105}^{[8]} - 24h_{107}^{[8]} - 20h_{109}^{[8]} - 10h_{111}^{[8]}\\
&\quad - 14h_{113}^{[8]} - 14h_{115}^{[8]} - 20h_{117}^{[8]} - 9h_{119}^{[8]} - 10h_{121}^{[8]} - 10h_{123}^{[8]}\\
&\quad - 5h_{125}^{[8]} + 60h_{129}^{[8]} + 60h_{131}^{[8]} + 50h_{133}^{[8]} + 54h_{135}^{[8]} + 50h_{137}^{[8]}\\
&\quad + 50h_{139}^{[8]} + 44h_{141}^{[8]} + 48h_{143}^{[8]} + 50h_{145}^{[8]} + 50h_{147}^{[8]} + 46h_{149}^{[8]}\\
&\quad + 47h_{151}^{[8]} + 44h_{153}^{[8]} + 44h_{155}^{[8]} + 41h_{157}^{[8]} + 45h_{159}^{[8]} + 45h_{161}^{[8]}\\
&\quad + 45h_{163}^{[8]} + 39h_{165}^{[8]} + 42h_{167}^{[8]} + 36h_{169}^{[8]} + 36h_{171}^{[8]} + 33h_{173}^{[8]}\\
&\quad + 39h_{175}^{[8]} + 39h_{177}^{[8]} + 39h_{179}^{[8]} + 33h_{181}^{[8]} + 39h_{183}^{[8]} + 36h_{185}^{[8]}\\
&\quad + 36h_{187}^{[8]} + 36h_{189}^{[8]} + 45h_{191}^{[8]} + 54h_{193}^{[8]} + 54h_{195}^{[8]} + 44h_{197}^{[8]}\\
&\quad + 50h_{199}^{[8]} + 44h_{201}^{[8]} + 44h_{203}^{[8]} + 40h_{205}^{[8]} + 46h_{207}^{[8]} + 43h_{209}^{[8]}\\
&\quad + 43h_{211}^{[8]} + 34h_{213}^{[8]} + 43h_{215}^{[8]} + 39h_{217}^{[8]} + 39h_{219}^{[8]} + 39h_{221}^{[8]}\\
&\quad + 45h_{223}^{[8]} + 48h_{225}^{[8]} + 48h_{227}^{[8]} + 41h_{229}^{[8]} + 47h_{231}^{[8]} + 38h_{233}^{[8]}\\
&\quad + 38h_{235}^{[8]} + 37h_{237}^{[8]} + 46h_{239}^{[8]} + 46h_{241}^{[8]} + 46h_{243}^{[8]} + 40h_{245}^{[8]}\\
&\quad + 46h_{247}^{[8]} + 45h_{249}^{[8]} + 45h_{251}^{[8]} + 45h_{253}^{[8]} + 105h_{255}^{[8]}\Big]\\
&+ \frac{\zeta_2}{8}\Big[4h_{17}^{[6]} + 4h_{19}^{[6]} - 25h_{21}^{[6]} + 11h_{23}^{[6]} + 4h_{25}^{[6]} + 10h_{27}^{[6]} + 11h_{29}^{[6]}\\
&\quad + 5h_{31}^{[6]} + 4h_{33}^{[6]} + 4h_{35}^{[6]} + h_{37}^{[6]} + 4h_{39}^{[6]} + 3h_{41}^{[6]} + 6h_{43}^{[6]}\\
&\quad + 6h_{45}^{[6]} + 9h_{47}^{[6]} + 6h_{49}^{[6]} + 6h_{51}^{[6]} + 9h_{53}^{[6]} + 6h_{55}^{[6]} + 6h_{57}^{[6]}
\end{aligned}
$$

$$
\begin{aligned}
&\quad + 9h_{59}^{[6]} + 6h_{61}^{[6]} + 60h_{63}^{[6]}\Big] \\
&+ \frac{\zeta_4}{8}\Big[115h_5^{[4]} - 21h_7^{[4]} + 10h_9^{[4]} + 10h_{11}^{[4]} - 11h_{13}^{[4]} + 186h_{15}^{[4]}\Big] \\
&+ \frac{3}{8}\left(5\zeta_5 - 2\zeta_2\zeta_3\right)\Big[2h_3^{[3]} + h_5^{[3]} + h_7^{[3]}\Big] - \frac{\zeta_6}{24}\Big[840h_1^{[2]} - 1373h_3^{[2]}\Big] \\
&- \frac{1}{2}\zeta_3^2 h_3^{[2]} + \frac{1}{2}\zeta_2\zeta_3^2 - \frac{35}{2}\zeta_3\zeta_5 + \frac{36271}{144}\zeta_8 - \frac{3}{2}\zeta_{5,3}\,, \qquad (1.115)
\end{aligned}
$$

$$
E^{(1)}(1,v,1) = -\frac{1}{2}h_3^{[2]} - \zeta_2\,, \qquad (1.116)
$$

$$
E^{(2)}(1,v,1) = \frac{1}{4}\Big[h_5^{[4]} + 3h_{15}^{[4]}\Big] - \frac{1}{2}\zeta_2\Big[h_1^{[2]} - 3h_3^{[2]}\Big] + \frac{13}{2}\zeta_4\,, \qquad (1.117)
$$

$$
\begin{aligned}
E^{(3)}(1,v,1) &= -\frac{1}{8}\Big[-4h_{21}^{[6]} + h_{23}^{[6]} + h_{29}^{[6]} + h_{53}^{[6]} + 15h_{63}^{[6]}\Big] \\
&\quad - \frac{1}{4}\zeta_2\Big[5h_5^{[4]} - h_7^{[4]} - h_{13}^{[4]} + 15h_{15}^{[4]}\Big] \\
&\quad + \frac{1}{4}\zeta_4\Big[21h_1^{[2]} - 55h_3^{[2]}\Big] - \frac{235}{6}\zeta_6 + \zeta_3^2\,, \qquad (1.118)
\end{aligned}
$$

$$
\begin{aligned}
E^{(4)}(1,v,1) &= \frac{1}{16}\Big[-18h_{65}^{[8]} - 18h_{67}^{[8]} - 18h_{69}^{[8]} - 14h_{71}^{[8]} - 18h_{73}^{[8]} - 18h_{75}^{[8]} \\
&\quad - 14h_{77}^{[8]} - 10h_{79}^{[8]} - 24h_{81}^{[8]} - 24h_{83}^{[8]} + 5h_{85}^{[8]} - 20h_{87}^{[8]} \\
&\quad - 20h_{89}^{[8]} - 20h_{91}^{[8]} - 16h_{93}^{[8]} - 5h_{95}^{[8]} - 18h_{97}^{[8]} - 18h_{99}^{[8]} \\
&\quad - 18h_{101}^{[8]} - 14h_{103}^{[8]} - 24h_{105}^{[8]} - 24h_{107}^{[8]} - 20h_{109}^{[8]} - 10h_{111}^{[8]} \\
&\quad - 14h_{113}^{[8]} - 14h_{115}^{[8]} - 20h_{117}^{[8]} - 9h_{119}^{[8]} - 10h_{121}^{[8]} - 10h_{123}^{[8]} \\
&\quad - 5h_{125}^{[8]} - 12h_{161}^{[8]} - 12h_{163}^{[8]} - 12h_{165}^{[8]} - 10h_{167}^{[8]} - 18h_{169}^{[8]} \\
&\quad - 18h_{171}^{[8]} - 16h_{173}^{[8]} - 8h_{175}^{[8]} - 12h_{177}^{[8]} - 12h_{179}^{[8]} - 18h_{181}^{[8]} \\
&\quad - 10h_{183}^{[8]} - 10h_{185}^{[8]} - 10h_{187}^{[8]} - 8h_{189}^{[8]} - 8h_{209}^{[8]} - 8h_{211}^{[8]} \\
&\quad - 14h_{213}^{[8]} - 5h_{215}^{[8]} - 8h_{217}^{[8]} - 8h_{219}^{[8]} - 5h_{221}^{[8]} - 6h_{233}^{[8]} \\
&\quad - 6h_{235}^{[8]} - 6h_{237}^{[8]} - 3h_{245}^{[8]} + 105h_{255}^{[8]}\Big] \\
&+ \frac{\zeta_2}{8}\Big[4h_{17}^{[6]} + 4h_{19}^{[6]} - 25h_{21}^{[6]} + 11h_{23}^{[6]} + 4h_{25}^{[6]} + 10h_{27}^{[6]} \\
&\quad + 11h_{29}^{[6]} + 5h_{31}^{[6]} + 2h_{41}^{[6]} + 8h_{43}^{[6]} + 8h_{45}^{[6]} + 8h_{47}^{[6]} \\
&\quad + 9h_{53}^{[6]} + 5h_{55}^{[6]} + 6h_{59}^{[6]} + 3h_{61}^{[6]} + 105h_{63}^{[6]}\Big] \\
&+ \frac{\zeta_4}{8}\Big[115h_5^{[4]} - 21h_7^{[4]} - 21h_{13}^{[4]} + 333h_{15}^{[4]}\Big]
\end{aligned}
$$

$$
\begin{aligned}
&+\frac{3}{4}\left(5\zeta_5-2\zeta_2\zeta_3\right)\Big[h_3^{[3]}+h_5^{[3]}+h_7^{[3]}\Big]\\
&-\frac{\zeta_6}{24}\Big[840h_1^{[2]}-2213h_3^{[2]}\Big]-\frac{1}{2}\zeta_3^2h_3^{[2]}\\
&+\frac{1}{2}\zeta_2\zeta_3^2-\frac{35}{2}\zeta_3\zeta_5+\frac{36271}{144}\zeta_8-\frac{3}{2}\zeta_{5,3}\,, \qquad (1.119)\\
\tilde{E}^{(2)}(u,1,1) &= \frac{1}{4}\Big[h_9^{[4]}+h_{11}^{[4]}+h_{13}^{[4]}\Big]-\frac{1}{2}\zeta_2h_3^{[2]}\,, \qquad (1.120)\\
\tilde{E}^{(3)}(u,1,1) &= -\frac{1}{8}\Big[6(h_{33}^{[6]}+h_{35}^{[6]}+h_{39}^{[6]}+h_{47}^{[6]}+h_{49}^{[6]})\\
&\qquad +6(h_{51}^{[6]}+h_{55}^{[6]}+h_{57}^{[6]}+h_{59}^{[6]}+h_{61}^{[6]})\\
&\qquad +5(h_{37}^{[6]}+h_{41}^{[6]}+h_{43}^{[6]}+h_{45}^{[6]}+h_{53}^{[6]})\Big]\\
&\quad -\frac{1}{4}\zeta_2\Big[h_9^{[4]}+h_{11}^{[4]}+h_{13}^{[4]}-6h_{15}^{[4]}\Big]+\frac{21}{4}\zeta_4h_3^{[2]}\,, \qquad (1.121)
\end{aligned}
$$

and

$$
\begin{aligned}
\tilde{E}^{(4)}(u,1,1) &= \frac{1}{16}\Big[40h_{205}^{[8]}+41(h_{157}^{[8]}+h_{229}^{[8]})+43(h_{237}^{[8]}+h_{245}^{[8]})\\
&\quad +44(h_{141}^{[8]}+h_{153}^{[8]}+h_{155}^{[8]}+h_{189}^{[8]}+h_{197}^{[8]}+h_{201}^{[8]}\\
&\qquad +h_{203}^{[8]}+h_{221}^{[8]}+h_{233}^{[8]}+h_{235}^{[8]})\\
&\quad +45(h_{159}^{[8]}+h_{191}^{[8]}+h_{223}^{[8]}+h_{249}^{[8]}+h_{251}^{[8]}+h_{253}^{[8]})\\
&\quad +46(h_{149}^{[8]}+h_{185}^{[8]}+h_{187}^{[8]}+h_{207}^{[8]}+h_{239}^{[8]}+h_{241}^{[8]}\\
&\qquad +h_{243}^{[8]}+h_{247}^{[8]})\\
&\quad +47(h_{151}^{[8]}+h_{175}^{[8]}+h_{217}^{[8]}+h_{219}^{[8]}+h_{231}^{[8]})\\
&\quad +48(h_{143}^{[8]}+h_{213}^{[8]}+h_{215}^{[8]}+h_{225}^{[8]}+h_{227}^{[8]})\\
&\quad +49(h_{173}^{[8]}+h_{183}^{[8]})\\
&\quad +50(h_{133}^{[8]}+h_{137}^{[8]}+h_{139}^{[8]}+h_{145}^{[8]}+h_{147}^{[8]}+h_{199}^{[8]})\\
&\quad +51(h_{165}^{[8]}+h_{177}^{[8]}+h_{179}^{[8]}+h_{181}^{[8]}+h_{209}^{[8]}+h_{211}^{[8]})\\
&\quad +52h_{167}^{[8]}\\
&\quad +54(h_{135}^{[8]}+h_{169}^{[8]}+h_{171}^{[8]}+h_{193}^{[8]}+h_{195}^{[8]})\\
&\quad +57(h_{161}^{[8]}+h_{163}^{[8]})+60(h_{129}^{[8]}+h_{131}^{[8]})\Big]
\end{aligned}
$$

$$
\begin{aligned}
&+\frac{1}{8}\zeta_2\Big[4(h^{[6]}_{33}+h^{[6]}_{35}+h^{[6]}_{39})+h^{[6]}_{37}+h^{[6]}_{41}\\
&\qquad\qquad+h^{[6]}_{47}+h^{[6]}_{55}-2(h^{[6]}_{43}+h^{[6]}_{45})\\
&\qquad\qquad+6(h^{[6]}_{49}+h^{[6]}_{51}+h^{[6]}_{57})\\
&\qquad\qquad+3(h^{[6]}_{59}+h^{[6]}_{61})-45h^{[6]}_{63}\Big]\\
&+\frac{1}{8}\zeta_4\Big[10(h^{[4]}_{9}+h^{[4]}_{11}+h^{[4]}_{13})-147h^{[4]}_{15}\Big]\\
&-\frac{3}{8}(5\zeta_5-2\zeta_2\zeta_3)(h^{[3]}_{5}+h^{[3]}_{7})-35\zeta_6 h^{[2]}_{3}\,.
\end{aligned}
\tag{1.122}
$$

We provide these formulae in the same ancillary file that contains the functions' values on the lines $(u,u,1)$ and $(u,1,u)$.

Actually, these functions are not all independent; they obey

$$\tilde{E}(u,1,1)=E(u,1,1)-E(1,u,1). \tag{1.123}$$

This relation follows from the spurious pole constraint (1.41), which holds for E and $\tilde{E}$ as well as for V and $\tilde{V}$ because R_6 and Y are totally symmetric. However, there is an issue of choosing the sign for the parity-odd function, or equivalently the choice of y_i versus $1/y_i$ as one approaches this limit. If one lets $u\to 1$, $v\to u$, $w\to 1$ in eq. (1.41), one obtains eq. (1.123). On the other hand, if one lets $u\to u$, $v\to 1$, $w\to 1$ in eq. (1.41), one obtains the same equation but with the opposite sign for $\tilde{E}(u,1,1)$.

The functions $\tilde{E}^{(L)}(u,1,1)$ have a relatively simple form because $d\tilde{E}(u,1,1)/du$ has the form of $1/u$ times a pure function, with no $1/(1-u)$ contribution. Inspecting these terms in the u derivative in eq. (A.2), after taking the limit $(u,v,w)\to(u,1,1)$, we find that the following linear combination of coproduct entries vanishes:

$$\tilde{E}^{1-u}(u,1,1)+2\,\tilde{E}^{y_u}(u,1,1)-\tilde{E}^{y_v}(u,1,1)-\tilde{E}^{y_w}(u,1,1)=0. \tag{1.124}$$

However, we have not yet been able to prove that this combination vanishes to all orders, for example as a consequence of the spurious-pole constraint and the $\bar{Q}$ relations.

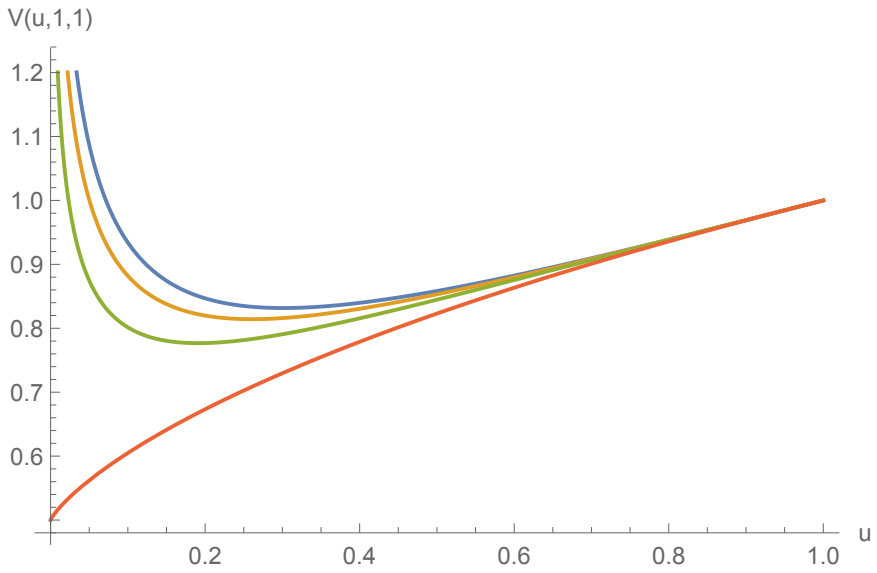

Figure 1.3: $V^{(1)}(u,1,1)$, $V^{(2)}(u,1,1)$, $V^{(3)}(u,1,1)$, and $V^{(4)}(u,1,1)$ normalized to one at $(1,1,1)$. One loop is in red, two loops is in green, three loops is in yellow, and four loops is in blue.

Next we plot the functions V and $\tilde{V}$ on the lines $(u,1,1)$ and $(1,v,1)$. For $V(u,1,1)$ and $V(1,v,1)$, shown in figures 1.3 and 1.4, respectively, we again normalize the plots so that each curve takes the value of unity at the point $(u,v,w)=(1,1,1)$.

We cannot use this normalization for $\tilde{V}(u,1,1)$, because this function vanishes at the point $(1,1,1)$. Instead, we normalize each loop order so that the coefficient of the $\ln^2 u$ term in the $u \to 0$ limit is equal to unity. As $u \to 0$, the functions (before normalization) behave as follows:

$$\tilde{V}^{(2)}(u,1,1)|_{u\to 0} = -\frac{1}{8}\zeta_2 \ln^2 u - \frac{5}{16}\zeta_4\,, \tag{1.125}$$

$$\tilde{V}^{(3)}(u,1,1)|_{u\to 0} = \frac{47}{32}\zeta_4 \ln^2 u + \frac{343}{128}\zeta_6 - \frac{1}{4}\zeta_3^2\,, \tag{1.126}$$

$$\begin{aligned}\tilde{V}^{(4)}(u,1,1)|_{u\to 0} = &-\frac{13}{512}\zeta_4 \ln^4 u + \frac{1}{64}\left(9\zeta_5 - 2\zeta_2\zeta_3\right)\ln^3 u \\ &- \frac{1}{768}\left(8173\zeta_6 + 48\zeta_3^2\right)\ln^2 u + \frac{1}{32}\left(27\zeta_2\zeta_5 - 40\zeta_3\zeta_4\right)\ln u \\ &- \frac{3}{8}\zeta_2\zeta_3^2 + \frac{73}{16}\zeta_3\zeta_5 - \frac{52217}{2560}\zeta_8 + \frac{33}{80}\zeta_{5,3}\,.\end{aligned} \tag{1.127}$$

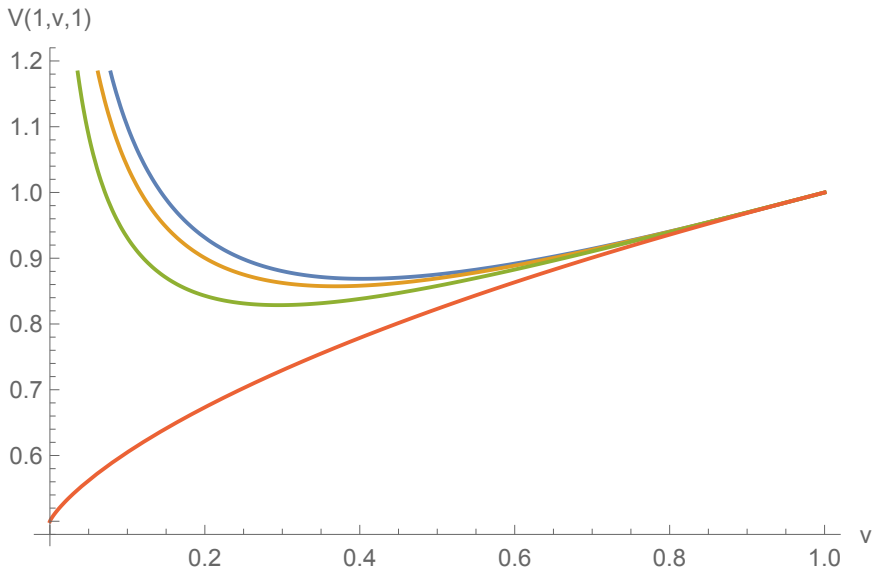

Figure 1.4: $V^{(1)}(1,v,1)$, $V^{(2)}(1,v,1)$, $V^{(3)}(1,v,1)$, and $V^{(4)}(1,v,1)$ normalized to one at $(1,1,1)$. One loop is in red, two loops is in green, three loops is in yellow, and four loops is in blue.

Note that when we use the normalization based on the $\ln^2 u$ coefficient, all three functions in figure 1.5 look almost identical! This is quite surprising, because $\tilde{V}^{(4)}(u,1,1)$ actually diverges like $\ln^4 u$ as $u \to 0$, while the lower-loop functions only diverge like $\ln^2 u$. The coefficient in front of the $\ln^4 u$ divergence is apparently small enough that it does little to change the shape of $\tilde{V}^{(4)}(u,1,1)$ over a large region of the u line.

1.7.4 The line (u,u,u)

Unlike the lines discussed above, the hexagon functions do not collapse to HPLs on the line where all of the cross ratios are equal. Instead they become cyclotomic polylogarithms [127]. Using the differential equations that they obey, it is relatively straightforward to evaluate these functions in terms of series expansions, either around $u = 0$, $u = 1$ or $u = \infty$. For the part of the line where $u < 1/4$, we have an alternate representation of V in terms of multiple polylogarithms. That is because $\Delta(u,u,u) = (1-u)^2(1-4u)$ is positive for $u < 1/4$, and this segment lies in the

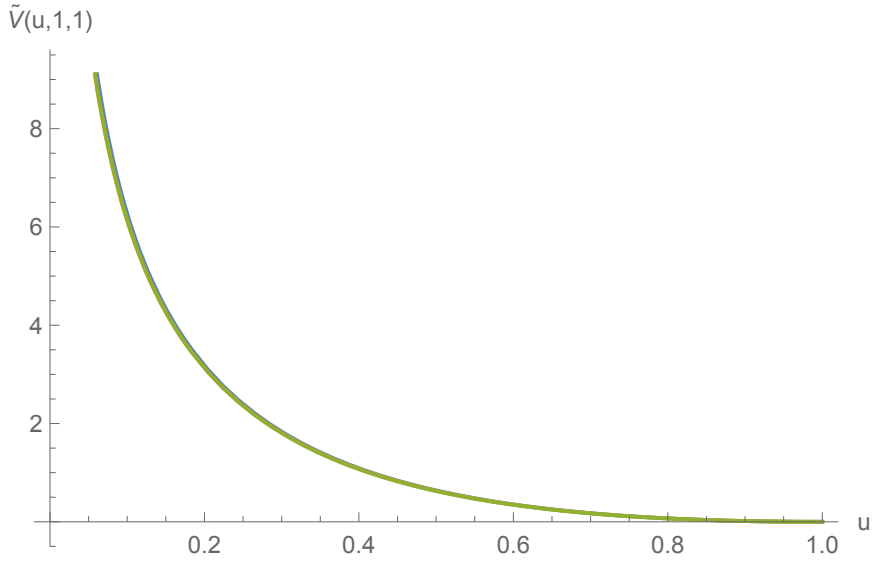

Figure 1.5: $\tilde{V}^{(2)}(u,1,1)$, $\tilde{V}^{(3)}(u,1,1)$ and $\tilde{V}^{(4)}(u,1,1)$ normalized so that the coefficient of the $\ln^2 u$ term in the $u \to 0$ limit is unity. Two loops is in green, three loops is in yellow, and four loops is in blue.

Region I defined in ref. [34]. On the whole line (u,u,u), $\tilde{V}$ vanishes by symmetry. We plot $V(u,u,u)$ in figure 1.6, normalized so that at each loop order the function has the value unity at the point $(1,1,1)$.

Among other uses, this line allows us to identify a place where the ratio function crosses zero, which is fairly stable with respect to the loop order. For each L, $V^{(L)}(u,u,u)$ crosses zero near $u = 1/3$, although the exact point shifts slightly with the loop order. Denoting by $u_0^{(L)}$ the value of u for which $V^{(L)}(u,u,u)$ equals zero, we have for this zero crossing,

$$\begin{aligned} u_0^{(1)} &= 0.372098\ldots, \quad u_0^{(2)} = 0.352838\ldots, \\ u_0^{(3)} &= 0.347814\ldots, \quad u_0^{(4)} = 0.346013\ldots. \end{aligned} \tag{1.128}$$

The functions $V^{(L)}(u,u,u)$ oscillate as $u \to 0$, leading to additional zero crossings near the origin. In particular, $V^{(2)}(u,u,u)$ has a zero crossing near 0.0015, while $V^{(3)}(u,u,u)$ crosses near 0.007 and again near 1.3×10^{-6}. $V^{(4)}(u,u,u)$ has three

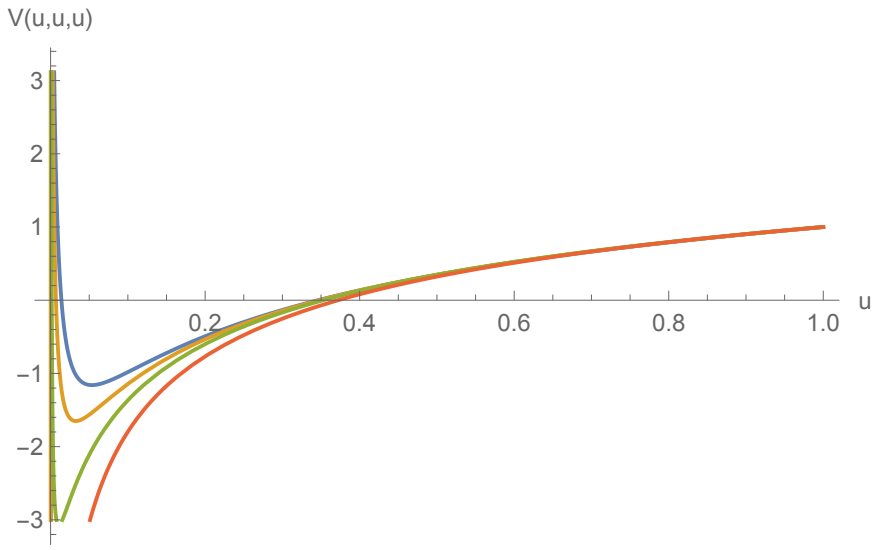

Figure 1.6: $V^{(1)}(u,u,u)$, $V^{(2)}(u,u,u)$, $V^{(3)}(u,u,u)$, and $V^{(4)}(u,u,u)$ normalized to one at $(1,1,1)$. One loop is in red, two loops is in green, three loops is in yellow, and four loops is in blue.

additional zero crossings, at roughly 0.014, 0.000025, and 7.2×10^{-10}. This can be seen from the small-u limits of these functions:

$$V^{(1)}(u,u,u) \sim \frac{1}{2}\ln^2 u + \frac{1}{2}\zeta_2\,, \tag{1.129}$$

$$V^{(2)}(u,u,u) \sim \frac{1}{16}\ln^4 u - \frac{3}{2}\zeta_2 \ln^2 u + \frac{1}{2}\zeta_3 \ln u - \frac{53}{16}\zeta_4\,, \tag{1.130}$$

$$\begin{aligned} V^{(3)}(u,u,u) \sim{}& \frac{1}{288}\ln^6 u - \frac{41}{96}\zeta_2 \ln^4 u + \frac{1}{8}\zeta_3 \ln^3 u + \frac{419}{32}\zeta_4 \ln^2 u \\ & - \left(2\,\zeta_5 + \frac{3}{4}\zeta_2\,\zeta_3\right)\ln u + \frac{2589}{128}\zeta_6 - \frac{1}{4}(\zeta_3)^2\,, \end{aligned} \tag{1.131}$$

$$\begin{aligned} V^{(4)}(u,u,u) \sim{}& \frac{1}{9216}\ln^8 u - \frac{43}{1152}\zeta_2 \ln^6 u + \frac{1}{96}\zeta_3 \ln^5 u + \frac{557}{96}\zeta_4 \ln^4 u \\ & - \frac{1}{48}\left(23\,\zeta_5 + 32\,\zeta_2\zeta_3\right)\ln^3 u - \frac{1}{256}\left(21971\,\zeta_6 - 8\,\zeta_3^2\right)\ln^2 u \\ & + \frac{1}{32}\left(300\,\zeta_7 + 108\,\zeta_2\zeta_5 + 121\,\zeta_3\zeta_4\right)\ln u \\ & - \frac{131867}{1024}\zeta_8 + \frac{3}{8}\zeta_2\zeta_3^2 + \frac{11}{4}\zeta_3\zeta_5\,. \end{aligned} \tag{1.132}$$

We note that the multiple zeta value $\zeta_{5,3}$ does not appear in this particular limit of the four-loop ratio function; nor did it appear in the same limit of the remainder function [35]. Its absence could be a hint that there might be a relatively simple description of this limit.

1.7.5 Faces of the unit cube

We can also examine V and $\tilde{V}$ on the faces of the unit cube in cross-ratio space. Here the functions do not collapse to HPLs, but they do still reduce to simpler bases of functions which can be readily treated numerically. There are two cases to consider: planes where one of the cross ratios goes to one, and planes where one of the cross ratios vanishes. We will consider each in turn.

First, we consider the plane where one of the cross ratios goes to one. For concreteness, we choose $w \to 1$, so the surface is $(u, v, 1)$. This limit was discussed in section 1.2, where it was used to ensure the vanishing of spurious poles. Recall that in this limit, our symbol entries behave as follows:

$$w \to 1\,, \quad y_u \to (1-w)\frac{u(1-v)}{(u-v)^2}\,, \quad y_v \to \frac{1}{(1-w)}\frac{(u-v)^2}{v(1-u)}\,, \quad y_w \to \frac{1-u}{1-v}\,. \tag{1.133}$$

Thus in this limit our set of nine symbol letters reduces to the following five:

$$\mathcal{S}_{w\to 1} \;=\; \{u,\, v,\, 1-u,\, 1-v,\, u-v\}\,. \tag{1.134}$$

We cannot represent this function space solely with one-dimensional HPLs ($H_{\vec{w}}(u)$ and $H_{\vec{w}}(v)$ with $\vec{w} \in \{0,1\}$), due to the $u-v$ entry. However, it is relatively straightforward to express any function with these symbol letters in terms of Goncharov polylogarithms, which in turn can be evaluated numerically with GiNaC [125, 126]. (We could have used instead the 2dHPL functions introduced by Gehrmann and Remiddi [128].)

For $V(u, v, w)$, there are two distinct cases to consider. We can either let $v \to 1$, or let $w \to 1$. The $u \to 1$ case is related to the $w \to 1$ case by $u \leftrightarrow w$ symmetry.

For the $w \to 1$ surface we find relatively simple behavior, shown in figure 1.7.

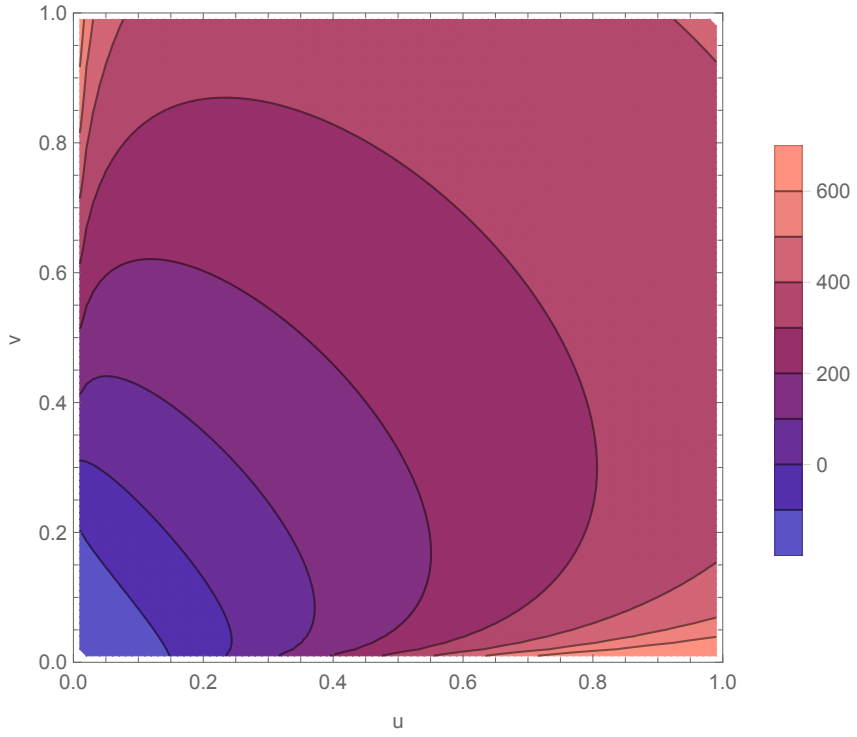

Figure 1.7: $V^{(4)}(u, v, 1)$ plotted in u and v.

The function $V^{(4)}(u, v, 1)$ is approximately symmetric under $u \leftrightarrow v$. It crosses zero around the line $u + v = 0.3$, and increases as u and v increase. Since the function crosses zero on this surface, plotting ratios between V at different loop orders is not especially informative, so here we plot only $V^{(4)}(u, v, 1)$.

If we instead take $v \to 1$, the function $V(u, 1, w)$ is exactly symmetric under exchange of u and w. It also has uniform sign. Taking advantage of both of these properties, we show in figure 1.8 the ratios of $V^{(4)}(u, 1, w)$ to $V^{(3)}(u, 1, w)$ and $V^{(3)}(u, 1, w)$ to $V^{(2)}(u, 1, w)$ on the same plot. Here $V^{(4)}(u, 1, w)/V^{(3)}(u, 1, w)$ is plotted in the top-left corner, while $V^{(3)}(u, 1, w)/V^{(2)}(u, 1, w)$ is in the bottom-right. In both cases, the missing part of the plot is just the mirror image, due to $u \leftrightarrow w$ symmetry. We find that these inter-loop ratios are quite heavily constrained, staying between -4 and -8. Note in particular that $V^{(4)}(u, 1, w)/V^{(3)}(u, 1, w)$ is significantly flatter than $V^{(3)}(u, 1, w)/V^{(2)}(u, 1, w)$. This is encouraging; we expect the ratios to continue to

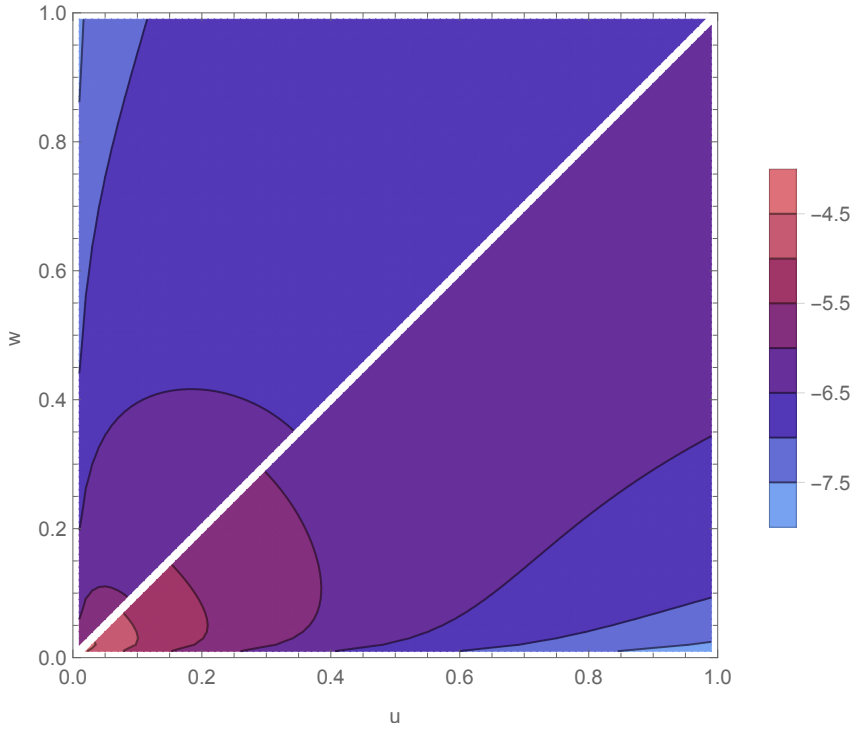

Figure 1.8: Ratios of $V(u, 1, w)$ between successive loop orders, plotted in u and w. $V^{(4)}/V^{(3)}$ is in the top-left corner, while $V^{(3)}/V^{(2)}$ is in the bottom-right.

become more constrained at higher loops due to the finite radius of convergence of the perturbative expansion. In non-singular regions, we expect the inter-loop ratios to approach -8 at very large loop order [35].

We can also look at the parity-odd functions on this plane. Here, we need to make a choice to avoid ambiguity. As discussed in section 1.2, $\tilde{V}$ has a "gauge" redundancy: we can add an arbitrary totally antisymmetric function to it without affecting the full ratio function. This ambiguity will have to be dealt with in order to present numerical results. Rather than fixing it in some arbitrary way, here we avoid the ambiguity altogether by taking differences of cyclic permutations of $\tilde{V}(u, v, w)$. Totally antisymmetric functions are cyclicly symmetric, so their contribution will cancel in these differences. The full ratio function can be expressed only in terms of the cyclic differences, with no independent appearance of $\tilde{V}$.

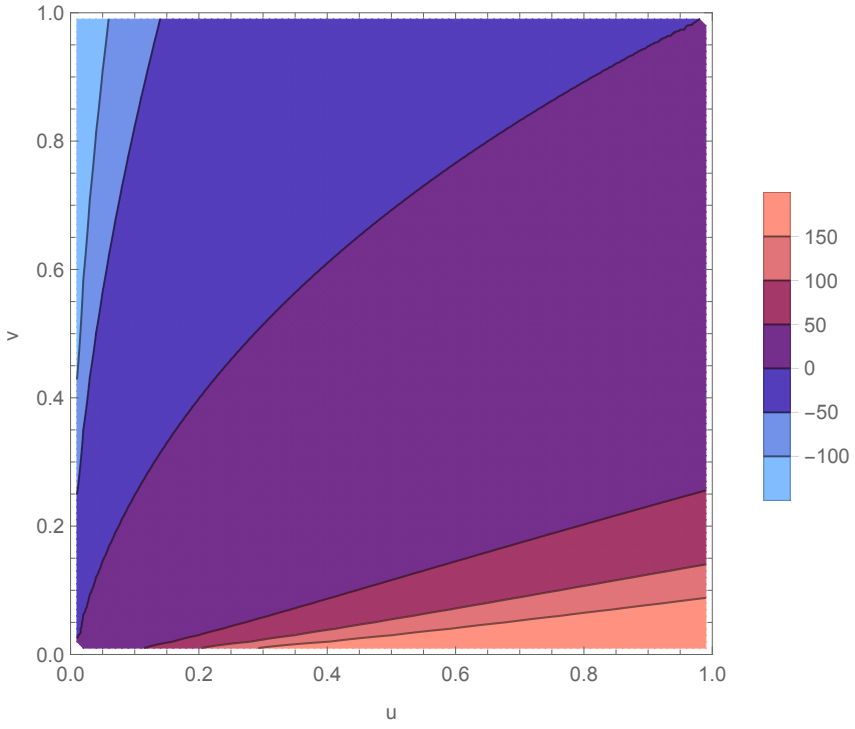

Figure 1.9: $\tilde{V}^{(4)}(v,1,u) - \tilde{V}^{(4)}(1,u,v)$ plotted in u and v.

There are three such differences to consider, $\tilde{V}(v,w,u) - \tilde{V}(w,u,v)$, $\tilde{V}(u,v,w) - \tilde{V}(v,w,u)$, and $\tilde{V}(w,u,v) - \tilde{V}(u,v,w)$. Taking $w \to 1$, this gives us $\tilde{V}(v,1,u) - \tilde{V}(1,u,v)$, $\tilde{V}(u,v,1) - \tilde{V}(v,1,u)$, and $\tilde{V}(1,u,v) - \tilde{V}(u,v,1)$. Of these, $\tilde{V}(v,1,u) - \tilde{V}(1,u,v)$ and $\tilde{V}(u,v,1) - \tilde{V}(v,1,u)$ exchange under $u \leftrightarrow v$, while $\tilde{V}(1,u,v) - \tilde{V}(u,v,1)$ is symmetric under $u \leftrightarrow v$. As it turns out, $\tilde{V}(v,1,u) - \tilde{V}(1,u,v)$ crosses zero while $\tilde{V}(1,u,v) - \tilde{V}(u,v,1)$ does not. As such, we can plot these cyclic differences of $\tilde{V}$ in the same format we used for V. Figure 1.9 plots $\tilde{V}^{(4)}(v,1,u) - \tilde{V}^{(4)}(1,u,v)$, while figure 1.10 shows the ratios $\left(\tilde{V}^{(4)}(1,u,v) - \tilde{V}^{(4)}(u,v,1)\right) / \left(\tilde{V}^{(3)}(1,u,v) - \tilde{V}^{(3)}(u,v,1)\right)$ and $\left(\tilde{V}^{(3)}(1,u,v) - \tilde{V}^{(3)}(u,v,1)\right) / \left(\tilde{V}^{(2)}(1,u,v) - \tilde{V}^{(2)}(u,v,1)\right)$ in the two panels separated by the diagonal line $u = v$. The latter plot again shows fairly constrained inter-loop ratios, varying between -3 and -8, and varying significantly less as the loop order increases.

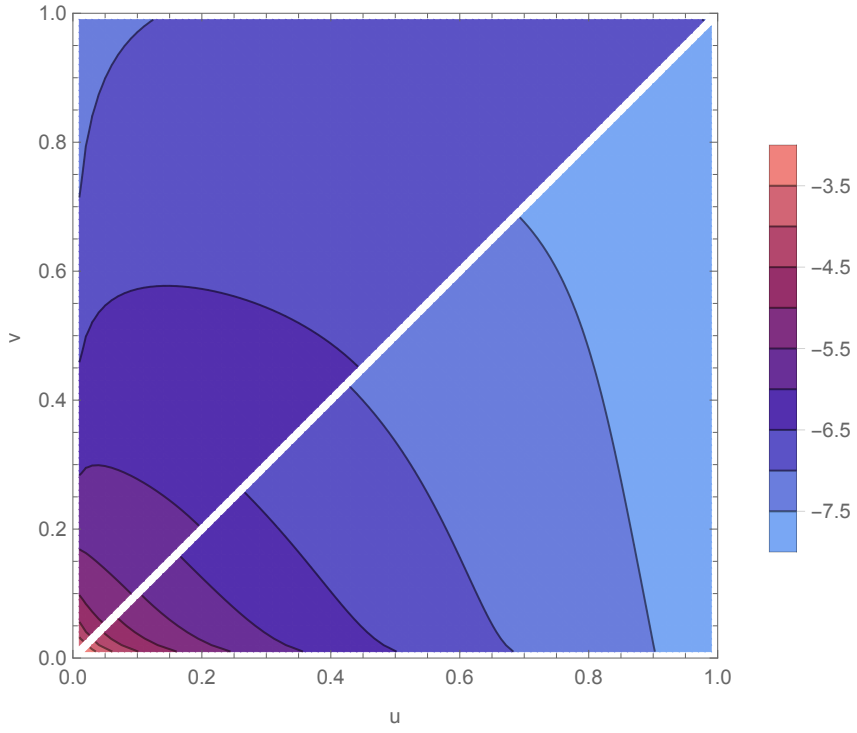

Figure 1.10: Ratios of $\tilde{V}(1,u,v) - \tilde{V}(u,v,1)$ between successive loop orders, plotted in u and v. $\tilde{V}^{(4)}/\tilde{V}^{(3)}$ is in the top-left corner, while $\tilde{V}^{(3)}/\tilde{V}^{(2)}$ is in the bottom-right.

Next, we consider the plane where one of the cross ratios goes to zero. For concreteness, take $v \to 0$. In this limit, as was also the case for the $w \to 1$ limit, the y variables become rational functions of u, v, and w:

$$y_u \to \frac{u}{1-w}\,, \qquad y_v \to \frac{v(1-u)(1-w)}{(1-u-w)^2}\,, \qquad y_w \to \frac{w}{1-u}\,. \tag{1.135}$$

(Equivalently, one could take the y_i to the inverse of these values.)

In contrast to the limit $w \to 1$, which is smooth (on the Euclidean branch), the hexagon functions can have logarithmically divergent behavior as $v \to 0$. As such, we expand all quantities in powers of $\ln v$. The coefficient of each power of $\ln v$ will then be a polylogarithmic function with symbol entries drawn from the following set:

$$\mathcal{S}_{v\to 0} \;=\; \{u,\, w,\, 1-u,\, 1-w,\, 1-u-w\}\,. \tag{1.136}$$

To plot these functions, we use a similar GiNaC-based implementation to that used for the $w = 1$ plane. Here there are two distinct regions to consider, due to the $1-u-w$ symbol entries. We can either consider $u+w > 1$, or $u+w < 1$. In general, these two regions require different implementations, which together can cover the whole positive quadrant $u, w > 0$. Here we just show results for the unit square.

In figure 1.11 we plot the $v \to 0$ limit of the parity-even functions $V^{(4)}(u,v,w)$ and $V^{(4)}(v,w,u)$ in the left and right columns, respectively, for each of the coefficients of $\ln^k v$ that are nonvanishing, $k = 0, 1, 2, 3, 4$. (In general, $V^{(L)}$ and $\tilde{V}^{(L)}$ have a maximum divergence of $\ln^L v$ at L loops, at least for $L \leq 4$.) Figure 1.12 plots the parity-odd functions $\tilde{V}^{(4)}(v,w,u) - \tilde{V}^{(4)}(w,u,v)$, and $\tilde{V}^{(4)}(u,v,w) - \tilde{V}^{(4)}(v,w,u)$. The other possible arguments are related by permutations. In both figures, the left panels are exactly symmetric under the exchange $u \leftrightarrow w$. Since the highest power of $\ln v$ in this limit increases with loop order there are no simple inter-loop ratios to show on this plane, which is why we plot only the four-loop functions.

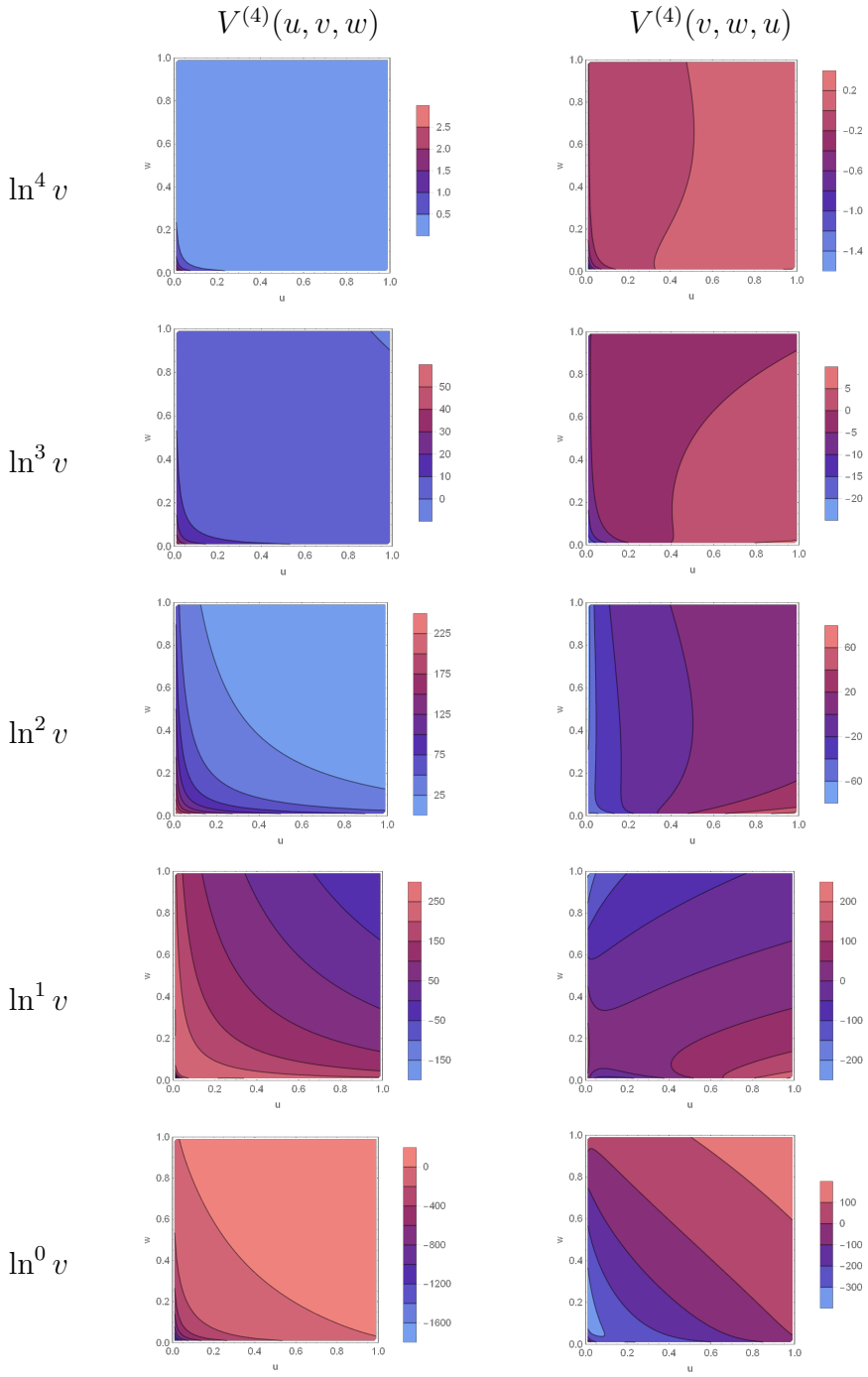

Figure 1.11: $V^{(4)}(u,v,w)$ and $V^{(4)}(v,w,u)$ plotted in the $v \to 0$ limit. The coefficient of each power of $\ln v$ is plotted separately.

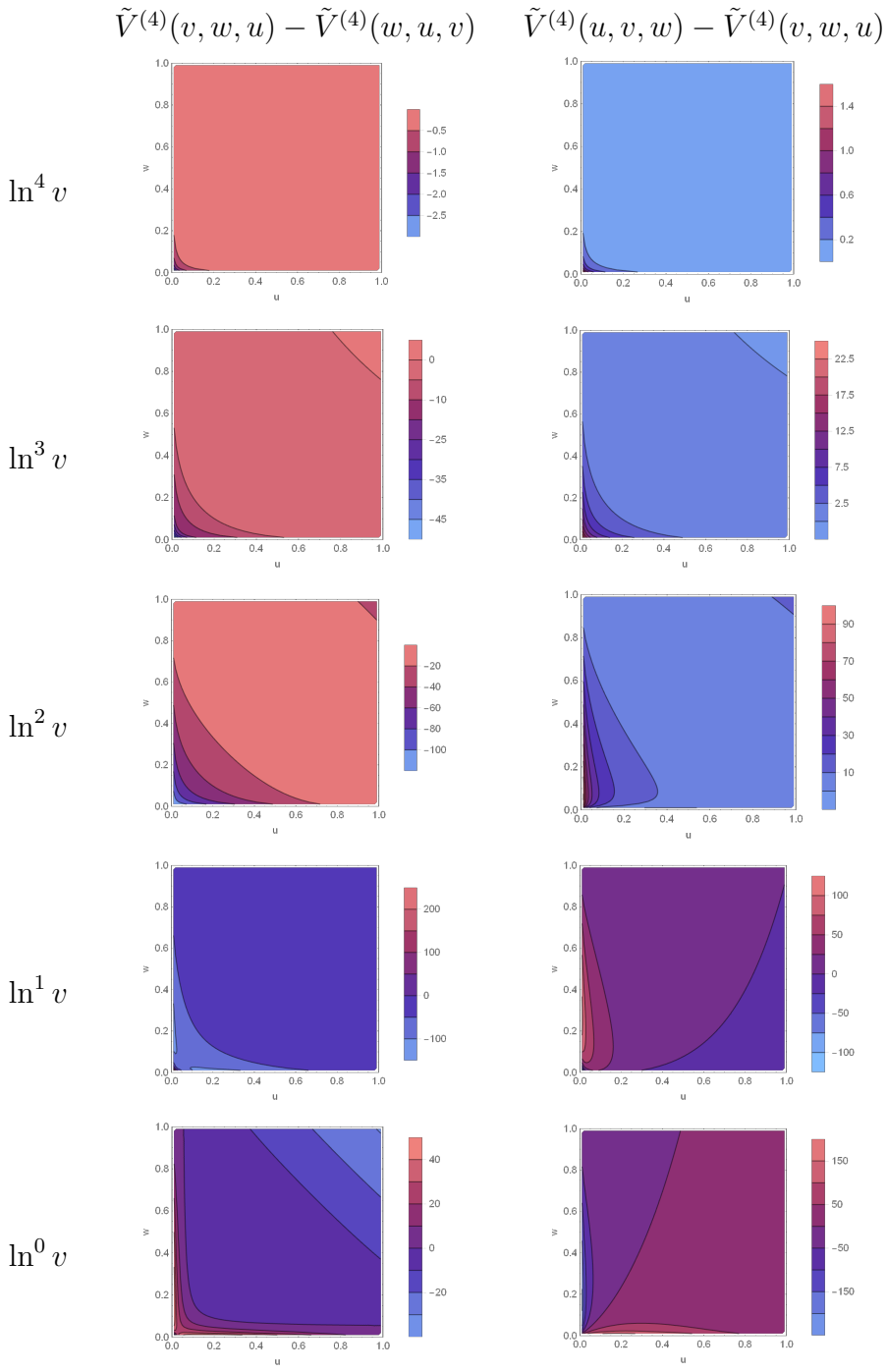

Figure 1.12: $\tilde{V}^{(4)}(v,w,u) - \tilde{V}^{(4)}(w,u,v)$ and $\tilde{V}^{(4)}(u,v,w) - \tilde{V}^{(4)}(v,w,u)$ plotted in the $v \to 0$ limit. The coefficient of each power of $\ln v$ is plotted separately.

1.8 Conclusions and outlook

In this paper we have continued the hexagon function bootstrap program initiated in ref. [32]. By calculating the six-particle NMHV ratio function through four loops, we have completed the description of six-point amplitudes at this loop order, complementing the earlier MHV results [35]. We extended the basis of hexagon functions constructed in ref. [34] to transcendental weight eight. We used the weight-seven part of this basis to construct an ansatz for the $\{7,1\}$ component of the coproduct of the NMHV coefficient functions V and $\tilde{V}$, which we then constrained through a series of physical inputs.

The most powerful such input comes from the $\bar{Q}$ equation. Previously, this equation was understood to imply a seven-final-entry condition. We now understand that it actually leads to a much more powerful set of relations between different permutations of the functions $E(u,v,w)$ and $\tilde{E}(u,v,w)$ [98]. This set of relations allowed us to work from an ansatz which, at four loops, had only 34 free parameters, and we could fix all but five of them by requiring the collinear limit of the ratio function to vanish.

The five remaining parameters were then fixed by appealing to the multi-Regge limit. By using an extension of the ansatz proposed in ref. [61] that we detailed in ref. [37], we used lower-loop information to predict the multi-Regge limit of the NMHV ratio function at leading-log and next-to-leading-log order. This allowed us to fix the remaining parameters in our ansatz. The terms in this limit that are of subleading logarithmic order have all been predicted using integrability [62]. They serve as a cross-check on our results.

With a unique result for the ratio function in hand, we proceeded to take the near-collinear limit and compare to the Pentagon OPE approach of Basso, Sever, and Vieira. Here we found perfect agreement with their published results [49] and those of Papathanasiou [121, 122] and Belitsky [53, 54, 116]. We also computed the multi-particle factorization limit, which takes a very simple form and agrees completely with integrability-based predictions [124].

Plotting V and $\tilde{V}$ over a variety of lines and planes through the space of cross

ratios, we found its behavior to be broadly similar across loop orders. In particular, we observed that, outside of regions where the functions vanish and corners containing logarithmic divergences, the ratios between successive loop orders are fairly flat, and generally stay between -4 and -8.

Recently, based on investigation of the positive Grassmannian [11], it was conjectured [129] that the remainder function ought to have uniform sign in a particular region of cross-ratio space. While this conjecture appears to be false near the origin for the remainder function, a similar conjecture seems to hold true for a bosonized version of the ratio function. Using the "data" found in this paper through four loops, we will explore this conjecture in future work [70].

Our new understanding of the $\bar{Q}$ equation has led to remarkably powerful constraints. After applying it, the number of free parameters remaining appears to only increase by around a factor of three at each loop order. If this trend continues, there should only be around a hundred unfixed parameters at five loops, comparable to the number that needed to be fixed for the four-loop MHV remainder function. This suggests that the five-loop ratio function may be well within reach. If so, it would be a great opportunity to see just how far the hexagon function program can extend.

Chapter 2

The Complete Amplitude at Five Loops

2.1 Introduction

To "bootstrap" generally refers to solving a problem via an ansatz constrained by symmetries and physical principles. This is naturally most successful in very special theories such as low-dimensional integrable models, but it has also proved powerful for conformal field theories in arbitrary dimensions. The hexagon function bootstrap [32, 38] is a perturbative version aimed at solving a scattering problem in a four-dimensional quantum field theory: the planar limit of $\mathcal{N} = 4$ super Yang-Mills (SYM). While scattering amplitudes in this theory are interesting in their own right, the methods developed to solve them have often had broader applicability, for example to computing amplitudes in QCD for scattering at the Large Hadron Collider.

The hexagon function bootstrap exploits the idea that, order by order in perturbation theory, the first nontrivial amplitude in planar $\mathcal{N} = 4$ SYM, the six-point amplitude, "lives" within a relatively small space of functions, which can be parametrized by a finite set of coefficients. This rigidity means that information from physical limits, such as when two gluons become collinear, or in a high-energy (Regge) limit, often suffices to fix the result. In turn this generates new predictions, a fact which

has led to much fruitful interplay with the pentagon operator-product-expansion program [48, 49, 53, 57].

The aim of this Letter is to point out that the relevant space of hexagon functions is far smaller than previously thought. This is due to constraints stemming from the classic work of Steinmann [65, 66, 67], which restrict the analytic structure of scattering amplitudes in any quantum field theory. We show that, when combined with Regge exponentiation and the so-called final-entry condition [64], this restriction makes it possible to bootstrap the six-gluon amplitude to at least 5 loops *without any external input*. Analogous constraints can be exploited for n-particle scattering with $n > 6$.

2.2 Hexagon Steinmann functions

We consider the scattering amplitude for six gluons (or other partons) in the planar limit of $\mathcal{N} = 4$ SYM. A priori, such an amplitude can depend, in four spacetime dimensions, on 8 Mandelstam invariants. Dual conformal symmetry of this model restricts the nontrivial dependence to be on 3 cross-ratios [26, 75, 76]

$$u = \frac{s_{12}s_{45}}{s_{123}s_{345}}, \quad v = \frac{s_{23}s_{56}}{s_{234}s_{123}}, \quad w = \frac{s_{34}s_{61}}{s_{345}s_{234}}, \tag{2.1}$$

where $s_{i\ldots k} \equiv (p_i + \cdots + p_k)^2$ are Mandelstam invariants. The same symmetry forces the four- and five-particle amplitudes to be essentially trivial, which is why we concentrate on six particles. It has been conjectured that the amplitude, which is a transcendental function of these three variables, lives in a restricted space of "hexagon" functions [32]. These are iterated integrals with singularities generated by logarithms of the nine letters [42]

$$\mathcal{S} \;=\; \{u, v, w, 1-u, 1-v, 1-w, y_u, y_v, y_w\}, \tag{2.2}$$

where

$$y_u = \frac{1+u-v-w-\sqrt{\Delta}}{1+u-v-w+\sqrt{\Delta}}, \quad \Delta = (1-u-v-w)^2 - 4uvw,$$

and cyclic rotations act as

$$C: \quad u \to v \to w \to u, \quad y_u \to 1/y_v \to y_w \to 1/y_u, \tag{2.3}$$

while parity acts as $u_i \to u_i$, $y_i \to 1/y_i$. These letters arise naturally as projectively invariant combinations of momentum twistors [81], variables that make manifest the dual conformal symmetry. Multiple zeta values $\zeta_{q_1,q_2,\ldots}$ with positive indices q_i also appear.

Branch cuts for massless scattering amplitudes start only at vanishing values of the Mandelstam invariants, $s_{i\ldots k} = 0$. Consequently, there is a canonical Riemann sheet on which the amplitude is analytic in the positive octant $u, v, w > 0$. This constraint is included in the definition of hexagon functions. It implies a "first-entry" condition [46]: discontinuities associated with the letters $(1-u) = 0$ or $y_u = 0$ are not visible in the canonical Riemann sheet; however, they can be exposed after analytic continuation. The physical interpretation of the restriction (2.2) is that, even after analytic continuation along an arbitrary complex path, the only possible branch points remain those characterized by $\mathcal{S}$.

The focus of this Letter is the Steinmann relations, which state that an amplitude A can have no double discontinuities in overlapping channels [65, 66, 67]. Using the correspondence between discontinuities and cut diagrams via the Cutkosky rules [130], overlapping channels correspond to cut lines that intersect. Thus for example the channels s_{345} and s_{234} overlap, which leads, schematically, to:

$$\text{Steinmann relation:} \quad \text{Disc}_{s_{345}}\left(\text{Disc}_{s_{234}} A\right) = 0, \tag{2.4}$$

illustrated in figure 2.1.

We focus on three-particle invariants s_{ijk} because these can change sign along fairly generic codimension-1 surfaces in the space of external momenta. The relation can therefore be probed with real external momenta. (In contrast, massless thresholds in two-particle invariants s_{ij} occur at phase space boundaries where other invariants may change sign; it is unclear to the authors how to extract putative constraints from these thresholds beyond the Regge limit [58].) For functions of the cross-ratios u, v, w,

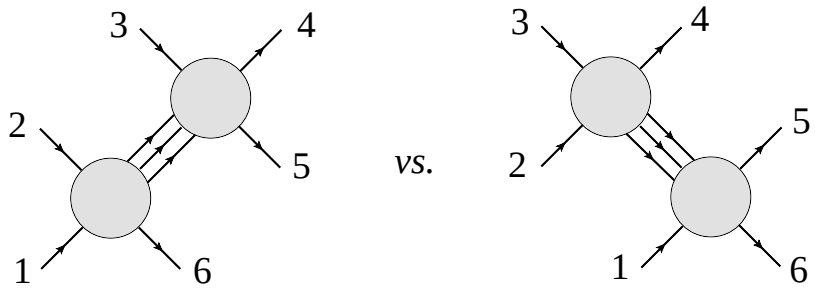

Figure 2.1: Illustration of the channels s_{345} and s_{234} for $3 \to 3$ kinematics. The discontinuity in one channel should not know about the discontinuity in the other channel.

the discontinuity with respect to s_{234} can be computed by rotating v, w by a common phase, as follows from eq. (2.1). The general Steinmann relation (2.4) thus implies — for the special case of dual-conformally invariant functions — that the following combination is analytic in a neighborhood of $r = \infty$:

$$0 = \text{Disc}_{r=\infty}[A(ru, ve^{i\pi}, re^{i\pi})) - A(ru, ve^{-i\pi}, re^{-i\pi})], \tag{2.5}$$

where $u, v > 0$ (and $r > 0$ before taking the discontinuity). The reason why $r = \infty$ appears is that the three-particle invariants appear in the denominators of eq. (2.1).

Focusing on the region where all three cross-ratios are large and combining this condition with its permutations, we obtain an equivalent but more practical statement: the amplitude must be expressible as a sum of terms with singularities in only one three-particle channel:

$$A = \sum_k \left[a_k^u \log^k\left(\frac{u}{vw}\right) + a_k^v \log^k\left(\frac{v}{wu}\right) + a_k^w \log^k\left(\frac{w}{uv}\right)\right], \tag{2.6}$$

with the $a_k^{u,v,w}$ analytic around $u = v = w = \infty$.

2.3 The Steinmann basis to weight 4

A complete basis of 88 hexagon functions at transcendental weight 4 was originally constructed in ref. [33]. The Steinmann relations imply that only a subspace is physically relevant, a subspace sufficiently small that it can be described in this Letter. We begin with weight 1, where the first entry condition allows only elementary logarithms: $\log u$, $\log v$, $\log w$. To build the higher weight basis, we use the fact that all derivatives of a Steinmann function also obey the Steinmann relations.

The derivative of a weight-k hexagon function F has the form [34]

$$dF = \sum_{i=1}^{9} F^i \; d\ln \mathcal{S}_i \,, \tag{2.7}$$

where F^i are weight-$(k-1)$ hexagon functions and $\mathcal{S}_i \in \mathcal{S}$ in eq. (2.2). We thus make an ansatz (2.7) for the derivatives of F where the F^i are Steinmann functions. For the ansatz to represent a function, the partial derivatives must commute ("integrability condition"). Once this condition is solved, the analyticity and Steinmann properties simplify dramatically. It suffices to impose the following constraints, which serve only to fix a few coefficients of zeta-values of weight $(k-1)$ and $(k-2)$:

- F^{1-u}, F^{y_v} and F^{y_w} must vanish at $(u, v, w) = (1, 0, 0)$ [34, 38].
- The s_{234}-discontinuity of $F^u + F^{1-u} + F^w + F^{1-w}$ must vanish at $(u, v, w) = (+\infty, 0, -\infty)$.

Cyclic rotations of these conditions are implied. The first condition enforces the absence of unwanted discontinuities [46] at function level; the second condition does the same for the Steinmann condition (2.5).

Following this procedure, at weight 2 we find 7 elements: the constant ζ_2 and two cyclic orbits containing

$$K^u_{1,1} \equiv \mathrm{Li}_2(1-1/u), \quad L^u_2 \equiv \tfrac{1}{2}\big[\log^2(u) + \log^2(v/w)\big] \,. \tag{2.8}$$

The naming convention will be explained shortly. Already, the Steinmann relations' impact is noticeable: without it there would be three additional functions, $\log^2 u$, $\log^2 v$ and $\log^2 w$, which do not satisfy eq. (2.6).

At weight 3, the basis contains 17 elements, the 5 cyclic 3-orbits of

$$\begin{aligned} K^u_3 &\equiv \tfrac{1}{3!}\log^3(1/u) + \tfrac{1}{2}\log(1/u)\log^2(v/w), \\ K^u_{2,1} &\equiv \mathrm{Li}_2(1/u)\log(1/u) - 2\mathrm{Li}_3(1/u) + 2\zeta_3, \\ K^u_{1,2} &\equiv K^u_{1,1}\log(v/w), \qquad K^u_{1,1,1} \equiv -\mathrm{Li}_3(1-1/u), \\ \zeta_2 K^u_1 &\equiv \zeta_2 \log(1/u), \end{aligned} \tag{2.9}$$

the constant ζ_3, and a single parity-odd element: the six-dimensional scalar hexagon integral $\tilde{\Phi}_6$ [131, 132, 34].

At this stage we see that the functions in eqs. (2.8)-(2.9) depend nontrivially on only u, apart from simple powers of $\log(v/w)$. We can construct $3 \times 2^{k-1}$ similar elements at weight k, as follows. We start from "seeds" which trivially satisfy eq. (2.6):

$$\begin{aligned} K^u_k(u, \tfrac{v}{w}) &\equiv \frac{1}{2\cdot k!}\left[\log^k\left(\frac{v}{uw}\right) - \log^k\left(\frac{uv}{w}\right)\right], \\ L^u_k(u, \tfrac{v}{w}) &\equiv \frac{1}{2\cdot k!}\left[\log^k\left(\frac{v}{uw}\right) + \log^k\left(\frac{uv}{w}\right)\right]. \end{aligned} \tag{2.10}$$

We then construct nontrivial functions as a simple generalization of harmonic polylogarithms (HPLs) [115] with argument $x = 1/u$, by integrating the seeds from the base point $u = \infty$. Using this base point automatically maintains the Steinmann relations. The constraint of analyticity for $u > 0$ is enforced by recursively removing values at $u = 1$:

$$K^u_{i,\ldots}(u, \tfrac{v}{w}) \equiv \sum_j c_j L^u_j + \int_0^{1/u} \frac{dx}{1-x}\frac{\log^{i-1}(\frac{1}{ux})}{(i-1)!} K^u_{\ldots}(\tfrac{1}{x}, \tfrac{v}{w}), \tag{2.11}$$

where the zeta-valued coefficients c_j are chosen uniquely to make the total vanish at $u = 1$. Without the c_j, the recursive definition would be identical to that of HPLs with argument $x = 1/u$, which makes it straightforward to express the K^u as combinations of HPLs. At weights 2 and 3, this definition agrees with the examples

Constraint	$L = 1$	$L = 2$	$L = 3$	$L = 4$	$L = 5$
0. Functions	(10,10)	(82,88)	(639,761)	(5153,6916)	(?????,?????)
1. Steinmann	(7,7)	(37,39)	(174,190)	(758,839)	(3105,3434)
2. Symmetry	(3,5)	(11,24)	(44,106)	(174,451)	(???,????)
3. Final-entry	(2,2)	(5,5)	(19,12)	(72,32)	(272,83)
4. Collinear	(0,0)	(0,0)	(1,1)	(3,5)	(9,15)
5. Regge	(0,0)	(0,0)	(0,0)	(0,0)	(0,0)

Table 2.1: Free parameters remaining after applying each constraint, for the 6-point (MHV,NMHV) amplitude at L loops.

given.

Defining K^v, K^w, L^v and L^w as cyclic images of K^u, L^u, the K functions with positive indices do generate $3 \times 2^{k-1}$ linearly independent elements. There is one exception: the three $K_k^{u,v,w}$ for even weight k are linearly dependent, so for even k we use $L_k^{u,v,w}$ instead.

At weight 4, the Steinmann basis contains the 8 3-orbits generated by:

$$L_4^u,\ K_{1,3}^u,\ K_{2,2}^u,\ K_{3,1}^u,\ K_{1,1,2}^u,\ K_{1,2,1}^u,\ K_{2,1,1}^u,\ K_{1,1,1,1}^u.$$

The iterative construction also generates 5 "non-K" functions: 3 parity-even functions — the integral $\Omega^{(2)}$ [33, 34] and its cyclic permutations — plus 2 parity-odd functions. Ten more functions come from multiplying ζ_2, ζ_3 and ζ_4 by the lower-weight Steinmann functions listed earlier. In summary, at weight 4 there are 39 physically relevant Steinmann functions, to be contrasted with 88 in the original hexagon function space.

This gap increases rapidly with higher weights, as evidenced by the first two lines of table 2.1, which was generated by implementing the construction iteratively. The paucity of Steinmann functions is because the space is not a ring: the product of two Steinmann functions is generically *not* an allowed function.

2.4 Application to two loops

Before using the Steinmann basis to help bootstrap the hexagon amplitude, we comment on the subtraction of its infrared divergences. A particularly convenient scheme for removing infrared divergences in the SYM model is to divide by the so-called BDS ansatz [31]. This soaks up the dual conformal anomaly, leaving a remainder which depends only on the cross-ratios u, v, w, and furthermore vanishes in soft and collinear limits [75, 76].[1]

However, in order to preserve the Steinmann relation (2.4), it is critical to divide only by quantities which are free of three-particle discontinuities. This singles out the so-called BDS-like ansatz [113, 38] $\mathcal{R}'_6$:

$$\mathcal{R}'_6 \equiv \mathcal{M}_6^{\text{bare}}/\mathcal{M}_6^{\text{BDS-like}}\,. \tag{2.12}$$

In fact, the amplitude is a function of the helicity of all 6 particles, in a way which can be neatly encoded in so-called R-invariants [29, 81]. In this Letter we thus deal with bosonic functions $\mathcal{E}$, E and $\tilde{E}$ which encode all the information and correspond to suitable components of the MHV and NMHV BDS-like remainders. Schematically, $\mathcal{R}'_6 \simeq \mathcal{E} \oplus E \oplus \tilde{E}$. The relations to the more conventional BDS MHV remainder ($\mathcal{R}_6$) and NMHV ratio function ($V, \tilde{V}$), defined for example in ref. [38] (to which we refer for further details), are:

$$e^{\mathcal{R}_6} \equiv \mathcal{E} e^{-\frac{1}{4}\Gamma_{\text{cusp}}\mathcal{E}^{(1)}}, \quad V \equiv E/\mathcal{E}, \quad \tilde{V} \equiv \tilde{E}/\mathcal{E}, \tag{2.13}$$

where $\frac{1}{4}\Gamma_{\text{cusp}} = g^2 - 2\zeta_2 g^4 + \ldots$ is the cusp anomalous dimension, known exactly as a function of the coupling $g^2 \equiv \frac{g^2_{\text{YM}} N_c}{16\pi^2}$ [114]. We stress that while $\mathcal{E}$, E and $\tilde{E}$ obey the Steinmann relations, $\mathcal{R}_6$, V and $\tilde{V}$ do not: the space of Steinmann functions is not a ring.

[1] The reader may object that higher-order poles in $\epsilon = (4-D)/2$ in the BDS ansatz mean that the full amplitude is not determined through $\mathcal{O}(\epsilon^0)$ by the remainder function alone. However, it has been proved [133] at next-to-next-to-leading order that the higher-order terms in ϵ in one-loop amplitudes are not needed, if one knows the two-loop remainder function to $\mathcal{O}(\epsilon^0)$. Based on the universal nature of infrared divergences and their cancellation, we expect the same result to hold to higher perturbative orders.

Let us describe a concrete example, the bootstrap of $\mathcal{E}$ at two loops. We begin by applying the following:

1. $\mathcal{E}$ is a hexagon Steinmann function

2. $\mathcal{E}$ is parity-even and dihedrally symmetric

3. The collinear limit to leading power is universal:

$$\lim_{v\to 0} \mathcal{E} = e^{-\frac{1}{4}\Gamma_{\text{cusp}}(L_2^v + 2\zeta_2)} + \mathcal{O}(\sqrt{v}\,\ln^{L-1} v).$$

In the weight 4 Steinmann space, no linear combination vanishes in all three collinear limits. Therefore the two-loop MHV amplitude is fully determined by just the above three conditions! Loop-expanding using $\mathcal{E} = \mathcal{E}^{(0)} + g^2\mathcal{E}^{(1)} + g^4\mathcal{E}^{(2)} + \ldots$, the result at tree-level is $\mathcal{E}^{(0)} = 1$, at one loop

$$\mathcal{E}^{(1)} = K^u_{1,1} + K^v_{1,1} + K^w_{1,1}\,, \tag{2.14}$$

and at two loops

$$\mathcal{E}^{(2)} = (1+C+C^2)[\Omega^{(2)} - K^u_{1,2,1} - 4K^u_{1,1,1,1} - \zeta_2 K^u_{1,1}] + 8\zeta_4\,, \tag{2.15}$$

where the cyclic rotation C is defined in eq. (2.3). This result agrees completely with refs. [42, 33].

For MHV at higher loops, and for NMHV, we imposed an additional "final-entry" condition, obtained by considering the action of the $\bar{Q}$ generator of dual superconformal transformations [64]. The MHV final-entry condition is simply $\mathcal{E}^{1-u} = -\mathcal{E}^u$, plus the cyclic relations. Similarly, the differential of the NMHV BDS-like remainder is spanned by the 18 elements listed in eq. (3.10) of ref. [38]. These conditions almost completely determine the higher-loop amplitudes; we need information from only one more limit.

2.5 Regge exponentiation and bootstrap

In the multi-Regge limit of $2 \to 4$ gluon scattering, the four outgoing gluons are strongly ordered in rapidity. The cross-ratios have the limits $u \to 1$, $v, w \to 0$, but on an analytically continued Riemann sheet which ensures nontrivial Lorentzian kinematics. This limit has been thoroughly analyzed for both MHV and NMHV amplitudes [58, 59, 60, 61, 62, 37]. Amplitudes exponentiate in terms of Fourier-Mellin variables ν, m which are conjugate to the transverse plane coordinates, schematically:

$$\mathcal{E}(\nu, m, vw) \xrightarrow{\text{Regge}} \Phi(\nu, m) \times \left(-1/\sqrt{vw}\right)^{\omega(\nu,m)} \tag{2.16}$$

where the Regge trajectory ω vanishes at tree level and Φ is an "impact factor". Exponentiation implies that terms with $\log^2(vw)$ or higher powers of the large logarithm are predicted by the multi-Regge limit at lower loops.

Remarkably, through five loops such terms suffice to fix all remaining parameters and uniquely determine $\mathcal{E}$, E, and $\tilde{E}$! Terms with $\log(vw)$ or lower were not needed, but rather led to predictions for the next loop order, enabling a pure bootstrap with no external information. The constraints are summarized in table 2.1.

With $\mathcal{E}$, E, and $\tilde{E}$ fixed through five loops we can evaluate them numerically on a variety of lines in cross-ratio space. Figure 2.2 shows the remainder function on the line (u, u, u). We have also used "hedgehog" variables [97] to generate multiple polylog representations of these functions in one bulk region [134].

Past implementations of the hexagon function bootstrap employed a variety of other constraints, which the Steinmann relations render unnecessary, or relegate to cross checks. For NMHV, the representation in terms of R-invariants has poles at kinematically spurious points that must cancel between different permutations of E and $\tilde{E}$ [33]. Now, after imposing the collinear constraint in table 2.1, the spurious poles cancel automatically. Similarly, for MHV and NMHV the $\bar{Q}$ equation predicts not only final entries, but next-to-final entries; however, again these constraints are satisfied automatically.

For both MHV and NMHV, the pentagon operator product expansion (POPE) [48, 49, 53, 57] served previously as a powerful bootstrap constraint [34, 37]. Now Regge

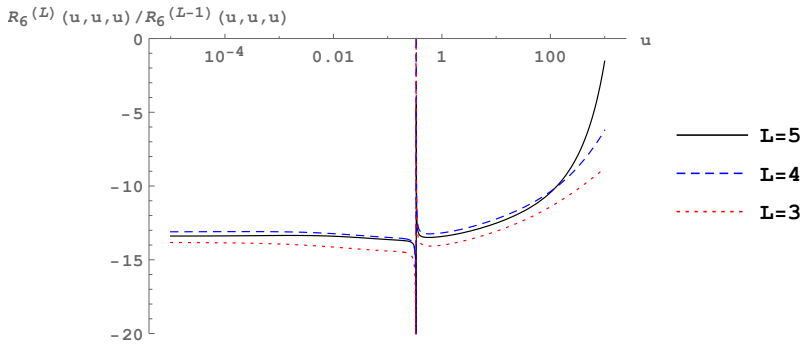

Figure 2.2: The remainder function $\mathcal{R}_6$, evaluated at ratios of successive loop orders L on the line $u = v = w$. The spike is an artifact due to $\mathcal{R}_6^{(L)}(u, u, u)$ crossing zero very close to $u = 1/3$ at each loop order.

exponentiation is enough to obtain a unique result. Nonetheless, we do check our results against the POPE predictions. We find complete agreement through five loops, to each order in the OPE we have computed (T^1 and T^2F^2 for MHV [48, 121, 50, 122, 109, 135] and T^1 for the (6134) component of NMHV [49, 121]).

In [37], two of the authors conjectured a relationship between the L-loop MHV amplitude and the $(L-1)$-loop NMHV amplitude. Our five-loop MHV amplitude allows us to verify this relation at one more loop order. Expressed in terms of the functions defined in eq. (2.13), it reads (using the coproduct notation [37])

$$\begin{aligned} g^2\,(2E-\mathcal{E}) \;&=\; \mathcal{E}^{y_u,y_u}+\mathcal{E}^{y_w,y_w}-3\mathcal{E}^{y_v,y_v}-\mathcal{E}^{v,v}-\mathcal{E}^{1-v,v} \\ &\quad +2(\mathcal{E}^{y_u,y_v}+\mathcal{E}^{y_w,y_v})-\mathcal{E}^{y_u,y_w}-\mathcal{E}^{y_w,y_u}. \end{aligned} \tag{2.17}$$

This relation calls out for explanation.

Remarkably, the space of Steinmann functions appears to be "not much larger" than required to contain $\mathcal{E}$, E and $\tilde{E}$, if we include all derivatives of higher loop amplitudes. Up to at least weight 6, the complete space is needed, apart from certain unexpected restrictions on zeta values. For example, the weight 2 functions found by taking 8 derivatives of $\mathcal{E}^{(5)}$, $E^{(5)}$ and $\tilde{E}^{(5)}$ span a 6 dimensional subspace of the 7 dimensional Steinmann space: $K^u_{1,1}$, $L^u_2 + 2\zeta_2$, plus cyclic; ζ_2 is not an independent element. In an ancillary file, we provide a coproduct representation of this trimmed

basis, which suffices to describe $\mathcal{E}$, E and $\tilde{E}$ through five loops. We also give HPL expressions for these functions on the lines $(1, v, v)$ and $(u, 1, 1)$ [134].

2.6 Conclusion

Leveraging the power of the Steinmann relations, we have bootstrapped six-point scattering amplitudes in planar $\mathcal{N} = 4$ super Yang-Mills through five loops. Loop by loop, these amplitudes are dramatically simpler than one would expect. Crucially, we did not need any external input: all constraints imposed are either general or are fixed by behavior at lower loops. Yet higher loops, or even finite coupling, may well be accessible too.

Unlike other techniques used to calculate in $\mathcal{N} = 4$ SYM, the Steinmann relations apply in general quantum field theories. Their strength here suggests that these often-neglected constraints may have broader applicability, perhaps making similar bootstrap techniques viable in other theories, such as QCD.

Chapter 3

Multi-Loop Positivity of the Amplitude

3.1 Introduction

There has been substantial progress from many different perspectives in understanding and calculating perturbative scattering amplitudes in $\mathcal{N} = 4$ super-Yang-Mills theory [15, 16], particularly in the planar limit of a large number of colors. The standard Feynman diagram expansion, as well as more modern methods such as generalized unitarity, are based on the expansion of the (multi)loop amplitude in terms of different sets of building blocks. These pieces are then individually integrated over the loop momenta, and the final amplitude corresponds to the sum over all terms. In recent years, it was shown that both the total integrand and the final amplitudes enjoy some extraordinary properties. As it turns out, there is a completely different way to think about each quantity, holistically and without reference to any expansion in building blocks.

For the integrand there exists a complete geometric reformulation in terms of the Amplituhedron, which is a generalization of projective polygons into Grassmannians [13, 14] (see also refs. [136, 137, 138, 139, 140, 141] for recent progress). The idea is to rewrite the kinematical and helicity variables in terms of bosonized momentum twistors Z serving as vertices of a geometric object – the Amplituhedron – whose

volume is equal to the integrand of scattering amplitudes in planar $\mathcal{N} = 4$ SYM. The definition of this space involves a generalization of the positive Grassmannian that appears in the context of on-shell diagrams [11].

On the other hand, there has also been great progress in understanding the space of transcendental functions that contains the final amplitudes. In many cases these functions are iterated integrals [87], also known as multiple polylogarithms [90, 91]. The weight, or number of integrations, is 2ℓ for perturbative amplitudes at loop order ℓ. While the origin of these functions comes from the "dlog" structure of the integrand, the precise connection is still not understood in general. For example, there may be obstructions to carrying out the dlog integrations in terms of iterated integrals. The two-loop equal-mass sunrise integral is in this elliptic class [142, 143], as is an integral entering the N^3MHV 10-point scattering amplitude in planar $\mathcal{N} = 4$ SYM [144]. However, it has been argued that MHV and NMHV amplitudes in this theory should be expressible solely in terms of multiple polylogarithms [11, 85, 86].

A function composed of multiple polylogarithms has a *symbol* [42], which is constructed essentially by repeated differentiation of the function. The alphabet, or set of letters appearing in the symbol, characterizes the function space. These letters seem to be closely related to cluster algebras [39, 40]. Once one knows the alphabet, as well as where the branch cuts are located, one can construct the function space iteratively. The number of such functions turns out to be much smaller than the number of independent physical constraints on them, allowing for a unique determination of the amplitude as a whole without ever inspecting the precise integrand or its decomposition into building blocks. This program has been carried out for the six-point amplitude through five loops [32, 33, 37, 35, 38, 68], and for the symbol of the seven-point amplitude through three loops [41].

Given this excellent progress in understanding both the integrand and amplitude holistically, it would be great to bring them together. It is not clear yet how the properties of the Amplituhedron extend from the integrand to the final amplitudes. However, there is an extension of the Amplituhedron conjecture, namely the existence of the *dual* Amplituhedron, which we will test indirectly in this paper. In ref. [69] it was argued that if the original Amplituhedron can be reformulated into a dual picture

where the integrand is directly a volume of this space, then this function should be positive when evaluated inside the Amplituhedron. This positivity property has been verified explicitly for various integrands up to high loop order. It also turns out to be true for the integrand of the ratio function – a ratio of amplitudes with different helicities which is free of infrared (IR) divergences.

It was then conjectured that this positivity property might also hold for the final transcendental function, rather than just the integrand. In general, the transcendental functions that determine scattering amplitudes are complex-valued. However, there exists a Euclidean region in which the amplitude is real-valued, and thus it is possible to define positivity consistently. For the six-point amplitude, the cross-ratios u, v, w are all real and positive in this Euclidean region. The conjecture is that the quantities under consideration are positive in a subregion of this Euclidean region that is selected by the properties of the Amplituhedron.

This conjecture was explicitly verified at one loop. In this paper we will check the statement through five loops for the NMHV case, providing strong evidence that the conjecture is indeed true. In addition, we show that the same is true for the IR-finite BDS-like normalized MHV amplitude. There are many ways to subtract IR divergences but the positivity conjecture more or less singles out this function. The positivity property is very non-trivial and we do not know how to prove it in full generality even at one loop, not to mention higher-loop examples where our analytic understanding is even more limited.

To show a simple example, let us consider a function of positive variables $u, w > 0$,

$$F(u, w) = \mathrm{Li}_2(1-u) + \mathrm{Li}_2(1-w) + \log u \log w - \zeta_2 \,. \tag{3.1}$$

This function will appear later in this paper in a particular limit of the NMHV one-loop ratio function, as well as of the BDS-like remainder function. In the first case the Amplituhedron picture dictates that $F(u, w) < 0$ whenever $u + w > 1$, while in the second case it requires $F(u, w) > 0$ for $u + w < 1$. Even in this simple case positivity is not manifest, i.e. the answer cannot be decomposed into a sum of obviously positive terms (although the positivity proof here is simple, see section 3.3.2). Note that for

$w = 1 - u$ we get the famous dilogarithm identity which sets $F(u, 1-u) = 0$, which also represents a physical vanishing condition on the ratio function in a collinear limit.

In general, positivity relies not only on the sign of transcendental functions like $F(u, w)$, but also on the sign of rational prefactors. For generic kinematics neither has uniform sign on its own. Nevertheless, the sign ambiguities of these individual parts conspire to produce quantities with uniform sign. The statement is even more interesting because not only the bosonic external data, but also the fermionic variables, play a crucial role in establishing this surprising and remarkable property. In the rest of this paper we will flesh out this statement, showcasing numerous regions in which positivity holds.

In this paper, whenever we refer to positivity, we mean that perturbative coefficients in the loop expansion of a given quantity are positive when the expansion parameter is the *negative* of the 't Hooft coupling, $-\lambda = -g^2 N_c$. Or, in terms of a standard, positive 't Hooft coupling (or multiple thereof), we will be testing for strict *sign-alternation* with loop order. That is, one-loop terms should be negative, two-loop terms positive, three-loop terms negative, and so on. From the point of view of the (dual) Amplituhedron, the overall sign at a given loop order is not dictated; what is really expected is a *uniform* sign as a function of the kinematics. However, we know empirically that the sign alternates for low loop orders, and we also expect it to alternate at very high loop orders. The reason for the latter statement is that planar $\mathcal{N} = 4$ SYM has no renormalons and no instantons, and so it is expected to have a finite radius of convergence of the perturbation theory. For some quantities, the radius of convergence is known: it is $\lambda_c = \pi^2$ for the light-like cusp anomalous dimension [114], and $\lambda_c \approx 14.7$ for the Bremsstrahlung function, which is another limit of the velocity-dependent cusp anomalous dimension [145, 146]. These quantities have no singularity on the positive λ axis. Hence their finite radius of convergence is controlled by a singularity for negative λ. This fact implies sign alternation at very large perturbative orders, with successive perturbative coefficients increasing by a factor that approaches $-1/\lambda_c$.

This paper is organized as follows. We begin in section 3.2 by describing the

regions in which the Amplituhedron construction leads to positive tree-level amplitudes; these regions are where we wish to test the corresponding loop amplitudes for positivity. Section 3.3 then presents some simple one-loop examples in which this positivity holds for the NMHV ratio function. We also define the double-scaling limit, in which certain monotonicity properties of the amplitude are manifest. In section 3.4 we explore this limit at higher loops, both analytically on certain special lines and numerically throughout the full region. We go on in section 3.5 to present numerical evidence for positivity outside of special limits, in the full space of cross-ratios selected by the Amplituhedron construction. Section 3.6 discusses the positivity properties of the MHV amplitude, and we conclude in section 3.7.

Appendix E proves positivity and monotonicity for a quantity, $c_1^{(2)}(u, w)$, relevant at two loops. We also attach ancillary files containing expressions for the quantities we consider on special lines threading the kinematic space.

3.2 From the Amplituhedron to positive kinematics

In this section we review the essential ingredients of the Amplituhedron construction of the multi-loop integrand for planar $\mathcal{N} = 4$ SYM, and show how this setup dictates where we should inspect the multi-loop six-point amplitudes for positivity.

The Amplituhedron space [13, 14] $\mathcal{Y}$ is implicitly labeled by n, k, and ℓ, where n is the number of external legs, k is the number of negative gluon helicities minus 2, and ℓ is the loop order. The formal definition of $\mathcal{Y}$ is given by the matrix multiplication

$$\mathcal{Y} = \mathcal{C} \cdot Z, \tag{3.2}$$

where $\mathcal{C}$ is a $(k+2\ell)\times n$ matrix with certain positivity properties, and Z is an $n\times(4+k)$ matrix with all $(4+k)\times(4+k)$ minors positive. The matrix Z corresponds to external data (momentum twistors and Grassmann variables); Z only depends on k while the $\mathcal{C}$ matrix also depends on ℓ. The loop integrand Ω is then a form which behaves logarithmically on the boundaries of $\mathcal{Y}$.

The conjecture made in ref. [69] is that the form Ω is positive when the measure is stripped off and it is evaluated inside the Amplituhedron, i.e. for $\mathcal{Y}$ satisfying eq. (3.2) with positive $\mathcal{C}$ and Z matrices. This property does not follow from the original Amplituhedron proposal. Rather it would provide evidence for the existence of a "dual Amplituhedron" of which Ω is literally the volume. This space has not been found yet, but the fact that Ω is observed to be positive is very encouraging.

Let us now consider the final amplitude rather than the integrand. It has a very complicated branch-cut structure, but no dependence on the loop momenta. If an Amplituhedron-like construction exists for the final amplitude then it is natural to impose the same positivity constraints, but now with $\ell = 0$, i.e.

$$Y = C \cdot Z, \tag{3.3}$$

where C is the matrix that appears in the definition of the tree-level Amplituhedron. The conjecture now is that a properly-defined amplitude must be positive – or rather, sign-alternating with loop order – if evaluated for Y and Z matrices satisfying the positivity conditions. We restrict ourselves to our cases of interest, MHV and NMHV amplitudes ($k = 0$ and 1), and review what these conditions imply.

3.2.1 MHV positive kinematics

For MHV amplitudes we have $k = 0$ and $l = 0$ so there is no C matrix. That is, the Y space in eq. (3.3) becomes trivial and the only conditions come from the positivity of the $(4 \times n)$ matrix Z. In this case the column vectors composing Z are directly the 4-dimensional momentum twistors Z_a and we have to keep them positive – in the sense that the following (4×4) minors of the Z matrix should be positive:

$$Z = \begin{pmatrix} \uparrow & \uparrow & \uparrow & \dots & \uparrow & \uparrow \\ Z_1 & Z_2 & Z_3 & \dots & Z_{n-1} & Z_n \\ \downarrow & \downarrow & \downarrow & \dots & \downarrow & \downarrow \end{pmatrix} \quad \begin{array}{c} \text{with } \langle abcd \rangle \equiv \det(Z_a, Z_b, Z_c, Z_d) > 0 \\ \text{for } a < b < c < d. \end{array} \tag{3.4}$$

Let us now parametrize the positive Z matrix for $n = 6$. Using a $GL(4)$ transformation we fix the first four columns to be the unit matrix, and parametrize the remaining two columns with eight positive parameters $x_a > 0$, $y_b > 0$. One solution that makes all (4×4) minors positive is

$$Z = \begin{pmatrix} 1 & 0 & 0 & 0 & -x_1 & -y_1 - y_2\frac{x_1}{x_2} - y_3\frac{x_1}{x_3} - y_4\frac{x_1}{x_4} \\ 0 & 1 & 0 & 0 & x_2 & y_2 + y_3\frac{x_2}{x_3} + y_4\frac{x_2}{x_4} \\ 0 & 0 & 1 & 0 & -x_3 & -y_3 - y_4\frac{x_3}{x_4} \\ 0 & 0 & 0 & 1 & x_4 & y_4 \end{pmatrix}. \tag{3.5}$$

We can now build three different dual-conformal cross ratios,

$$u = \frac{\langle 6123\rangle\langle 3456\rangle}{\langle 6134\rangle\langle 2356\rangle}, \quad v = \frac{\langle 1234\rangle\langle 4561\rangle}{\langle 1245\rangle\langle 3461\rangle}, \quad w = \frac{\langle 2345\rangle\langle 5612\rangle}{\langle 2356\rangle\langle 4512\rangle}. \tag{3.6}$$

We also consider the combinations

$$\varepsilon \equiv 1 - u - v - w, \qquad \Delta = \varepsilon^2 - 4uvw. \tag{3.7}$$

From the positive parametrization (3.5) of the Z matrix we get,

$$u = \frac{x_2^2 x_3^2 y_1 y_4}{PQ}, \quad v = \frac{x_3 x_4 y_2}{P}, \quad w = \frac{x_1 x_2 y_3}{Q}, \tag{3.8}$$

$$\varepsilon = \frac{x_2 x_3 (x_2 x_4 y_1 y_3 + x_1 x_3 y_2 y_4)}{PQ}, \quad \Delta = \frac{x_2^2 x_3^2 (x_1 x_3 y_2 y_4 - x_2 x_4 y_1 y_3)^2}{P^2 Q^2}, \tag{3.9}$$

where $P = x_3x_4y_2 + x_2x_4y_3 + x_2x_3y_4$, $Q = x_2x_3y_1 + x_1x_3y_2 + x_1x_2y_3$. For positive values of x_a, y_b the cross ratios u, v, w and ε, Δ are all manifestly positive. These inequalities combine to define conditions for the MHV positive region,

$$u, v, w > 0, \quad u + v + w < 1, \quad (1 - u - v - w)^2 > 4uvw, \tag{3.10}$$

which restrict the cross ratios to be relatively close to the origin, in contrast to what we will find for the NMHV positive region. We refer to this region as Region I (see

ref. [34] and eq. (3.79) below). The only place that ε can approach zero in Region I, given the constraint on Δ, is for $v \to 0$, $u + w \to 1$, or cyclic permutations of this line. In this limit, two gluons become collinear.

Now that we have identified MHV positive kinematics, we would like to conjecture that a properly-defined IR-finite part of the MHV amplitude is positive for any positive values $x_a, y_b > 0$. However, individual on-shell amplitudes are IR divergent, and there is not a unique way to obtain a finite quantity by removing the IR divergences. The original way that IR divergences were removed (while preserving dual conformal symmetry) was to divide by the BDS ansatz [31]. While this procedure leads to remainder functions with smooth collinear limits [75, 76], it breaks a global analytic property known as the Steinmann relations [65, 66, 67]. To preserve the Steinmann relations [68], at six points (or seven points) one can divide by a unique "BDS-like" ansatz [113, 38]. Yet this procedure sacrifices the vanishing in collinear limits of the six-point BDS remainder function, and the collinear limits form a boundary of the positive region (e.g. $v \to 0$, $u + w \to 1$ makes ε and Δ both vanish). There are also dual-conformal IR regulators based on the Wilson loop interpretation of the amplitude [48], but they break a dihedral symmetry. In short, there is no unique way to define an IR finite part of the MHV amplitude, nor one that is clearly optimal. We will discuss the positivity properties of these various choices in section 3.6.

3.2.2 NMHV positive kinematics

In contrast, when we also consider the NMHV amplitude there is a natural way to form an IR finite quantity, the *ratio function*, which is defined (at six points) by dividing the NMHV super-amplitude by the MHV super-amplitude [29]. IR divergences are helicity-independent and cancel between numerator and denominator. We will inspect the ratio function for NMHV positive kinematics.

For the NMHV case, $k = 1$, the Amplituhedron lives in a projective space $\mathbb{P}^4$. It is defined as all points Y that are linear combinations of Z_a with positive coefficients,

$$Y = C \cdot Z = c_1 Z_1 + c_2 Z_2 + \cdots + c_n Z_n \quad \text{with } c_a > 0, \tag{3.11}$$

where the Z_a are now five-dimensional. They can be written as

$$Z_a = \begin{pmatrix} z_a \\ \phi \cdot \eta_a \end{pmatrix}, \tag{3.12}$$

where the first four components are momentum twistor variables z_a associated with each particle label, $a = 1, 2, \ldots, n$ for n-point scattering. The fifth (last) component is the contraction $\phi \cdot \eta_a = \epsilon_{IJ}\phi^I \eta_a^J$, $I, J = 1, 2, 3, 4$, of an auxiliary Grassmann variable ϕ^I with the standard Grassmann variable η_a^J of on-shell superspace [77, 78, 29, 80]. These bosonic variables then carry all information about the external particles in the scattering. The bosonized momentum twistors are projective variables, defined up to rescaling $Z_a \to tZ_a$.

Positivity conditions are then imposed directly on the five-dimensional Z_a rather than the four-dimensional part z_a. The $(n \times 5)$-dimensional matrix Z has all (5×5) minors positive; that is,

$$\langle abcde \rangle \equiv \det(Z_a, Z_b, Z_c, Z_d, Z_e) > 0 \qquad \text{for} \quad a < b < c < d < e. \tag{3.13}$$

Geometrically, the Z_a form a convex configuration in real projective space $\mathbb{P}^4$.

In addition to five-brackets containing five Z_a, we can also have five-brackets including the point Y in eq. (3.11), which lies inside the Amplituhedron. The Y-containing five-brackets are given by,

$$\langle Y abcd \rangle \equiv \det(Y, Z_a, Z_b, Z_c, Z_d). \tag{3.14}$$

A subset of these five-brackets is positive when Y is in the Amplituhedron, specifically those with two pairs of consecutive indices: $\langle Y\, a\, a{+}1\, b\, b{+}1 \rangle > 0$ for all a, b. The three-planes $(Z_a\, Z_{a+1}\, Z_b\, Z_{b+1})$ are boundaries of the Amplituhedron. The condition $\langle Y\, a\, a{+}1\, b\, b{+}1 \rangle > 0$ puts the point Y on the correct side of the boundary, inside the Amplituhedron. From a physics perspective, the term $\langle Y\, a\, a{+}1\, b\, b{+}1 \rangle \sim s_{a+1\ldots b} \equiv (p_{a+1} + \cdots + p_b)^2$ corresponds to a factorization pole of the tree-level amplitude.

For the six-point case, we redefine the three cross ratios defined in eq. (3.6) by

inserting Y into all the four-brackets to make them five-brackets,

$$u = \frac{\langle Y6123\rangle\langle Y3456\rangle}{\langle Y6134\rangle\langle Y2356\rangle}\,, \quad v = \frac{\langle Y1234\rangle\langle Y4561\rangle}{\langle Y1245\rangle\langle Y3461\rangle}\,, \quad w = \frac{\langle Y2345\rangle\langle Y5612\rangle}{\langle Y2356\rangle\langle Y4512\rangle}\,. \tag{3.15}$$

The positive parametrization is now much simpler than in the MHV case because the matrix Z is (6×5) rather than (6×4). A natural parametrization of Z in terms of five positive parameters $x_a > 0$ is,

$$Z = \begin{pmatrix} 1 & 0 & 0 & 0 & 0 & x_1 \\ 0 & 1 & 0 & 0 & 0 & -x_2 \\ 0 & 0 & 1 & 0 & 0 & x_3 \\ 0 & 0 & 0 & 1 & 0 & -x_4 \\ 0 & 0 & 0 & 0 & 1 & x_5 \end{pmatrix} \qquad \begin{aligned} &\langle 12345\rangle = 1, \quad \langle 23456\rangle = x_1, \\ &\langle 13456\rangle = x_2, \quad \langle 12456\rangle = x_3, \\ &\langle 12356\rangle = x_4, \quad \langle 12346\rangle = x_5. \end{aligned} \tag{3.16}$$

Using this parametrization and $Y = C\cdot Z$ from eq. (3.11), we can compute all $\binom{6}{2} = 15$ five-brackets $\langle Yabcd\rangle$:

$$\begin{aligned} &\langle Y1234\rangle = c_5x_6 + c_6x_5, \quad \langle Y1235\rangle = c_6x_4 - c_4x_6, \quad \langle Y6123\rangle = c_4x_5 + c_5x_4, \\ &\langle Y1245\rangle = c_3x_6 + c_6x_3, \quad \langle Y1246\rangle = c_3x_5 - c_5x_3, \quad \langle Y1256\rangle = c_3x_4 + c_4x_3, \\ &\langle Y1345\rangle = c_6x_2 - c_2x_6, \quad \langle Y3461\rangle = c_2x_5 + c_5x_2, \quad \langle Y1356\rangle = c_4x_2 - c_2x_4, \\ &\langle Y4561\rangle = c_2x_3 + c_3x_2, \quad \langle Y2345\rangle = c_1x_6 + c_6x_1, \quad \langle Y2346\rangle = c_1x_5 - c_5x_1, \\ &\langle Y2356\rangle = c_1x_4 + c_4x_1, \quad \langle Y2456\rangle = c_1x_3 - c_3x_1, \quad \langle Y3456\rangle = c_1x_2 + c_2x_1, \end{aligned} \tag{3.17}$$

where $x_6 \equiv 1$ is added to make the expressions more uniform.

From eq. (3.15), the cross ratios are now

$$u = \frac{(c_1x_2 + c_2x_1)(c_4x_5 + c_5x_4)}{(c_2x_5 + c_5x_2)(c_1x_4 + c_4x_1)}\,, \qquad v = \frac{(c_2x_3 + c_3x_2)(c_5x_6 + c_6x_5)}{(c_2x_5 + c_5x_2)(c_3x_6 + c_6x_3)}\,,$$
$$w = \frac{(c_1x_6 + c_6x_1)(c_3x_4 + c_4x_3)}{(c_1x_4 + c_4x_1)(c_3x_6 + c_6x_3)}\,. \tag{3.18}$$

As in the MHV case, the cross ratios are all positive.

Denoting $W = (c_1x_4 + c_4x_1)(c_2x_5 + c_5x_2)(c_3x_6 + c_6x_3)$, we get for the quantities ε and Δ defined in eq. (3.7),

$$\varepsilon = -\frac{P_1(x_a, c_b)}{W} < 0, \qquad \Delta = \frac{[P_2(x_a, c_b)]^2}{W^2} > 0, \tag{3.19}$$

where the $P_j(x_a, c_b)$ are polynomials in x_a, c_b with positive coefficients. Notice that the sign condition on ε has flipped from the MHV case, pushing the cross ratios away from the origin.

The NMHV amplitude also contains R-invariants, defined as the following function of momentum twistors z_a and Grassmann variables η_a:

$$R[a\,b\,c\,d\,e] = \frac{(\eta_a\langle bcde\rangle + \eta_b\langle cdea\rangle + \eta_c\langle deab\rangle + \eta_d\langle eabc\rangle + \eta_e\langle abcd\rangle)^4}{\langle abcd\rangle\langle bcde\rangle\langle cdea\rangle\langle deab\rangle\langle eabc\rangle}. \tag{3.20}$$

In the bosonized language, the R-invariants become functions of five-brackets, projective in all variables, which we denote as

$$[a\,b\,c\,d\,e] = \frac{\langle Y\,d^4Y\rangle\langle abcde\rangle^4}{\langle Y\,abcd\rangle\langle Y\,bcde\rangle\langle Y\,cdea\rangle\langle Y\,deab\rangle\langle Y\,eabc\rangle}, \tag{3.21}$$

where $\langle Y\,d^4Y\rangle$ is the measure in Y. For the six-point case, it is convenient to label this object by the missing index, and to omit the measure, defining

$$(1) \equiv \frac{[23456]}{\langle Y\,d^4Y\rangle} = \frac{\langle 23456\rangle^4}{\langle Y2345\rangle\langle Y2346\rangle\langle Y2456\rangle\langle Y2356\rangle\langle Y3456\rangle} \tag{3.22}$$

and similarly for $(2) = [34561]$, $(3) = [45612]$, etc.

The form for the tree-level NMHV Amplituhedron is then

$$\Omega^{\text{tree}}_{6,1} = (1) + (3) + (5) = (2) + (4) + (6). \tag{3.23}$$

This is also the bosonized version of the tree-level NMHV ratio function $\mathcal{P}^{\text{tree}}_{6,1}$, see section 3.2.3.

Using the positive parametrization (3.11), we can rewrite the bosonized R-invariants

as

$$
\begin{aligned}
(1) &= \frac{x_1^4}{(c_1x_6+c_6x_1)(c_1x_2+c_2x_1)(c_1x_3-c_3x_1)(c_1x_4+c_4x_1)(c_1x_5-c_5x_1)},\\
(2) &= \frac{x_2^4}{(c_1x_2+c_2x_1)(c_2x_3+c_3x_2)(c_2x_4-c_4x_2)(c_2x_5+c_5x_2)(c_2x_6-c_6x_2)},\\
(3) &= \frac{x_3^4}{(c_2x_3+c_3x_2)(c_3x_4+c_4x_3)(c_3x_5-c_5x_3)(c_3x_6+c_6x_3)(c_3x_1-c_1x_3)},\\
(4) &= \frac{x_4^4}{(c_3x_4+c_4x_3)(c_4x_5+c_5x_4)(c_4x_6-c_6x_4)(c_1x_4+c_4x_1)(c_4x_2-c_2x_4)},\\
(5) &= \frac{x_5^4}{(c_4x_5+c_5x_4)(c_5x_6+c_6x_5)(c_1x_5-c_5x_1)(c_2x_5+c_5x_2)(c_3x_5-c_5x_3)},\\
(6) &= \frac{x_6^4}{(c_5x_6+c_6x_5)(c_1x_6+c_6x_1)(c_2x_6-c_6x_2)(c_3x_6+c_6x_3)(c_4x_6-c_6x_4)}.
\end{aligned}
\tag{3.24}
$$

Five-brackets corresponding to spurious poles can be identified in eq. (3.17) as the expressions containing minus signs, while those corresponding to physical poles are manifestly positive. Each R-invariant (a) contains two spurious poles. For example, (1) has $\langle Y2346\rangle$ and $\langle Y2456\rangle$. The spurious poles do not have a fixed sign for all $c_b, x_a > 0$, e.g. $\langle Y2346\rangle = c_1x_5 - c_5x_1$. Therefore, the invariant (1) also does not have a fixed sign and it is not a manifestly positive object, and similarly for the other (a). Only in the sum (3.23) do these poles cancel, so that $\Omega^{\text{tree}}_{6,1}$ can be positive in the full positive region.

In fact, we can write the tree amplitude in the form,

$$
\Omega^{\text{tree}}_{6,1} = \frac{\mathcal{N}(x_a, c_b)}{\prod\limits_{|j-k|=1 \text{ or } 3} (c_jx_k + c_kx_j)}\,, \tag{3.25}
$$

where $\mathcal{N}(x_a, c_b)$ is a polynomial in x_a, c_b with all positive coefficients [69].

3.2.3 The ratio function

Scattering amplitudes of massless particles suffer from IR divergences from both soft and collinear virtual exchange. It is necessary to introduce a regulator to get a well-defined answer. In the planar theory, for gauge group $SU(N_c)$ with $N_c \to \infty$, the IR divergences exponentiate in a relatively simple fashion. In dimensional regularization with $D = 4 - 2\epsilon$, the poles in ϵ in planar $\mathcal{N} = 4$ SYM amplitudes are captured by the BDS ansatz [31],

$$\mathcal{M}_{n,k} = \mathcal{M}^{\text{tree}}_{n,k} \cdot \exp\left[\sum_{\ell=1}^{\infty} a^\ell \left(f^{(\ell)}(\epsilon) \cdot \mathcal{A}^{1-\text{loop}}_{n,0}(\ell\epsilon) + \text{finite}\right)\right], \tag{3.26}$$

where $a = g^2 N_c/(8\pi^2)$ is the 't Hooft coupling, $f^{(\ell)}(\epsilon) = f_0^{(\ell)} + f_1^{(\ell)}\epsilon + f_2^{(\ell)}\epsilon^2$ for some constants $f_k^{(\ell)}$, and $\mathcal{A}^{1-\text{loop}}_{n,0}(\epsilon)$ is the regulated one-loop MHV amplitude $\mathcal{M}^{1-\text{loop}}_{n,0}(\epsilon)$ divided by the tree-level amplitude $\mathcal{M}^{\text{tree}}_{n,0}$.

In the MHV case, $k = 0$, the finite part in the exponential in eq. (3.26) is called the remainder function $R_n^{(\ell)}$,

$$\begin{aligned}\mathcal{M}_{n,0} &= \mathcal{M}^{\text{tree}}_{n,0} \cdot \exp\left[\sum_{\ell=1}^{\infty} a^\ell \left(f^{(\ell)}(\epsilon) \cdot \mathcal{A}^{1-\text{loop}}_{n,0}(\ell\epsilon) + R_n^{(\ell)}\right)\right] \\ &\equiv \mathcal{M}^{\text{BDS}}_{n,0}(\epsilon) \cdot \exp[R_n]\,,\end{aligned} \tag{3.27}$$

and it is dual conformally invariant. However, we can still move finite, dual conformally invariant terms between the first and second terms in this expression. Correspondingly, there are a few possible different definitions of the remainder function. In section 3.6 we will discuss the possibilities in more detail, and describe one choice which appears to satisfy MHV positivity properties.

There is a cleaner and less ambiguous way to define an IR-finite object in the context of scattering amplitudes, simply by taking a ratio of two amplitudes with different helicities [29]. Because the IR divergences (3.26) are universal, one can divide any amplitude $\mathcal{M}_{n,k}$ by the MHV amplitude $\mathcal{M}_{n,0}$ and get an IR finite ratio function $\mathcal{P}_{n,k}$. Expanding the ratio in the coupling constant a, we define the loop

expansion coefficients of the ratio function as,

$$\mathcal{P}_{n,k} = \frac{\mathcal{M}_{n,k}}{\mathcal{M}_{n,0}} = \mathcal{P}_{n,k}^{\text{tree}} + a \cdot \mathcal{P}_{n,k}^{1-\text{loop}} + a^2 \cdot \mathcal{P}_{n,k}^{2-\text{loop}} + \dots , \tag{3.28}$$

while those of the amplitude normalized by the MHV tree super-amplitude (an IR divergent quantity) are denoted by

$$\mathcal{A}_{n,k} = \frac{\mathcal{M}_{n,k}}{\mathcal{M}_{n,0}^{\text{tree}}} = \mathcal{P}_{n,k}^{\text{tree}} + a \cdot \mathcal{A}_{n,k}^{1-\text{loop}} + a^2 \cdot \mathcal{A}_{n,k}^{2-\text{loop}} + \dots . \tag{3.29}$$

The two sets of expansion coefficients are related by,

$$\begin{aligned} \mathcal{P}_{n,k}^{1-\text{loop}} &= \mathcal{A}_{n,k}^{1-\text{loop}} - \mathcal{P}_{n,k}^{\text{tree}} \cdot \mathcal{A}_{n,0}^{1-\text{loop}} , \\ \mathcal{P}_{n,k}^{2-\text{loop}} &= \mathcal{A}_{n,k}^{2-\text{loop}} - \mathcal{P}_{n,k}^{\text{tree}} \cdot \mathcal{A}_{n,0}^{2-\text{loop}} - \mathcal{P}_{n,k}^{1-\text{loop}} \cdot \mathcal{A}_{n,0}^{1-\text{loop}} , \end{aligned} \tag{3.30}$$

and so on.

The ratio function $\mathcal{P}_{n,k}^{\ell-\text{loop}}$ corresponds to a linear combination of products of amplitudes with different signs. Therefore, it would be quite surprising if it had any positivity properties. However, numerical checks performed in ref. [69] for the one-loop NMHV n-point amplitude for $n \leq 12$, and for the one-loop N^{2}MHV amplitude for $n \leq 9$ show that this is indeed true!

Let us now focus on the six-point case in more detail. As was pointed out in ref. [29], the ratio function can be expressed in terms of two transcendental functions, $V(u, v, w)$ and $\widetilde{V}(y_u, y_v, y_w)$,

$$\begin{aligned} \mathcal{P}_{6,1} = \frac{1}{2}\Big(&[(1)+(4)]V(u,v,w) + [(2)+(5)]V(v,w,u) + [(3)+(6)]V(w,u,v) \\ &+ [(1)-(4)]\widetilde{V}(y_u,y_v,y_w) - [(2)-(5)]\widetilde{V}(y_v,y_w,y_u) + [(3)-(6)]\widetilde{V}(y_w,y_u,y_v)\Big) , \end{aligned} \tag{3.31}$$

where the cross ratios u, v, w are written in terms of our bosonized variables in

eq. (3.15), and the extended cross ratios y_u, y_v, y_w [33] are also bosonized:

$$y_u = \frac{\langle Y1345\rangle\langle Y2456\rangle\langle Y1236\rangle}{\langle Y1235\rangle\langle Y3456\rangle\langle Y1246\rangle}\,, \quad y_v = \frac{\langle Y1235\rangle\langle Y2346\rangle\langle Y1456\rangle}{\langle Y1234\rangle\langle Y2456\rangle\langle Y1356\rangle}\,,$$
$$y_w = \frac{\langle Y2345\rangle\langle Y1356\rangle\langle Y1246\rangle}{\langle Y1345\rangle\langle Y2346\rangle\langle Y1256\rangle}\,. \tag{3.32}$$

The function V is even under a parity symmetry that inverts $y_i \leftrightarrow 1/y_i$, and leaves u, v, w invariant. The function $\widetilde{V}$ is parity-odd, changing sign under this inversion. For this reason, it is better to think of $\widetilde{V}$ as a function of y_u, y_v, y_w rather than u, v, w.

Note that the extended cross ratios do not have any positivity properties due to the presence of spurious poles. Under a cyclic shift $Z_a \to Z_{a+1}$ they transform as

$$y_u \to \frac{1}{y_v}\,, \qquad y_v \to \frac{1}{y_w}\,, \qquad y_w \to \frac{1}{y_u}\,, \tag{3.33}$$

and the standard cross ratios transform as $u \to v$, $v \to w$, $w \to u$. The ratio function is symmetric under both cyclic shifts and dihedral flips. The combined symmetry group is D_6, although acting on the cross ratios u, v, w it reduces to S_3, i.e. all permutations of u, v, w. The individual functions V and $\tilde{V}$ are (anti)symmetric under a Z_2 subgroup of S_3 that leaves v fixed:

$$V(u, v, w) = V(w, v, u), \qquad \tilde{V}(y_u, y_v, y_w) = -\tilde{V}(y_w, y_v, y_u). \tag{3.34}$$

The transcendental functions V and $\tilde{V}$ have a Euclidean sheet on which they are real, when the cross ratios lie in the positive octant $u, v, w > 0$. We evaluate them on this sheet, with the cross ratios and R-invariants further restricted by the positive parametrization $c_b, x_a > 0$. (In some physical scattering regions V and $\tilde{V}$ would acquire imaginary parts, which would make discussing positivity difficult.)

3.3 One-loop ratio function

At one loop, the parity-odd part vanishes, $\widetilde{V}^{(1)} = 0$, and the full ratio function can be written as

$$2\mathcal{P}_{6,1}^{1-\text{loop}} = [(1)+(4)]V^{(1)}(u,v,w) + [(2)+(5)]V^{(1)}(v,w,u) + [(3)+(6)]V^{(1)}(w,u,v), \tag{3.35}$$

where the one-loop function $V^{(1)}(u,v,w)$ is given by

$$\begin{aligned} V^{(1)}(u,v,w) &= \frac{1}{2}\Big[\text{Li}_2(1-u) + \text{Li}_2(1-v) + \text{Li}_2(1-w) \\ &\qquad + \log u \log v - \log u \log w + \log v \log w - 2\zeta_2\Big]\,. \end{aligned} \tag{3.36}$$

Our claim is that eq. (3.35) is negative (because the loop order is odd) within the positive region. Note that the individual pieces in this formula do not have definite signs, neither the R-invariants (a), nor the function $V^{(1)}$ which has both plus and minus signs in front of individual terms. Depending on the values of u, v, w, different terms can dominate.

For some purposes it is convenient to separate out the Li_2 part of the expression. Note that the Li_2 part is invariant under S_3 permutations, and therefore it multiplies all R-invariants (a), which can be assembled into the tree-level amplitude,

$$\begin{aligned} 2\mathcal{P}_{6,1}^{1-\text{loop}} = \mathcal{P}_{6,1}^{\text{tree}} \cdot [&\text{Li}_2(1-u) + \text{Li}_2(1-v) + \text{Li}_2(1-w) - 2\zeta_2] \\ &+ [(1)-(2)+(3)]\log u \log v + [(2)-(3)+(4)]\log v \log w \\ &+ [(3)-(4)+(5)]\log w \log u\,, \end{aligned} \tag{3.37}$$

where we have used the identity $(1)+(3)+(5) = (2)+(4)+(6)$. For some purposes it is more convenient to use eq. (3.35), for others eq. (3.37).

3.3.1 Simple examples of positivity

Let us give a few examples where the overall sign can be easily understood.

Example 1

Our first case is the point $(u, v, w) = (1, 1, 1)$, which was studied in detail in ref. [69]. To reach this point, we set $c_3 = c_1 x_3/x_1$ and $c_5 = c_1 x_5/x_1$. This preserves positivity of c_b, x_a, and so it is inside the Amplituhedron. Kinematically, it corresponds to setting $\langle Y2456\rangle = \langle Y2346\rangle = 0$, which is a spurious boundary of the tree-level Amplituhedron, so we are not on the true physical boundary. Therefore, the tree-level term $\mathcal{P}^{\text{tree}}_{6,1}$ is completely regular and positive here. However, individual R-invariants (a) do blow up. In order to approach this point, we first set all cross-ratios to be equal, $u = v = w$, and then take $u \to 1$,

$$\mathcal{P}^{1-\text{loop}}_{6,1} \xrightarrow[u=v=w]{} \frac{1}{2}\mathcal{P}^{\text{tree}}_{6,1} \cdot \left[3\text{Li}_2(1-u) + \log^2 u - 2\zeta_2\right] \xrightarrow[u=1]{} -\mathcal{P}^{\text{tree}}_{6,1} \cdot \zeta_2 < 0. \tag{3.38}$$

Thus we obtain the desired negative value. In section 3.5.1 we will study the point $(1, 1, 1)$ at higher loops.

Example 2

Another interesting case is the point $(u, v, w) = (1, 0, 0)$, which can be reached by setting $c_2 = c_3 = c_4 = 0$. Naively, the term $\log v \log w$ dominates, but there is a conspiracy of prefactors which makes the situation more complicated. We can approach this limit by setting $c_2 \to \epsilon c_2$, $c_3 \to \epsilon c_3$, $c_4 \to \epsilon c_4$ and then letting $\epsilon \to 0$. There are many ways to approach the point $(u, v, w) = (1, 0, 0)$, but this limit always keeps us in the positive region.

For analyzing the one-loop ratio function in this limit, it is good to use the second representation (3.37). The relevant combinations of R-invariants behave in this limit as

$$\begin{aligned}
\mathcal{P}^{\text{tree}}_{6,1} &= \frac{1}{\epsilon^2} \cdot \frac{x_3}{c_1 c_5 c_6 (c_3 x_2 + c_2 x_3)(c_4 x_3 + c_3 x_4)}\,, \\
(1) - (2) + (3) &= -\frac{1}{\epsilon^2} \cdot \frac{x_4}{c_1 c_5 c_6 (c_4 x_2 - c_2 x_4)(c_4 x_3 + c_3 x_4)}\,, \\
(3) - (4) + (5) &= \frac{1}{\epsilon^2} \cdot \frac{x_2}{c_1 c_5 c_6 (c_3 x_2 + c_2 x_3)(c_4 x_2 - c_2 x_4)}\,.
\end{aligned} \tag{3.39}$$

while the term $(2)-(3)+(4)=\mathcal{O}(1)$ is subleading. Combining these limits with those of the polylog parts, the individual pieces in eq. (3.37) behave like

$$\mathcal{P}_{6,1}^{\text{tree}}\cdot(\dots)=\frac{\log\epsilon}{\epsilon}\cdot\frac{X}{c_1^2c_5^2c_6^2x_2x_4(c_3x_2+c_2x_3)(c_4x_3+c_3x_4)}\,, \tag{3.40}$$

$$[(1)-(2)+(3)]\cdot(\dots)=-\frac{\log\epsilon}{\epsilon}\cdot\frac{c_1x_5-c_5x_1}{c_1^2c_5^2c_6x_2(c_4x_3+c_3x_4)}\,, \tag{3.41}$$

$$[(3)-(4)+(5)]\cdot(\dots)=\frac{\log\epsilon}{\epsilon}\cdot\frac{c_1x_5-c_5x_1}{c_1^2c_5^2c_6x_4(c_3x_2+c_2x_3)}\,, \tag{3.42}$$

where

$$\begin{aligned}X=\;&c_4c_5x_2x_3(c_6x_1+c_1x_6)+c_1c_2x_3x_4(c_6x_5+c_5x_6)\\&+c_3x_2x_4(c_5c_6x_1+c_1c_6x_5+2c_1c_5x_6),\end{aligned} \tag{3.43}$$

while the last term is subleading in this limit, $[(2)-(3)+(4)]\cdot(\dots)=\mathcal{O}(\log^2\epsilon)$. This suppression may be counter-intuitive (as that term had the dominant logarithms), but the rational prefactor is regular in this limit, while the prefactors of other terms diverge. We see that the terms (3.41) and (3.42) do not have fixed sign, but if we combine all three pieces together we get

$$\mathcal{P}_{6,1}^{1-\text{loop}}=\frac{\log\epsilon}{\epsilon}\cdot\frac{Y}{2c_1^2c_5^2c_6^2x_2x_4(c_3x_2+c_2x_3)(c_4x_3+c_3x_4)}\,, \tag{3.44}$$

where

$$\begin{aligned}Y=\;&c_5c_6x_1x_4(c_3x_2+c_2x_3)+c_1c_6x_2x_5(c_4x_3+c_3x_4)\\&+c_1c_5x_6(c_4x_2x_3+2c_3x_2x_4+c_2x_3x_4),\end{aligned} \tag{3.45}$$

which is manifestly negative for $\epsilon\to 0$ while keeping $c_a,x_b>0$. The negativity of the final expression requires a conspiracy between the rational prefactors and the polylog part, as well as between different parts of the answer in eq. (3.37). We can also start with representation (3.35), but in this case the cancellation is even more complicated. Individual pieces would also contain logs of c_a,x_b as prefactors of $\frac{\log\epsilon}{\epsilon}$. These logs

would all cancel when taking the sum, leaving us with the rational expression (3.44).

3.3.2 Double-scaling limit

In the previous examples the rational prefactors played a central role in proving positivity. Let us now discuss an example where positivity relies on a relation between polylogarithms. Such a case can be found near the boundary $\langle Y1234\rangle = 0$, which we can approach by setting $c_5 = \epsilon\hat{c}_5$, $c_6 = \epsilon\hat{c}_6$ and taking the limit $\epsilon \to 0$ with $\hat{c}_5, \hat{c}_6$ fixed. As can be seen from eq. (3.24), the two dominant R-invariants are equal to each other in this limit,

$$(5) = (6) = \frac{1}{\epsilon} \cdot \frac{1}{c_1 c_2 c_3 c_4 (\hat{c}_6 x_5 + \hat{c}_5 x_6)}, \tag{3.46}$$

while the R-invariants $(1), (2), (3)$ and (4) remain finite. Similarly, the cross ratios become

$$u = \frac{c_4(c_2 x_1 + c_1 x_2)}{c_2(c_4 x_1 + c_1 x_4)}, \quad v = \mathcal{O}(\epsilon), \quad w = \frac{c_1(c_4 x_3 + c_3 x_4)}{c_3(c_4 x_1 + c_1 x_4)} \tag{3.47}$$

in this limit.

Thus this limit sends the cross ratio $v \to 0$, but leaves u, w fixed. This limit has been studied in the context of the operator product expansion (OPE), where it is referred to as the double-scaling limit and corresponds to contributions with the maximum number of gluonic flux-tube excitations [46, 51, 109]. While the conventional OPE addresses configurations near the collinear limit $v \to 0$, $u + w \to 1$, the double-scaling limit allows u and w to be generic.

For NMHV positive kinematics, u and w are not totally generic, because we have

$$[u + w]_{c_5, c_6 \to 0} = 1 + \frac{c_1 c_4 (c_2 x_3 + c_3 x_2)}{c_2 c_3 (c_1 x_4 + c_4 x_1)} > 1. \tag{3.48}$$

This turns out to be the only additional constraint; that is, the correct NMHV positive region within the double-scaling limit is the semi-infinite plane

$$u > 0, \quad w > 0, \quad u + w > 1. \tag{3.49}$$

In order to show that the entire region (3.49) corresponds to positive kinematics, we use the fact that the lines $u = 1$ and $w = 1$ divide the region (3.49) into four subregions. Each of the four subregions corresponds to solving eq. (3.47) for two of the c_b, $b = 1, 2, 3, 4$, in terms of u, w and the remaining c_b, x_a, in a manifestly positive manner. There are six possible pairs of c_b, but the pairs $\{c_1, c_3\}$ and $\{c_2, c_4\}$ do not work. For example, solving eq. (3.47) for c_2, c_3 gives

$$c_2 = \frac{c_1 c_4 x_2}{u c_1 x_4 + (u-1) c_4 x_1}\,, \qquad c_3 = \frac{c_1 c_4 x_3}{w c_4 x_1 + (w-1) c_1 x_4}\,, \tag{3.50}$$

which is manifestly positive in the subregion $u > 1$, $w > 1$. This solution shows that this entire subregion is covered. The other subregions work in the same way.

Since polylogarithms can generate at most $\log \epsilon$ behavior, the one-loop ratio function in the double-scaling limit becomes dominated by terms involving the singular (and equal) R-invariants (5) and (6):

$$\mathcal{P}_{6,1}^{1-\text{loop}}\Big|_{c_5,c_6\to 0} = \frac{1}{2\epsilon} \cdot \frac{1}{c_1 c_2 c_3 c_4 (\hat{c}_6 x_5 + \hat{c}_5 x_6)} \cdot C^{(1)}(u, w), \tag{3.51}$$

where

$$C^{(1)}(u, w) = \text{Li}_2(1-u) + \text{Li}_2(1-w) + \log u \log w - \zeta_2\,. \tag{3.52}$$

While the rational prefactor in this expression is manifestly positive for all positive values of the c_a, it's not yet obvious what can be said about the sign of the polylogarithmic part $C^{(1)}(u, w)$ in region (3.49). In fact, $\mathcal{P}_{6,1}^{1-\text{loop}}|_{c_5,c_6\to 0}$, and hence also $C^{(1)}(u, w)$, are required to vanish on the boundary $u + w = 1$, because this line corresponds to a limit in which two adjacent particles become collinear. In general, this would mean that the six-point ratio function should match onto the five-point ratio function – but the five-point ratio function receives no loop-level corrections [31]. The vanishing boundary condition holds to all loop orders. At one loop, it is a trivial dilog identity, $\text{Li}_2(1-u) = \zeta_2 - \log u \log(1-u) - \text{Li}_2(u)$.

Given a vanishing boundary condition at the boundary $u + w = 1$, we can learn about the sign of the one-loop ratio function throughout the NMHV positive region

by looking instead at the radial derivative of $C^{(1)}(u,w)$,

$$(u\partial_u + w\partial_w)C^{(1)}(u,w) = \frac{\log u}{1-u} + \frac{\log w}{1-w}\,. \tag{3.53}$$

This derivative is manifestly negative for all $u, w > 0$. Also, radial flow can be used to reach any point (u,w) starting from some point on the boundary, namely the point $(\frac{u}{u+w}, \frac{w}{u+w})$. Thus $C^{(1)}(u,w)$ and $\mathcal{P}_{6,1}^{1-\text{loop}}|_{c_5,c_6\to 0}$ must be negative throughout region (3.49).

3.4 Positivity in the double-scaling limit

We now begin to extend our investigation of positivity from one loop to higher loop orders. In this section, we focus on the double-scaling limit just discussed in section 3.3.2. Because the R-invariants are independent of loop order, the only difference in going to higher loops is that the transcendental function $C^{(1)}(u,w)$ in eq. (3.52) is replaced by the sum of the coefficients of the R-invariants (5) and (6), in eq. (3.31) for $\mathcal{P}_{6,1}$. Up to a factor of $1/2$, we denote this sum by $C(u,v,w)$. In terms of the functions V and $\widetilde{V}$, it is given by

$$C(u,v,w) = V(v,w,u) + V(w,u,v) + \widetilde{V}(y_v, y_w, y_u) - \widetilde{V}(y_w, y_u, y_v)\,. \tag{3.54}$$

The limit $v \to 0$ with u, w held fixed (or $c_5, c_6 \to 0$ in the positive parametrization) acts on the extended cross ratios y_i by sending

$$y_u \to \frac{1-w}{u}\,, \quad y_v \to \frac{(1-u-w)^2}{v(1-u)(1-w)}\,, \quad y_w \to \frac{1-u}{w}\,. \tag{3.55}$$

(Because u, v, w remain stationary under parity, while y_u, y_v, y_w invert, one might think that one could send the y_i variables instead to the reciprocal of the three values chosen in eq. (3.55). However, this choice is inconsistent with the positive parametrization (3.32).)

In general, the functions V and $\widetilde{V}$ diverge logarithmically in this limit, because the amplitude has a physical branch cut at $v = 0$, where the Mandelstam variables

s_{23} and s_{56} vanish. We therefore parametrize the limiting behavior of $C(u, v, w)$ as an expansion in powers of $\log(1/v)$ as well as loop order,

$$C(u, v \to 0, w) = \sum_{\ell=0}^{\infty} \sum_{n=0}^{\ell-1} (-a)^{\ell} c_n^{(\ell)}(u, w) \log^n(1/v), \tag{3.56}$$

up to power-suppressed terms. The upper limit on the sum over n reflects the empirical observation that the leading-logarithmic contribution is $\log^{\ell-1}(1/v)$ at ℓ loops. We expect that this observation should have a OPE-based explanation.

The one-loop case studied in the previous section is the only one with no logarithmic divergence:

$$C^{(1)}(u, v \to 0, w) = C^{(1)}(u, w) = -c_0^{(1)}(u, w). \tag{3.57}$$

The use of $(-a)$ in eq. (3.56) ensures that all the coefficients $c_n^{(\ell)}(u, w)$ will be empirically positive, given the overall sign alternation with loop order discussed in the introduction. The boundary condition discussed in the previous subsection, that the ratio function vanishes in the collinear limit, tells us that

$$c_n^{(\ell)}(u, 1-u) = 0, \tag{3.58}$$

for all ℓ and n.

The limiting values (3.55) for the y_i imply that the coefficient functions $c_n^{(\ell)}(u, w)$ in eq. (3.56) can be expressed as multiple polylogarithms [90, 91] of weight $2\ell - n$ with symbol letters drawn from the set [37, 109]

$$\mathcal{S}_{\text{DS}} = \{u, w, 1-u, 1-w, 1-u-w\}, \tag{3.59}$$

and branch cuts only in the letters u and w. This "double-scaling" function space is a subspace of the 2dHPL function space introduced by Gehrmann and Remiddi [128] for four-point scattering with one massive leg and three massless legs.

The $c_n^{(\ell)}(u, w)$ can be computed from V and $\widetilde{V}$ by expressing them as multiple polylogarithms and taking the double scaling limit directly using the replacements (3.55) for the y_i variables. In this process, one can also extract the $\log(1/v)$ dependence.

Alternatively, one can construct the double-scaling function space more abstractly at first, using the set of relations between derivatives and coproducts implied by the symbol alphabet $\mathcal{S}_{\rm DS}$. These relations are limiting versions of the coproduct relations used in the hexagon function bootstrap. Then one can find matching conditions between these functions and the $v \to 0$ limit of one's basis of hexagon functions. For an example of the latter procedure see Appendix D.

In the latter approach, at high loop order it may be preferable to perform intermediate steps using the BDS-like normalized MHV and NMHV amplitudes that satisfy the Steinmann relations, because the space of Steinmann-satisfying hexagon functions is much smaller [68]. The limiting behavior of the (non-Steinmann) functions V and $\tilde{V}$ can then be computed from the limiting values of the Steinmann functions.

In section 3.4.2 we will show plots for the coefficient functions $c_n^{(\ell)}(u,w)$ on the full two-dimensional double-scaling surface (3.49). First, however, we would like to examine their behavior on three one-dimensional lines that trace through this surface.

3.4.1 Positivity along lines in the double-scaling limit

The space of functions relevant for six-gluon scattering amplitudes simplifies further in three one-dimensional subspaces of the double-scaling limit, where everything can be expressed in terms of harmonic polylogarithms (HPLs) of a single variable [115]. On these lines, we can evaluate the ratio function numerically in Mathematica using the HPL package [147]. Correspondingly, we first explore the behavior of the functions $c_n^{(\ell)}(u,w)$ in these special kinematic regions, before enlarging the scope of our study to the full double-scaling limit. As we will see later, these lines turn out to capture most of the interesting information about the ratio function in the double-scaling limit.

The line $w = 1$

The first simple line in the double-scaling limit corresponds to setting $w = 1$. This collapses $\mathcal{S}_{\rm DS}$ to the simpler set of letters $\{u, 1-u\}$, which implies that the functions $c_n^{(\ell)}(u,1)$ can be written as a sum of HPLs with argument $1-u$. This representation can be built up through iterative integrations, using the fact that the u derivative of

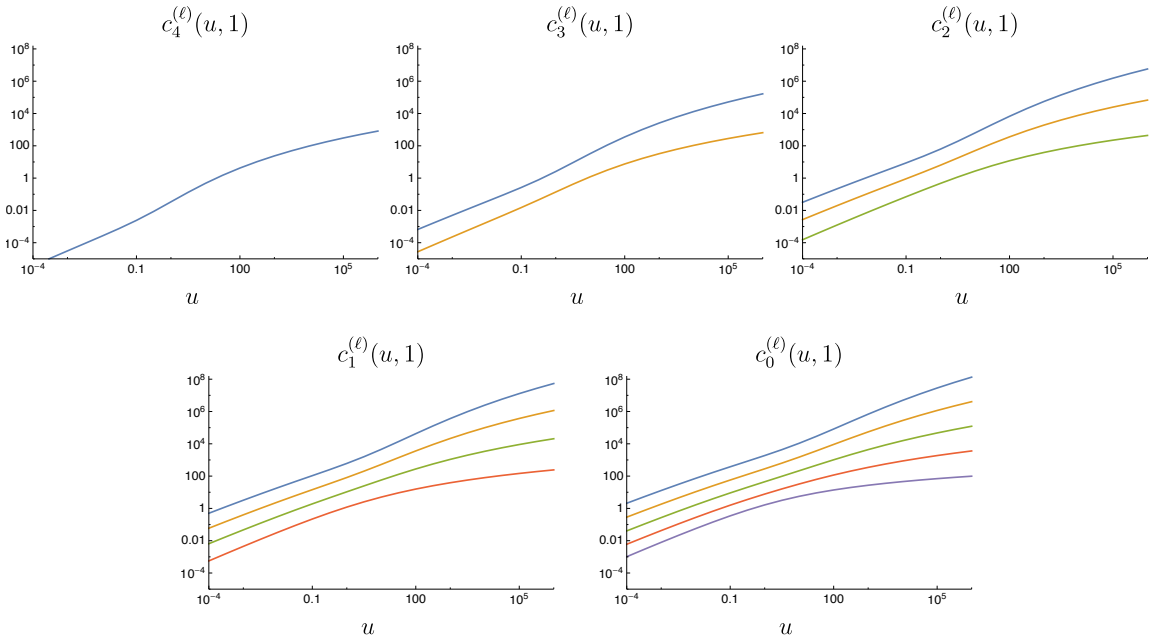

Figure 3.1: The coefficient functions $c_n^{(\ell)}(u,1)$ that multiply $\log^n(1/v)$ in the double-scaling limit at ℓ loops. Five loops is shown in blue, four loops in yellow, three loops in green, two loops in red, and one loop in purple.

a generic hexagon function F collapses to

$$\left.\frac{\partial F}{\partial u}\right|_{v\to 0;w=1} = \frac{F^u - F^{y_u} + 2F^{y_v}}{u} - \frac{F^{1-u} - F^{y_v} + F^{y_w}}{1-u} \tag{3.60}$$

along this line. To carry out this integration on a generic hexagon function, one must also set the integration constant at each weight. This can be done by integrating from the point $(u,v,w) = (1,1,1)$, where the additive constants of hexagon functions are usually defined, to the point $(1,0,1)$ along the line $(1,v,1)$. Hexagon functions all collapse to HPLs with argument $1-v$ along the line $(1,v,1)$, so this integration is also simple [34]. Using this procedure, we have computed the functions $c_n^{(\ell)}(u,1)$ through five loops, which we plot in figure 3.1. We also provide their HPL expressions in an ancillary file.

The vanishing of the ratio function along the collinear line $u+w=1$, eq. (3.58), requires that the $c_n^{(\ell)}(u,1)$ all vanish at the point $u=0$. We can also check the

behavior of these functions as $u \to \infty$, where they reduce to polynomials in $\log u$. For instance, the coefficient functions $c_0^{(\ell)}(u \to \infty, 1)$ become

$$c_0^{(1)}(u \to \infty, 1) = \frac{1}{2}\log^2 u + 2\zeta_2\,, \tag{3.61}$$

$$c_0^{(2)}(u \to \infty, 1) = \frac{1}{12}\log^4 u + \frac{7}{4}\zeta_2 \log^2 u + \frac{1}{2}\zeta_3 \log u + \frac{59}{4}\zeta_4\,, \tag{3.62}$$

$$\begin{aligned} c_0^{(3)}(u \to \infty, 1) = {} & \frac{1}{80}\log^6 u + \frac{25}{48}\zeta_2 \log^4 u + \frac{1}{24}\zeta_3 \log^3 u + \frac{287}{16}\zeta_4 \log^2 u \\ & + \frac{7}{4}\zeta_5 \log u + \frac{3}{2}\zeta_3^2 + \frac{6303}{64}\zeta_6\,, \end{aligned} \tag{3.63}$$

$$\begin{aligned} c_0^{(4)}(u \to \infty, 1) = {} & \frac{37}{20160}\log^8 u + \frac{11}{96}\zeta_2 \log^6 u - \frac{1}{480}\zeta_3 \log^5 u + \frac{459}{64}\zeta_4 \log^4 u \\ & - \left(\frac{1}{2}\zeta_2\zeta_3 + \frac{19}{48}\zeta_5\right)\log^3 u + \left(\frac{3}{2}\zeta_3^2 + \frac{108763}{768}\zeta_6\right)\log^2 u \\ & + \left(\frac{381}{128}\zeta_7 - \frac{443}{32}\zeta_4\zeta_3 - \frac{107}{16}\zeta_5\zeta_2\right)\log u \\ & - \frac{1}{4}\zeta_{5,3} + \frac{3299555}{4608}\zeta_8 + \frac{63}{4}\zeta_5\zeta_3 + \frac{85}{16}\zeta_3^2\zeta_2\,, \end{aligned} \tag{3.64}$$

$$\begin{aligned} c_0^{(5)}(u \to \infty, 1) = {} & \frac{13}{48384}\log^{10} u + \frac{899}{40320}\zeta_2 \log^8 u - \frac{7}{5760}\zeta_3 \log^7 u + \frac{2559}{1280}\zeta_4 \log^6 u \\ & - \left(\frac{223}{960}\zeta_3\zeta_2 + \frac{71}{320}\zeta_5\right)\log^5 u + \left(\frac{103}{192}\zeta_3^2 + \frac{105113}{1536}\zeta_6\right)\log^4 u \\ & - \left(\frac{1613}{96}\zeta_4\zeta_3 + \frac{1769}{192}\zeta_2\zeta_5 + \frac{1913}{256}\zeta_7\right)\log^3 u \\ & + \left(\frac{691}{64}\zeta_2\zeta_3^2 + \frac{659}{32}\zeta_5\zeta_3 - \frac{3}{8}\zeta_{5,3} + \frac{21436813}{18432}\zeta_8\right)\log^2 u \\ & - \left(\frac{79}{48}\zeta_3^3 + \frac{60801}{256}\zeta_6\zeta_3 + \frac{3209}{16}\zeta_4\zeta_5 + \frac{6913}{64}\zeta_7\zeta_2 + \frac{66545}{1152}\zeta_9\right)\log u \\ & - \frac{101}{160}\zeta_2\zeta_{5,3} - \frac{543}{512}\zeta_{7,3} + \frac{10267}{128}\zeta_4\zeta_3^2 + \frac{2707}{32}\zeta_2\zeta_5\zeta_3 \\ & + \frac{1717}{16}\zeta_7\zeta_3 + \frac{28635}{512}\zeta_5^2 + \frac{592519707}{102400}\zeta_{10}\,, \end{aligned} \tag{3.65}$$

which all approach positive infinity, as expected. More generally, we have checked that $c_n^{(\ell)}(u \to \infty, 1) \to +\infty$ for all $\ell \leq 5$ and for all n between 0 and $\ell - 1$.

Since v is very small, positivity strictly requires only the leading-log coefficients $c_{\ell-1}^{(\ell)}(u, 1)$ to be positive. However, we find a much stronger result: The coefficients

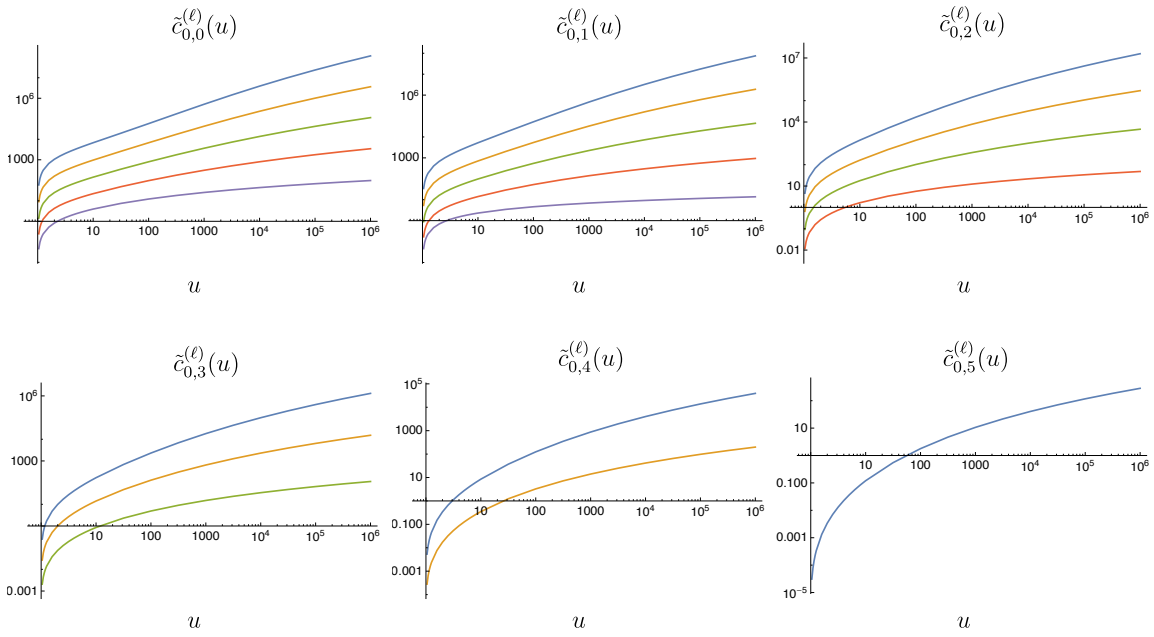

Figure 3.2: The coefficient functions $\tilde{c}^{(\ell)}_{0,k}(u)$ for the $w \to 0$ edge of the double-scaling limit at ℓ loops. Five loops is shown in blue, four loops in yellow, three loops in green, two loops in red, and one loop in purple.

$c^{(\ell)}_n(u,1)$ are all positive for $u > 0$ and for any n between 0 and $\ell - 1$. Furthermore, figure 3.1 shows that they all increase monotonically with u.

The line $w = 0$

The second simple line we will look at is $w = 0$. It forms an edge of the positive double-scaling region (3.49). As was the case for the $w = 1$ line, $\mathcal{S}_{\text{DS}}$ collapses to $\{u, 1-u\}$. However, $c^{(\ell)}_n(u, w \to 0)$ diverges logarithmically in w due to a physical branch cut analogous to the branch cut in v. The functions $c^{(\ell)}_n(u, w \to 0)$ are therefore expressible as an expansion in powers of $\log(1/w)$,

$$c^{(\ell)}_n(u, w \to 0) = \sum_{k=0}^{\ell-n} \tilde{c}^{(\ell)}_{n,k}(u) \log^k(1/w). \tag{3.66}$$

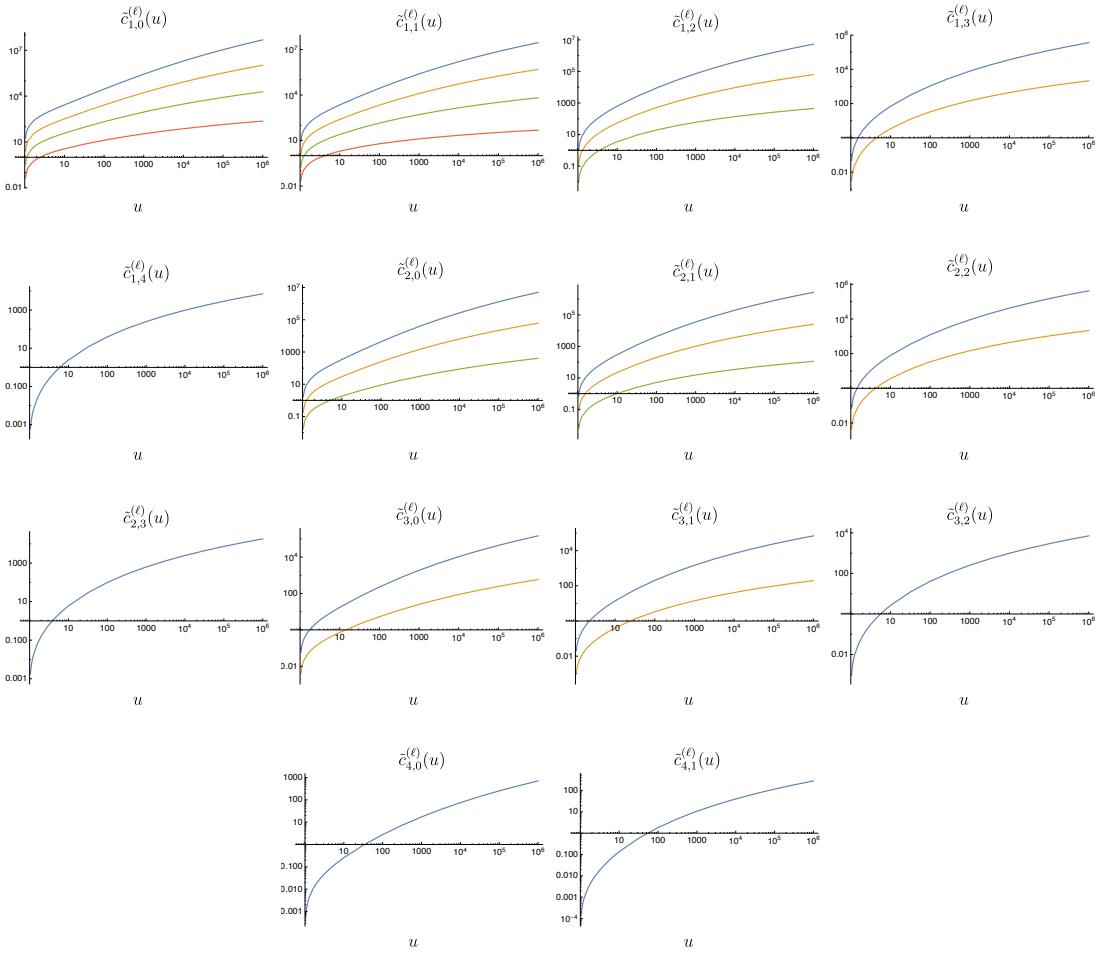

Figure 3.3: The coefficient functions $\tilde{c}^{(\ell)}_{n,k}(u)$ for the $w \to 0$ edge of the double-scaling limit at ℓ loops. Five loops is shown in blue, four loops in yellow, three loops in green, and two loops in red.

The coefficients $\tilde{c}^{(\ell)}_{n,k}(u)$ are drawn from the space of HPLs with argument $1-u$, and empirically they vanish unless k is between 0 and $\ell - n$, where we recall that n is the power of $\log(1/v)$ in the expansion (3.56).

The derivative of a generic hexagon function F along the line $(u, w \to 0)$ is given by

$$\left.\frac{\partial F}{\partial u}\right|_{v,w\to 0} = \frac{F^u - F^{y_u}}{u} - \frac{F^{1-u} + F^{y_v} + F^{y_w}}{1-u}\,. \tag{3.67}$$

The integration constant can be set at $u = 1$, using the $v \to 0$ endpoint of the line $(u, v, w) = (1, v, 0)$, which is just an S_3 permutation of the line $(u, 0, 1)$ considered in the previous subsection.

We have carried out the corresponding integration through five loops and we include HPL representations of all the $\tilde{c}^{(\ell)}_{n,k}(u)$ in an ancillary file. The functions $\tilde{c}^{(\ell)}_{0,k}(u)$, which multiply different powers of $\log(1/w)$ in the non-$\log(1/v)$ part, are plotted in figure 3.2, while the functions $\tilde{c}^{(\ell)}_{n>0,k}(u)$ that multiply $\log^n(1/v)$ on this line are plotted in figure 3.3.

The vanishing of the ratio function along the collinear line $u + w = 1$, eq. (3.58), requires these coefficient functions to become zero at $u = 1$. We have also checked analytically that each of these functions approaches positive infinity in the limit $u \to \infty$. Once again, we observe that all the coefficient functions – not just the leading-log ones – are positive, and furthermore that they are monotonically increasing with u.

Interestingly, there is an HPL representation in which the positivity and monotonicity of the $\tilde{c}^{(\ell)}_{n,k}(u)$ is *almost* manifest. We let the argument of the HPLs be $z = 1 - 1/u$. As u increases from 1 to ∞, z increases from 0 to 1. In this range of z, the HPLs with trailing 1's in their weight vectors are manifestly positive and monotonic, simply from their integral definition,

$$H_{0,\vec{w}}(z) = \int_0^z \frac{dt}{t} H_{\vec{w}}(t), \quad H_{1,\vec{w}}(u) = \int_0^z \frac{dt}{1-t} H_{\vec{w}}(t), \tag{3.68}$$

because the integrand is a lower-weight HPL of the same form, $H_{\vec{w}}(t)$, multiplied by a kernel that is positive for $0 < t < 1$. Hence if the $\tilde{c}^{(\ell)}_{n,k}(u)$ could be written in terms of such HPLs with only positive coefficients, positivity and monotonicity would both be manifest.

At one and two loops, this is the case; the non-vanishing coefficients are

$$\begin{aligned}
\tilde{c}^{(1)}_{0,1} &= H_1\,, \\
\tilde{c}^{(1)}_{0,0} &= H_{0,1} + H_{1,1}\,, \\
\tilde{c}^{(2)}_{1,1} &= \frac{1}{2} H_{0,1} + \frac{1}{2} H_{1,1}\,,
\end{aligned}$$

$$
\begin{aligned}
\tilde{c}^{(2)}_{1,0} &= H_{0,0,1} + H_{0,1,1} + \frac{1}{2}H_{1,0,1} + \frac{1}{2}H_{1,1,1}\,, \\
\tilde{c}^{(2)}_{0,2} &= \frac{1}{4}H_{0,1} + \frac{1}{2}H_{1,1}\,, \\
\tilde{c}^{(2)}_{0,1} &= 2H_{0,0,1} + \frac{5}{2}H_{0,1,1} + \frac{3}{2}H_{1,0,1} + 2H_{1,1,1} + \zeta_2 H_1\,, \\
\tilde{c}^{(2)}_{0,0} &= \frac{9}{2}H_{0,0,0,1} + 5H_{0,0,1,1} + 3H_{0,1,0,1} + \frac{7}{2}H_{0,1,1,1} + 2H_{1,0,0,1} + \frac{5}{2}H_{1,0,1,1} \\
&\quad + \frac{3}{2}H_{1,1,0,1} + 2H_{1,1,1,1} + \zeta_2\Big(\frac{1}{2}H_{0,1} + H_{1,1}\Big)\,,
\end{aligned}
\tag{3.69}
$$

where we have suppressed the argument $z = 1 - 1/u$ of the HPLs $H_{\vec{w}}(z)$, displaying only their weight vector $\vec{w}$.

Since all the coefficients in eq. (3.69) are positive, positivity and monotonicity on the line $w = 0$ is manifest through two loops. However, the plot thickens at three loops. All 9 nonzero coefficient functions $\tilde{c}^{(3)}_{n,k}$ have positive coefficients in their representations, except for $\tilde{c}^{(3)}_{1,0}$ and $\tilde{c}^{(3)}_{0,0}$. The only negative coefficients in these functions are those in terms containing ζ_3 – for example,

$$
\begin{aligned}
\tilde{c}^{(3)}_{1,0} &= 6H_{0,0,0,0,1} + \frac{45}{4}H_{0,0,0,1,1} + 6H_{0,0,1,0,1} + \frac{45}{4}H_{0,0,1,1,1} + 4H_{0,1,0,0,1} + \frac{31}{4}H_{0,1,0,1,1} \\
&\quad + 4H_{0,1,1,0,1} + \frac{23}{4}H_{1,0,1,1,1} + 2H_{1,1,0,0,1} + 4H_{1,1,0,1,1} + 2H_{1,1,1,0,1} + 4H_{1,1,1,1,1} \\
&\quad + \frac{31}{4}H_{0,1,1,1,1} + 3H_{1,0,0,0,1} + \frac{23}{4}H_{1,0,0,1,1} + 3H_{1,0,1,0,1} \\
&\quad + \zeta_2\Big(\frac{3}{2}H_{0,0,1} + \frac{7}{4}H_{0,1,1} + \frac{3}{4}H_{1,0,1} + H_{1,1,1}\Big) - \frac{1}{2}\zeta_3 H_{0,1}\,.
\end{aligned}
\tag{3.70}
$$

Because the numerical coefficient in front of the ζ_3 is relatively small, it doesn't change the actual positivity or monotonicity properties; it just makes them less manifest.

Continuing on to four and five loops, there are 14 and 20 nonzero coefficient functions, respectively, with weights that range from 4 up to 10. The sign in front of each HPL in each coefficient function is completely predictable: positive, unless the term has an odd number of odd zeta values, in which case it is negative. The (mostly) consistent signs for the HPL coefficients are reminiscent of the behavior found for the velocity-dependent cusp anomalous dimension $\Omega_0(x)$ in ref. [148].

The line $u = w$

The final simple line in the double-scaling limit is given by setting $u = w$. Here, the symbol letters in $\mathcal{S}_{\rm DS}$ collapse to the set $\{u, 1-u, 1-2u\}$. This makes the functions $c_n^{(\ell)}(u,u)$ expressible as HPLs of argument $x \equiv 1-2u$ with weight vectors involving -1, 0, and 1. The derivative of a generic hexagon function F along this line takes the form

$$\left.\frac{\partial F}{\partial x}\right|_{v\to 0;u,w=(1-x)/2} = \frac{2F^{y_v}}{x} + \frac{F^{1-u}+F^{1-w}+F^{y_u}+F^{y_w}-2F^{y_v}}{1+x} - \frac{F^u+F^w-F^{y_u}-F^{y_w}}{1-x}\,, \tag{3.71}$$

while the integration constant can be set by matching to the $v \to 0$ endpoint of the line $(u,v,w) = (1,v,1)$. This requires setting the argument $x = -1$, which introduces transcendental constants beyond the multiple zeta values ζ_m and $\zeta_{m,n}$. At low weights, there are identities relating these new constants to multiple zeta values, $\log 2$, and $\mathrm{Li}_n(1/2)$ with $n \geq 4$, but starting at weight 6 new alternating sums $\mathrm{alt}_{\vec{w}} \equiv (-1)^{|\vec{w}|} H_{\vec{w}}(-1)$ are needed [149], where $|\vec{w}|$ is the depth of $\vec{w}$. The numerical values of these constants can be calculated using the HPL package.

We have computed the functions $c_n^{(\ell)}(u,u)$ through five loops and include their HPL representations in an ancillary file. The functions governing the leading-log and next-to-leading-log contributions in $1/v$ are plotted in figure 3.4. These functions must vanish at $u = \frac{1}{2}$ where they intersect the collinear line $u + w = 1$. While $c_n^{(\ell)}(u,w)$ diverges at large u along the $w = 1$ and $w = 0$ lines, it has a finite large u limit along the line $u = w$. That is, figure 3.4 shows that the coefficient functions $c_n^{(\ell)}(u,u)$ all asymptote to a constant as $u \to \infty$. This constant can be computed analytically using our HPL representation; for instance, the constants for $n = 0$ are given through four loops by

$$\begin{aligned} c_0^{(1)}(u,u)|_{u\to\infty} &= 3\zeta_2\,, \\ c_0^{(2)}(u,u)|_{u\to\infty} &= 27\zeta_4 + 6\zeta_2\log^2 2 - 6\mathrm{Li}_4(1/2) - \frac{1}{4}\log^4 2\,, \end{aligned}$$

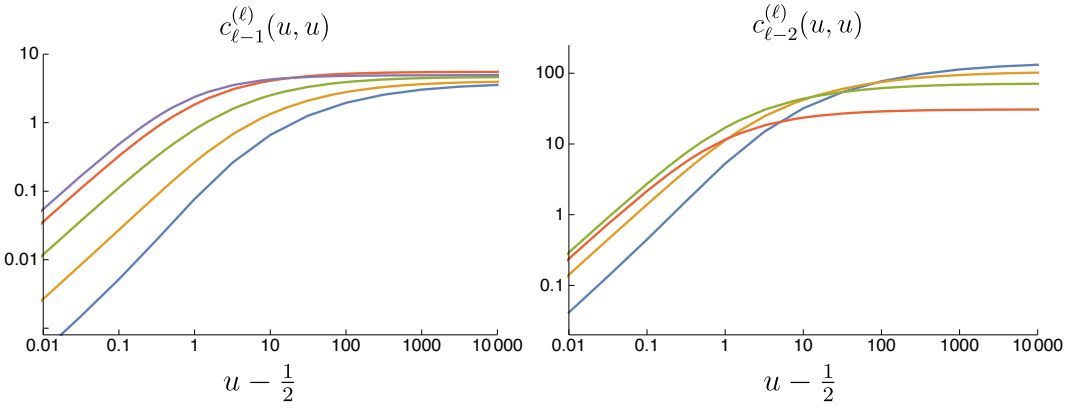

Figure 3.4: The functions $c^{(\ell)}_{\ell-1}(u,u)$ and $c^{(\ell)}_{\ell-2}(u,u)$ governing the leading-log and next-to-leading-log behavior of the ratio function at ℓ loops in the double scaling limit. The variable u has been shifted by $\frac{1}{2}$ to make it possible to plot on a log scale. Five loops is shown in blue, four loops in yellow, three loops in green, two loops in red, and one loop in purple.

$$
\begin{aligned}
c_0^{(3)}(u,u)|_{u\to\infty} &= 213\zeta_6 + \frac{55}{16}\zeta_3^2 + \frac{341}{64}\zeta_5\log 2 + \frac{2835}{32}\zeta_4\log^2 2 + \frac{23}{16}\zeta_2\log^4 2 \\
&\quad - \frac{51}{2}\zeta_2\mathrm{Li}_4(1/2) - 30\mathrm{Li}_6(1/2) - \frac{1}{24}\log^6 2 - \frac{11}{4}\mathrm{alt}_{5,1}\,, \\
c_0^{(4)}(u,u)|_{u\to\infty} &= \frac{2714608937}{1474560}\zeta_8 + \frac{6793}{512}\zeta_2\zeta_3^2 + \frac{10285}{4096}\zeta_3\zeta_5 - \frac{11683}{20480}\zeta_{5,3} \\
&\quad + \frac{20489}{512}\zeta_3\zeta_4\log 2 + \frac{2871}{64}\zeta_2\zeta_5\log 2 + \frac{354801}{16384}\zeta_7\log 2 \\
&\quad - \frac{729}{512}\zeta_3^2\log^2 2 + \frac{477873}{512}\zeta_6\log^2 2 + \frac{787}{192}\zeta_2\zeta_3\log^3 2 \\
&\quad + \frac{2015}{384}\zeta_5\log^3 2 + \frac{7423}{128}\zeta_4\log^4 2 - \frac{221}{960}\zeta_3\log^5 2 \\
&\quad - \frac{457}{720}\zeta_2\log^6 2 + \frac{11}{768}\log^8 2 - \frac{5231}{16}\mathrm{Li}_4(1/2)\zeta_4 \\
&\quad - \frac{43}{2}\mathrm{Li}_4(1/2)\zeta_2\log^2 2 + \frac{43}{48}\mathrm{Li}_4(1/2)\log^4 2 + \frac{43}{4}\mathrm{Li}_4(1/2)^2 \\
&\quad + \frac{221}{8}\mathrm{Li}_5(1/2)\zeta_3 + \frac{9}{2}\mathrm{Li}_5(1/2)\zeta_2\log 2 - 135\mathrm{Li}_6(1/2)\zeta_2 \\
&\quad - 175\mathrm{Li}_8(1/2) - \frac{67}{16}\mathrm{alt}_{5,1,1,1} + \frac{193}{64}\mathrm{alt}_{4,2,1,1} + \frac{5281}{256}\mathrm{alt}_{7,1} \\
&\quad - \frac{327}{16}\mathrm{alt}_{5,1}\zeta_2 + \frac{67}{16}\mathrm{alt}_{5,1,1}\log 2
\end{aligned}
$$

$$- \frac{193}{64}\mathrm{alt}_{4,2,1}\log 2 - \frac{65}{8}\mathrm{alt}_{5,1}\log^2 2\,, \tag{3.72}$$

while the five loop expression $c_0^{(5)}(u,u)|_{u\to\infty}$ proves too unwieldy to present. At one loop this constant is manifestly positive. Evaluating the higher-loop expressions numerically confirms that they are positive as well:

$$\begin{aligned} c_0^{(1)}(u,u)|_{u\to\infty} &= 4.93480220054\ldots, \\ c_0^{(2)}(u,u)|_{u\to\infty} &= 30.8020253462\ldots, \\ c_0^{(3)}(u,u)|_{u\to\infty} &= 235.199512804\ldots, \\ c_0^{(4)}(u,u)|_{u\to\infty} &= 2091.54312703\ldots, \\ c_0^{(5)}(u,u)|_{u\to\infty} &= 22406.9101345\ldots. \end{aligned} \tag{3.73}$$

Indeed, numerical checks reveal that the functions $c_n^{(\ell)}(u,u)$ are positive throughout the positive region, and increase monotonically with u. This has been checked exhaustively through four loops and for $n > 1$ at five loops. The higher-weight expressions $c_1^{(5)}(u,u)$ and $c_0^{(5)}(u,u)$ are more computationally challenging to check at finite u, and have only been checked in the limit $u \to \infty$.

3.4.2 The full double-scaling surface

Figures 3.1, 3.2, 3.3, and 3.4 exhibit a remarkable feature – the functions $c_n^{(\ell)}(u,w)$ are not only positive along these lines, but increase monotonically as they move away from the $u+w=1$ line. We proved this radial monotonicity at one loop, for $c_0^{(1)}(u,w)$, in section 3.3.2. In appendix E we show it for the next simplest case, $c_1^{(2)}(u,w)$, a weight-3 function. These results make it natural to conjecture that the monotonicity of $c_n^{(\ell)}(u,w)$ holds to all loop orders.

In the rest of this section we check the monotonicity of the $c_n^{(\ell)}(u,w)$ numerically throughout the double-scaling surface. This can be done by expressing the functions in terms of Goncharov polylogarithms, which can be numerically evaluated using the program GiNaC [125, 126] wherever these functions admit a convergent series expansion. The convergence condition for a Goncharov polylogarithm $G(\vec{a},z)$ is that

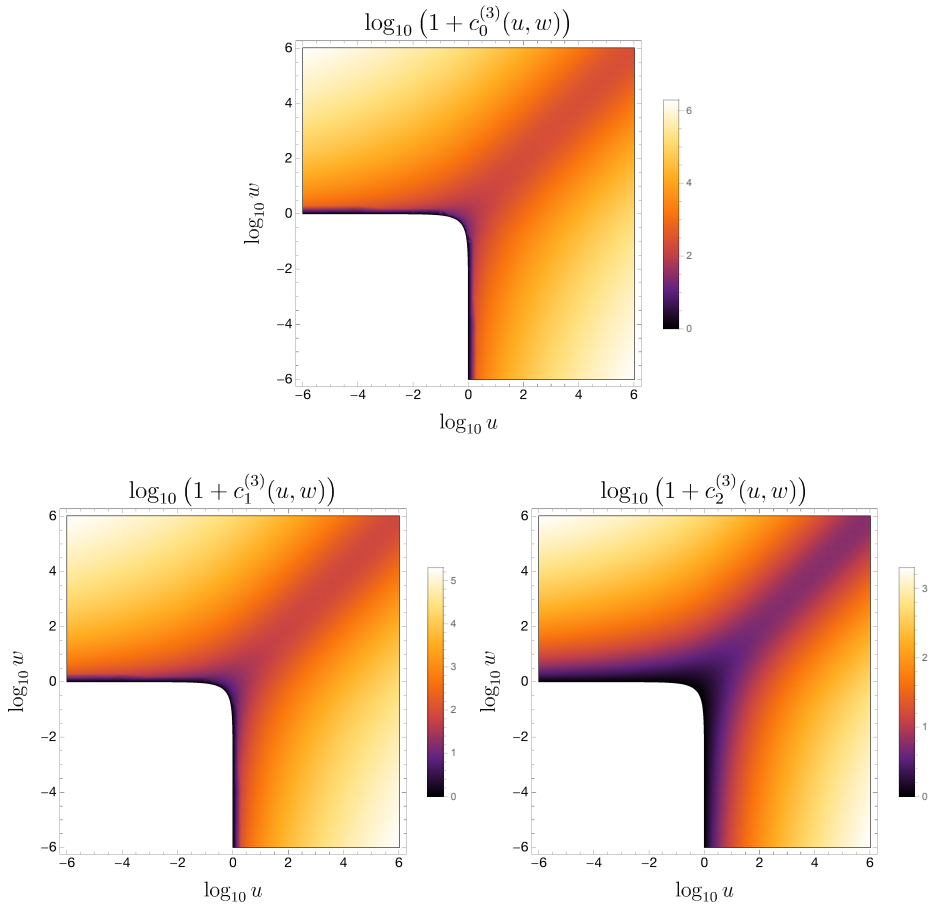

Figure 3.5: The three-loop coefficient functions $c_n^{(3)}(u,w)$ in the double-scaling limit, shifted to make it possible to plot them on a log scale. By plotting these functions against $\log u$ and $\log w$ we deform the $u+w=1$ line to the concave boundary seen in each plot.

$|z| \leq |a_i|$ for all nonzero a_i. This condition is satisfied in the triangle subregion $u+w>1$, $u<1$, $w<1$ if we work in the following basis of Goncharov polylogarithms:

$$G_{\text{DS}} = \left\{ G(\vec{a};1-w) \middle| a_i \in (0,u,1) \right\} \cup \left\{ G(\vec{a};1-u) \middle| a_i \in (0,1) \right\}. \tag{3.74}$$

This basis can also be used in the remainder of the NMHV positive region, where u and/or w is larger than 1, because GiNaC automatically employs identities to relate functions outside their region of convergence to ones that do admit a convergent

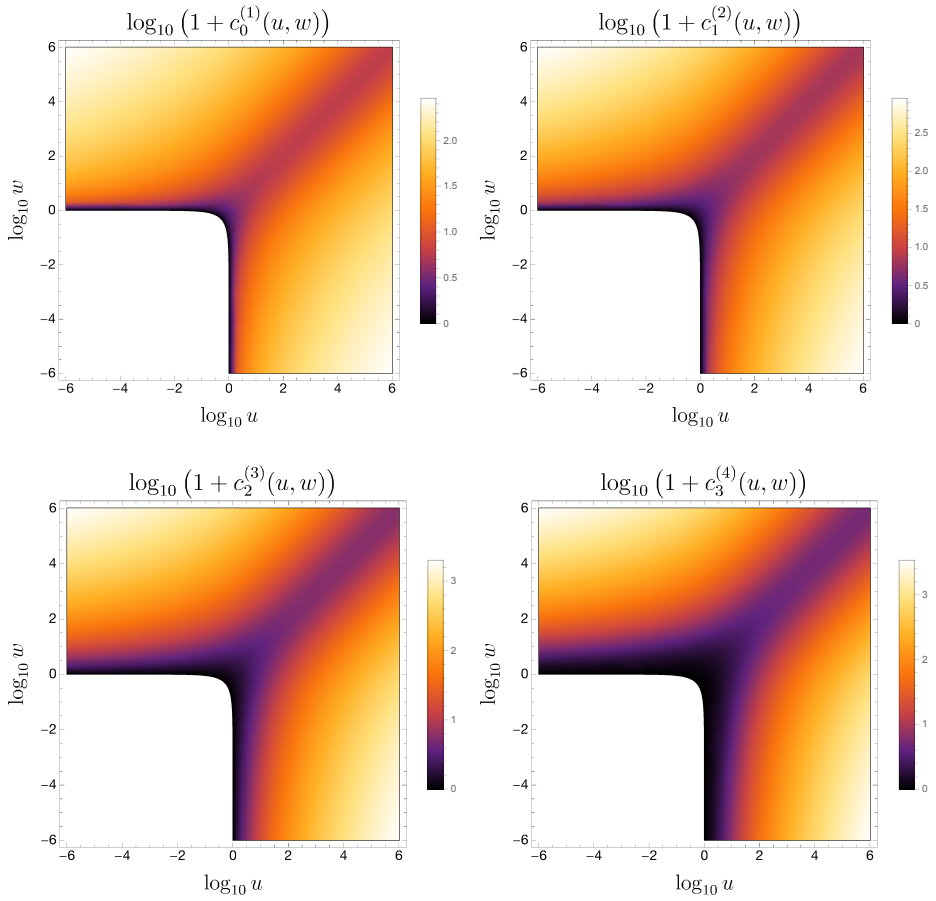

Figure 3.6: The leading-log coefficient functions $c_{\ell-1}^{(\ell)}(u,w)$ in the double-scaling limit from one to four loops, shifted to make it possible to plot them on a log scale. By plotting these functions against $\log u$ and $\log w$ we deform the $u+w=1$ line to the concave boundary seen in each plot.

expansion. This procedure can generate imaginary parts for individual G functions, but the imaginary parts cancel out in the final result.

All the numerical checks we have performed on the double-scaling surface support both positivity and monotonic radial growth for every function $c_n^{(\ell)}(u,w)$. We plot the functions, rather than their radial derivatives, in order to make interpretation of the magnitudes appearing in these plots more clear. In particular, we provide two sequences of plots that illustrate the trends the functions $c_n^{(\ell)}(u,w)$ exhibit as n and ℓ are varied. The first sequence, in figure 3.5, shows how the three-loop result

$c_n^{(3)}(u,w)$ changes as we move from the coefficient of the next-to-next-to-leading log in $1/v$ ($n=0$) to the leading log in $1/v$ ($n=2$) in the expansion (3.56). The plots all display the $u \leftrightarrow w$ symmetry of $C(u,v,w)$, which is manifest from its definition (3.54) and the (anti)symmetry properties of V and $\tilde{V}$, eq. (3.34). More interestingly, the coefficient of the leading log term grows the most slowly in the radial direction at a given loop order, particularly near the line of symmetry, $u=w$, where it asymptotes to a constant. This result holds at least through four loops. (The five loop expressions proved too computationally taxing to explore exhaustively.)

In figure 3.6 we plot the slowest-growing, leading-log coefficient functions $c_{\ell-1}^{(\ell)}(u,w)$ from one to four loops. As the loop order increases, the functions experience slower radial growth. Moreover, the functions $c_n^{(\ell)}(u,w)$ interpolate smoothly between the lines $u=w$ and $w=0$, implying that most of the interesting information about these functions in present on these two lines. In particular, the functions always grow the most slowly along the line $u=w$.

3.5 Bulk positivity at higher loops

The previous sections verified the positivity of the ratio function in various limits, nearly all of which were on the boundary of the positive octant, i.e. the double-scaling limit. In this section, we check the positivity of the ratio function in the bulk, where all three cross ratios are bounded away from zero. Except for the point $(u,v,w)=(1,1,1)$, the topic of the next subsection, our investigations will be numerical. After a brief review of our procedure for numerically evaluating hexagon functions, we outline the checks performed. Positivity appears to continue to hold in the bulk through at least four loops, after which it gets too computationally taxing to check.

3.5.1 The point $(u,v,w)=(1,1,1)$

The parity-odd functions $\tilde{V}^{(\ell)}$ all vanish at the point $(1,1,1)$, because they are odd about the surface $\Delta(u,v,w)=0$, which includes this point. Thus we can repeat the

analysis from Example 1 in section 3.3.1, obtaining

$$\mathcal{P}_{6,1}^{\ell-\text{loop}} \xrightarrow[u=v=w]{} \mathcal{P}_{6,1}^{\text{tree}} \times V^{(\ell)}(1,1,1). \tag{3.75}$$

So all we need to do is check that the sign of $V^{(\ell)}(1,1,1)$ alternates with loop order ℓ. The value of the functions $V^{(\ell)}(1,1,1)$ were supplied through four loops in ref. [38], and we have extracted the five-loop value from ref. [68]:

$$\begin{aligned}
V^{(1)}(1,1,1) &= -\zeta_2\,, \\
V^{(2)}(1,1,1) &= 9\,\zeta_4\,, \\
V^{(3)}(1,1,1) &= -\frac{243}{4}\,\zeta_6\,, \\
V^{(4)}(1,1,1) &= \frac{5051}{12}\,\zeta_8 + 3\,\zeta_2\,(\zeta_3)^2 - 15\,\zeta_3\,\zeta_5 - 3\,\zeta_{5,3}\,, \\
V^{(5)}(1,1,1) &= -\frac{244257}{80}\,\zeta_{10} - \frac{93}{2}\,\zeta_4\,(\zeta_3)^2 - 21\,\zeta_2\,\zeta_3\,\zeta_5 + \frac{399}{2}\,\zeta_3\,\zeta_7 \\
&\quad + \frac{777}{8}\,(\zeta_5)^2 + \frac{9}{2}\,\zeta_2\,\zeta_{5,3} + \frac{57}{4}\,\zeta_{7,3}\,.
\end{aligned} \tag{3.76}$$

The desired sign alternation is manifest from eq. (3.76) through three loops; after that it relies on the numerical values of the multiple zeta values:

$$\begin{aligned}
V^{(1)}(1,1,1) &= -1.64493406684\ldots, \\
V^{(2)}(1,1,1) &= +9.74090910340\ldots, \\
V^{(3)}(1,1,1) &= -61.8035910155\ldots, \\
V^{(4)}(1,1,1) &= +410.9535753669\ldots, \\
V^{(5)}(1,1,1) &= -2825.3845732862\ldots.
\end{aligned} \tag{3.77}$$

We remark that the numerical result for $V^{(\ell)}(1,1,1)$ is dominated by the $\zeta_{2\ell}$ term through five loops (it gives the correct value to within 10%).

3.5.2 Method for obtaining bulk numerics and positivity tests

Next we turn to numerical evaluation of the ratio function at random points in the bulk of the NMHV positive region. To evaluate the ratio function numerically at higher loops, we followed the procedure pioneered in ref. [34].

Representing the ratio function in terms of multiple polylogarithms allows us to evaluate them using powerful existing code like GiNaC [125, 126]. In order to do this, we choose a representation in which the multiple polylogarithms have convergent series expansions. We also prefer our representations to be manifestly real to reduce the potential for numerical error.

These conditions lead to two conditions on our multiple polylogarithms. For a multiple polylogarithm $G(w_1, \ldots, w_n; z)$, we obtain a convergent series expansion when $|z| \leq |w_i|$ for all nonzero w_i, and our result is manifestly real if z and all w_i are real and positive.

In order to avoid square roots and their attendant branch-cut ambiguities, we work in the variables (y_u, y_v, y_w). Following ref. [34], we find four different multiple polylog representations, corresponding to four different kinematic regions. In particular, for MHV studies we use

$$\begin{aligned}\mathcal{G}_I^L = &\left\{ G(\vec{w}; y_u) | w_i \in (0,1) \right\} \cup \left\{ G(\vec{w}; y_v) \Big| w_i \in \left(0, 1, \frac{1}{y_u}\right) \right\} \\ &\cup \left\{ G(\vec{w}; y_w) \Big| w_i \in \left(0, 1, \frac{1}{y_u}, \frac{1}{y_v}, \frac{1}{y_u y_v}\right) \right\}\end{aligned} \tag{3.78}$$

which is manifestly convergent for points in Region I, the MHV positive kinematic region defined by

$$\text{Region I}: \quad \begin{cases} \Delta > 0\,, \quad 0 < u_i < 1\,, \quad \text{and} \quad u + v + w < 1, \\ 0 < y_i < 1\,. \end{cases} \tag{3.79}$$

For studying the ratio function in NMHV positive kinematics, we use

$$\begin{aligned}\mathcal{G}_{II}^{L} =&\left\{G\Big(\vec{w};\frac{1}{y_u}\Big)\Big|w_i\in(0,1)\right\}\cup\left\{G\Big(\vec{w};\frac{1}{y_v}\Big)\Big|w_i\in(0,1,y_u)\right\}\\ &\cup\left\{G(\vec{w};y_w)\Big|w_i\in\Big(0,1,\frac{1}{y_u},\frac{1}{y_v},\frac{1}{y_u y_v}\Big)\right\}\end{aligned} \tag{3.80}$$

for points in Region II:

$$\text{Region II}: \quad \begin{cases}\Delta>0\,, \quad 0<u_i<1\,, \quad \text{and} \quad u+v-w>1,\\ 0<y_w<\frac{1}{y_u y_v}<\frac{1}{y_u},\frac{1}{y_v}<1\,.\end{cases} \tag{3.81}$$

Cycling the y_i in Region II lets us define two other regions, Region III and Region IV, where we have multiple polylog representations in the bulk. Because the bosonized ratio function is S_3 symmetric, Regions III and IV do not add any new information. The NMHV positive region always has $\Delta > 0$ (see eq. (3.19)). However, Region II lies entirely within the unit cube in (u, v, w), and the bulk NMHV positive region extends well beyond it (as is clear from the double-scaling plots in the previous section). So our bulk positivity tests will be confined to points inside the unit cube.

In order to perform this test, we randomly generate a phase-space point in the NMHV positive region by picking eleven random values of the positive parameters (c_b, x_a), each between 0 and 100 (x_6 is set to 1, as discussed in section 3.2.2). For each set of values we use eqs. (3.17) and (3.15) to compute the three cross ratios u, v, w. If the point (u, v, w) is not inside the unit cube, we stop and generate a new point. If it is inside the unit cube, we use eqs. (3.24) and (3.32) to compute the R-invariants and extended cross ratios y_u, y_v, y_w. We plug the latter into the arguments of the multiple polylogarithms in our Region II (or III or IV) representation of the ratio function, performing the numerical evaluation with GiNaC. We examined 585 points at loop orders from one through four, and the ratio function always has the expected sign, alternating with loop order.

3.6 MHV positivity

Having found strong evidence that the NMHV ratio function is positive through five loops in the NMHV positive region, we now return to studying various IR-finite versions of the MHV amplitude in the MHV positive region.

3.6.1 The remainder function fails

As mentioned in section 3.2.1, there are a variety of possibilities. They are all fairly simply related to each other analytically, but they still can have different positivity properties. First we consider the six-point remainder function R_6, which is defined as the logarithm of the MHV amplitude divided by the BDS ansatz, as in eq. (3.27),

$$\exp[R_6] \;=\; \frac{\mathcal{M}_{6,0}}{\mathcal{M}_{6,0}^{\rm BDS}}\,. \tag{3.82}$$

The remainder function vanishes at one loop by construction. Its positivity in the MHV positive region (3.10) was investigated at two loops [69], three loops [34], and four loops [35]. All points investigated numerically were found to have the correct sign.

However, it turns out that there are regions close to the origin in (u, v, w) that have the wrong sign for $R_6^{(4)}$. To exhibit such points, we consider the same line $v = 0$, $w = 0$ on which the ratio function was studied for $u > 1$ in section 3.4.1, but now we take $0 < u < 1$ in order to be in the MHV positive region. As was true for the ratio function, the remainder function develops logarithmic singularities in both v and w as they approach zero,

$$R_6(u, v \to 0, w \to 0) = \sum_{\ell=2}^{\infty} \sum_{n,k=0}^{\ell-1} (-a)^\ell\, r_{n,k}^{(\ell)}(u)\, \log^n(1/v) \log^k(1/w), \tag{3.83}$$

up to power-suppressed terms in v and w. Since R_6 is S_3 permutation symmetric, $r_{k,n}(u) = r_{n,k}(u)$. Also, the coefficient functions vanish unless $n + k \leq \ell$.

At two and three loops, there are no problems in this region. The independent

nonzero coefficient functions are given by,

$$\begin{aligned} r^{(2)}_{1,1} &= \frac{1}{4}H_{0,1}\,, \\ r^{(2)}_{1,0} &= \frac{1}{4}\Big[2H_{0,0,1}+H_{1,0,1}\Big]\,, \\ r^{(2)}_{0,0} &= \frac{1}{4}\Big[6H_{0,0,0,1}+3H_{0,1,0,1}+4H_{1,0,0,1}+2H_{1,1,0,1}-2\zeta_2(H_{0,1}+H_{1,1})\Big], \end{aligned} \tag{3.84}$$

and

$$\begin{aligned} r^{(3)}_{2,1} &= \frac{1}{16}\Big[H_{0,0,1}-H_{0,1,1}\Big]\,, \\ r^{(3)}_{2,0} &= \frac{1}{16}\Big[3H_{0,0,0,1}-2H_{0,0,1,1}+H_{0,1,0,1}+H_{1,0,0,1}-H_{1,0,1,1}\Big]\,, \\ r^{(3)}_{1,1} &= \frac{1}{4}\Big[3H_{0,0,0,1}-2H_{0,0,1,1}+H_{1,0,0,1}-H_{1,0,1,1}+2\zeta_2 H_{0,1}\Big]\,, \\ r^{(3)}_{1,0} &= \frac{1}{8}\Big[18H_{0,0,0,0,1}-9H_{0,0,0,1,1}+3H_{0,0,1,0,1}+7H_{0,1,0,0,1}-4H_{0,1,0,1,1}+H_{0,1,1,0,1} \\ &\quad +9H_{1,0,0,0,1}-6H_{1,0,0,1,1}+H_{1,0,1,0,1}+3H_{1,1,0,0,1}-3H_{1,1,0,1,1} \\ &\quad +\zeta_2(5H_{0,0,1}-H_{0,1,1}+2H_{1,0,1})\Big]\,, \\ r^{(3)}_{0,0} &= \frac{1}{4}\Big[30H_{0,0,0,0,0,1}-12H_{0,0,0,0,1,1}+6H_{0,0,0,1,0,1}+12H_{0,0,1,0,0,1}-5H_{0,0,1,0,1,1} \\ &\quad +2H_{0,0,1,1,0,1}+15H_{0,1,0,0,0,1}-8H_{0,1,0,0,1,1}+2H_{0,1,0,1,0,1}+5H_{0,1,1,0,0,1} \\ &\quad -4H_{0,1,1,0,1,1}+18H_{1,0,0,0,0,1}-9H_{1,0,0,0,1,1}+3H_{1,0,0,1,0,1}+7H_{1,0,1,0,0,1} \\ &\quad -4H_{1,0,1,0,1,1}+H_{1,0,1,1,0,1}+9H_{1,1,0,0,0,1}-6H_{1,1,0,0,1,1}+H_{1,1,0,1,0,1} \\ &\quad +3H_{1,1,1,0,0,1}-3H_{1,1,1,0,1,1} \\ &\quad +\zeta_2(3H_{0,0,0,1}-2H_{0,0,1,1}+H_{0,1,0,1}+H_{1,0,0,1}-H_{1,0,1,1}) \\ &\quad -2\zeta_3(H_{0,0,1}+H_{0,1,1})-11\zeta_4(H_{0,1}+H_{1,1})\Big]\,, \end{aligned} \tag{3.85}$$

where the suppressed HPL argument is $1-u$. It can be checked that they are all positive for $0<u<1$.

The problem starts at four loops with the leading log coefficients,

$$r^{(4)}_{3,1}(u) = \frac{1}{96}\Big[H_{0,0,0,1}-2H_{0,0,1,1}-2H_{0,1,0,1}+H_{0,1,1,1}\Big]\,,$$

$$r^{(4)}_{2,2}(u) \;=\; \frac{1}{32}\Big[H_{0,0,0,1} - 5H_{0,0,1,1} - H_{0,1,0,1} + H_{0,1,1,1}\Big]\,, \tag{3.86}$$

which turn negative for $u < 0.15$ and $u < 0.2$, respectively, and stay negative as $u \to 0$. The leading terms in their expansions around $u = 0$ are clearly negative:

$$\begin{aligned} r^{(4)}_{3,1}(u) &\sim -\frac{u}{96}\Big[\frac{1}{6}\log^3(1/u) + \frac{1}{2}\log^2(1/u) - (2\zeta_2 - 1)\log(1/u) + 3\zeta_3 - 2\zeta_2 + 1\Big]\,, \\ r^{(4)}_{2,2}(u) &\sim -\frac{u}{32}\Big[\frac{1}{6}\log^3(1/u) + \frac{1}{2}\log^2(1/u) - (\zeta_2 - 1)\log(1/u) - 2\zeta_3 - \zeta_2 + 1\Big], \end{aligned} \tag{3.87}$$

Thus $R^{(4)}_6(u, v, w)$ is negative for very small v and w and $u < 0.14$.

3.6.2 Logarithmic fixes fail

One might first try to fix the problem with $R^{(4)}_6$ at the logarithmic level. Consider the logarithm of the BDS-like normalized amplitude,

$$\mathcal{E} \;=\; \frac{\mathcal{M}_{6,0}}{\mathcal{M}^{\text{BDS-like}}_{6,0}} = \exp\left[R_6 - \frac{\gamma_K}{8} Y\right], \tag{3.88}$$

where γ_K is the cusp anomalous dimension and

$$Y(u, v, w) \;=\; \mathrm{Li}_2(1-u) + \mathrm{Li}_2(1-v) + \mathrm{Li}_2(1-w) + \frac{1}{2}\Big(\log^2 u + \log^2 v + \log^2 w\Big), \tag{3.89}$$

so that

$$\log \mathcal{E}(u, v, w) = R_6(u, v, w) - \frac{\gamma_K}{8} Y(u, v, w). \tag{3.90}$$

This attempt immediately runs into trouble, because the limiting behavior of Y,

$$Y(u, v \to 0, w \to 0) \sim \frac{1}{2}\log^2 v + \frac{1}{2}\log^2 w + \frac{1}{2}\log^2 u + \mathrm{Li}_2(1-u) + 2\zeta_2\,, \tag{3.91}$$

like that of any one-loop function, does not have enough logarithms of v or w to compete with the four powers of logs in the problematic terms in $R^{(4)}_6$.

One can also consider the logarithm of the hexagonal Wilson loop framed by two

pentagons and a box [44, 48],

$$W_{\rm ratio} = \frac{\langle W_{\rm hex}\rangle\langle W_{\rm box}\rangle}{\langle W_{\rm pent}\rangle\langle W_{\rm pent'}\rangle} = \exp\left[R_6 + \frac{\gamma_K}{8}X\right], \tag{3.92}$$

where

$$\begin{aligned} X(u,v,w) &= -{\rm Li}_2(1-u) - {\rm Li}_2(1-v) - {\rm Li}_2(1-w) \\ &\quad - \log\left(\frac{uv}{w(1-v)}\right)\log(1-v) - \log u \log w + 2\zeta_2\,. \end{aligned} \tag{3.93}$$

Since X is a one-loop function, it cannot produce enough logs in the limit to compete with $R_6^{(4)}$, and thus $\log W_{\rm ratio}$ cannot be strictly positive either by four loops.

3.6.3 Other fixes fail

Next we turn to functions that are defined at the level of the MHV amplitude, rather than its logarithm. First we consider the BDS-normalized amplitude $\exp[R_6]$. At one and two loops, it is the same as R_6, while its four-loop coefficient receives an extra positive contribution:

$$\Big[\exp[R_6]\Big]^{(4)} = R_6^{(4)} + \frac{1}{2}\Big[R_6^{(2)}\Big]^2\,. \tag{3.94}$$

Taking into account eq. (3.84), the leading-log $[r_{1,1}^{(2)}]^2$ part of $[R_6^{(2)}]^2$ can and does flip the sign of the $\log^2(1/v)\log^2(1/w)$ coefficient function to positive. But it clearly leaves the $\log^3(1/v)\log(1/w)$ term unaltered. So the addition of $[R_6^{(2)}]^2$ cannot cancel the negative behavior of $R_6^{(4)}$ for kinematics with $0 < v \ll w \ll u < 0.14$, for which $\log^3(1/v)\log(1/w) \gg \log^2(1/v)\log^2(1/w)$.

Can the negative behavior be fixed by the framed Wilson loop $W_{\rm ratio}$ defined in eq. (3.92)? Now X is not S_3 symmetric, and the three cyclically-related line segments all belong to the MHV positive regions: $v, w \to 0$, $0 < u < 1$; $w, u \to 0$, $0 < v < 1$; $u, v \to 0$, $0 < w < 1$. We need to ensure positivity along all three lines and for both orderings of the two vanishing cross ratios. Equivalently, since R_6 is S_3 symmetric, we should consider the $v, w \to 0$, $0 < u < 1$ limits of all six permutations of X. The

original orientation $X(u,v,w)$ already reveals a problem:

$$X(u, v \to 0, w \to 0) \sim -\log(1/w)\log(1/u) - \mathrm{Li}_2(1-u)\,. \tag{3.95}$$

Because there are no $\log(1/v)$'s in this expression, powers of X cannot fix the sign problem that $\exp[R_6]$ still has in the region $0 < v \ll w \ll u < 0.14$.

3.6.4 BDS-like normalized amplitude works

Finally, we consider the BDS-like normalized amplitude itself, $\mathcal{E}(u,v,w)$ defined in eq. (3.88). Since the limiting behavior of Y in eq. (3.91) contains both $\log^2(1/v)$ and $\log^2(1/w)$, it can potentially fix the negative behavior. Indeed it does fix the problem through five loops, at least for $v, w \to 0$, $0 < u < 1$, or (by symmetry) on cyclic permutations of this line segment. It also leads to monotonically increasing behavior as u decreases from 1. The expansion on this line segment now contains many higher powers of the singular logs, all the way up to 2ℓ,

$$\mathcal{E}(u, v \to 0, w \to 0) = \sum_{\ell=0}^{\infty} \sum_{n,k=0}^{2\ell} (-a)^\ell\, \tilde{e}^{(\ell)}_{n,k}(u)\, \log^n(1/v)\log^k(1/w), \tag{3.96}$$

up to power-suppressed terms. Here $\tilde{e}^{(\ell)}_{k,n} = \tilde{e}^{(\ell)}_{n,k}$ and $n + k \leq 2\ell$ for a nonzero coefficient.

As was the case for the NMHV ratio function on the continuation of this line to $u > 1$, discussed in section 3.4.1, there is an HPL representation which *almost* makes manifest the positivity and monotonicity. In this case we use the argument $1-u$ rather than $1-1/u$, since the argument $1-u$ runs from 0 to 1 as u runs from the collinear point $u = 1$ down to the origin. Positivity is manifest from the signs in front of the HPLs at one and two loops:

$$\tilde{e}^{(1)}_{2,0} = \frac{1}{4}\,, \qquad \tilde{e}^{(1)}_{1,1} = 0\,, \qquad \tilde{e}^{(1)}_{1,0} = 0\,, \qquad \tilde{e}^{(1)}_{0,0} = \frac{1}{2}\Big[H_{0,1} + H_{1,1} + 2\zeta_2\Big]\,, \tag{3.97}$$

$$
\begin{aligned}
\tilde{e}^{(2)}_{4,0} &= \frac{1}{32}\,, \qquad \tilde{e}^{(2)}_{3,1} = 0\,, \qquad \tilde{e}^{(2)}_{2,2} = \frac{1}{16}\,, \qquad \tilde{e}^{(2)}_{3,0} = 0\,, \qquad \tilde{e}^{(2)}_{2,1} = 0\,, \\
\tilde{e}^{(2)}_{2,0} &= \frac{1}{8}\Big[H_{0,1} + H_{1,1} + 4\zeta_2\Big]\,, \qquad \tilde{e}^{(2)}_{1,1} = \frac{1}{4}H_{0,1}\,, \qquad \tilde{e}^{(2)}_{1,0} = \frac{1}{4}\Big[2H_{0,0,1} + H_{1,0,1}\Big]\,, \\
\tilde{e}^{(2)}_{0,0} &= \frac{1}{4}\Big[6H_{0,0,0,1} + 2H_{0,0,1,1} + 4H_{0,1,0,1} + 3H_{0,1,1,1} + 4H_{1,0,0,1} + 2H_{1,0,1,1} \\
&\qquad + 3H_{1,1,0,1} + 3H_{1,1,1,1} + 2\zeta_2(H_{0,1} + H_{1,1}) + 15\zeta_4\Big]\,. \qquad (3.98)
\end{aligned}
$$

At three loops the HPL representation no longer makes manifest the positivity of all terms; for example,

$$
\begin{aligned}
\tilde{e}^{(3)}_{2,1} &= \frac{1}{16}\Big[3H_{0,0,1} + H_{1,0,1} - H_{0,1,1}\Big]\,, \\
\tilde{e}^{(3)}_{1,0} &= \frac{1}{8}\Big[18H_{0,0,0,0,1} + 3H_{0,0,0,1,1} + 9H_{0,0,1,0,1} + 6H_{0,0,1,1,1} + 9H_{0,1,0,0,1} + 2H_{0,1,0,1,1} \\
&\qquad + 5H_{0,1,1,0,1} + 9H_{1,0,0,0,1} + 2H_{1,0,0,1,1} + 5H_{1,0,1,0,1} + 3H_{1,0,1,1,1} + 5H_{1,1,0,0,1} \\
&\qquad + H_{1,1,0,1,1} + 3H_{1,1,1,0,1} + \zeta_2(9H_{0,0,1} + 4H_{1,0,1} - H_{0,1,1})\Big]\,. \qquad (3.99)
\end{aligned}
$$

In both of these cases, it is easy to see that the terms with a minus sign are overpowered by the previous term. At higher-loop orders, positivity and monotonicity of the coefficient functions becomes tricky to prove analytically, but we have verified it numerically for all $\tilde{e}^{(\ell)}_{n,k}$ coefficients through five loops.

What about positivity of $\mathcal{E}$ in other parts of the MHV positive region? The double-scaling limit intersects this region in the triangle,

$$
u > 0, \quad w > 0, \quad u + w < 1. \qquad (3.100)
$$

which is the complement of the NMHV double-scaling positive region (3.49) in the positive quadrant. The expansion of $\mathcal{E}$ in this limit is

$$
\mathcal{E}(u, v \to 0, w) = \sum_{\ell=0}^{\infty} \sum_{n=0}^{2\ell} (-a)^\ell \, e^{(\ell)}_n(u, w) \, \log^n(1/v). \qquad (3.101)
$$

The one-loop coefficient functions are,

$$\begin{aligned} e_2^{(1)}(u,w) &= \frac{1}{4}\,, \\ e_1^{(1)}(u,w) &= 0\,, \\ e_0^{(1)}(u,w) &= \frac{1}{4}\log^2(u/w) + \zeta_2 + \frac{1}{2}C^{(1)}(u,w). \end{aligned} \tag{3.102}$$

Now $C^{(1)}(u,w)$ is negative in the NMHV positive region, but the same radial-derivative argument shows that it flips sign around the collinear boundary, where it vanishes. So $C^{(1)}(u,w)$ is positive in the MHV positive region, and the representation (3.102) makes manifest the desired sign (and monotonicity) for $\mathcal{E}^{(1)}(u,v,w)$ in the double-scaling limit of the MHV positive region.

Similarly at two loops we have,

$$\begin{aligned} e_4^{(2)}(u,w) &= \frac{1}{32}\,, \\ e_3^{(2)}(u,w) &= 0\,, \\ e_2^{(2)}(u,w) &= \frac{1}{4}\Big[e_0^{(1)}(u,w) + \zeta_2\Big]\,, \\ e_1^{(2)}(u,w) &= -\frac{1}{2}c_1^{(2)}(u,w), \end{aligned} \tag{3.103}$$

where $e_0^{(1)}(u,w)$ was just argued to be positive. The positivity of $c_1^{(2)}(u,w)$ is proved in the NMHV positive region in appendix E. But again the argument does not rely on $u+w>1$ – except for the overall sign, which flips when crossing the collinear boundary dividing the MHV and NMHV positive regions. Hence $c_1^{(2)}(u,w)$ is negative in the MHV positive region, implying that $e_1^{(2)}(u,w)$ is positive.

The positivity and monotonicity of the last two-loop coefficient, $e_0^{(2)}(u,w)$, is not as simple to prove, but has been confirmed numerically with GiNaC using the basis of multiple polylogarithms given in eq. (3.74). Similar numerical checks confirm the positivity and monotonicity of all the three loop coefficient functions $e_n^{(3)}(u,w)$; we plot the functions governing the leading-log and next-to-leading log behavior in figure 3.7. As can be seen in these plots, $\mathcal{E}$ is not generically required to vanish on the line $u+w=1$. However, the collinear vanishing of R_6 on this line is inherited by the

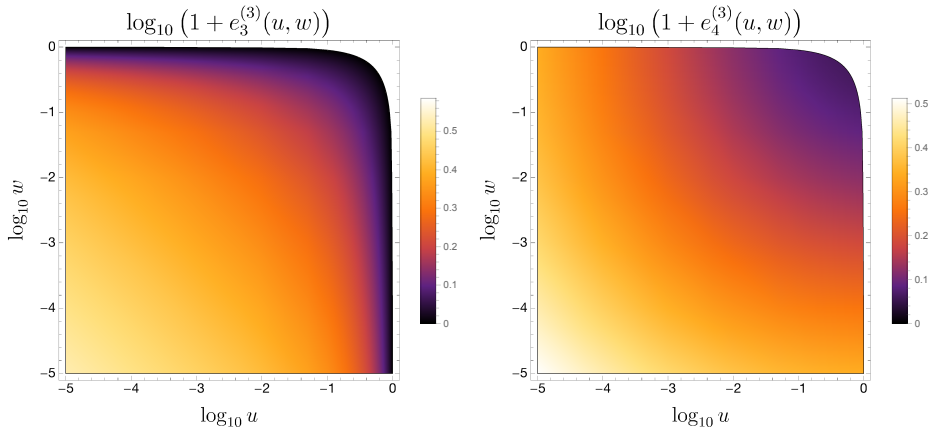

Figure 3.7: The three-loop coefficient functions $e_3^{(3)}(u,w)$ and $e_4^{(3)}(u,w)$ in the double-scaling limit, shifted to make it possible to plot them on a log scale. By plotting these functions against $\log u$ and $\log w$ we deform the $u+w=1$ line to the convex boundary seen in each plot.

coefficient functions $e_n^{(\ell)}(u,w)$ that multiply odd powers of logs. This is due to the fact that the function Y that converts between $\mathcal{E}$ and R_6 in eq. (3.88) can only provide even powers of logs, as can be seen from its definition in eq. (3.89). Correspondingly, $e_3^{(3)}(u,w)$ vanishes along the line $u+w=1$ while $e_4^{(3)}(u,w)$ does not. These plots also exhibit the $u \leftrightarrow w$ symmetry that the functions $e_n^{(\ell)}(u,w)$ inherit from the total symmetry of $\mathcal{E}$.

Finally, we examined the values for $\mathcal{E}^{(\ell)}(u,v,w)$ in the bulk MHV positive region (Region I), from one to four loops, using the representations for $\mathcal{E}^{(\ell)}$ in terms of multiple polylogarithms referred to in section 3.5.2. After randomly generating 1608 points in this region, we found that $\mathcal{E}^{(\ell)}$ had the correct sign through four loops for every point examined.

3.7 Conclusion

In this paper we have demonstrated that the positivity properties of the Amplituhedron persist after momentum integration, at least in some cases. In particular, the ratio function (the IR-finite ratio of the NMHV and MHV amplitudes) has uniform

sign in the same region in which the Amplituhedron is positive. The MHV amplitude also has uniform sign provided that we normalize by a "BDS-like" ansatz. In both cases, it appears that the Minkowski contour of integration preserves positivity more completely than would have been expected.

While we have not provided a general proof, we do provide analytic evidence on a variety of lines, as well as numerical checks through the bulk of kinematic space, all of which support positivity. In doing so, we have observed that the ratio function and $\mathcal{E}$ both appear to be not just of uniform sign but, at least in the double-scaling limit, they are monotonic in a radial direction away from the collinear limit. This property appears to be quite robust, and falls in line with older observations of ratio function numerics, all of which suggest that the ratio function is significantly simpler than the complicated expressions used to represent it might imply.

In the future, it would be interesting to explore whether a more general proof of positivity can be devised. It seems possible that one could find rules for which positive integrands result in positive amplitudes, and such rules would likely be useful in much broader contexts. This would likely involve finding some contour of integration that, unlike the usual Minkowski contour, manifestly preserves positivity. Understanding such a contour could also shed new light on the Amplituhedron, suggesting that there could be an Amplituhedron-like construction of finite quantities such as ratio functions or BDS-like normalized MHV amplitudes, both for the integrands and the final results.

Part II

Seven-Particle Kinematics

Chapter 4

The MHV (NMHV) Symbol at Four (Three) Loops

4.1 Introduction

The desire to construct general scattering amplitudes from their analytic and physical properties has been a goal since the birth of the analytic S-matrix program (see e.g. ref. [150]). More recently, such a procedure has been applied in a perturbative context and referred to as bootstrapping. Aspects of this approach have been applied to theories such as quantum chromodynamics at one loop [151, 152, 153] and more recently at two loops [154, 155, 156]. However, the most powerful applications to date have been to the planar limit of $\mathcal{N} = 4$ super-Yang-Mills (SYM) theory in four dimensions [15, 16]. Fueled by an increased understanding of the classes of analytic functions appearing in amplitudes in general quantum field theories, as well as the stringent constraints obeyed by amplitudes in planar $\mathcal{N} = 4$ SYM, it has been possible to advance as far as five loops [32, 37, 41, 36, 40, 68]. These results in turn provide a rich mine of theoretical data for understanding how scattering amplitudes behave.

The planar limit of a large number of colors in $\mathcal{N} = 4$ SYM has received a great deal of attention because of the remarkable properties it exhibits. In addition to superconformal symmetry it respects a dual conformal symmetry [23, 26, 27, 28, 157], and amplitudes are dual to polygonal light-like Wilson loops [19, 20, 21, 22, 23, 75,

76]. Dual (super)conformal symmetry fixes the four-point and five-point amplitudes uniquely to match the Bern-Dixon-Smirnov (BDS) ansatz [31], which captures all the infrared divergences of planar scattering amplitudes. Starting at six points, the BDS ansatz receives corrections from finite functions of dual conformal invariants [158, 58, 76, 75]. The correction to the maximally helicity violating (MHV) amplitude has traditionally been expressed in terms of a (BDS) remainder function [75, 76, 32, 34, 41], while the correction to the next-to-maximally helicity violating (NMHV) amplitude has traditionally been expressed in terms of the infrared-finite NMHV ratio function [29, 111, 159, 33, 37, 38].

The cluster bootstrap program is built on the idea that certain scattering amplitudes can be determined order by order in perturbation theory using a set of basic building blocks known as cluster coordinates [160, 161]. Inspired by the results of refs. [42, 39], the bootstrap approach developed in refs. [32, 37, 41, 36, 40, 68] assumes that the MHV and NMHV amplitudes at each loop order belong to a particular class of iterated integrals, or generalized polylogarithms. More specifically, the L-loop contribution to the remainder and ratio functions is expected to lie within the space spanned by polylogarithms of weight $2L$ [11] whose symbols can be written in terms of cluster $\mathcal{A}$-coordinates. A further constraint on the relevant space of functions comes from the restriction that only physical branch cuts can appear in the remainder and ratio functions [46].

To make use of this expectation, in the bootstrap program one first constructs a general linear combination of the above set of functions to serve as an ansatz. Then one tries to determine all free coefficients in the ansatz by imposing analytic and physical constraints. This procedure becomes increasingly computationally expensive at higher loop orders, largely due to the fact that the number of relevant functions increases exponentially with the weight. It is hoped that one day a constructive procedure for determining these amplitudes can be developed that does not require constructing the full weight-$2L$ space as an intermediate step. A promising candidate in this respect is the Wilson loop Operator Product Expansion (OPE) [44, 46, 162] and the Pentagon OPE program [48, 49, 51, 163, 56, 57, 164] which provides finite-coupling expressions for the amplitudes as an expansion around (multi-)collinear

kinematics. The main challenge in this framework is to resum the infinite series around these kinematics; there has been progress recently in this direction at weak coupling [109, 165, 166]. Another potential constructive approach could involve the Amplituhedron [13, 14] description of the multi-loop integrand. Perhaps one can extend the methods of ref. [167] for reading off the branch-point locations, in order to enable reading off the entire function.

To date, six- and seven-point amplitudes have been computed in the cluster bootstrap program through the study of so-called hexagon and heptagon functions. Both helicity configurations of the six-point amplitude have been determined through five loops [68], while the MHV seven-point amplitude has been determined at symbol level through three loops [41]. The seven-point NMHV amplitude has not yet received attention in the bootstrap program, but it has been calculated through two loops using slightly different methods [64]. Surprisingly, bootstrapping the seven-point remainder function has thus far proven to be conceptually simpler (i.e. requiring the imposition of fewer constraints) than bootstrapping its six-point counterpart. The collinear limit of the seven-point remainder function must be nonsingular and a well-defined hexagon function. This requirement is so restrictive that it entirely determines the two-loop heptagon remainder function, up to an overall scale. It similarly determines the three-loop remainder function, once the full implications of dual superconformal symmetry are taken into account [41]. The corresponding hexagon remainder function symbols may then be obtained by taking a collinear limit.

In a recent breakthrough [68], the classic work of Steinmann [65, 66] on the compatibility of branch cuts in different channels has been used to supercharge the hexagon function bootstrap program. The Steinmann relations dramatically reduce the size of the functional haystack one must search through in order to find amplitudes, putting higher-loop amplitudes that were previously inaccessible within reach. In this paper we reformulate the heptagon bootstrap of ref. [41] to exploit the power of the Steinmann relations. With their help, we are able to fully determine the symbol of the seven-point three-loop NMHV and four-loop MHV amplitude in planar $\mathcal{N} = 4$ SYM, using only a few simple physical and mathematical inputs. In a separate paper [168], we will investigate various kinematical limits of these amplitudes in

more detail, including the multi-Regge limit [58, 59, 102, 169, 60, 61, 105, 170, 171, 172, 173, 174], the OPE limit [44, 46, 162, 48, 49, 51, 163, 56], and the self-crossing limit [175, 176]. In this paper, we study one of the simpler limits, where the NMHV seven-point amplitude factorizes on a multi-particle pole.

This paper is organized as follows. In section 4.2 we begin by reviewing the general structure of seven-particle MHV and NMHV (super)amplitudes, and different schemes for subtracting their infrared divergences. Section 4.3 discusses the essential ingredients of the amplitude bootstrap for constructing heptagon functions, which are believed to describe the nontrivial kinematical dependence of these amplitudes. Section 4.4 focuses on the additional physical constraints that allow us to single out the MHV or NMHV amplitude from this space of functions.

Our main results, including the analysis of the general space of heptagon symbols, and the determination of the three-loop NMHV and four-loop MHV amplitude symbols, are presented in section 4.5. Section 4.6 describes a sample kinematical limit, the behavior of the NMHV amplitude as a multi-particle Mandelstam invariant vanishes. Finally, section 4.7 contains our conclusions, and discusses possible avenues for future study.

Many of the analytic results in this paper are too lengthy to present in the manuscript; instead, we include them as ancillary files. These files can also be downloaded from [177].

4.2 Seven-Particle Scattering Amplitudes

4.2.1 MHV: The Remainder Function

In planar $\mathcal{N} = 4$ SYM, n-particle amplitudes are completely characterized by the color-ordered partial amplitudes A_n, which are the coefficients of specific traces $\mathrm{Tr}(T^{a_1}T^{a_2}\cdots T^{a_n})$ in the color decomposition of the amplitudes. The MHV helicity configuration has precisely two gluons with negative helicity and $(n-2)$ with positive helicity (in a convention where all particles are outgoing). The MHV amplitude is encoded in the remainder function R_n, which is defined by factoring out the BDS

ansatz A_n^{BDS} [31] (reviewed in appendix F):

$$A_n^{\text{MHV}} = A_n^{\text{BDS}} \exp\left[R_n\right]. \tag{4.1}$$

The BDS ansatz captures all the infrared and collinear divergences [178, 179, 180] in the planar amplitude, so the remainder function is infrared finite. It is also invariant under dual conformal transformations [26, 27, 19, 28, 23]. Moreover, since the BDS ansatz accounts for collinear factorization to all orders in perturbation theory [31], the n-point remainder function smoothly tends to the $(n-1)$-point remainder function in its collinear limits, a fact that will prove to be an important ingredient in the bootstrap program.

In the definition (4.1), R_n is the finite-coupling (or all-loop) remainder function. Here we will be interested in its perturbative expansion. For any function F of the coupling, we denote the coefficients of its perturbative expansion with a superscript according to the definition

$$F = \sum_{L=0}^{\infty} g^{2L} F^{(L)}, \tag{4.2}$$

where $g^2 = g_{YM}^2 N/(16\pi^2)$, g_{YM} is the Yang-Mills coupling constant, and N is the number of colors. Elsewhere in the literature, the coupling constant $a = 2g^2$ is often used. The L-loop contribution to the remainder function, $R_n^{(L)}$, is expected to be a weight-$2L$ iterated integral.

The remainder function vanishes for the four- and five-particle amplitudes, because dual conformally invariant cross ratios cannot be formed with fewer than six external lightlike momenta (in other words, the BDS ansatz is correct to all loop orders for $n = 4$ or 5) [158, 76, 75]. The first nontrivial case, the six-point remainder function, has been successfully computed at two loops [42], three loops [32, 64, 34], four loops [35] and recently five loops [68]. At seven points, the remainder function has been computed at two loops [181, 64, 182, 183] and its symbol has been computed at three loops [41]. The symbol of the four-loop seven-point MHV remainder function $R_7^{(4)}$ is one of the main results of this paper.

4.2.2 NMHV: The Ratio Function and R-invariants

Beyond the MHV case, scattering amplitudes in SYM theory are most efficiently organized by exploiting the (dual) superconformal symmetry [29] of the theory, as reviewed in ref. [184].

In a nutshell, one starts by packaging the on-shell particle content of the theory into a single superfield Φ with the help of four Grassmann variables η^A, whose index transforms in the fundamental representation of the $SU(4)$ R-symmetry group. In other words, all external states, gluons $G^{\pm}$, fermions Γ_A and $\bar{\Gamma}^A$, and scalars S_{AB}, can be simultaneously described by the superfield

$$\Phi = G^+ + \eta^A \Gamma_A + \tfrac{1}{2!}\eta^A\eta^B S_{AB} + \tfrac{1}{3!}\eta^A\eta^B\eta^C \epsilon_{ABCD}\bar{\Gamma}^D + \tfrac{1}{4!}\eta^A\eta^B\eta^C\eta^D\epsilon_{ABCD}G^- \,, \quad (4.3)$$

which allows us to combine all n-point amplitudes into a superamplitude $\mathcal{A}_n(\Phi_1, \ldots, \Phi_n)$.

Expanding the superamplitude in the Grassmann variables separates out its different helicity components. The MHV amplitude is contained in the part of $\mathcal{A}_n^{\text{MHV}}$ with 8 powers of Grassmann variables, or Grassmann degree 8. Specifically, the MHV amplitude discussed in the previous subsection is given in the MHV superamplitude by the term

$$\mathcal{A}_n^{\text{MHV}} = (2\pi)^4\delta^{(4)}\Big(\sum_{i=1}^n p_i\Big) \sum_{1\le j<k\le n} (\eta_j)^4(\eta_k)^4 A_n^{\text{MHV}}(1^+ \ldots j^- \ldots k^- \ldots n^+) + \ldots, \quad (4.4)$$

where we have shown only the pure-gluon terms explicitly. Similarly, the terms of Grassmann degree 12 make up the NMHV superamplitude. Since NMHV amplitudes in this theory have the same infrared-divergent structure as MHV amplitudes, the two superamplitudes can be related by

$$\mathcal{A}_n^{\text{NMHV}} = \mathcal{A}_n^{\text{MHV}}\,\mathcal{P}_n \,, \quad (4.5)$$

where the infrared-finite quantity $\mathcal{P}_n$ is called the NMHV ratio function and has Grassmann degree 4. On the basis of tree-level and one-loop amplitude computations, it was argued in ref. [29] that $\mathcal{P}_n$ is dual conformally invariant.

At tree level, the dual conformal symmetry is enhanced to dual superconformal symmetry, and the ratio function can be written as a sum of *dual superconformal invariants* or '*R-invariants*' [29, 111]. These quantities, which carry the dependence on the fermionic variables, are algebraic functions of the kinematics and can be written as Grassmannian contour integrals [82]. From this representation it is also possible to prove their invariance under ordinary superconformal transformations [12, 185], or in other words their Yangian invariance [30].

As shown in ref. [82], R-invariants are most easily expressed in terms of the momentum supertwistors $\mathcal{Z}_i$ defined by[1] [81]

$$\mathcal{Z}_i = (Z_i \,|\, \chi_i)\,, \qquad Z_i^{\alpha,\dot{\alpha}} = (\lambda_i^\alpha, x_i^{\beta\dot{\alpha}}\lambda_{i\beta})\,, \qquad \chi_i^A = \theta_i^{\alpha A}\lambda_{i\alpha}\,. \tag{4.6}$$

Their fermionic components χ_i are associated with the fermionic dual coordinates θ_i in the same way that the bosonic twistors Z_i are associated with the bosonic dual coordinates x_i. Differences between color-adjacent dual coordinates x_i and θ_i are related to the external momenta p_i and supermomenta q_i, respectively:

$$p_i^{\alpha\dot{\alpha}} = \lambda_i^\alpha \tilde{\lambda}_i^{\dot{\alpha}} = x_{i+1}^{\alpha\dot{\alpha}} - x_i^{\alpha\dot{\alpha}}\,, \qquad q_i^{\alpha A} = \lambda_i^\alpha \eta_i^A = \theta_{i+1}^{\alpha A} - \theta_i^{\alpha A}\,. \tag{4.7}$$

Given any set of five supertwistors $\mathcal{Z}_a, \mathcal{Z}_b, \mathcal{Z}_c, \mathcal{Z}_d, \mathcal{Z}_e$, we may define a corresponding NMHV R-invariant as a 5-bracket

$$[abcde] = \frac{\delta^{0|4}(\chi_a\langle bcde\rangle + \text{cyclic})}{\langle abcd\rangle\langle bcde\rangle\langle cdea\rangle\langle deab\rangle\langle eabc\rangle}\,, \tag{4.8}$$

in terms of dual conformally invariant bosonic 4-brackets

$$\langle ijkl\rangle \equiv \langle Z_i Z_j Z_k Z_l\rangle = \epsilon_{ABCD} Z_i^A Z_j^B Z_k^C Z_l^D = \det(Z_i Z_j Z_k Z_l)\,, \tag{4.9}$$

and a fermionic delta function $\delta^{0|4}(\xi) = \xi^1\xi^2\xi^3\xi^4$ for the different $SU(4)$ components of ξ. The original definition of the R-invariants [29, 111] (there denoted $R_{r;ab}$) in

[1] The indices $\alpha, \dot{\alpha} = 1, 2$ denote the components of the spinor representation of the Lorentz group $SO(3,1) \simeq SL(2,\mathbb{C})$.

normal twistor space corresponds to the special case $R_{r;ab} = [r, a{-}1, a, b{-}1, b]$.

From the definition (4.8), we can see that R-invariants are antisymmetric in the exchange of any pair of supertwistor indices (hence also invariant under cyclic permutations). They are also manifestly dual conformally invariant, since they don't depend on spinor products $\langle ij\rangle$. The aforementioned Grassmannian contour integral representation in momentum twistor space [82] makes the full dual conformal invariance manifest. It also allows one to prove more transparently the following important identity between R-invariants: Given any six momentum supertwistors $\mathcal{Z}_a, \mathcal{Z}_b, \mathcal{Z}_c, \mathcal{Z}_d, \mathcal{Z}_e, \mathcal{Z}_f$, their R-invariants are related by [29]

$$[abcde] - [bcdef] + [cdefa] - [defab] + [efabc] - [fabcd] = 0\,. \tag{4.10}$$

For n-particle scattering, there exist $\binom{n}{6}$ such equations for the $\binom{n}{5}$ distinct R-invariants; however, it turns out that only $\binom{n-1}{5}$ are independent. So in the end we are left with

$$\#\text{ linearly independent } n\text{-particle } R\text{-invariants} = \binom{n}{5} - \binom{n-1}{5} = \binom{n-1}{4}\,. \tag{4.11}$$

For example, there are 5, 15, and 35 independent R-invariants relevant for 6-, 7- and 8-particle NMHV scattering amplitudes, respectively.

Let us now focus on the seven-particle NMHV superamplitude. For compactness we may express the corresponding R-invariants in terms of the particle indices that are *not* present in the 5-brackets (4.8), for example

$$[12345] = (67) = (76)\,, \tag{4.12}$$

where (by convention) the 5-bracket on the left-hand side of this definition is always ordered, so ordering on the right-hand side doesn't matter.

In this notation, the representation for the tree-level ratio function found in ref. [111] may be rewritten as

$$\mathcal{P}_7^{(0)} = \frac{3}{7}\,(12) + \frac{1}{7}\,(13) + \frac{2}{7}\,(14) \;+ \text{cyclic}\,. \tag{4.13}$$

Following the same reference, we find it convenient to use a basis of 15 independent R-invariants consisting of $\mathcal{P}_7^{(0)}$ together with (12), (14), and their cyclic permutations. (Because $\mathcal{P}_7^{(0)}$ is totally symmetric, it has no independent cyclic images.) In particular, the remaining R-invariants $(i, i+2)$ are related to this set by

$$(13) = -(15) - (17) - (34) - (36) - (56) + \mathcal{P}_7^{(0)}\,, \tag{4.14}$$

plus the cyclic permutations of this identity.

Beyond tree level, the independent R-invariants are dressed by transcendental functions of dual conformal invariants, and the ratio function can be put in the form

$$\mathcal{P}_7 = \mathcal{P}_7^{(0)}\, V_0 + [(12)\, V_{12} + (14)\, V_{14} \ + \text{cyclic}]\,. \tag{4.15}$$

As we will review in section 4.4.2, $\mathcal{P}_7$ is symmetric under the dihedral group D_7. The component V_0 inherits the full dihedral symmetry of $\mathcal{P}_7^{(0)}$, whereas V_{12} and V_{14} are only invariant under the flip $i \to 3-i$ and $i \to 5-i$ of their momentum twistor labels, respectively.

The dependence of $\mathcal{P}_7$ on the coupling enters only through the functions V_0 and V_{ij}. Their L-loop contributions, $V_0^{(L)}$ and $V_{ij}^{(L)}$, like the remainder function, $R_7^{(L)}$, are expected to be weight-$2L$ iterated integrals. Using the notation introduced in eq. (4.2) we must have

$$V_0^{(0)} = 1\,, \quad V_{12}^{(0)} = V_{14}^{(0)} = 0 \tag{4.16}$$

at tree level. At one loop, these functions become [111]

$$\begin{aligned}
V_0^{(1)} &= \mathrm{Li}_2\,(1-u_1) - \mathrm{Li}_2\,(1-u_1u_4) - \log u_1 \log u_3 + \ \text{cyclic}\,,\\
V_{12}^{(1)} &= -\mathrm{Li}_2\,(1-u_6) + \mathrm{Li}_2\,(1-u_1u_4) + \mathrm{Li}_2\,(1-u_2u_6) + \mathrm{Li}_2\,(1-u_3u_6)\,,\\
&\quad + \log u_1 \log u_2 - \log u_3 \log u_2 + \log u_4 \log u_2 + \log u_1 \log u_3 + \log u_3 \log u_4\\
&\quad + \log u_1 \log u_6 + \log u_4 \log u_6 - \zeta_2\,,\\
V_{14}^{(1)} &= \mathrm{Li}_2\,(1-u_1u_4) + \mathrm{Li}_2\,(1-u_3u_6) + \log u_1 \log u_3 + \log u_4 \log u_3 + \log u_1 \log u_6\\
&\quad + \log u_4 \log u_6 - \zeta_2\,.
\end{aligned} \tag{4.17}$$

See also ref. [186] for a more recent, compact representation of the same amplitude. In the above relations and everything that follows, the cross ratios u_i are defined by,

$$u_{ij} = \frac{x^2_{i,j+1}\, x^2_{i+1,j}}{x^2_{i,j}\, x^2_{i+1,j+1}}\,, \qquad\qquad u_i = u_{i+1,i+4} = \frac{x^2_{i+1,i+5}\, x^2_{i+2,i+4}}{x^2_{i+1,i+4}\, x^2_{i+2,i+5}}\,. \tag{4.18}$$

The u_i are dual conformally invariant combinations of the Mandelstam invariants, see eq. (4.7) and also eq. (4.32) below.

Finally, the symbol of the two-loop NMHV heptagon has been computed in ref. [64] using the same choice of independent R-invariants as in eq. (4.15), with the help of an anomaly equation for the $\bar{Q}$ dual superconformal symmetry generators. Here we will use the Steinmann cluster bootstrap to push to three loops: The symbols of the functions $V_0^{(3)}$, $V_{12}^{(3)}$, and $V_{14}^{(3)}$ constituting the three-loop seven-point NMHV ratio function are another of the main results of this paper.

4.2.3 The BDS- and BDS-like Normalized Amplitudes

In the previous sections we mentioned that MHV and NMHV amplitudes have the same infrared-divergent structure, which is accurately captured by the BDS ansatz. This fact allows us to define the MHV and NMHV *BDS-normalized* superamplitudes,

$$\mathcal{B}_n \equiv \frac{\mathcal{A}_n^{\text{MHV}}}{\mathcal{A}_n^{\text{BDS}}} = \frac{A_n^{\text{MHV}}}{A_n^{\text{BDS}}} = \exp\left[R_n\right], \tag{4.19}$$

$$B_n \equiv \frac{\mathcal{A}_n^{\text{NMHV}}}{\mathcal{A}_n^{\text{BDS}}} = \frac{\mathcal{A}_n^{\text{NMHV}}}{\mathcal{A}_n^{\text{MHV}}} \frac{\mathcal{A}_n^{\text{MHV}}}{\mathcal{A}_n^{\text{BDS}}} = \mathcal{P}_n\, \mathcal{B}_n\,, \tag{4.20}$$

where $\mathcal{A}_n^{\text{BDS}}$ is the superamplitude obtained from the bosonic BDS ansatz by replacing the tree-level MHV Parke-Taylor factor [2, 187] it contains with its supersymmetrized version [77]. Indeed, normalizations (4.19), (4.20) were found to be more natural for the study of the dual superconformal symmetry anomaly equation [64].

In what follows, it will prove greatly beneficial to define yet another set of infrared-finite quantities, using an alternate normalization factor that is compatible with the

Steinmann relations. The BDS ansatz is essentially the exponential of the full one-loop amplitude, which includes a finite part with nontrivial dependence on Mandelstam invariants involving all possible numbers of external momenta. Dividing by the BDS ansatz produces a quantity with altered dependence on three-particle Mandelstam invariants. As we will see, such a quantity does not satisfy the Steinmann relations. In the case of seven-particle scattering (indeed, whenever n is not a multiple of four), all the dependence on the three-particle invariants (and higher-particle invariants) can be assembled into a dual conformally invariant function Y_n, which we may remove from the one-loop amplitude in order to define a *BDS-like* ansatz,

$$\mathcal{A}_n^{\text{BDS-like}} \equiv \mathcal{A}_n^{\text{BDS}} \exp\left[\frac{\Gamma_{\text{cusp}}}{4} Y_n\right], \tag{4.21}$$

where

$$Y_6 = -\text{Li}_2\left(1-\frac{1}{u}\right) - \text{Li}_2\left(1-\frac{1}{v}\right) - \text{Li}_2\left(1-\frac{1}{w}\right), \tag{4.22}$$

$$Y_7 = -\sum_{i=1}^{7}\left[\text{Li}_2\left(1-\frac{1}{u_i}\right) + \frac{1}{2}\log\left(\frac{u_{i+2}u_{i-2}}{u_{i+3}u_i u_{i-3}}\right)\log u_i\right], \tag{4.23}$$

and

$$\Gamma_{\text{cusp}} = \sum_{L=1}^{\infty} g^{2L}\Gamma_{\text{cusp}}^L = 4g^2 - \frac{4\pi^2}{3}g^4 + \frac{44\pi^4}{45}g^6 - 4\left(\frac{73\pi^6}{315} + 8\zeta_3^2\right)g^8 + \mathcal{O}(g^{10}), \tag{4.24}$$

is the cusp anomalous dimension in the normalization of e.g. [49].[2] In eq. (4.22), u, v, w are the three cross ratios for six-point kinematics, defined below in eq. (4.58). The difference between the BDS- and BDS-like-normalized ansätze for seven-point kinematics is reviewed in more detail in appendix F. The utility of the BDS-like ansatz was first noticed in the strong coupling analysis of amplitudes via the AdS/CFT correspondence [113] (see also ref. [188]). At weak coupling, it was found to simplify the six-point multi-particle factorization limit [37], self-crossing limit [176] and NMHV

[2] In particular, $\Gamma_{\text{cusp}} = \gamma_K/2$ compared to the normalization of [31] and subsequent papers of Dixon and collaborators.

$\bar{Q}$ relations [38], before its role in applying the six-point Steinmann relations was noticed [68]. We will see its advantages as well in our seven-point analysis.

When n is a multiple of four it is not possible to simultaneously remove the dependence on all three-particle and higher-particle Mandelstam invariants in a conformally invariant fashion [189]. However, for $n = 8$ it is still possible to separately remove the dependence of all three-particle invariants, *or* of all four-particle invariants, giving rise to two different BDS-like ansätze.

Restricting our attention to the case $n \neq 4$, we may thus define the *BDS-like-normalized* MHV and NMHV amplitudes as

$$\begin{aligned}
\mathcal{E}_n &\equiv \frac{\mathcal{A}_n^{\text{MHV}}}{\mathcal{A}_n^{\text{BDS-like}}} = \frac{\mathcal{A}_n^{\text{MHV}}}{\mathcal{A}_n^{\text{BDS}}} \frac{\mathcal{A}_n^{\text{BDS}}}{\mathcal{A}_n^{\text{BDS-like}}} = \mathcal{B}_n \exp\left[-\frac{\Gamma_{\text{cusp}}}{4} Y_n\right] = \exp\left[R_n - \frac{\Gamma_{\text{cusp}}}{4} Y_n\right], \\
E_n &\equiv \frac{\mathcal{A}_n^{\text{NMHV}}}{\mathcal{A}_n^{\text{BDS-like}}} = \frac{\mathcal{A}_n^{\text{NMHV}}}{\mathcal{A}_n^{\text{BDS}}} \frac{\mathcal{A}_n^{\text{BDS}}}{\mathcal{A}_n^{\text{BDS-like}}} = B_n \exp\left[-\frac{\Gamma_{\text{cusp}}}{4} Y_n\right] = \mathcal{P}_n \, \mathcal{E}_n \,,
\end{aligned} \tag{4.25}$$

where we have also spelled out their relation to the previously-considered normalizations. Note that

$$\mathcal{E}_n^{(1)} = -Y_n \,, \tag{4.26}$$

since R_n starts at two loops.

Because we will focus almost exclusively on heptagon amplitudes in this paper, we will usually drop the particle index n from of all of its associated quantities in order to avoid clutter, e.g. $\mathcal{P}_7 \to \mathcal{P}$, $\mathcal{E}_7 \to \mathcal{E}$ and $E_7 \to E$. In the NMHV case we will instead use subscripts to denote components multiplying the different R-invariants. For example, the BDS-normalized and BDS-like-normalized analogs of eq. (4.15) are

$$B = \mathcal{P}^{(0)} \, B_0 + [(12) \, B_{12} + (14) \, B_{14} + \text{ cyclic}] \,, \tag{4.27}$$

$$E = \mathcal{P}^{(0)} \, E_0 + [(12) \, E_{12} + (14) \, E_{14} + \text{ cyclic}] \,. \tag{4.28}$$

It is important to note that because the R-invariants are coupling-independent, the same coupling-dependent factor that relates NMHV superamplitudes in different normalizations will also relate the respective coefficient functions of the R-invariants. In

other words,

$$E_* = B_* \exp\left[-\frac{\Gamma_{\text{cusp}}}{4} Y\right] = \mathcal{E}\, V_*\,, \tag{4.29}$$

where $*$ can be any index, 0 or ij.

Given that in this paper we will be focusing exclusively on symbols, it's also worth emphasizing that when expanding eq. (4.25) or equivalently eq. (4.29) at weak coupling, we may replace $\Gamma_{\text{cusp}} \to 4g^2$, as a consequence of the fact that the symbol of any term containing a transcendental constant, such as ζ_n, is zero. Thus, the conversion between the BDS-like-normalized quantities $F \in \{\mathcal{E}, E, E_0, E_{ij}\}$ and the corresponding BDS-normalized quantities $\mathcal{F} \in \{\mathcal{B}, B, B_0, B_{ij}\}$ at symbol level and at fixed order in the coupling, simply becomes

$$F^{(L)} = \sum_{k=0}^{L} \mathcal{F}^{(k)} \frac{(-Y_n)^{L-k}}{(L-k)!}\,, \qquad \mathcal{F}^{(L)} = \sum_{k=0}^{L} F^{(k)} \frac{Y_n^{L-k}}{(L-k)!}\,. \tag{4.30}$$

In particular, for R_7, which sits in the exponent, its analogous conversion to $\mathcal{E}_7$ through four loops is given by

$$\begin{aligned}
\mathcal{E}_7^{(2)} &= R_7^{(2)} + \frac{1}{2}\Big(\mathcal{E}_7^{(1)}\Big)^2\,,\\
\mathcal{E}_7^{(3)} &= R_7^{(3)} + \mathcal{E}_7^{(1)} R_7^{(2)} + \frac{1}{6}\Big(\mathcal{E}_7^{(1)}\Big)^3\,,\\
\mathcal{E}_7^{(4)} &= R_7^{(4)} + \frac{1}{2}\Big(R_7^{(2)}\Big)^2 + \mathcal{E}_7^{(1)} R_7^{(3)} + \frac{1}{2}\Big(\mathcal{E}_7^{(1)}\Big)^2 R_7^{(2)} + \frac{1}{24}\Big(\mathcal{E}_7^{(1)}\Big)^4\,.
\end{aligned} \tag{4.31}$$

In summary, all the nontrivial kinematic dependence of seven-particle scattering can be encoded in the four transcendental functions R_7, B_0, B_{12} and B_{14} using BDS normalization, or equivalently $\mathcal{E}, E_0, E_{12}$ and E_{14} using BDS-like normalization. (The other E_{ij} that are needed are related to E_{12} and E_{14} by cyclic permutations.) These functions are all expected to belong to a very special class of transcendental functions called heptagon functions, whose definition and construction we turn to in the next section. However, we will see that it is only the BDS-like-normalized amplitudes that inherit a specific analytic property from the full amplitudes: they satisfy the Steinmann relations. Taking this restriction into account hugely trims the space

of heptagon functions needed to bootstrap the BDS-like normalized functions, thus allowing for a far more efficient construction of the amplitude.

4.3 The Steinmann Cluster Bootstrap

The heptagon bootstrap approach we use in this paper is a slight refinement of that used in ref. [41], which in turn is a generalization of the hexagon function bootstrap [32, 33, 34, 35, 37, 36]. We begin this section by reviewing some basics of the bootstrap approach and defining heptagon functions. Then we express the seven-point Steinmann relations in the language of cluster $\mathcal{A}$-coordinates. We assume a basic working knowledge of both symbols [42, 93, 94, 90, 91, 92, 39, 190] and momentum twistor notation [81].

4.3.1 Symbol Alphabet

In the cluster bootstrap program for n-point amplitudes in planar SYM theory, we assume that the symbol alphabet consists of certain objects known as cluster $\mathcal{A}$-coordinates. These coordinates have been discussed extensively in the context of scattering amplitudes; see for example ref. [39]. Here we will only briefly recall that the kinematic data for a scattering process in planar SYM theory may be specified by a collection of n momentum twistors [81], each of which is a homogeneous coordinate Z_i on $\mathbb{P}^3$. The configuration space for SYM theory is $\mathrm{Conf}_n(\mathbb{P}^3) = \mathrm{Gr}(4,n)/(\mathbb{C}^*)^{n-1}$, and cluster $\mathcal{A}$-coordinates on this space can be expressed in terms of the Plücker coordinates of 4-brackets $\langle ijkl\rangle$, which we defined in eq. (4.9).

Mandelstam invariants constructed from sums of cyclically adjacent external momenta $p_i, p_{i+1}, \ldots, p_{j-1}$ can be expressed nicely in terms of dual coordinates x_i satisfying the relation $p_i = x_{i+1} - x_i$. Using the notation $x_{ij} = x_i - x_j$, the Mandelstam invariant $s_{i,\ldots,j-1}$ can be written as

$$s_{i,\ldots,j-1} = (p_i + p_{i+1} + \cdots + p_{j-1})^2 = x_{ij}^2 = \frac{\langle i{-}1\, i\, j{-}1\, j\rangle}{\langle i{-}1\, i\rangle\langle j{-}1\, j\rangle}\,. \tag{4.32}$$

Here we have also shown how to express the Mandelstam invariant $s_{i,\ldots,j-1}$ in terms of Plücker coordinates and the usual spinor products $\langle ij\rangle = \epsilon_{\alpha\beta}\lambda_i^\alpha\lambda_j^\beta$, see also eq. (4.7). The denominator factors in eq. (4.32) drop out of any dual conformally invariant quantity and so may be ignored for our purposes. We will use eq. (4.32) to establish the connection between the cluster $\mathcal{A}$-coordinates (defined in terms of Plücker coordinates) and the Steinmann relations (formulated in terms of Mandelstam invariants). More general Plücker coordinates $\langle ijkl\rangle$ not of the form $\langle i{-}1\, i\, j{-}1\, j\rangle$ have more complicated (algebraic) representations in terms of Mandelstam invariants. (A systematic approach for finding such representations was discussed in the appendix of ref. [191].)

In this paper we focus on $n = 7$ where there are a finite number of $\mathcal{A}$-coordinates. In addition to the Plücker coordinates $\langle ijkl\rangle$ there are 14 Plücker bilinears of the form $\langle a(bc)(de)(fg)\rangle \equiv \langle abde\rangle\langle acfg\rangle - \langle abfg\rangle\langle acde\rangle$. A convenient complete and multiplicatively independent set of 42 dual conformally invariant ratios, introduced in ref. [41], is given in terms of these building blocks by

$$\begin{aligned} a_{11} &= \frac{\langle 1234\rangle\langle 1567\rangle\langle 2367\rangle}{\langle 1237\rangle\langle 1267\rangle\langle 3456\rangle}\,, & a_{41} &= \frac{\langle 2457\rangle\langle 3456\rangle}{\langle 2345\rangle\langle 4567\rangle}\,,\\ a_{21} &= \frac{\langle 1234\rangle\langle 2567\rangle}{\langle 1267\rangle\langle 2345\rangle}\,, & a_{51} &= \frac{\langle 1(23)(45)(67)\rangle}{\langle 1234\rangle\langle 1567\rangle}\,,\\ a_{31} &= \frac{\langle 1567\rangle\langle 2347\rangle}{\langle 1237\rangle\langle 4567\rangle}\,, & a_{61} &= \frac{\langle 1(34)(56)(72)\rangle}{\langle 1234\rangle\langle 1567\rangle}\,, \end{aligned} \tag{4.33}$$

with a_{ij} for $1 < j \leq 7$ given by cyclic permutation of the particle labels; specifically,

$$a_{ij} = a_{i1}\big|_{Z_k\to Z_{k+j-1}}\,. \tag{4.34}$$

The Steinmann relations, to be reviewed in section 4.3.4, are expressed simply in terms of Mandelstam invariants. We therefore note that with the help of eq. (4.32) we can express a_{1j} quite simply as

$$a_{11} = \frac{s_{23}s_{67}s_{712}}{s_{12}s_{71}s_{45}}\,, \tag{4.35}$$

with the remaining six a_{1j} again given by cyclic permutations. The remaining 35 cluster $\mathcal{A}$-coordinates do not admit simple representations in terms of Mandelstam invariants because they involve brackets not of the form $\langle i{-}1\, i\, j{-}1\, j\rangle$.

Finally, it is useful to relate the cross ratios u_i, defined in eq. (4.18), to the letters a_{ij}. Eq. (4.35) can alternatively be written as

$$a_{11} = \frac{x_{24}^2 x_{61}^2 x_{73}^2}{x_{13}^2 x_{72}^2 x_{46}^2}\,. \tag{4.36}$$

Combining this equation with cyclic permutations of it, and using eq. (4.18), we find that

$$\frac{a_{11}}{a_{14}a_{15}} = \frac{x_{73}^2 x_{46}^2}{x_{74}^2 x_{36}^2} = u_{36} = u_2\,, \tag{4.37}$$

plus cyclic permutations of this relation. Note that, although we can define 7 of these cross ratios u_i in seven-point kinematics, an n-point scattering process in this theory only has $3n-15$ algebraically independent dual conformal invariants. Thus only 6 of the 7 u_i (or a_{1i}) are algebraically independent. The seven u_i obey a single algebraic equation, the condition that a particular Gram determinant vanishes, which restricts the kinematics to a six-dimensional surface within the seven-dimensional space of cross ratios. We will not need the explicit form of the Gram determinant in this paper.

4.3.2 Integrability

The heptagon bootstrap is based on the working hypothesis that any seven-point L-loop amplitude in planar $\mathcal{N}=4$ SYM theory can be expressed as a linear combination of weight-$2L$ generalized polylogarithm functions written in the 42-letter alphabet shown in eq. (4.33). Using this alphabet one can write 42^k distinct symbols of weight k. Fortunately, relatively few linear combinations of these 42^k symbols are actually the symbol of some function. A symbol $\mathcal{S}$ of the form

$$\mathcal{S}(f_k) = \sum_{\alpha_1,\ldots,\alpha_k} f_0^{(\alpha_1,\ldots,\alpha_k)}(\phi_{\alpha_1}\otimes\cdots\otimes\phi_{\alpha_k}), \tag{4.38}$$

where the ϕ_{α_j} are letters, corresponds to an actual function only if it satisfies the integrability condition

$$\sum_{\alpha_1,\ldots,\alpha_k} f_0^{(\alpha_1,\ldots,\alpha_k)} \underbrace{(\phi_{\alpha_1}\otimes\cdots\otimes\phi_{\alpha_k})}_{\text{omitting } \alpha_j\otimes\alpha_{j+1}} d\log\phi_{\alpha_j}\wedge d\log\phi_{\alpha_{j+1}} = 0 \quad \forall j\in\{1,2,\ldots,k-1\}\,, \tag{4.39}$$

where the wedge product between two letters ϕ_p, ϕ_q that are functions of the independent variables x^i is defined to be

$$d\log\phi_p\wedge d\log\phi_q = \sum_{m,n}\left[\frac{\partial\log\phi_p}{\partial x^m}\frac{\partial\log\phi_q}{\partial x^n} - \frac{\partial\log\phi_p}{\partial x^n}\frac{\partial\log\phi_q}{\partial x^m}\right] dx^m\wedge dx^n\,. \tag{4.40}$$

The symbols of physical amplitudes have several additional properties, to which we will now turn our attention.

4.3.3 Symbol Singularity Structure

Locality requires that amplitudes can only have singularities when an intermediate particle goes on-shell. In a planar theory the momenta of intermediate particles can always be expressed as a sum of cyclically adjacent momenta, and thresholds in massless theories are always at the origin. Hence perturbative amplitudes in planar SYM theory can only have branch points when the corresponding Mandelstam invariants $s_{i,\ldots,j-1} = x_{ij}^2$ vanish.

When some letter ϕ appears in the first entry of a symbol it indicates that the corresponding function has branch points at $\phi = 0$ and $\phi = \infty$. Therefore the first entry of a symbol that corresponds to a physical scattering amplitude must be a ratio of products of x_{ij}^2 [46]. We see from eqs. (4.32) and (4.33) that only the seven a_{1j} are valid first entries. The remaining 35 cluster $\mathcal{A}$-coordinates contain terms that may be zero (or infinite) without any intermediate particles going on-shell. There is no possibility of cancellation in a sum over terms in a symbol since the letters of the alphabet are multiplicatively independent. The restriction that the first entry of the symbol of any seven-point amplitude must be one of the seven a_{1j} is called the first-entry condition.

4.3.4 Steinmann Relations

The classic work of Steinmann provided powerful restrictions on the analytic form of discontinuities [65, 66]. Expanding upon his work, Cahill and Stapp found that the generalized Steinmann relations hold and that double discontinuities vanish for any pair of overlapping channels [67].[3] A channel is labelled by a Mandelstam invariant, but it also corresponds to an assignment of particles to incoming and outgoing states. Two channels overlap if the four sets into which they divide the particles – (incoming,incoming), (incoming,outgoing), (outgoing,incoming) and (outgoing,outgoing) – are all non-empty. Fig. 4.1 shows a pair of overlapping channels for the seven-point process, s_{345} and s_{234}. They overlap because they divide the seven particles into the four non-empty sets $\{2\}$, $\{3,4\}$, $\{5\}$, and $\{6,7,1\}$.

Unlike two-particle invariants, three-particle invariants can cross zero "gently", without any other invariants having to change sign. Fig. 4.1 is drawn for the $3 \to 4$ configuration with particles 1, 2 and 3 incoming. Within that configuration, the left panel shows that s_{345} can be either negative or positive. As s_{345} moves from negative to positive, a branch cut opens up, due to one or more on-shell particles being allowed to propagate between the two blobs. The discontinuity in the amplitude across the branch cut is given by the sum of all such on-shell intermediate-state contributions, integrated over their respective phase space. The same is true for the s_{234} discontinuity illustrated in the right panel. However, once one takes the s_{345} discontinuity, the resulting function cannot have a second discontinuity in the s_{234} channel, because it is impossible for states to propagate on-shell simultaneously in both the s_{345} and s_{234} "directions". Thus we require the Steinmann conditions,

$$\text{Disc}_{s_{i+1,i+2,i+3}}\left[\text{Disc}_{s_{i,i+1,i+2}}F\right] = \text{Disc}_{s_{i+2,i+3,i+4}}\left[\text{Disc}_{s_{i,i+1,i+2}}F\right] = 0, \tag{4.41}$$

to hold for all $i = 1, 2, \ldots 7$.

In contrast, the s_{234} channel does not overlap the s_{567} channel (or the s_{671} channel). For example, in the right panel of the figure, one can have a second discontinuity,

[3] The implications of the Steinmann relations for the multi-Regge limit of amplitudes in planar $\mathcal{N} = 4$ SYM have been analyzed in refs. [192, 193, 58, 59].

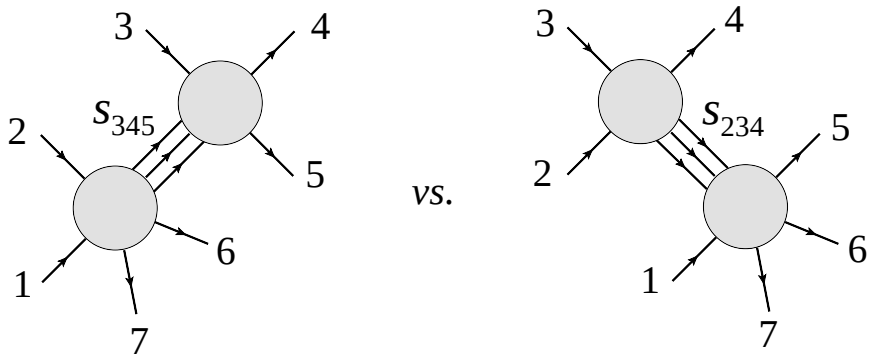

Figure 4.1: The figure on the left (right) shows the discontinuity of an amplitude in the s_{345} (s_{234}) channel due to the respective intermediate states. These two channels overlap, which implies that the states that cross the first cut cannot produce a discontinuity in the second channel (or vice versa).

after taking $\text{Disc}_{s_{234}}$, in the s_{567} channel, as particle 1 and the particles crossing the s_{234} cut rescatter into another set of intermediate states, which then materializes into particles 5, 6 and 7. That is, the following double discontinuities can be nonvanishing,

$$\text{Disc}_{s_{i+3,i+4,i+5}}\left[\text{Disc}_{s_{i,i+1,i+2}}F\right] \neq 0, \qquad \text{Disc}_{s_{i+4,i+5,i+6}}\left[\text{Disc}_{s_{i,i+1,i+2}}F\right] \neq 0, \tag{4.42}$$

and they provide us with no useful constraints. Also, the "self" double discontinuities are nonvanishing,

$$\text{Disc}_{s_{i,i+i,i+2}}\left[\text{Disc}_{s_{i,i+1,i+2}}F\right] \neq 0, \tag{4.43}$$

and are not of use to us. A recent analysis of the Steinmann relations, focusing on the six-point case, can be found in ref. [68].

We will only consider restrictions imposed on the symbol letters a_{ij} by the Steinmann relations on overlapping three-particle cuts, eq. (4.41). If there are any restrictions imposed by using two-particle cuts, they are considerably more subtle for generic kinematics. Flipping the sign of a two-particle invariant generally entails moving a particle from the initial state to the final state, or vice versa, and other invariants can flip sign at the same time, making it hard to assess the independence of the two-particle discontinuities.

Because the discontinuities of a symbol are encoded in its first entries, double

discontinuities are encoded by the combinations of first and second entries that appear together. Correspondingly, the Steinmann relations tell us that the symbol of an amplitude cannot have any terms in which overlapping three-particle Mandelstam invariants appear together as first and second entries. Eqs. (4.32)–(4.33) imply that this only imposes a constraint on the letters a_{1j}, since the other letters do not contain three-particle Mandelstam invariants $s_{i-1,i,i+1} \propto \langle i{-}2\, i{-}1\, i{+}1\, i{+}2\rangle$. More specifically, we see in eq. (4.35) that each a_{1i} is proportional to a single three-particle invariant $s_{i-1,i,i+1}$, so a first entry of a_{1i} cannot be followed by a second entry of $a_{1,i+1}, a_{1,i+2}, a_{1,i+5}$, or $a_{1,i+6}$, all of which contain a three-particle invariant involving p_{i-1}, p_i, or p_{i+1}. A first entry of a_{1i} *can* be followed by a second entry of a_{1i}, $a_{1,i+3}$, $a_{1,i+4}$, or any a_{ki} for $k > 1$ (subject to the constraint of integrability).

Everything stated thus far about the Steinmann constraint applies to full, infrared-divergent amplitudes. However, the BDS-like-normalized amplitudes straightforwardly inherit this constraint, due to the fact that the BDS-like ansatz, given explicitly in eqs. (F.14) and (F.15), contains no three-particle invariants; it therefore acts as a spectator when taking three-particle discontinuities, e.g.

$$\mathrm{Disc}_{s_{i-1,i,i+1}} \mathcal{A}_7^{\mathrm{MHV}} = \mathrm{Disc}_{s_{i-1,i,i+1}} \left[\mathcal{A}_7^{\text{BDS-like}}\, \mathcal{E} \right] = \mathcal{A}_7^{\text{BDS-like}}\, \mathrm{Disc}_{s_{i-1,i,i+1}} \mathcal{E}\,. \tag{4.44}$$

This is no longer true for the BDS-normalized amplitude, which according to eq. (4.25) comes with an extra factor of $\exp[\frac{\Gamma_{\mathrm{cusp}}}{4} Y_n]$. When expanded at weak coupling this factor will produce powers of Y_n. The function Y_n is itself Steinmann since $Y_n = -\mathcal{E}_n^{(1)}$. However, products of Steinmann functions are not generically Steinmann functions, because overlapping discontinuities can arise from different factors in the product. Indeed, once we observe that Y_n has a cut in one three-particle channel, and that it is dihedrally invariant, we know it has cuts in all three-particle channels. Whereas Y_n itself is a *sum* of terms having cuts in overlapping channels, it is the *cross terms* in $(Y_n)^2$, or higher powers of Y_n, that violate the Steinmann relations. Similarly, the ratio function $V_* = E_*/\mathcal{E}$, when expanded out perturbatively, contains products of Steinmann functions and therefore does not obey the Steinmann relations. The lesson here is that the proper normalization of the amplitude is critical for elucidating its

analytic properties.

To summarize, the Steinmann relations require that any BDS-like-normalized seven-point function F, such as $\mathcal{E}_7$ or E_7, must satisfy

$$\text{Disc}_{a_{1i}}\left[\text{Disc}_{a_{1j}}F\right] = 0 \quad \text{if } j \neq i, i+3, i+4\,. \tag{4.45}$$

At the level of the symbol, this statement is equivalent to requiring that the symbol of F contains no first entries a_{1i} followed by second entries $a_{1,i+1}$, $a_{1,i+2}$, $a_{1,i+5}$, or $a_{1,i+6}$.

4.3.5 Absence of Triple Discontinuity Constraints

At the seven-point level, it is interesting to ask whether there could be new constraints on amplitudes of the following type:

$$\text{Disc}_{a_{17}}\left[\text{Disc}_{a_{14}}\left[\text{Disc}_{a_{11}}F\right]\right] \stackrel{?}{=} 0. \tag{4.46}$$

The three-particle channels corresponding to a_{11} and a_{14} do not overlap, nor do the channels corresponding to a_{14} and a_{17}. The channels corresponding to a_{11} and a_{17} *do* overlap, but the two discontinuities are separated by the a_{14} discontinuity in between. (An analogous situation never arises for three-particle cuts in the six-point case, because the only allowed double three-particle cut in that case involves cutting the same invariant twice.) We have inspected the symbols of the MHV and NMHV seven-point amplitudes, and we find that eq. (4.46) is generically non-vanishing. The act of taking the non-overlapping second discontinuity of the amplitude apparently alters the function's properties enough that the third discontinuity is permitted.

4.3.6 Steinmann Heptagon Functions

We define a heptagon function of weight k to be a generalized polylogarithm function of weight k whose symbol may be written in the alphabet of 42 cluster $\mathcal{A}$-coordinates, eq. (4.33), and which satisfies the first entry condition. These functions have been

studied in ref. [41], where it was found that the vector space of heptagon function symbols at weight $k = 1, 2, 3, 4, 5$ has dimension 7, 42, 237, 1288, 6763, respectively.

In this paper our goal is to sharpen the heptagon bootstrap of ref. [41] by taking advantage of the powerful constraint provided by the Steinmann relations. We thus define Steinmann heptagon functions to be those heptagon functions that additionally satisfy the Steinmann relations (4.45). This corresponds to a restriction on the second entry of their symbols, as discussed in section 4.3.4. We stress again that while both BDS-normalized and BDS-like-normalized amplitudes are heptagon functions, only the BDS-like-normalized ones, $\mathcal{E}$, E_0, and E_{ij}, are Steinmann heptagon functions.

We will see in subsection 4.5.1 that a drastically reduced number of heptagon functions satisfy the Steinmann relations. The reduction begins at weight 2, where there are 42 heptagon function symbols, but only 28 that obey the Steinmann relations. The corresponding 28 functions fall into 4 orbits:

$$\mathrm{Li}_2\left(1 - \frac{a_{13}a_{14}}{a_{17}}\right), \quad \mathrm{Li}_2\left(1 - a_{14}a_{16}\right), \quad \log^2 a_{13}, \quad \log a_{13} \log a_{16}, \tag{4.47}$$

together with their cyclic permutations. This fractional reduction, by one third, is the same as in the hexagon case [68], where the number of weight-2 functions was reduced from 9 to 6. At higher weight, we will see that the reductions are much more dramatic, and even more so for heptagon functions than hexagon functions. This reduction in the number of relevant functions vastly decreases the size of our ansatz, making this version of the bootstrap program more computationally tractable than its predecessor.

4.4 MHV and NMHV Constraints

Starting from a basis of weight-k Steinmann heptagon symbols, we impose known analytic and physical properties as constraints in order to identify the amplitudes uniquely within this space. Here we review these properties and the constraints they impose.

4.4.1 Final Entry Condition

The final entry condition is a restriction on the possible letters that may appear in the final entry of the symbol of an amplitude. As a consequence of the dual superconformal symmetry of SYM, the differential of an MHV amplitude must be expressible as a linear combination of $d\log\langle i\,j{-}1\,j\,j{+}1\rangle$ factors [181]. The differential of a generalized polylogarithm of weight k factors into linear combinations of weight-$(k{-}1)$ polylogarithms multiplied by $d\log\phi$ terms where ϕ is the final entry of the symbol. Therefore the final entries of the symbol of an MHV amplitude must be composed entirely of Plücker coordinates with three adjacent momentum twistors, $\langle i\,j{-}1\,j\,j{+}1\rangle$. In the symbol alphabet (4.33) we have chosen, the final entries can only be drawn from the set of 14 letters $\{a_{2j}, a_{3j}\}$.

The MHV final entry condition we just described can be derived from an anomaly equation for the $\bar{Q}$ dual superconformal generators [64]. The same anomaly equation can also be used to constrain the final entries of the symbol of the NMHV superamplitude E. In particular, using as input the leading singularities of the N^{2}MHV 8-point amplitude obtained from the Grassmannian [12], and refining the $\bar{Q}$ equation so as to act on the BDS-like normalized amplitude rather than the BDS-normalized one, Caron-Huot has found [194] that only 147 distinct (R-invariant) $\times$ (final entry) combinations are allowed in E, namely these 21:

$$\begin{gathered}
(34)\log a_{21},\quad (14)\log a_{21},\quad (15)\log a_{21},\quad (16)\log a_{21},\quad (13)\log a_{21},\\
(12)\log a_{21},\quad (45)\log a_{37},\quad (47)\log a_{37},\quad (37)\log a_{37},\quad (27)\log a_{37},\\
(57)\log a_{37},\quad (67)\log a_{37},\quad (45)\log\frac{a_{34}}{a_{11}},\quad (14)\log\frac{a_{34}}{a_{11}},\quad (14)\log\frac{a_{11}a_{24}}{a_{46}},\\
(14)\log\frac{a_{14}a_{31}}{a_{34}},\quad (24)\log\frac{a_{44}}{a_{42}},\quad (56)\log a_{57},\quad (12)\log a_{57},\quad (16)\log\frac{a_{67}}{a_{26}},\\
(13)\log\frac{a_{41}}{a_{26}a_{33}}+((14)-(15))\log a_{26}-(17)\log a_{26}a_{37}+(45)\log\frac{a_{22}}{a_{34}a_{35}}-(34)\log a_{33},
\end{gathered}\tag{4.48}$$

together with their cyclic permutations.[4]

[4]We thank Simon Caron-Huot for sharing these results with us.

4.4.2 Discrete Symmetries

The n-particle superamplitudes $\mathcal{A}_n$ are invariant under dihedral transformations acting on the external particle labels. The generators of the dihedral group D_n are the cyclic permutation $i \to i+1$ and the flip permutation $i \to n+1-i$ of the particle labels, or equivalently of the momentum twistors. For the heptagon a-letters (4.33), these correspond to

$$\begin{aligned} &\text{Cyclic transformation:} \quad a_{li} \to a_{l,i+1}\,, \\ &\text{Flip transformation:} \begin{cases} a_{2i} \leftrightarrow a_{3,8-i} \\ a_{li} \to a_{l,8-i} \quad \text{for} \quad l \neq 2,3\,. \end{cases} \end{aligned} \tag{4.49}$$

MHV and $\overline{\text{MHV}}$ amplitudes differ only in their tree-level prefactors. Hence the functions $\mathcal{E}_n$ and R_n must remain invariant under spacetime parity transformations. Parity maps NMHV amplitudes to $\overline{\text{NMHV}}$ ones and therefore acts nontrivially on E_0, E_{12} and E_{14}. In the language of our symbol alphabet (4.33), a parity transformation leaves the letters a_{1i} and a_{6i} invariant. The remaining letters transform under parity according to

$$\text{Parity transformation:} \quad a_{21} \longleftrightarrow a_{37}, \qquad a_{41} \longleftrightarrow a_{51}, \tag{4.50}$$

and the cyclic permutations thereof.

The parity and dihedral symmetries of the (super)amplitude are inherited by its BDS(-like) normalized counterpart because the BDS(-like) ansätze are also dihedrally invariant.

4.4.3 Collinear Limit

So far we have primarily focused on the BDS-like normalized amplitude and the Steinmann functions describing it. However for the study of collinear limits it proves advantageous to switch, using eq. (4.30), to the BDS-normalized amplitude, since in the limit the former becomes divergent, whereas the latter remains finite.

In more detail, the BDS ansatz $A_n^{\rm BDS}$ entering eq. (4.1) is defined in such a way that the n-point BDS-normalized amplitude (or equivalently the remainder function for MHV) reduces to the same quantity but with one fewer particle:

$$\begin{aligned}\lim_{i+1||i} R_n &= R_{n-1}\,,\\ \lim_{i+1||i} B_n &= B_{n-1}\,.\end{aligned} \tag{4.51}$$

To take one of these collinear limits, one of the $s_{i,i+1}$ must be taken to zero. From eq. (4.32), we see that this can be accomplished by taking a limit of one of the momentum twistor variables. In the case of the NMHV superamplitude we also need to specify the limit of the fermionic part of the supertwistors (4.6). The (MHV degree preserving) 7||6 collinear limit can be taken by sending

$$\mathcal{Z}_7 \to \mathcal{Z}_6 + \epsilon\frac{\langle 1246\rangle}{\langle 1245\rangle}\mathcal{Z}_5 + \epsilon\tau\frac{\langle 2456\rangle}{\langle 1245\rangle}\mathcal{Z}_1 + \eta\frac{\langle 1456\rangle}{\langle 1245\rangle}\mathcal{Z}_2\,, \tag{4.52}$$

for fixed τ, and by taking the limit $\eta \to 0$ followed by $\epsilon \to 0$.

Of course for bosonic quantities, only the bosonic part $\mathcal{Z}_i \to Z_i$ of the supertwistor is relevant. As noted in ref. [41], in the limit (4.52) the heptagon alphabet (4.33) reduces to the hexagon alphabet, plus the following 9 additional letters,

$$\begin{gathered}\eta\,,\quad \epsilon\,,\quad \tau\,,\quad 1+\tau\,,\\ \langle 1235\rangle\langle 1246\rangle + \tau\langle 1236\rangle\langle 1245\rangle\,,\quad \langle 1245\rangle\langle 3456\rangle + \tau\langle 1345\rangle\langle 2456\rangle\,,\\ \langle 1246\rangle\langle 2356\rangle + \tau\langle 1236\rangle\langle 2456\rangle\,,\quad \langle 1246\rangle\langle 3456\rangle + \tau\langle 1346\rangle\langle 2456\rangle\,,\\ \langle 1235\rangle\langle 1246\rangle\langle 3456\rangle + \tau\langle 1236\rangle\langle 1345\rangle\langle 2456\rangle\,.\end{gathered} \tag{4.53}$$

Therefore the collinear limits of heptagon functions are not generically hexagon functions. We say that a heptagon symbol has a well-defined 7||6 limit only if in this limit it is independent of all 9 of the additional letters (4.53).

We must also take the limit (4.52) of the R-invariants. Since these invariants are antisymmetric under the exchange of any pair of twistor indices, the invariants that contain both indices 6 and 7 will vanish. All other invariants reduce to six-point

R-invariants. Denoting the six-point invariants by

$$[12345] = (6) \tag{4.54}$$

and its cyclic permutations (under the six-point dihedral group), and solving the single identity of type (4.10) among them to eliminate (6), we deduce that

$$\begin{aligned}\lim_{7\|6} B =&(1)[\hat{B}_{17} + \hat{B}_{67} + \hat{B}_0] + (2)[\hat{B}_{26} - \hat{B}_{67}] + (3)[\hat{B}_{36} + \hat{B}_{37} + \hat{B}_{67} + \hat{B}_0] \\ &+ (4)[\hat{B}_{47} - \hat{B}_{67}] + (5)[\hat{B}_{56} + \hat{B}_{67} + \hat{B}_0]\,,\end{aligned} \tag{4.55}$$

where the hats denote the collinear limit of the corresponding bosonic functions.

Finally, we should note that in this work we will be focusing on collinear limits of dihedrally invariant functions. Therefore it will be sufficient to consider the 7||6 limit shown above, and the remaining $i{+}1 \parallel i$ collinear limits will be automatically satisfied as a consequence of dihedral symmetry.

4.5 Results

4.5.1 Steinmann Heptagon Symbols and Their Properties

As defined in section 4.3.6, a Steinmann heptagon function of weight k is a polylogarithm of weight k that has a symbol satisfying the following properties:

(i) it can be expressed entirely in terms of the heptagon symbol alphabet of eq. (4.33),

(ii) only the seven letters a_{1i} appear in its first entry,

(iii) a first entry a_{1i} is not followed by a second entry a_{1j} with $j \in \{i+1, i+2, i+5, i+6\}$.

We will frequently use the term 'Steinmann heptagon symbol' to mean the symbol of a Steinmann heptagon function. We begin by investigating how the number of Steinmann heptagon symbols compares to the number of heptagon symbols reported in ref. [41] through weight 5.

Weight $k =$	1	2	3	4	5	6	7	$7''$
parity +, flip +	4	16	48	154	467	1413	4163	3026
parity +, flip −	3	12	43	140	443	1359	4063	2946
parity −, flip +	0	0	3	14	60	210	672	668
parity −, flip −	0	0	3	14	60	210	672	669
Total	7	28	97	322	1030	3192	9570	7309

Table 4.1: Number of Steinmann heptagon symbols at weights 1 through 7, and those satisfying the MHV next-to-final entry condition at weight 7.

Table 4.1 presents the number of Steinmann heptagon symbols through weight 7; these numbers can be compared to $7, 42, 237, 1288$, and 6763 linearly independent heptagon symbols at weights 1 through 5, respectively [41]. By weight 5, the size of the Steinmann heptagon space has already been reduced by a factor of six compared to the size of the standard heptagon space! (The corresponding reduction factor for hexagon symbols at weight 5 is only about 3.5.)

The total number of Steinmann heptagon symbols at each weight was calculated without imposing spacetime parity or dihedral symmetries. The first four rows show the number of Steinmann heptagon symbols that have the specified eigenvalue under the $\mathbb{Z}_2 \times \mathbb{Z}_2$ generators of parity and the dihedral flip symmetry. There are many more parity even (parity +) Steinmann heptagon functions than parity odd. At each weight there are approximately the same number of flip + as flip −. Up through weight 7, there are an equal number of flip + and flip − parity odd functions.

Table 4.1 has two columns for weight 7. The column $7''$ counts the number of weight 7 symbols that satisfy an additional constraint we call the MHV next-to-final entry condition. Paired with the MHV final entry condition, which requires the final entry of the symbol to be a_{2j} or a_{3j}, integrability imposes an additional constraint that prohibits the seven letters a_{6i} from appearing in the next-to-final entry of any MHV symbol. Symbols satisfying this additional constraint are useful for bootstrapping the

four-loop MHV heptagon, to be discussed in subsection 4.5.3 below.

The fact that there are many more parity-even than parity-odd Steinmann heptagon functions is also true in the hexagon case [68]. In that case, it is possible to give a closed-form construction of an infinite series of parity-even "K" functions. The K functions apparently saturate the subspace of Steinmann hexagon functions having no parity-odd letters. This series of functions can also be repurposed, with appropriate arguments, to describe some, but not all, of the Steinmann heptagon symbols having no parity-odd letters.

Before concluding this section, let us emphasize that we are here counting integrable symbols, not functions. We expect each such symbol to be completable into a function. However, there are other functions (with vanishing symbol) obtained by multiplying lower-weight functions by multiple zeta values. When we impose physical constraints on the full function space, parameters associated with these additional functions will also have to be determined. On the other hand, sometimes the function-level constraints are more powerful than the symbol-level constraints. As first observed in the case of the 3-loop MHV hexagon [32, 34], the number of n-gon functions obeying additional constraints, such as well-defined collinear limits, may be smaller than the number of the corresponding symbols. That is, completing a symbol to a function with proper branch cuts may require adding to it functions of lower weight that don't have a well-defined collinear limit, even if the symbol does. We leave the problem of upgrading our heptagon bootstrap from symbol to function level to a later work.

4.5.2 The Three-Loop NMHV Heptagon

Once we have constructed the Steinmann heptagon symbol space, we can assemble it into an ansatz for the seven-particle amplitude and apply the constraints outlined in section 4.4 to fix the free parameters. Let us describe the steps of this computation in the NMHV case.

The NMHV amplitude is a linear combination of 15 transcendental functions multiplying the independent R-invariants. Therefore the initial number of free parameters

Loop order $L =$	1	2	3
Steinmann symbols	15×28	15×322	15×3192
NMHV final entry	42	85	226
Dihedral symmetry	5	11	31
Well-defined collinear	0	0	0

Table 4.2: Number of free parameters after applying each of the constraints in the leftmost column, to an ansatz for the symbol of the L-loop seven-point NMHV BDS-like-normalized amplitude. The first row in column L is equal to the last line of column $k = 2L$ of table 4.1, multiplied by 15 for the 15 linearly independent R-invariants.

at L loops, shown in table 4.2, is given by 15 times the entry in table 4.1 that counts the total number of Steinmann heptagon symbols of weight $2L$.[5]

We then impose the heptagon NMHV final entry condition discussed in subsection 4.4.1. Similarly to the NMHV hexagon case [38], the list of allowed final entries in eq. (4.4.1) can be translated into relations between the 42 different $\{k-1, 1\}$ coproduct components for each of the 15 functions multiplying the independent R-invariants, for a total of $42\times15 = 630$ independent objects. Note that eq. (4.4.1) contains all 21 distinct R-invariants, so in order to obtain the aforementioned equations we first need to eliminate the dependent R-invariants with the help of eqs. (4.13) and (4.14).

In principle, one can impose the NMHV final entry equations at $L = k/2$ loops on the ansatz of weight-k integrable symbols appearing in the first line of table 4.2. In practice, we have found it more efficient to solve these equations simultaneously

[5]If we had imposed dihedral symmetry first, we would have had only three independent functions E_0, E_{12} and E_{14} to parametrize, each with some dihedral symmetry, and there would have been fewer than 3 times the number of independent Steinmann heptagon symbols in the first line of the table. This part of the computation is not a bottleneck either way. This alternative procedure would also give rise to a different set of numbers in the second line of table 4.2.

with the weight-k integrability equations (4.39), namely the equations imposing integrability on the last two slots of an ansatz for E. The number of free parameters after imposing this condition (using either method) is reported in the second line of table 4.2. We see that the final entry condition is already very restrictive; out of the 47880 possible NMHV symbols with generic final entry at three loops, only 226 of them obey the NMHV final entry. Next we impose invariance of E under dihedral transformations, as discussed in subsection 4.4.2. The dihedral restriction leads to the small number of remaining free parameters reported in the third line of table 4.2.

We then examine the behavior of the amplitude in the collinear limit. To this end, we recall from subsection 4.4.3 that it is advantageous to convert to the BDS normalization, since the BDS-normalized amplitude is finite in the collinear limit, while the BDS-like normalized one becomes singular. Converting our partially-determined ansatz for E to an equivalent ansatz for B with the help of eq. (4.30), we then take its collinear limit using eq. (4.52).

Quite remarkably, demanding that the right-hand side of eq. (4.55) be well-defined, namely independent of the spurious letters (4.53) (and thus also finite), suffices to uniquely fix B through 3 loops! Even an overall rescaling is not allowed in the last line of table 4.2, because the condition of well-defined collinear limits, while homogeneous for BDS-normalized amplitudes, is inhomogeneous for the BDS-like normalization with which we work. We did not need to require that the collinear limit (4.55) of the solution agrees with the six-point ratio function computed at three loops in ref. [37], but of course we have checked that it does agree.

In this manner, we arrive at a unique answer for the symbol of the NMHV heptagon through three loops. Our results are included in the ancillary files, which can also be downloaded from [177]. The one- and two-loop results match the amplitudes computed in refs. [111] and [64], respectively. The fact that six-point boundary data is not even needed to fix the symbol through three loops points to a strong tension between the Steinmann relations, dual superconformal symmetry (in the guise of the final entry condition), and the collinear limit.

4.5.3 The Four-Loop MHV Heptagon

For the MHV remainder function at $L = k/2$ loops, we could in principle start from an ansatz for $\mathcal{E}_7^{(L)}$ involving all heptagon Steinmann symbols of weight k. As with the NMHV case, however, it is simpler to impose the MHV final-entry condition discussed in section 4.4.1 at the same time as integrability on the last two entries of the symbol. In fact, our initial four-loop MHV ansatz was constructed using not just the MHV final-entry condition, but also the MHV next-to-final entry condition discussed in section 4.5.1.

Loop order $L =$	1	2	3	4
Steinmann symbols	28	322	3192	?????
MHV final entry	1	1	2	4
Well-defined collinear	0	0	0	0

Table 4.3: Free parameter count after applying each of the constraints in the left-most column to an ansatz for the symbol of the L-loop seven-point MHV BDS-like-normalized amplitude.

In the first line of table 4.3, we reiterate the number of Steinmann heptagon functions with general final entry. In the second line of the table, we report the number of symbols that satisfy the MHV final entry condition. Clearly, there are only a few Steinmann heptagon functions at each weight that satisfy even these few constraints. Note that we have not even imposed dihedral invariance, nor that the symbol have even spacetime parity.

To determine the third line of the table, we convert the ansatz to one for the BDS normalized amplitude, using eq. (4.30) and the symbol of Y_7. We then ask that this quantity have a well-defined collinear limit. As in the NMHV case, there is a unique solution to this constraint, this time through four loops, as reported in the last line of table 4.3; this unique solution must be the symbol of $\mathcal{E}_7^{(L)}$. Our results are included in the ancillary files, which can also be downloaded from [177]. Again the overall normalization is fixed because the last constraint is an inhomogeneous one

for a BDS-like normalized amplitude. The symbols of the two- and three-loop seven-point BDS remainder functions $R_7^{(2)}$, $R_7^{(3)}$ are known [181, 41]. We have converted these quantities to the BDS-like normalization with the help of eq. (4.31), and they agree with our unique solutions. At four loops, when we convert our unique solution for $\mathcal{E}_7^{(4)}$ (which has 105,403,942 terms) to $R_7^{(4)}$ (which has 899,372,614 terms), we find that its well-defined collinear limit agrees perfectly with the symbol of the four-loop six-point MHV remainder function $R_6^{(4)}$ computed in ref. [35]. Because we did not need to impose dihedral invariance, nor spacetime parity, we can say that even less input is needed to fix the symbol of the MHV amplitude through four loops than was needed for the three-loop NMHV amplitude!

Before concluding, let us note that although we used the Steinmann constraint to tightly constrain the space of symbols through which we had to sift in order to find the four-loop MHV heptagon, it is possible that the same result could have been obtained (in principle, with much more computer power), without it. In the second row of table 4.3 we see, for example, that at weight 6 there are precisely 2 Steinmann heptagon symbols satisfying the MHV final-entry condition. Ref. [41] imposed the MHV final-entry condition, without considering the Steinmann relations, and found 4 different symbols at weight 6: $(Y_7)^3$, $Y_7\, R_7^{(2)}$, $R_7^{(3)}$ and one more. Modulo the reducible (product) functions $(Y_7)^3$ and $Y_7\, R_7^{(2)}$, heptagon functions satisfying the MHV final-entry condition automatically satisfy the Steinmann relations as well, at least at weight 6! We cannot rule out the possibility that the Steinmann constraint is also superfluous at weight 8 (or, perhaps, even higher), but certainly the complexity of the computation is significantly reduced if one allows oneself to input this knowledge.

4.5.4 Three Loops from Dihedral Symmetry

In this subsection we consider dropping the final entry condition, which derives from dual superconformal invariance. One motivation for doing this is to check independently the NMHV final entry conditions detailed in eq. (4.4.1). Another possible motivation, in the MHV case, is to try to widen the applicability of the bootstrap approach to the study of (bosonic) light-like Wilson loops in weakly-coupled conformal

theories with less supersymmetry than $\mathcal{N} = 4$ SYM.

Let us consider adding general L-loop Steinmann heptagon symbols $\tilde{\mathcal{E}}_7^{(L)}$ (with no restrictions on the final entry) to the known answer $\mathcal{E}_7^{(L)}$ and see whether we can preserve the conditions of dihedral symmetry and good collinear behavior. We can ask this question through three loops, because we have a complete basis of Steinmann heptagon symbols up to (and beyond) weight six. Since such symbols appear additively in the BDS-normalized quantity $\mathcal{B}_7^{(L)}$, we need the Steinmann symbols $\tilde{\mathcal{E}}_7^{(L)}$ themselves to be well-defined in the collinear limit. The numbers of Steinmann heptagon symbols obeying the successive conditions of cyclic invariance, flip symmetry, and well-defined collinear behavior are detailed in table 4.4.

We find that the first dihedrally invariant Steinmann symbol with well-defined collinear limits appears at weight six, i.e. at three loops. We denote this symbol by $\tilde{\mathcal{E}}_7$. In fact the collinear limit of $\tilde{\mathcal{E}}_7$, which we denote by $\tilde{\mathcal{E}}_6$, automatically turns out to possess six-point dihedral invariance as well. Furthermore the collinear limit of $\tilde{\mathcal{E}}_6$ from six points to five is vanishing. Therefore the symbol $\tilde{\mathcal{E}}_7$ could be added to that for $\mathcal{E}_7^{(3)}$ (and simultaneously $\tilde{\mathcal{E}}_6$ to $\mathcal{E}_6^{(3)}$) without breaking dihedral symmetry or good collinear behavior either at seven points or at six points.

Neither $\tilde{\mathcal{E}}_7$ nor $\tilde{\mathcal{E}}_6$ obey the MHV final entry condition, as required to be consistent with the results of section 4.5.3. Thus at the three-loop order, $\bar{Q}$-supersymmetry is really fixing only a single parameter, after the consequences of the Steinmann relations, dihedral symmetry and good collinear behavior are taken into account. A different criterion that can be used to uniquely determine $\mathcal{E}_7^{(3)}$ is that the three-loop remainder $R_6^{(3)}$ should have at most a double discontinuity around the locus $u = 0$ where u is one of three the cross ratios available at six points. The double discontinuity is in fact predicted from the original implementation of the Wilson line OPE [46], which we will not delve into here. We may simply observe that $\tilde{\mathcal{E}}_6$ has a triple discontinuity and hence we can rule out adding $\tilde{\mathcal{E}}_7$ to $\mathcal{E}_7^{(3)}$ on these grounds.

We may similarly examine the consequences of dihedral symmetry and collinear behavior for the NMHV amplitude. In this case there are some additional conditions which we can impose, from requiring the absence of spurious poles. We recall the form of the NMHV ratio function given in eq. (4.15), or equivalently the form of E

Loop order $L =$	1	2	3
Steinmann symbols	28	322	3192
Cyclic invariance	4	46	456
Dihedral invariance	4	30	255
Well-defined collinear	0	0	1

Table 4.4: Number of linearly independent Steinmann heptagon symbols obeying, respectively: cyclic invariance, dihedral invariance, and well-defined collinear behavior together with dihedral symmetry.

given in eq. (4.28). The tree-level amplitude $\mathcal{P}^{(0)}$ obviously possesses only physical poles, but the individual R-invariants have spurious poles. Requiring that the NMHV amplitude as a whole has no spurious poles leads us to the following conditions:

$$\text{Spurious I:} \quad E_{47}|_{\langle 1356\rangle=0} = 0\,, \tag{4.56}$$

$$\text{Spurious II:} \quad E_{23}|_{\langle 1467\rangle=0} = E_{25}|_{\langle 1467\rangle=0}\,. \tag{4.57}$$

In table 4.5 we detail the number of Steinmann symbols obeying the successive conditions of cyclic symmetry, absence of spurious poles, well-defined collinear behavior, and flip symmetry. At weight two, we find a single combination obeying all conditions, which is precisely the combination $B^{(1)}$ itself, which is therefore determined up to an overall scale by these conditions. Note that unlike the $B^{(L)}$ for $L > 1$, the function $B^{(1)}$ obeys the Steinmann relations.

At weight four, we find no Steinmann symbols obeying all the conditions. This is not in contradiction with the results of section 4.5.2: we recall that the quantity $E^{(2)}$ does not exhibit well-defined, finite collinear behavior; rather it is the (non-Steinmann) function $B^{(2)}$ which manifests this. The zero in the final row of the $L = 2$ column in table 4.5 rather reflects the fact that there is no Steinmann symbol which could be added to $E^{(2)}$ while preserving the good collinear behavior of $B^{(2)}$, even if we are willing to abandon the NMHV final entry condition.

At weight six, we find a single Steinmann symbol with all the properties listed in table 4.5. It is precisely the same symbol $\tilde{\mathcal{E}}_7$ appearing in table 4.4 multiplied by the tree-level amplitude $\mathcal{P}^{(0)}$. Hence it only appears as a potential contribution to $E_0^{(3)}$. In other words, the symbols of $E_{12}^{(3)}$ and $E_{14}^{(3)}$ are uniquely fixed by the constraints of dihedral symmetry, absence of spurious poles and correct collinear behavior. The appearance of the same ambiguity $\tilde{\mathcal{E}}_7$ in $E_0^{(3)}$ is to be expected since the only additional criterion imposed in table 4.5, that of spurious-pole cancellation, cannot constrain potential contributions to E_0. Finally, we note that the addition of $\tilde{\mathcal{E}}_7$ in $E_0^{(3)}$ is connected to its addition to $\mathcal{E}_7^{(3)}$ by the NMHV to MHV collinear limit which relates E_7 to $\mathcal{E}_6$. Thus dropping the final entry condition from $\bar{Q}$-supersymmetry allows only a single potential contribution at weight 6 in all of the heptagon and hexagon amplitudes.

Loop order $L =$	1	2	3
Steinmann symbols	15×28	15×322	15×3192
Cyclic invariant	$4 + (2 \times 28)$	$46 + (2 \times 322)$	$456 + (2 \times 3192)$
Spurious vanishing I	$4 + 1 + 28$	$46 + 19 + 322$	$456 + 208 + 3192$
Spurious vanishing II	$4 + 6$	$46 + 89$	$456 + 927$
Well-defined collinear	1	0	11
Flip invariant	1	0	1

Table 4.5: Number of Steinmann heptagon symbols entering the NMHV amplitude obeying respectively cyclic invariance, vanishing on spurious poles, well-defined collinear behavior and flip symmetry.

We conclude that, up to three loops, starting from an ansatz of Steinmann heptagon functions, all heptagon amplitudes and hence all hexagon amplitudes (by collinear limits) in planar $\mathcal{N} = 4$ SYM can be determined just by imposing dihedral symmetry and well-defined collinear limits, combined with the requirement of no

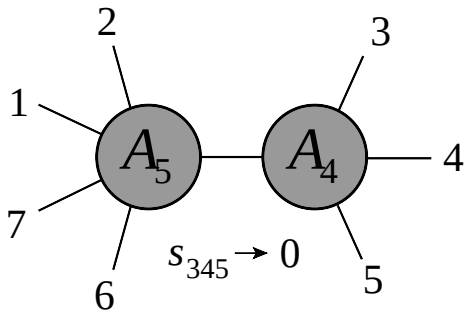

Figure 4.2: Factorization of a seven-point amplitude in the limit $s_{345} \to 0$. Notice that the collinear limit $p_7 \parallel p_1$ can be taken "inside" the factorization limit.

triple discontinuity in $R_6^{(3)}$ and no spurious poles in the NMHV amplitudes. These results provide an independent check of the NMHV final entry conditions (4.4.1). It would be interesting to investigate whether the ambiguity functions $\tilde{\mathcal{E}}_7$ and $\tilde{\mathcal{E}}_6$ could play a role in the perturbative expansion of any weakly-coupled conformal theories with less supersymmetry than $\mathcal{N} = 4$ SYM.

4.6 The Multi-Particle Factorization Limit

One of the kinematic limits we can study using our explicit seven-point results is the multi-particle factorization limit. In this limit, one of the three-particle invariants goes on shell, $s_{i,i+1,i+2} \to 0$. Figure 4.2 shows the limit $s_{345} \to 0$. In this limit the seven-point NMHV amplitude factorizes at leading power into a product of four-point and five-point amplitudes, multiplied by the $1/s_{345}$ pole. The seven-point MHV amplitude vanishes at leading power. Indeed, all supersymmetric MHV amplitudes are required to vanish at leading power when a three-particle (or higher-particle) invariant goes on shell. This result holds because all possible helicity assignments for the intermediate state require at least one lower-point amplitude to have fewer than two negative-helicity gluons; such amplitudes vanish by supersymmetry Ward identities [195, 196]. For the same reason, MHV tree amplitudes [2] have no multi-particle poles.

Before turning to the behavior of the seven-point NMHV amplitude, we recall the multi-particle factorization behavior of the BDS-like-normalized six-point NMHV

amplitude [37]. As $s_{345} \to 0$, two of the six-point R-invariants become much larger than the rest, and they become equal to each other. Therefore the singular behavior of the six-point amplitude is controlled by a single coefficient function, which we denote by $\mathcal{U}_6$ and whose limiting behavior takes an especially simple form.[6] Up to power-suppressed terms, the limit of $\mathcal{U}_6$ was found to be a polynomial in $\log(uw/v)$, whose coefficients are rational linear combinations of zeta values, and whose overall weight is $2L$. Here, u, v, and w are the three dual conformal invariant cross ratios for the hexagon, whose expressions in terms of six-point kinematics are

$$u = \frac{x_{13}^2\, x_{46}^2}{x_{14}^2\, x_{36}^2} = \frac{s_{12}\, s_{45}}{s_{123}\, s_{345}}\,, \qquad v = \frac{x_{24}^2\, x_{51}^2}{x_{25}^2\, x_{41}^2} = \frac{s_{23}\, s_{56}}{s_{234}\, s_{123}}\,, \qquad w = \frac{x_{35}^2\, x_{62}^2}{x_{36}^2\, x_{52}^2} = \frac{s_{34}\, s_{61}}{s_{345}\, s_{234}}\,. \tag{4.58}$$

The six-point limit $s_{345} \to 0$ sends $uw/v \to \infty$.

The logarithm of $\mathcal{U}_6$, called U in ref. [37], has an even simpler behavior than $\mathcal{U}_6$. The L-loop contribution $U^{(L)}$ is also a polynomial in $\log(uw/v)$, but it has only degree L at L loops, for $L > 1$. This three-loop result was later found to hold also at four and five loops [38, 68]. Because $U^{(L)}$ has weight $2L$, but a maximum of L powers of $\log(uw/v)$ for $L > 1$, every term in it contains zeta values, and its symbol vanishes. The only exception is the one-loop result,

$$U^{(1)}(u,v,w) \xrightarrow{s_{345}\to 0} -\frac{1}{2}\log^2\left(\frac{uw}{v}\right) - 2\zeta_2\,, \tag{4.59}$$

where we have converted the result in ref. [37] to that for expansion parameter g^2. The results for $U^{(L)}$ agree with the perturbative expansion of an all-orders prediction based on the Pentagon OPE [197, 198].

Ref. [37] also made a prediction for the multi-particle factorization behavior of NMHV n-point amplitudes, which we can now test at 7 points at the symbol level. Define the factorization function F_n by

$$A_n^{\text{NMHV}}(k_i) \to A_{j-i+1}(k_i, k_{i+1}, \ldots, k_{j-1}, K) \tag{4.60}$$

[6] The function $\mathcal{U}_6$ can be identified with the function E in refs. [38, 68], but we prefer to adopt a different notation here to emphasize that this function is *not* the BDS-like-normalized NMHV superamplitude E_6.

$$\times \frac{F_n(K^2, s_{l,l+1})}{K^2} A_{n-(j-i)+1}(-K, k_j, k_{j+1}, \ldots, k_{i-1}) \,,$$

as $K^2 \to 0$, or in the seven-point case,

$$A_7^{\rm NMHV}(k_i) \xrightarrow{s_{345}\to 0} A_5(k_6, k_7, k_1, k_2, K) \frac{F_7(K^2, s_{l,l+1})}{K^2} A_4(-K, k_3, k_4, k_5) \,, \qquad (4.61)$$

where $K = k_3 + k_4 + k_5$, $K^2 = s_{345}$. Then F_7 was predicted to have the form

$$\begin{aligned}
[\log F_7]^{(L)}_{\rm symbol} \;=\; \delta_{L,1} \Bigg\{ & \frac{1}{8\epsilon^2} \left[\left(\frac{(-s_{712})(-s_{34})}{(-s_{56})} \right)^{-\epsilon} + \left(\frac{(-s_{45})(-s_{671})}{(-s_{23})} \right)^{-\epsilon} \right] \\
& - \frac{1}{2} \log^2 \left(\frac{(-s_{712})(-s_{34})}{(-s_{56})} \Big/ \frac{(-s_{45})(-s_{671})}{(-s_{23})} \right) \\
& - \frac{1}{2} \log^2 \left(\frac{x_{73}^2 x_{35}^2 x_{46}^2 x_{62}^2}{x_{57}^2 x_{24}^2 (x_{36}^2)^2} \right) \Bigg\} \,. \qquad (4.62)
\end{aligned}$$

For simplicity, we have dropped all terms that vanish at symbol level, which kills all terms in $\log F_7$ beyond one loop, and we have converted to the g^2 expansion parameter.

We should now convert this prediction to one for the BDS-like normalized amplitude. Apart from trivial tree-level factors, we have

$$\log F_7 \;=\; \log \left(\frac{A_7^{\rm NMHV}}{A_5^{\rm BDS}\, A_4^{\rm BDS}} \right) \;=\; \log \left(\frac{A_7^{\rm NMHV}}{A_7^{\rm BDS-like}} \right) - \log \left(\frac{A_5^{\rm BDS}\, A_4^{\rm BDS}}{A_7^{\rm BDS-like}} \right) . \qquad (4.63)$$

So to obtain $\log(A_7^{\rm NMHV}/A_7^{\rm BDS-like})$ we need to add to $[\log F_7]^{(1)}$ the quantity

$$-\hat{M}_7^{(1)} + M_5^{(1)} + M_4^{(1)} \,, \qquad (4.64)$$

where $\hat{M}_7$ is given in eq. (F.14), and $M_4^{(1)}$ and $M_5^{(1)}$ are the four- and five-point MHV amplitudes, for the kinematics shown in fig. 4.2, and normalized by their respective tree amplitudes.

Adding eqs. (4.63) and (4.64), we find, in terms of dual variables,

$$\log\left(\frac{A_7^{\rm NMHV}}{A_7^{\rm BDS-like}}\right)^{(1)} \to -\frac{1}{2}\log^2\left(\frac{x_{73}^2 x_{35}^2 x_{46}^2 x_{62}^2}{x_{57}^2 x_{24}^2 (x_{36}^2)^2}\right) - \frac{1}{2}\log^2\left(\frac{x_{46}^2 x_{72}^2 x_{13}^2}{x_{73}^2 x_{24}^2 x_{61}^2}\right) - \frac{1}{2}\log^2\left(\frac{x_{35}^2 x_{72}^2 x_{61}^2}{x_{62}^2 x_{57}^2 x_{13}^2}\right), \tag{4.65}$$

at symbol level, and a vanishing contribution to the logarithm beyond one loop. Note that the first term in eq. (4.65) comes directly out of eq. (4.62), and is the "naive" generalization of $-\frac{1}{2}\log^2(uw/v)$ to the seven-point case. The first term diverges logarithmically as $s_{345} = x_{36}^2 \to 0$, while the last two terms are finite in this limit.

The one-loop factorization behavior in eq. (4.65) could have been extracted, of course, from the one-loop seven-point amplitude. Thus the symbol-level content of the prediction is really the vanishing of the logarithm beyond one loop. Beyond symbol level, the all-loop-order prediction of ref. [37] is that (up to an additive constant) the first term gets upgraded to the function appearing in the six-point limit, namely $U(x)$, where $x = (x_{73}^2 x_{35}^2 x_{46}^2 x_{62}^2)/(x_{57}^2 x_{24}^2 (x_{36}^2)^2)$, while the last two terms should simply get multiplied by the cusp anomalous dimension.

Now let us test the symbol-level prediction (4.65) by taking the limit $s_{345} \to 0$ of the seven-point NMHV amplitude. Referring back to (4.32), we have

$$s_{345} = x_{36}^2 = \frac{\langle 2356\rangle}{\langle 23\rangle\langle 56\rangle} \to 0. \tag{4.66}$$

Keeping s_{23} and s_{56} generic requires us to take this limit by sending $\langle 2356\rangle \to 0$. This limit can be accomplished using the replacement

$$\mathcal{Z}_2 \to \mathcal{Z}_3 + a\frac{\langle 1436\rangle}{\langle 1456\rangle}\mathcal{Z}_5 + b\frac{\langle 1453\rangle}{\langle 1456\rangle}\mathcal{Z}_6 + \epsilon\frac{\langle 3456\rangle}{\langle 1456\rangle}\mathcal{Z}_1 \tag{4.67}$$

where $a, b \in \mathbb{C}$ are generic and ϵ is a regulator. In the limit $\epsilon \to 0$, a_{14} vanishes while the other a_{ij} map into a space of 31 finite letters.

The map works out to be

$$\begin{aligned} a_{25} &\to \frac{a_{11}a_{17}}{a_{21}a_{24}}, \qquad a_{33} \to \frac{a_{17}}{a_{24}}, \qquad a_{34} \to \frac{a_{21}a_{24}}{a_{17}}, \qquad a_{37} \to \frac{a_{11}a_{17}}{a_{21}} \\ a_{42} &\to a_{24} \qquad a_{46} \to \frac{a_{21}a_{24}}{a_{17}}, \qquad a_{52} \to \frac{a_{17}}{a_{24}}, \qquad a_{56} \to \frac{a_{11}a_{17}}{a_{21}a_{24}} \\ a_{63} &\to -1, \qquad a_{65} \to -1, \end{aligned} \tag{4.68}$$

which removes 10 of the 42 letters, leaving a_{14} and the 31 finite letters.

We also need the limiting behavior of the seven-point R-invariants. Referring back to their definition (4.8), we see that the invariants (71), (14) and (47) become singular as $\langle 2356\rangle \to 0$ while all others remain finite. The finite R-invariants are suppressed in the identities (4.10) in this limit, giving us

$$(71)_{s_{345}\to 0} \;=\; (14)_{s_{345}\to 0} \;=\; (47)_{s_{345}\to 0}\,. \tag{4.69}$$

The function controlling the behavior of E_7 as $s_{345} \to 0$ is thus given by the sum of functions multiplying these singular invariants in eq. (4.28), corresponding to the combination

$$\mathcal{U}_7 \equiv \Big[E_{71} + E_{14} + E_{47} + E_0\Big]_{s_{345}\to 0}\,. \tag{4.70}$$

Note that from eq. (4.13), the coefficient of E_0 receives a $3/7$ contribution from (71), and $2/7 + 2/7$ from (14) and (47).

Ignoring the tree amplitude, the quantity $\mathcal{U}_7$ is the exponential of $\log(A_7^{\rm NMHV}/A_7^{\rm BDS-like})$, whose prediction is given in eq. (4.65). Using eq. (4.68) to compute $\mathcal{U}_7$ from eq. (4.70) in terms of the letters a_{ij}, we find at one, two, and three loops,

$$\mathcal{U}_7^{(1)} = -\frac{1}{2}\log^2\left(\frac{a_{14}^2}{a_{11}a_{17}}\right) - \frac{1}{2}\log^2 a_{11} - \frac{1}{2}\log^2 a_{17}\,, \tag{4.71}$$

$$\mathcal{U}_7^{(2)} = \frac{\left(\mathcal{U}_7^{(1)}\right)^2}{2!}\,, \tag{4.72}$$

$$\mathcal{U}_7^{(3)} = \frac{\left(\mathcal{U}_7^{(1)}\right)^3}{3!}\,. \tag{4.73}$$

Hence $\mathcal{U}_7$ exponentiates at symbol level, as predicted by eq. (4.65). Substituting eq. (4.36) for a_{11}, and its cyclic permutations, into eq. (4.71), we find perfect agreement with eq. (4.65). We can also express the result in terms of the cross ratios u_i:

$$\mathcal{U}_7^{(1)} = -\frac{1}{2}\log^2\left(\frac{u_1u_2}{u_3u_7}\right) - \frac{1}{2}\log^2\left(\frac{u_1u_4u_5}{u_3u_6}\right) - \frac{1}{2}\log^2\left(\frac{u_2u_6u_5}{u_7u_4}\right). \tag{4.74}$$

Once this analysis is repeated at function level, we expect the first term in $\mathcal{U}_7^{(1)}$ to receive higher-loop zeta-valued contributions, dictated by the six-point function $U(x)$, while the last two terms simply get multiplied by the cusp anomalous dimension.

The last two terms in eq. (4.71) or eq. (4.74) do not diverge in the factorization limit. On the other hand, they play an essential role in endowing $\mathcal{U}_7$ with the correct behavior as p_7 and p_1 become collinear. Fig. 4.2 shows that this collinear limit is well away from the factorization pole, in the sense of color ordering. So it should be possible to take this collinear limit "inside" the $s_{345} \to 0$ multi-particle factorization limit, i.e. as a further limit of it.

The $p_7 \parallel p_1$ collinear limit takes $x_{72}^2 \to 0$, and hence the cross ratio $u_5 \to 0$. Equation (4.74) shows that the last two terms of $\mathcal{U}_7^{(1)}$ diverge logarithmically in this collinear limit, while the first term behaves smoothly. Recall that the n-point BDS ansatz smoothly tends to the $(n-1)$-point BDS ansatz in all collinear limits. However, this is not true for the BDS-like ansatz; that is, $Y_7 \not\to Y_6$ in collinear limits, rather it diverges logarithmically. Essentially, the last two terms of eq. (4.71) account for this non-smooth behavior. In the $p_7 \parallel p_1$ collinear limit,

$$-\frac{1}{2}\log^2\left(\frac{a_{14}^2}{a_{11}a_{17}}\right) \xrightarrow{p_7\parallel p_1} -\frac{1}{2}\log^2\left(\frac{uw}{v}\right), \tag{4.75}$$

$$-\frac{1}{2}\log^2 a_{11} - \frac{1}{2}\log^2 a_{17} + Y_7 \xrightarrow{p_7\parallel p_1} Y_6\,. \tag{4.76}$$

Thus the last two terms in eq. (4.71) precisely account for the non-smooth collinear behavior of the BDS-like-normalized amplitude at seven points, within the multi-particle factorization limit.

4.7 Discussion

Following the inclusion of the Steinmann relations in the hexagon function bootstrap program [68], we have applied these constraints to heptagon symbols, in order to drastically reduce the number of symbols needed to bootstrap seven-point scattering amplitudes. We have been able to construct a basis of Steinmann heptagon symbols through weight 7, and those which further satisfy the MHV final-entry condition at weight 8. In order to apply the Steinmann relations transparently, we have shifted our focus from the familiar BDS-normalized amplitudes to BDS-like normalized analogues. The simple conversions (4.30) and (4.31) between functions in these two normalizations allow us to simultaneously take advantage of the smaller space of Steinmann heptagon symbols, and utilize the simple behavior exhibited by BDS-normalized functions near the collinear limit. With these advances, we have completely determined, in a conceptually simple manner, the symbols of the seven-point three-loop NMHV and four-loop MHV amplitudes in planar $\mathcal{N} = 4$ SYM theory.

Calculating the symbol of these particular component amplitudes is only the tip of the Steinmann iceberg. The main limiting factor in applying the bootstrap at higher weight is the computational complexity resulting from the size of the space of Steinmann heptagon functions, which still grows close to exponentially, despite its small size relative to the general heptagon function space. This growth can be especially prohibitive when generating the general basis of Steinmann heptagon symbols at each higher weight. At the same time, nearly the entire space of Steinmann heptagon symbols is needed to describe the amplitudes we have bootstrapped – including derivatives (coproducts) of higher-loop amplitudes. That is, the full space of Steinmann heptagon symbols is spanned by the derivatives of our amplitudes at weights 2 and 3. Only 15 of the 322 Steinmann heptagon symbols are absent from the span of these derivatives at weight 4. This situation resembles what is observed in the hexagon function bootstrap [68], where the derivatives of the five-loop six-point amplitude also span the full weight-2 and weight-3 Steinmann hexagon symbol spaces, while only 3, 12, and 30 symbols are absent from the span of these derivatives at weights 4, 5, and 6. In the hexagon case, all of these symbols are observed to drop

out due to lower-weight restrictions on the appearance of zeta values (i.e. the zeta values only appear in certain linear combinations with other hexagon functions, and this leads to symbol-level restrictions at higher weights). We expect that a similar set of function-level restrictions will explain why a small set of weight-4 Steinmann heptagon symbols are not needed to describe the seven-point amplitude. (Only 386 of the 1030 weight-5 Steinmann heptagon symbols are currently needed to describe the four-loop MHV and three-loop NMHV amplitudes, but here we expect significantly more of these symbols to be needed to describe coproducts of yet higher-loop contributions.) No physical explanation for the restrictions on the occurrence of zeta values at six points has yet been discerned, indicating that there remains some physics to be discovered.

More generally, the task of upgrading our symbol-level results to full functions will be left to future work. A full functional representation would be valuable for checking seven-point predictions in both the near-collinear [162, 48, 49, 51, 163, 56, 57, 164] and multi-Regge limits [58, 59, 102, 60, 61, 105, 169, 170, 171, 172, 173, 174]. An important problem is to generalize the all-loop results for six-point scattering in the multi-Regge limit [62] to the seven-point case. The full functional form of the seven-point amplitude could assist the construction of an all-loop multi-Regge heptagon formula.

Bootstrapping amplitudes with eight or more external legs will require more than a simple extension of the heptagon bootstrap presented in this work. Both the hexagon and heptagon bootstrap approaches depend on the assumption that the weight-$2L$ generalized polylogarithms can be built from a finite symbol alphabet, corresponding to an appropriate set of cluster $\mathcal{A}$-coordinates. Going to $n = 8$, we move into a cluster algebra with infinitely many $\mathcal{A}$-coordinates. It is expected that only a finite number of letters will appear at any finite loop order, but it is currently unknown how to characterize what sets may appear. In principle, this information ought to follow from a careful consideration of the Landau singularities of these amplitudes (see for example refs. [199, 167] for recent related work). There is hope that patterns may emerge at currently accessible loop orders, which may provide insight into the letters appearing for $n > 7$.

Appendices

Appendix A

Hexagon Function Basis at Weights 6, 7, and 8

Building on the basis of hexagon functions through weight five introduced in ref. [34], we describe here a complete basis of hexagon functions at weight six, seven and eight. These functions can be defined in terms of their $\{n-1,1\}$ coproduct components, which for a generic hexagon function F take the form

$$\Delta_{n-1,1}(F) \equiv \sum_{i=1}^{3} F^{u_i} \otimes \ln u_i + F^{1-u_i} \otimes \ln(1-u_i) + F^{y_i} \otimes \ln y_i, \tag{A.1}$$

where the functions $\{F^{u_i}, F^{1-u_i}, F^{y_i}\}$ uniquely determine the derivatives of F to be

$$\begin{aligned}\left.\frac{\partial F}{\partial u}\right|_{v,w} &= \frac{F^u}{u} - \frac{F^{1-u}}{1-u} + \frac{1-u-v-w}{u\sqrt{\Delta}}F^{y_u} \\ &\quad + \frac{1-u-v+w}{(1-u)\sqrt{\Delta}}F^{y_v} + \frac{1-u+v-w}{(1-u)\sqrt{\Delta}}F^{y_w}\,, \end{aligned}\tag{A.2}$$

$$\begin{aligned}\sqrt{\Delta}y_u\left.\frac{\partial F}{\partial y_u}\right|_{y_v,y_w} &= (1-u)(1-v-w)F^u - u(1-v)F^v - u(1-w)F^w \\ &\quad - u(1-v-w)F^{1-u} + uvF^{1-v} + uwF^{1-w} + \sqrt{\Delta}F^{y_u}\,, \end{aligned}\tag{A.3}$$

and the cyclic permutations of these formulae. We fix the overall integration constant of each function by stipulating that it vanish at the point $F(u,v,w) = F(1,1,1)$.

The process of constructing such functions is described in ref. [34], and proceeds analogously to the construction of the spurious pole functions which we cover in detail in appendix D. The definitions of the basis functions in terms of their $\{n-1,1\}$ coproduct components are lengthy and unilluminating, so instead of writing them out explicitly we will only describe their formal properties; these definitions can be found in the ancillary files.

One way of organizing the space of irreducible hexagon functions is by the maximum number of times the y_i variables appears in a single term of a function's symbol. Since this number is additive under function multiplication, it endows the space of hexagon functions with a grading which naturally separates parity-odd functions (those with odd numbers of y entries) from parity-even functions (those with even numbers of y entries). The dimension of the hexagon function space with each y-grading through weight eight is given in table A.1. The hexagon function space also has an S_3 symmetry that acts by permuting the variables u, v, and w. We have selected basis functions that form orbits under this S_3 symmetry, and we only label one representative of each orbit, since the other members can be found by permuting the arguments of the representative.

At weight six, we denote the i^{th} odd function by $A_i(u,v,w)$ and the i^{th} even function by $B_i(u,v,w)$. Up to the action of the S_3 symmetry there are 11 independent odd functions and 11 independent even functions. The size of each basis function's orbit is specified alongside its y-grading in table A.2. Similarly, we denote the weight seven odd functions by $C_i(u,v,w)$ and the weight seven even functions by $D_i(u,v,w)$. All 28 odd functions and 36 even functions fit into orbits of S_3, and these orbits are specified with the y-gradings of these functions in table A.3. Finally, at weight eight there are 86 odd functions, denoted by $S_i(u,v,w)$, and 102 even functions, denoted by $T_i(u,v,w)$. In table A.4 we give their S_3 orbits and y-gradings. We suppress the arguments of the basis functions in the tables.

Weight	y^0	y^1	y^2	y^3	y^4	y^5	y^6
1	3	-	-	-	-	-	-
2	3	-	-	-	-	-	-
3	6	1	-	-	-	-	-
4	9	3	3	-	-	-	-
5	18	4	13	6	-	-	-
6	27	4	27	29	18	-	-
7	54	4	41	63	108	39	-
8	90	4	50	108	306	238	114

Table A.1: The dimension of the space of irreducible hexagon functions at each weight, graded by the maximum number of y entries appearing in each function's symbol. The y^0 column counts one-dimensional HPLs, but the other columns are nontrivial.

S_3 orbit	y^4	y^3	y^2	y^1
6-cycle	B_1, B_2	A_1, A_2	B_5, B_6	-
3-cycle	B_3, B_4	$A_3 \dots A_7$	$B_7 \dots B_{11}$	A_{10}
singlet	-	A_8, A_9	-	A_{11}

Table A.2: The weight-six hexagon basis functions organized by the size of their S_3 orbits and y-grading.

S_3 orbit	y^5	y^4	y^3	y^2	y^1
6-cycle	$C_1 \dots C_3$	$D_1 \dots D_{12}$	$C_{11} \dots C_{15}$	D_{25}, D_{26}, D_{27}	-
3-cycle	$C_4 \dots C_{10}$	$D_{13} \dots D_{24}$	$C_{16} \dots C_{26}$	$D_{28} \dots D_{34}$	C_{27}
singlet	-	-	-	D_{35}, D_{36}	C_{28}

Table A.3: The weight-seven hexagon basis functions organized by the size of their S_3 orbits and y-grading.

S_3 orbit	y^6	y^5	y^4	y^3	y^2	y^1
6-cycle	$T_1 \dots T_{15}$	$S_1 \dots S_{26}$	$T_{16} \dots T_{54}$	$S_{27} \dots S_{34}$	$T_{55} \dots T_{58}$	-
3-cycle	$T_{59} \dots T_{66}$	$S_{35} \dots S_{61}$	$T_{67} \dots T_{89}$	$S_{62} \dots S_{80}$	$T_{90} \dots T_{97}$	S_{81}
singlet	-	S_{82}	T_{98}, T_{99}, T_{100}	S_{83}, S_{84}, S_{85}	T_{101}, T_{102}	S_{86}

Table A.4: The weight-eight hexagon basis functions organized by the size of their S_3 orbits and y-grading.

Appendix B

$R_6^{(3)}$, $V^{(3)}$ and $\tilde{V}^{(3)}$ in Terms of Weight 6 Basis

The weight-six basis for the parity-odd sector includes functions $A_i(u,v,w)$, $i = 1,2,\ldots,11$, and for the parity-even sector, $B_i(u,v,w)$, $i = 1,2,\ldots,11$. This basis allows us to write the three-loop remainder and ratio functions directly, instead of in terms of their $\{5,1\}$ coproduct components, as was done previously [34, 37].

Using the parity-even weight-six functions and the total symmetry of the remainder function, we can write the three-loop result as

$$\begin{aligned} R_6^{(3)}(u,v,w) &= R_{6,A}^{(3)}(u,v,w) + R_{6,A}^{(3)}(v,w,u) + R_{6,A}^{(3)}(w,u,v) \\ &\quad + R_{6,A}^{(3)}(u,w,v) + R_{6,A}^{(3)}(v,u,w) + R_{6,A}^{(3)}(w,v,u)\,, \end{aligned} \tag{B.1}$$

where

$$\begin{aligned} R_{6,A}^{(3)} &= \frac{1}{128}\Big\{30\Big(B_1+B_2\Big) + 18B_3 + 14B_4 - 2\Big(B_5+B_6\Big) + 12B_7 - 2B_8 \\ &\quad - 264B_9 + 2B_{10} - 24B_{11} + 4\ln(u/v)M_1 + \frac{128}{3}\ln(w/v)Q_{\rm ep} \\ &\quad - \Big(400H_2^u + 200H_2^w - 10\ln^2 u - 2\ln^2 w - 204\ln u\ln v \\ &\qquad + 412\ln u\ln w - 408\zeta_2\Big)\Omega^{(2)} + \frac{104}{3}(\tilde{\Phi}_6)^2 - 96H_6^u \\ &\quad + 56H_{5,1}^u - 6H_{4,2}^u - 204H_{4,1,1}^u - 44H_{3,2,1}^u - 6H_{3,1,2}^u + 168H_{3,1,1,1}^u \end{aligned}$$

$$
\begin{aligned}
&+ 6H^u_{2,2,1,1} - 210H^u_{2,1,1,1,1} - 2(H^u_3)^2 - 4H^u_3 H^u_{2,1} + 14(H^u_{2,1})^2 \\
&+ H^u_2\Big(- 376H^u_4 + 8H^u_{3,1} + 594H^u_{2,1,1} + 96(H^u_2)^2\Big) \\
&+ \ln u\Big(96H^u_5 - 56H^u_{4,1} + 10H^u_{3,2} + 168H^u_{3,1,1} + 26H^u_{2,2,1} \\
&\qquad - 144H^u_{2,1,1,1} + H^u_2\Big(380H^u_3 + 2H^u_{2,1}\Big)\Big) \\
&+ \ln^2 u\Big(- 26H^u_4 + 38H^u_{3,1} - 60H^u_{2,1,1} - 100(H^u_2)^2\Big) \\
&- 4\ln^3 u\Big(H^u_3 + 2H^u_{2,1}\Big) + \frac{7}{4}\ln^4 u\, H^u_2 \\
&- H^v_3\Big(338H^u_3 + 4H^u_{2,1} + \frac{10}{3}\ln u\, H^u_2 - \frac{7}{3}\ln^3 u\Big) \\
&+ H^v_{2,1}\Big(690H^u_{2,1} - \frac{34}{3}\ln u\, H^u_2 - \frac{5}{3}\ln^3 u\Big) \\
&+ H^v_2\Big(- 760H^u_4 - 8H^u_{3,1} + 1224H^u_{2,1,1} + \frac{575}{2}(H^u_2)^2 \\
&\qquad - \frac{64}{3}H^u_2 H^w_2 + \ln u\left(\frac{2314}{3}H^u_3 + \frac{82}{3}H^u_{2,1}\right) \\
&\qquad - \frac{610}{3}\ln^2 u H^u_2 - \frac{5}{2}\ln^4 u\Big) \\
&+ \ln v\Big(- 8H^u_{4,1} - 10H^u_{3,2} + 120H^u_{3,1,1} + 38H^u_{2,2,1} \\
&\qquad - 48H^u_{2,1,1,1} + H^u_2\Big(4H^u_3 - 18H^u_{2,1}\Big) \\
&\qquad + \ln u\Big(- 276H^u_4 - 320H^u_{3,1} - 174H^u_{2,1,1} + 197(H^u_2)^2\Big) \\
&\qquad + 2\ln^2 u\Big(- 30H^u_{2,1} + 119H^u_3\Big) - 51\ln^3 u H^u_2\Big) \\
&+ \ln^2 v\Big(34H^u_4 - 10H^u_{3,1} - 6H^u_{2,1,1} - 9\Big(H^u_2\Big)^2 \\
&\qquad - \ln u\left(\frac{403}{3}H^u_3 + \frac{1837}{3}H^u_{2,1}\right) - \frac{1687}{6}\ln^2 u H^u_2 - 2\ln^4 u\Big) \\
&- \ln^3 v\left(\frac{631}{3}\ln u H^u_2 + \frac{103}{2}\ln^3 u\right) + \frac{256}{3}\ln v H^v_2 \ln u H^u_2 \\
&+ \ln w\Big(H^v_2\Big(16H^u_{2,1} + 1018\ln u H^u_2 + 201\ln^3 u\Big) \\
&\qquad + \ln v\Big(-764H^u_4 - 164H^u_{3,1} + 846H^u_{2,1,1} + 126(H^u_2)^2 \\
&\qquad + \ln u\Big(334H^u_3 + 582H^u_{2,1}\Big) + \frac{1037}{2}\ln^2 u H^u_2 + \frac{9}{2}\ln^4 u\Big)
\end{aligned}
$$

$$
\begin{aligned}
&\quad + \ln^2 v \left(114 H_3^u + 643 H_{2,1}^u + \frac{913}{2} \ln u H_2^u + \frac{773}{12} \ln^3 u \right) \Big) \\
&- \ln^2 w \Big(8 H_2^u H_2^v + \frac{335}{2} \ln^2 v H_2^u + \frac{457}{6} \ln^2 u \ln^2 v \Big) \\
&+ \zeta_2 \Big(788 H_4^u - 4 H_{3,1}^u - 1236 H_{2,1,1}^u + 220 (H_2^u)^2 \\
&\quad - 783 \ln u H_3^u + 4 \ln u H_{2,1}^u + 407 \ln^2 u H_2^u - \frac{5}{2} \ln^4 u \\
&\quad + \ln v \Big(-13 H_3^u + 2244 H_{2,1}^u + 297 \ln u H_2^u - 39 \ln^3 u \Big) \\
&\quad + \ln^2 v \Big(822 H_2^u + 314 \ln^2 u \Big) + 858 H_2^u H_2^v \\
&\quad - \Big(400 H_2^u + 314 \ln^2 u \Big) \ln v \ln w \Big) \\
&+ \zeta_3 \Big(28 \ln u H_2^u + 6 \ln^3 u + \ln v \Big(-40 H_2^u + 125 \ln^2 u \Big) \\
&\quad + 58 \ln u \ln v \ln w \Big) + \frac{41860}{9} \zeta_6 + \frac{64}{3} (\zeta_3)^2 \\
&- \zeta_4 \Big(5704 H_2^u + 980 \ln^2 u + 464 \ln u \ln v \Big) \Big\} , \qquad \text{(B.2)}
\end{aligned}
$$

and we dropped the arguments (u, v, w) on B_i, M_1, $Q_{\rm ep}$, $\Omega^{(2)}$ and $\tilde{\Phi}_6$ to save space.

The parity-even part of the three-loop ratio function is

$$
V^{(3)}(u, v, w) \;=\; V_A^{(3)}(u, v, w) + V_A^{(3)}(w, v, u), \qquad \text{(B.3)}
$$

where

$$
\begin{aligned}
V_A^{(3)}(u, v, w) \;=\; & \frac{1}{128} \Big\{ -42 B_1(u, v, w) - 38 B_1(v, w, u) - 54 B_1(w, u, v) \\
& - 38 B_2(u, v, w) - 54 B_2(v, w, u) - 42 B_2(w, u, v) \\
& - 60 B_3(u, v, w) - 18 B_3(v, w, u) - 40 B_4(u, v, w) \\
& - 20 B_4(v, w, u) + 2 B_5(u, v, w) + 2 B_5(v, w, u) \\
& + 10 B_5(w, u, v) + 2 B_6(u, v, w) + 2 B_6(v, w, u) \\
& + 10 B_6(w, u, v) - 36 B_7(u, v, w) - 20 B_7(v, w, u) \\
& + 4 B_8(u, v, w) + 816 B_9(u, v, w) + 348 B_9(v, w, u) \\
& - 12 B_{10}(u, v, w) - 2 B_{10}(v, w, u) + 64 B_{11}(u, v, w)
\end{aligned}
$$

$$
\begin{aligned}
&+ 48B_{11}(v,w,u) - 154(\tilde{\Phi}_6(u,v,w))^2 \\
&+ \ln(v/u)\Big(4M_1(u,v,w) + \frac{128}{3}\Big(5Q_{\rm ep}(v,w,u) - Q_{\rm ep}(w,u,v)\Big)\Big) \\
&+ \ln(w/v)\Big(4M_1(v,w,u) + \frac{128}{3}\Big(5Q_{\rm ep}(v,w,u) - Q_{\rm ep}(u,v,w)\Big)\Big) \\
&+ 2\Big(292\Big(H_2^u + H_2^v + H_2^w\Big) - 6\ln^2 u - 3\ln^2 w - 5\ln^2 v \\
&\qquad - 312\ln u\ln v + 298\ln w\ln v + 316\ln u\ln w \\
&\qquad - 596\zeta_2\Big)\Omega^{(2)}(u,v,w) \\
&+ 2\Big(142\Big(2H_2^u + H_2^v\Big) - 12\ln^2 u - 3\ln^2 v \\
&\qquad + \Big(298\ln v - 145\ln\Big)\ln u \\
&\qquad - 286\zeta_2\Big)\Omega^{(2)}(w,u,v) \;+\; \text{pure HPLs}\Big\}. \qquad \text{(B.4)}
\end{aligned}
$$

The pure HPL terms are quite lengthy, so we only present them in an ancillary file.

The parity-odd part of the three-loop ratio function can be presented here in its entirety,

$$\tilde{V}^{(3)}(u,v,w) \;=\; \tilde{V}_A^{(3)}(u,v,w) - \tilde{V}_A^{(3)}(w,v,u), \qquad \text{(B.5)}$$

where

$$
\begin{aligned}
\tilde{V}_A^{(3)}(u,v,w) \;=\; &\frac{1}{128}\Big\{-\frac{4}{3}\,A_1(u,v,w) - \frac{28}{3}\,A_1(v,w,u) + \frac{32}{3}\,A_1(w,u,v) \\
&+ \frac{8}{3}\,A_2(u,v,w) - \frac{28}{3}\,A_2(v,w,u) + \frac{20}{3}\,A_2(w,u,v) \\
&+ 12\,A_3(u,v,w) + 4\,A_4(u,v,w) - 12\,A_6(u,v,w) \\
&+ 12\,A_7(u,v,w) - 120\,A_{10}(u,v,w) - \frac{4}{3}\,\ln u\,H_1(u,v,w) \\
&- \frac{4}{3}\Big(3\,\ln w - \ln u - 2\,\ln v\Big)\,H_1(v,w,u) - \frac{23}{3}\,\ln u\,J_1(u,v,w) \\
&+ \frac{1}{3}\Big(3\,\ln w - 13\,\ln u + 10\,\ln v\Big)\,J_1(v,w,u) \\
&- 2\Big(4\Big(H_2^u + H_2^v + H_2^w\Big) + 5\,\ln^2 u + 4\,\ln^2 w - 4\,\ln u\,\ln w \\
&\qquad - 2\,\ln u\,\ln v + 3\,\ln^2 v - 12\,\zeta_2\Big)\,F_1(u,v,w) \\
&+ 2\Big(\ln^2 u - 2\,\ln u\,\ln v\Big)\,F_1(v,w,u)
\end{aligned}
$$

$$+ 4 \Big(2 \Big(\ln u - \ln w \Big) H_2^u + 2 \ln^3 u - \ln^2 u \Big(3 \ln w + \ln v \Big) + 2 \ln u \Big(H_2^v + \ln^2 v \Big) - 26 \zeta_2 \ln u \Big) \tilde{\Phi}_6(u,v,w) \Big\} . \quad \text{(B.6)}$$

Appendix C

$R_6^{(4)}$, $V^{(4)}$ and $\tilde{V}^{(4)}$ in Terms of Weight 8 Basis

Using the weight-eight basis, we can describe the four-loop quantities $R_6^{(4)}$, $V^{(4)}$ and $\tilde{V}^{(4)}$ directly, instead of via their $\{7,1\}$ coproduct components.

First we present the four-loop remainder function $R_6^{(4)}$. Because this function is totally symmetric in $(u,v,w)=(u_1,u_2,u_3)$, we can express it in terms of the weight-eight basis as,

$$\begin{aligned}
R_6^{(4)} \;=\; \frac{1}{1024}\Bigg\{\sum_{\sigma\in S_3}\Big[&-320T_1^\sigma - 324T_2^\sigma - 290T_3^\sigma - 268T_4^\sigma - 252T_5^\sigma - 292T_6^\sigma \\
&- 248T_7^\sigma - 252T_9^\sigma - 248T_{10}^\sigma - 248T_{11}^\sigma - 272T_{12}^\sigma - 296T_{13}^\sigma \\
&- 256T_{14}^\sigma - 296T_{15}^\sigma + 4848T_{16}^\sigma + 5268T_{17}^\sigma - 4T_{18}^\sigma - 4T_{19}^\sigma \\
&+ 1173T_{20}^\sigma - 254T_{21}^\sigma - 4T_{22}^\sigma + 12T_{23}^\sigma + 312T_{24}^\sigma + 292T_{25}^\sigma \\
&+ 24T_{26}^\sigma + 252T_{27}^\sigma + 8T_{29}^\sigma + 4T_{30}^\sigma + \frac{725}{3}T_{31}^\sigma + 20T_{32}^\sigma \\
&+ 24T_{33}^\sigma + 12T_{34}^\sigma + \frac{1165}{3}T_{35}^\sigma + 724T_{36}^\sigma + 4T_{37}^\sigma + 24T_{38}^\sigma \\
&+ 24T_{39}^\sigma + 20T_{40}^\sigma - 32T_{41}^\sigma - 48T_{42}^\sigma - 32T_{43}^\sigma + 4T_{44}^\sigma - 16T_{45}^\sigma \\
&- 48T_{46}^\sigma - 16T_{47}^\sigma + 40T_{48}^\sigma - 28T_{49}^\sigma - 28T_{50}^\sigma - 40T_{51}^\sigma \\
&+ 16T_{52}^\sigma + 20T_{53}^\sigma + 20T_{54}^\sigma - 336T_{55}^\sigma + 177T_{57}^\sigma - 4T_{58}^\sigma\Big]
\end{aligned}$$

$$
\begin{aligned}
&+ \sum_{\sigma\in Z_3}\Big[-200T_{59}^{\sigma} - 128T_{60}^{\sigma} - 136T_{61}^{\sigma} - 132T_{62}^{\sigma} - 132T_{64}^{\sigma} \\
&\qquad - 128T_{65}^{\sigma} - 145T_{66}^{\sigma} + 2712T_{67}^{\sigma} + 2520T_{68}^{\sigma} - \frac{502}{3}T_{69}^{\sigma} \\
&\qquad - 114T_{70}^{\sigma} - \frac{122}{3}T_{71}^{\sigma} + \frac{2216}{3}T_{72}^{\sigma} + 8T_{73}^{\sigma} + 390T_{74}^{\sigma} + 8T_{75}^{\sigma} \\
&\qquad - 8T_{76}^{\sigma} - 24T_{77}^{\sigma} - 8T_{78}^{\sigma} + \frac{3827}{9}T_{80}^{\sigma} - 24T_{81}^{\sigma} + \frac{215}{6}T_{83}^{\sigma} \\
&\qquad - 160T_{84}^{\sigma} + 20T_{85}^{\sigma} - T_{86}^{\sigma} - 4T_{87}^{\sigma} + 2T_{88}^{\sigma} - 116T_{89}^{\sigma} \\
&\qquad + \frac{11102}{3}T_{90}^{\sigma} + 197232T_{91}^{\sigma} + 336T_{92}^{\sigma} - \frac{18465}{4}T_{93}^{\sigma} \\
&\qquad + \frac{12643}{3}T_{94}^{\sigma} - 79T_{95}^{\sigma} + \frac{6113}{6}T_{96}^{\sigma} - \frac{3427}{6}T_{97}^{\sigma}\Big] \\
&- \frac{5741}{6}T_{100} + \frac{17467}{6}T_{101} - \frac{292661}{72}T_{102} \\
&+ \text{ products of lower weight functions}\Big\}, \qquad \text{(C.1)}
\end{aligned}
$$

where T_i^{σ} denotes a permuted version of $T_i \equiv T_i(u,v,w) = T_i(u_1,u_2,u_3)$, namely

$$T_i^{\sigma} \;\equiv\; T_i(u_{\sigma(1)}, u_{\sigma(2)}, u_{\sigma(3)}). \qquad \text{(C.2)}$$

We sum over all six permutations of the 6-cycle basis functions, $T_1,\ldots,T_{58}$, and over the three cyclic permutations of the 3-cycle ones, $T_{59},\ldots,T_{97}$. We have dropped the terms that are products of lower weight functions because they are very lengthy, but they are given in an ancillary file.

The parity-even part of the four-loop ratio function can be expressed in terms of the same T_i functions as

$$V^{(4)}(u,v,w) = V_A^{(4)}(u,v,w) + V_A^{(4)}(w,v,u) + V_B^{(4)}(u,v,w)\,, \qquad \text{(C.3)}$$

where

$$
\begin{aligned}
V_A^{(4)} \;=\; \frac{1}{1024}\Big\{&380T_1^u + 620T_1^v + 500T_1^w + 596T_2^u + 516T_2^v + 396T_2^w \\
&+ 542T_3^u + 440T_3^v + 398T_3^w + 376T_4^u + 450T_4^v + 446T_4^w \\
&+ 380T_5^u + 434T_5^v + 392T_5^w + 436T_6^u + 564T_6^v + 394T_6^w
\end{aligned}
$$

$$
\begin{aligned}
&+ 400T_7^u + 414T_7^v + 388T_7^w + 422T_9^u + 404T_9^v + 396T_9^w \\
&+ 388T_{10}^u + 426T_{10}^v + 376T_{10}^w + 392T_{11}^u + 426T_{11}^v + 376T_{11}^w \\
&+ 374T_{12}^u + 464T_{12}^v + 448T_{12}^w + 404T_{13}^u + 554T_{13}^v + 446T_{13}^w \\
&+ 432T_{14}^u + 406T_{14}^v + 406T_{14}^w + 554T_{15}^u + 446T_{15}^v + 404T_{15}^w \\
&- 6984T_{16}^u - 7584T_{16}^v - 8604T_{16}^w - 8347T_{17}^u - 9102T_{17}^v \\
&- 7576T_{17}^w + 28T_{18}^u + 4T_{18}^v + 16T_{18}^w + 16T_{19}^u - 8T_{19}^v + 4T_{19}^w \\
&- \frac{7689}{4}T_{20}^u - \frac{22685}{12}T_{20}^v - 1852T_{20}^w + 376T_{21}^u + 403T_{21}^v \\
&+ 428T_{21}^w + 16T_{22}^u + 4T_{22}^v + 28T_{22}^w - 12T_{23}^u - 26T_{23}^v - 24T_{23}^w \\
&- 482T_{24}^u - 562T_{24}^v - 388T_{24}^w - 408T_{25}^u - 434T_{25}^v - 542T_{25}^w \\
&+ 12T_{26}^u - 72T_{26}^v - 24T_{26}^w - 456T_{27}^u - 394T_{27}^v - 422T_{27}^w \\
&+ 40T_{28}^u - 36T_{28}^v - 36T_{28}^w - 8T_{29}^u - 32T_{29}^v - 20T_{29}^w - 4T_{30}^u \\
&- 28T_{30}^v - 16T_{30}^w - \frac{2621}{6}T_{31}^u - \frac{605}{2}T_{31}^v - \frac{1219}{3}T_{31}^w - 6T_{32}^u \\
&- 20T_{32}^v - 26T_{32}^w - 24T_{33}^u - 10T_{33}^v + 16T_{33}^w - 26T_{34}^u - 12T_{34}^v \\
&- 24T_{34}^w - \frac{2965}{6}T_{35}^u - \frac{1405}{2}T_{35}^v - 729T_{35}^w - 1031T_{36}^u - 1159T_{36}^v \\
&- \frac{2537}{2}T_{36}^w - 4T_{37}^u - 4T_{37}^v - 4T_{37}^w - 24T_{38}^u - 96T_{38}^v - 42T_{39}^u \\
&+ 12T_{39}^v - 54T_{39}^w + 2T_{40}^u - 20T_{40}^v - 90T_{40}^w + 102T_{41}^u + 32T_{41}^v \\
&+ 46T_{41}^w + 120T_{42}^u + 48T_{42}^v + 18T_{42}^w + 38T_{43}^u + 32T_{43}^v + 26T_{43}^w \\
&- 4T_{44}^u - 16T_{44}^v + 8T_{44}^w - 20T_{45}^u + 16T_{45}^v - 56T_{45}^w + 80T_{46}^u \\
&+ 128T_{46}^v + 48T_{46}^w + 4T_{47}^u + 16T_{47}^v - 8T_{47}^w - 40T_{48}^u - 24T_{48}^v \\
&- 96T_{48}^w + 36T_{49}^u + 38T_{49}^v + 28T_{49}^w + 28T_{50}^u + 108T_{50}^v + 42T_{50}^w \\
&+ 24T_{51}^u + 96T_{51}^v + 40T_{51}^w - 16T_{52}^u - 28T_{52}^v - 22T_{52}^w - 20T_{53}^u \\
&- 26T_{53}^v - 6T_{53}^w - 10T_{54}^u - 78T_{54}^v - 20T_{54}^w + 264T_{55}^u + 756T_{55}^v \\
&+ 336T_{55}^w + 3T_{57}^u - 177T_{57}^v - 102T_{57}^w - 6T_{58}^u - 2T_{58}^v + 4T_{58}^w \\
&+ 200T_{59}^u + 213T_{60}^u + 190T_{61}^u + 186T_{62}^u + 186T_{64}^u + 213T_{65}^u \\
&+ \frac{419}{2}T_{66}^u - 3468T_{67}^u - \frac{8119}{2}T_{68}^u + 235T_{69}^u + 204T_{70}^u + 49T_{71}^u \\
&- 1166T_{72}^u - 44T_{73}^u - 544T_{74}^u - 20T_{75}^u + 8T_{76}^u + 48T_{77}^u + 8T_{78}^u
\end{aligned}
$$

$$
\begin{aligned}
&- 18T^u_{79} - \frac{23861}{36}T^u_{80} + 24T^u_{81} + 22T^u_{82} - \frac{190}{3}T^u_{83} + \frac{1291}{6}T^u_{84} \\
&- 20T^u_{85} - \frac{7}{2}T^u_{86} + 4T^u_{87} - 22T^u_{88} + 202T^u_{89} - 4999T^u_{90} \\
&- 284328T^u_{91} - 510T^u_{92} + \frac{42173}{6}T^u_{93} - \frac{64501}{12}T^u_{94} \\
&+ 79T^u_{95} - \frac{34631}{24}T^u_{96} + \frac{4467}{4}T^u_{97} \\
&+ \text{ products of lower weight functions}\Big\}, \qquad \text{(C.4)}
\end{aligned}
$$

and

$$
\begin{aligned}
V_B^{(4)} \;=\; \frac{1}{1024}\Big\{ & 500T^v_{59} + 193T^v_{60} + 252T^v_{61} + 244T^v_{62} + 256T^v_{64} + 193T^v_{65} \\
& + 271T^v_{66} - 5712T^v_{67} - 3922T^v_{68} + \frac{1012}{3}T^v_{69} + 173T^v_{70} + \frac{304}{3}T^v_{71} \\
& - 1215T^v_{72} + 100T^v_{73} - \frac{1561}{2}T^v_{74} + 28T^v_{75} - 100T^v_{76} + 24T^v_{77} \\
& - 28T^v_{78} + 22T^v_{79} - \frac{13825}{18}T^v_{80} + 144T^v_{81} + 18T^v_{82} - \frac{157}{6}T^v_{83} \\
& + \frac{839}{3}T^v_{84} - 68T^v_{85} + \frac{1}{2}T^v_{86} + 4T^v_{87} + 30T^v_{88} + 170T^v_{89} - \frac{46967}{6}T^v_{90} \\
& - 367344T^v_{91} - 336T^v_{92} + \frac{49109}{6}T^v_{93} - 9155T^v_{94} + 364T^v_{95} \\
& - \frac{8521}{4}T^v_{96} + \frac{1633}{3}T^v_{97} + 12T^u_{98} + 4T^u_{99} + \frac{9155}{6}T^u_{100} - \frac{170141}{36}T^u_{101} \\
& + \frac{145829}{24}T^u_{102} + \text{ products of lower weight functions}\Big\}. \qquad \text{(C.5)}
\end{aligned}
$$

Here $T^u_i = T_i(u,v,w)$, $T^v_i = T_i(v,w,u)$, $T^w_i = T_i(w,u,v)$. The 3-cycle functions $T_{59}, \ldots, S_{97}$ are chosen to be symmetric in their last two arguments, so for these functions the permutation $T_i(v,w,u)$ appears only in $V_B^{(4)}$.

Similarly, the parity-odd part of the four-loop ratio function can be expressed as

$$
\tilde{V}^{(4)}(u,v,w) = \tilde{V}_A^{(4)}(u,v,w) - \tilde{V}_A^{(4)}(w,v,u)\,, \qquad \text{(C.6)}
$$

where

$$\begin{aligned}
\tilde{V}_A^{(4)} \;=\; \frac{1}{3072}\Big\{ & -300S_1^u + 60S_1^v + 240S_1^w - 126S_2^u + 18S_2^v + 108S_2^w \\
& + 156S_3^u - 222S_3^v + 66S_3^w - 40S_4^u + 206S_4^v - 166S_4^w \\
& - 166S_5^u - 112S_5^v + 278S_5^w - 976S_6^u + 278S_6^v + 698S_6^w \\
& + 44S_7^u - 52S_7^v + 8S_7^w - 124S_8^u + 224S_8^v - 100S_8^w + 48S_9^u \\
& + 192S_9^v - 240S_9^w + 720S_{10}^u - 1110S_{10}^v + 390S_{10}^w + 178S_{11}^u \\
& - 242S_{11}^v + 64S_{11}^w + 150S_{12}^u - 150S_{12}^v - 196S_{13}^u - 38S_{13}^v \\
& + 234S_{13}^w - 96S_{14}^u - 18S_{14}^v + 114S_{14}^w + 78S_{15}^u - 78S_{15}^w \\
& + 114S_{16}^v - 114S_{16}^w - 78S_{17}^u - 18S_{17}^v + 96S_{17}^w - 122S_{18}^u \\
& - 26S_{18}^v + 148S_{18}^w - 122S_{19}^u - 26S_{19}^v + 148S_{19}^w + 96S_{20}^u \\
& + 18S_{20}^v - 114S_{20}^w - 454S_{21}^u + 56S_{21}^v + 398S_{21}^w + 12S_{22}^u \\
& + 12S_{22}^v - 24S_{22}^w - 18S_{23}^u + 96S_{23}^v - 78S_{23}^w + 114S_{24}^u \\
& - 96S_{24}^v - 18S_{24}^w - 166S_{25}^u - 40S_{25}^v + 206S_{25}^w - 166S_{26}^u \\
& - 40S_{26}^v + 206S_{26}^w + 396S_{27}^u - 2664S_{27}^v + 2268S_{27}^w + 2831S_{28}^u \\
& - 259S_{28}^v - 2572S_{28}^w - 8S_{29}^u - 146S_{29}^v + 154S_{29}^w - \frac{215}{2}S_{30}^u \\
& + 218S_{30}^v - \frac{221}{2}S_{30}^w - 20S_{31}^u - 966S_{31}^v + 986S_{31}^w - 136S_{32}^u \\
& + 8S_{32}^v + 128S_{32}^w + 34S_{33}^u - 8S_{33}^v - 26S_{33}^w + 1053S_{34}^u \\
& - 1239S_{34}^v + 186S_{34}^w + 126S_{35}^u + 126S_{36}^u - 1666S_{38}^u + 228S_{39}^u \\
& + 360S_{40}^u + 712S_{41}^u + 2843S_{42}^u - 72S_{43}^u + 376S_{45}^u - 153S_{46}^u \\
& - 492S_{47}^u + 610S_{48}^u + 200S_{49}^u - 846S_{50}^u + 884S_{52}^u - 462S_{53}^u \\
& + 27S_{54}^u + 78S_{55}^u + 114S_{57}^u + 78S_{58}^u - 2313S_{62}^u + 177S_{63}^u \\
& - 3060S_{64}^u + \frac{14490793}{44}S_{65}^u + 81S_{66}^u - \frac{84153}{2}S_{67}^u + 2227S_{68}^u \\
& + 20S_{69}^u + 1354S_{70}^u + \frac{1484251}{44}S_{71}^u + \frac{1203}{2}S_{72}^u + \frac{657}{4}S_{73}^u \\
& - \frac{34985}{2}S_{75}^u - 808S_{76}^u + 62S_{77}^u - \frac{28471}{4}S_{78}^u + 759S_{79}^u \\
& + 1065S_{80}^u - 249048S_{81}^u
\end{aligned}$$

$$+ \text{ products of lower weight functions} \Big\}, \tag{C.7}$$

and $S_i^u = S_i(u,v,w)$, $S_i^v = S_i(v,w,u)$, $S_i^w = S_i(w,u,v)$. Note that the singlet functions $S_{82}, \ldots, S_{86}$ cannot appear in an antisymmetric quantity such as $\tilde{V}$. Again, the 3-cycle functions $S_{35}, \ldots, S_{81}$ are chosen to be symmetric in their last two arguments, so for these functions the permutation $S_i(v,w,u)$ cannot appear, and $S_i(w,u,v)$ is related by the $u \leftrightarrow w$ exchange. The products of lower weight functions for both $V^{(4)}$ and $\tilde{V}^{(4)}$ are too lengthy to present here, but they are given in ancillary files.

Appendix D

Functions on the Spurious Pole Surface $w = 1$

In section 1.7.5 we explored the behavior of the ratio function in the limit $w \to 1$. We also need to understand this limit in order to impose the spurious-pole constraint. We call the functions that the hexagon functions approach in this limit *spurious pole surface functions (SP functions)*. Just as for the hexagon functions, the space of SP functions can be built up iteratively in the weight. Because the construction is simpler than for the full hexagon function space, but contains the same essential ingredients, it may be useful for the reader to see it in some detail.[1]

The SP functions must have only physical branch cuts, and their symbol entries can only be drawn from the set of letters that appear in the $w \to 1$ limit of the hexagon function letters (1.29). These conditions translate to functions with symbols constructed out of the letters

$$\mathcal{S}_{w\to 1} \;=\; \{u,\, v,\, 1-u,\, 1-v,\, u-v\}\,, \tag{D.1}$$

with only u and v appearing in the first entry. The $\{n-1, 1\}$ coproduct component

[1] One can always use multiple polylogarithms, or the 2dHPLs of Gehrmann and Remiddi [128] to describe this function space. The main virtue of the construction described here, as with the hexagon function approach, is imposing the branch-cut condition at the beginning, which reduces the size of the space dramatically at high weights.

of a generic SP function $f(u, v)$ of weight n thus takes the form

$$\begin{aligned}\Delta_{n-1,1}(f) \equiv f^u \otimes \ln u + f^v \otimes \ln v + f^{1-u} \otimes \ln(1-u) \\ + f^{1-v} \otimes \ln(1-v) + f^{u-v} \otimes \ln(u-v),\end{aligned} \tag{D.2}$$

where its derivatives are given by

$$\begin{aligned}\left.\frac{\partial f}{\partial u}\right|_v &= \frac{f^u}{u} - \frac{f^{1-u}}{1-u} + \frac{f^{u-v}}{u-v}\,, \\ \left.\frac{\partial f}{\partial v}\right|_u &= \frac{f^v}{v} - \frac{f^{1-v}}{1-v} - \frac{f^{u-v}}{u-v}\,.\end{aligned} \tag{D.3}$$

We can take the u and v partial derivatives of a full hexagon function $F(u, v, w)$ using eq. (A.2), let $w \to 1$ in the rational prefactors, and compare with eq. (D.3). This comparison relates the $\{n-1, 1\}$ coproduct components for F to the corresponding ones for the function $f(u, v)$ that it approaches on the $w = 1$ surface:

$$\begin{aligned}f^u &= F^u \pm F^{y_u}\,, \\ f^v &= F^v \mp F^{y_v}\,, \\ f^{1-u} &= F^{1-u} \mp F^{y_v} \pm F^{y_w}\,, \\ f^{1-v} &= F^{1-v} \pm F^{y_u} \mp F^{y_w}\,, \\ f^{u-v} &= \mp 2F^{y_u} \pm 2F^{y_v}\,.\end{aligned} \tag{D.4}$$

The overall sign ambiguity associated with the F^{y_i} components simply reflects an ambiguity as to whether the limit (1.133) holds, or the same limit with the y_i's inverted, so it holds globally for all functions. We note that "coproduct matching relations" like eq. (D.4) provide a very useful way to collapse hexagon functions into functions on generic limiting surfaces, beyond the specific case of SP functions treated here.

We'll construct the irreducible part of the SP function space through weight three here, in order to illustrate the same methods used to construct hexagon functions.

At weight one, the only functions satisfying the branch-cut constraints are $\ln u$ and

$\ln v$. Functions of higher weight n can be constructed at the symbol level by requiring that their symbol satisfy an integrability condition. This condition connects pairs of adjacent entries, and there are $n-1$ such conditions, one for each pair. Imposing all these conditions ensures that the symbol can be integrated up to a single-valued function, or equivalently that partial derivatives acting on it commute. However, integrability can also be imposed iteratively. Suppose we have classified all functions with weight $n-1$. Then we can construct an ansatz for the space of functions with weight n by requiring that their derivatives are given by eq. (D.3) (for the case of SP functions) where each of the coproduct entries $f^u, f^v, f^{1-u}, f^{1-v}, f^{u-v}$ is a generic linear combination of weight $n-1$ functions. Now we just need to impose integrability on the last two entries of the corresponding symbol. At function level, this is a linear constraint on the $\{n-2,1,1\}$ coproduct entries $f^{x,y}$, which is a set of linear equations for the coefficients of $f^u, f^v, f^{1-u}, f^{1-v}, f^{u-v}$, when they are expanded in terms of the weight $n-1$ functions.

On the spurious pole surface, the requirement that partial derivatives commute,

$$\frac{\partial^2 f}{\partial u \partial v} = \frac{\partial^2 f}{\partial v \partial u}\,, \tag{D.5}$$

gives rise to six relations between the $\{n-2,1,1\}$ coproduct entries of a weight n function f:

$$\begin{aligned}
f^{[u,1-v]} &= 0,\\
f^{[v,1-u]} &= 0,\\
f^{[u,u-v]} &= f^{[v,u]},\\
f^{[v,u-v]} &= f^{[u,v]},\\
f^{[1-u,u-v]} &= f^{[1-v,1-u]},\\
f^{[1-v,u-v]} &= f^{[1-u,1-v]},
\end{aligned} \tag{D.6}$$

where the square brackets indicate that an antisymmetric combination of coproduct entries is being taken, $f^{[x,y]} \equiv f^{x,y} - f^{y,x}$. These relations are the analogs of the relations (1.35) for hexagon functions.

However, the relations (D.6) don't completely exhaust the conditions we must impose on an SP function. Note that transcendental constants of weight $n-1$ are in the kernel of the $\{n-2,1,1\}$ coproduct, so their coefficients remain undetermined by the above equations. Some of these coefficients will lead to unwanted branch cuts for f, even if all of the $\{n-1,1\}$ coproducts f^x have only the proper branch cuts. We must also check the first derivatives of our candidate functions at particular locations, in order to make sure that they remain finite away from the allowed physical singularities ($u \to 0$, $v \to 0$). From eq. (D.3) we see that we must inspect the lines $u = 1$, $v = 1$ and $u = v$, where the symbol letters (other than u and v) vanish. We must impose

$$f^{1-u}|_{u=1} = f^{1-v}|_{v=1} = f^{u-v}|_{u=v} = 0, \tag{D.7}$$

which are the analogs for SP functions of eqs. (1.37) and (1.38) for the hexagon functions.

After we have found the space of functions with good branch cuts, we remove the ones that are reducible, i.e. products of lower weight functions, as well as the one-dimensional HPLs in u and v. The remaining irreducible functions can be classified by the discrete symmetry. For hexagon functions this symmetry group includes parity and the S_3 symmetry permuting (u, v, w). For the SP functions, there is no parity; eq. (D.4) shows that parity even and odd hexagon functions such as F^u and F^{y_u} combine to give SP functions. Also, the S_3 symmetry is broken to S_2, generated by the exchange $u \leftrightarrow v$.

When we apply the integrability constraint, eq. (D.6), at weight two we find, interestingly, that it already allows for the appearance of an irreducible function. (In the hexagon function case, the first irreducible function is $\tilde{\Phi}_6$, at weight three.) We choose to define this function's $\{1,1\}$ coproduct to be

$$\begin{aligned}\Delta_{1,1}\Big(\mathrm{SP}_1^{(2)}(u,v)\Big) &= -\ln u \otimes \ln(u-v) + \frac{1}{2}\ln u \otimes \ln v \\ &\quad + \ln v \otimes \ln(u-v) - \frac{1}{2}\ln v \otimes \ln u\,,\end{aligned} \tag{D.8}$$

so that it is antisymmetric under the exchange of u and v.[2]

No other integrable symbols at weight two involve the letter $u - v$. We can see this easily from eq. (D.6): The right-hand sides of the last two relations vanish for weight two because a first entry is never $1-u$ or $1-v$. Thus $f^{1-u,u-v} = f^{1-v,u-v} = 0$. The third and fourth relations show that $f^{u,u-v} = -f^{v,u-v}$, which determines all the $(u-v)$-dependent terms up to an overall constant. The rest of the space is spanned by products of HPLs in u and v.

The derivative of $\mathrm{SP}_1^{(2)}$ follows from eq. (D.8):

$$\frac{\partial}{\partial u}\mathrm{SP}_1^{(2)}(u,v) = -\frac{\ln v}{2u} + \frac{\ln v - \ln u}{u - v}\,. \tag{D.9}$$

It is indeed singular only in the $u \to 0$ limit. At this weight, there would be no possibility of adding a transcendental constant to the (weight one) functions in the $\{n-1, 1\}$ coproducts to fix such a singularity, had it been there.

We set the additive constant of all SP functions by requiring that they vanish in the limit $(u, v) \to (1, 1)$.

At weight three, there are four independent solutions to the integrability condition, besides the reducible space of HPLs and $\mathrm{SP}_1^{(2)}$ times $\ln u$ or $\ln v$. These four irreducible solutions can be organized into two orbits of the S_2 group that permutes u and v,

$$\Big\{\mathrm{SP}_1^{(3)}(u,v), \mathrm{SP}_1^{(3)}(v,u), \mathrm{SP}_2^{(3)}(u,v), \mathrm{SP}_2^{(3)}(v,u)\Big\}\,. \tag{D.10}$$

Each orbit is a two-cycle represented by one of the following functions, defined by its $\{2,1\}$ coproduct:

$$\begin{aligned}\Delta_{2,1}\Big(\mathrm{SP}_1^{(3)}(u,v)\Big) = &-H_2^u \otimes \ln(1-v) + H_2^u \otimes \ln(u-v) - H_2^v \otimes \ln(u-v)\\ &+ \frac{1}{2}\ln u \ln v \otimes \ln(1-v) + \mathrm{SP}_1^{(2)}(u,v) \otimes \ln(1-v)\,,\end{aligned} \tag{D.11}$$

$$\begin{aligned}\Delta_{2,1}\Big(\mathrm{SP}_2^{(3)}(u,v)\Big) = &-\frac{1}{2}\ln u \ln v \otimes \ln v + \mathrm{SP}_1^{(2)}(u,v) \otimes \ln v\\ &- 2\ \mathrm{SP}_1^{(2)}(u,v) \otimes \ln(u-v)\,.\end{aligned} \tag{D.12}$$

[2] $\ln(u-v)$ should be considered inert under this transformation.

Note that, since each of these two-cycles represents two linearly independent SP functions, the dimension of the weight three irreducible space (four) is larger than the number of functions we have indexed (two). Moreover, these definitions are relatively simple, compared to the number of terms required to specify each function's symbol. This feature becomes increasingly true as we move to higher weight.

Next we inspect the behavior of these functions at $u = 1$, $v = 1$ and $u = v$. For $\mathrm{SP}_1^{(3)}(u, v)$, eq. (D.11) has no $\ln(1 - u)$, so there can be no singularity as $u \to 1$. The singularity as $u \to v$ is cancelled because the first entry multiplying $\ln(u - v)$ is $H_2^u - H_2^v$, which vanishes in this limit. The only subtlety is for $v \to 1$, where we require, from setting $v = 1$ in the first entry multiplying $\ln(1 - v)$ in eq. (D.11),

$$\mathrm{SP}_1^{(2)}(u, 1) = H_2^u = \mathrm{Li}_2(1 - u). \tag{D.13}$$

But this equation follows by evaluating the u derivative using eq. (D.9) for $v = 1$, and the fact that they match at $u = 1$: $\mathrm{SP}_1^{(2)}(1, 1) = 0 = \mathrm{Li}_2(0)$. For the other weight three irreducible function, the only singularity that has to be checked is the limit $u \to v$, where the antisymmetry of $\mathrm{SP}_1^{(2)}(u, v)$ ensures it. So again at weight three, we do not need to add any transcendental constants (in this case only ζ_2 would be expected) to the weight two functions appearing in the $\{2, 1\}$ coproducts to fix the branch-cut behavior. It turns out that such weight $n - 1$ constants are never needed in the $\{n - 1, 1\}$ coproducts of SP functions. (In contrast, they do appear in the coproducts of many hexagon functions, in order to enforce smoothness as $u_i \to 1$.)

A complete basis of SP functions through weight seven was constructed using this method, and can be found in an ancillary file. The symmetry properties of these basis functions under the permutation group S_2 are laid out in Table D.1. We divide them into two-cycles, symmetric and antisymmetric functions. Clearly one could form symmetric and antisymmetric combinations of each member of a two-cycle, but it is convenient to leave it as a two-cycle, in analogy to how we treat S_3 for the hexagon functions. We introduced some explicitly symmetric functions into our basis starting at weight five. We provide another ancillary file which uses this SP basis to describe the ratio function and remainder function on the spurious pole surface through three

Weight	two-cycles	symmetric	antisymmetric
2	-	-	$\mathrm{SP}_1^{(2)}$
3	$\mathrm{SP}_1^{(3)}, \mathrm{SP}_2^{(3)}$	-	-
4	$\mathrm{SP}_1^{(4)} \ldots \mathrm{SP}_5^{(4)}$	-	$\mathrm{SP}_6^{(4)}, \mathrm{SP}_7^{(4)}$
5	$\mathrm{SP}_1^{(5)} \ldots \mathrm{SP}_{16}^{(5)}$	$\mathrm{SP}_{17}^{(5)}, \mathrm{SP}_{18}^{(5)}$	$\mathrm{SP}_{19}^{(5)}, \mathrm{SP}_{20}^{(5)}$
6	$\mathrm{SP}_1^{(6)} \ldots \mathrm{SP}_{44}^{(6)}$	$\mathrm{SP}_{45}^{(6)}, \mathrm{SP}_{46}^{(6)}, \mathrm{SP}_{47}^{(6)}$	$\mathrm{SP}_{48}^{(6)} \ldots \mathrm{SP}_{54}^{(6)}$
7	$\mathrm{SP}_1^{(7)} \ldots \mathrm{SP}_{126}^{(7)}$	$\mathrm{SP}_{127}^{(7)} \ldots \mathrm{SP}_{138}^{(7)}$	$\mathrm{SP}_{139}^{(7)} \ldots \mathrm{SP}_{150}^{(7)}$

Table D.1: The symmetry orbits of the SP basis functions through weight seven. The functional dependence on u and v has been suppressed. Upon exchange of u and v, each two-cycle is sent to a linearly independent function within the SP function space. Symmetric and antisymmetric functions are mapped back to themselves, with an overall sign change in the antisymmetric case.

loops.

Appendix E

Proof that $c_1^{(2)}(u,w)$ is Positive and Monotonic

The coefficient function $c_1^{(2)}(u,w)$ has weight 3, which guarantees that it can be represented in terms of classical polylogarithms. From its coproduct representation we found that

$$\begin{aligned} c_1^{(2)}(u,w) &= -\mathrm{Li}_3\left(\frac{u+w-1}{uw}\right) + \mathrm{Li}_3\left(\frac{u+w-1}{u}\right) + \mathrm{Li}_3\left(\frac{u+w-1}{w}\right) \\ &\quad - \log w\,\mathrm{Li}_2\left(\frac{u+w-1}{u}\right) - \log u\,\mathrm{Li}_2\left(\frac{u+w-1}{w}\right) \\ &\quad - \frac{1}{2}\,\log(uw)\left(\mathrm{Li}_2(1-u) + \mathrm{Li}_2(1-w) - \zeta_2\right) \\ &\quad - \frac{1}{2}\left(\log^2 u\,\log(1-u) + \log^2 w\,\log(1-w)\right). \end{aligned} \tag{E.1}$$

Note that it vanishes on the collinear boundary $u+w=1$: $c_1^{(2)}(u,1-u)=0$. The representation (E.1) is manifestly real for $u,w>0$ and $u,w<1$. It can acquire an imaginary part in other regions, so another representation might be preferable in principle.

However, we are going to take its radial derivative now, and write the result in a

manifestly real form:

$$\begin{aligned} c_{1,r}^{(2)}(u,w) &\equiv (u\partial_u + w\partial_w)c_1^{(2)}(u,w) \\ &= \frac{c_0^{(1)}(u,w)}{u+w-1} - \frac{1}{2}\left[\frac{1}{1-u} + \frac{1}{1-w}\right]\log u\,\log w\,, \end{aligned} \tag{E.2}$$

where

$$c_0^{(1)}(u,w) = -C^{(1)}(u,w) = -\mathrm{Li}_2(1-u) - \mathrm{Li}_2(1-w) - \log u \log w + \zeta_2 \tag{E.3}$$

is positive and monotonically increasing, from the previous one-loop analysis.

Although the first term in eq. (E.2) is positive in the positive double-scaling region (3.49), the second term can be negative (say, for $u < 1$ and $w < 1$). So we have to show that the second term is outweighed by the first term.

Rather than working with dilogarithms, we take another radial derivative. First we multiply by the quantity $(u + w - 1)$, which is uniformly positive in the positive region. So if we can show that $(u + w - 1)c_{1,r}^{(2)}$ is positive, it's the same as showing $c_{1,r}^{(2)}$ is positive. It's easy to see that $c_{1,r}^{(2)}(u,w)$ is regular on the collinear boundary, because $c_0^{(1)}(u,w)$ vanishes there. Hence $(u + w - 1)c_{1,r}^{(2)}$ vanishes there, which allows a radial flow argument to work. Multiplication by $(u + w - 1)$ before differentiating also allows the radial derivative to kill the polylogarithms:

$$\begin{aligned} c_{1,rr}^{(2)}(u,w) &\equiv (u\partial_u + w\partial_w)\Big[(u+w-1)c_{1,r}^{(2)}(u,w)\Big] \\ &= -\frac{1}{2}\left[\frac{u}{(1-w)^2} + \frac{w}{(1-u)^2}\right]\log u\,\log w \\ &\quad -\frac{1}{2}\left[\frac{u}{1-w} + \frac{w+2u}{1-u}\right]\log u - \frac{1}{2}\left[\frac{w}{1-u} + \frac{u+2w}{1-w}\right]\log w\,. \\ &= \frac{1}{2}\log u\left[-\frac{u\,\log w}{(1-w)^2} - \frac{u}{1-w} - \frac{w+2\,u}{1-u}\right] \;+\; (u \leftrightarrow w). \end{aligned} \tag{E.4}$$

In the second form, it is enough to show that the term shown is positive everywhere in the positive region; the same will then be true of the term obtained by $(u \leftrightarrow w)$ reflection.

Note that the contribution of the third term in brackets, $-(w+2u)(\log u)/(1-u)$, always has the desired sign, positive. Suppose first that $u > 1$. Then we combine the first two terms to get $(-u) \times (\log w + 1 - w)/(1-w)^2$. The last factor is always negative, including $w = 1$ where it approaches a finite limit. So we are done with the $u > 1$ case.

Now let $u < 1$. In this case we have to combine all three terms, and use the identity,

$$\frac{u}{1-w} + \frac{w+2\,u}{1-u} \;>\; \frac{u}{w(1-w)}\,, \tag{E.5}$$

which can be established by writing the difference, left minus right, as

$$\frac{w(w+u)+u(u+w-1)}{w(1-u)} \;>\; 0. \tag{E.6}$$

Therefore

$$\frac{u\,\log w}{(1-w)^2} + \frac{u}{1-w} + \frac{w+2\,u}{1-u} \;>\; \frac{u\,\log w}{(1-w)^2} + \frac{u}{w(1-w)} \;=\; u \times \frac{\log w + \frac{1-w}{w}}{(1-w)^2}\,. \tag{E.7}$$

The last factor is always positive, so the quantity in brackets in eq. (E.4) is negative for $u < 1$. Combined with the fact that $\log u < 0$ for $u < 1$, we are done proving that $c_{1,rr}^{(2)} > 0$ in the positive region. This in turn proves that $c_{1,r}^{(2)} > 0$, and hence that $c_1^{(2)}(u,w)$ itself is positive.

For the next simplest quantity, the weight-4 function $c_0^{(2)}(u,w)$, we tried to apply the same method of taking repeated radial derivatives, but we were unable to remove all the trilogarithms in the second iteration, because they come with different rational prefactors. So an analytic proof would probably require another method. However, we could establish numerically that the second such derivative, $c_{1,rr}^{(2)}(u,w)$ was positive in the positive region, consistent with the more general numerical study in section 3.4.2.

Appendix F

The BDS and BDS-like Ansätze

The BDS ansatz [31] for the n-particle MHV amplitude (with the Parke-Taylor tree amplitude scaled out) is given by

$$M_n \equiv \frac{A_n}{A_n^{(0)}} = \exp\left[\sum_{L=1}^{\infty} a^L \left(f^{(L)}(\epsilon)\frac{1}{2}M_n^{(1)}(L\epsilon) + C^{(L)}\right)\right] \tag{F.1}$$

with

$$f^{(L)}(\epsilon) = f_0^{(L)} + \epsilon f_1^{(L)} + \epsilon^2 f_2^{(L)}, \tag{F.2}$$

and where ϵ is the dimensional regularization parameter in $D = 4 - 2\epsilon$. Here $f_0^{(L)}$ is the planar cusp anomalous dimension with

$$f_0^{(L)} = \frac{1}{4}\gamma_K^{(L)} = \frac{1}{2}\Gamma_{\text{cusp}}^{(L)}\,, \tag{F.3}$$

according to the definition (4.24). However, note that in the above relation the superscript L refers to coefficients in the expansion with respect to $a = 2g^2$, and not g^2.

For $n = 7$, the BDS ansatz takes the form

$$A_7^{\text{BDS}} = A_7^{\text{MHV}(0)}\exp\left[\sum_{L=1}^{\infty} a^L \left(f^{(L)}(\epsilon)\frac{1}{2}M_7^{(1)}(L\epsilon) + C^{(L)}\right)\right]. \tag{F.4}$$

Here we have explicitly factored out 1/2 from the definition of $M_7^{(1)}(\epsilon)$ appearing in the original BDS paper. The seven-particle one-loop MHV amplitude (again with the tree amplitude scaled out) appearing in the BDS ansatz is given by

$$M_7^{(1)}(\epsilon) = -\frac{1}{\epsilon^2}\sum_{i=1}^{7}\left(\frac{\mu^2}{-s_{i,i+1}}\right)^{\epsilon} + F_7^{(1)}(0) + \mathcal{O}(\epsilon) \tag{F.5}$$

where

$$F_7^{(1)}(0) = \sum_{i=1}^{7}\left[-\log\left(\frac{-s_{i,i+1}}{-s_{i,i+1,i+2}}\right)\log\left(\frac{-s_{i+1,i+2}}{-s_{i,i+1,i+2}}\right) + D_{7,i} + L_{7,i} + \frac{3}{2}\zeta_2\right] \tag{F.6}$$

with

$$D_{7,i} = -\mathrm{Li}_2\left(1-\frac{s_{i,i+1}\,s_{i-1,i,i+1,i+2}}{s_{i,i+1,i+2}\,s_{i-1,i,i+1}}\right) \tag{F.7}$$

and

$$L_{7,i} = -\frac{1}{2}\log\left(\frac{-s_{i,i+1,i+2}}{-s_{i,i+1,i+2,i+3}}\right)\log\left(\frac{-s_{i+1,i+2,i+3}}{-s_{i-1,i,i+1,i+2}}\right). \tag{F.8}$$

Notice that all of the dependence on the three-particle Mandelstam invariants is contained within $F_7^{(1)}(0)$, so we will focus on determining its dependence. We can replace the four-particle invariants with three-particle invariants in both $D_{7,i}$ and $L_{7,i}$. The two equations then become

$$\begin{aligned} D_{7,i} &= -\mathrm{Li}_2\left(1-\frac{s_{i,i+1}s_{i+3,i+4,i+5}}{s_{i,i+1,i+2}s_{i-1,i,i+1}}\right), \\ L_{7,i} &= -\frac{1}{2}\log\left(\frac{s_{i,i+1,i+2}}{s_{i+4,i+5,i+6}}\right)\log\left(\frac{s_{i+1,i+2,i+3}}{s_{i+3,i+4,i+5}}\right). \end{aligned} \tag{F.9}$$

At this point, it is convenient to switch to the $n = 7$ dual conformal cross ratios u_i, defined in terms of the Mandelstam variables by

$$u_i = u_{i+1,i+4} = \frac{s_{i+2,i+3}\,s_{i+5,i+6,i+7}}{s_{i+1,i+2,i+3}\,s_{i+2,i+3,i+4}}, \tag{F.10}$$

where all indices are understood mod 7. We can see from this definition that $D_{7,i}$ can be expressed simply in the u_i variables as $D_{7,i} = -\mathrm{Li}_2\,(1-u_{i-2})$. Using the dilogarithm

identity $\mathrm{Li}_2(z) + \mathrm{Li}_2(1-1/z) = -\frac{1}{2}\log^2 z$, we then rewrite $D_{7,i} = \mathrm{Li}_2\left(1-1/u_{i-2}\right) + \frac{1}{2}\log^2 u_{i-2}$, and express $F_7^{(1)}(0)$ as

$$\begin{aligned} F_7^{(1)}(0) = \sum_{i=1}^{7} \Bigg[&- \log\left(\frac{s_{i,i+1}}{s_{i,i+1,i+2}}\right) \log\left(\frac{s_{i+1,i+2}}{s_{i,i+1,i+2}}\right) + \mathrm{Li}_2\left(1-1/u_i\right) + \frac{1}{2}\log^2 u_i \\ &- \frac{1}{2}\log\left(\frac{s_{i,i+1,i+2}}{s_{i+4,i+5,i+6}}\right) \log\left(\frac{s_{i+1,i+2,i+3}}{s_{i+3,i+4,i+5}}\right) + \frac{3}{2}\zeta_2 \Bigg]. \end{aligned} \tag{F.11}$$

After some algebra, $F_7^{(1)}(0)$ can be shown to be

$$\begin{aligned} F_7^{(1)}(0) \;=\; \sum_{i=1}^{7} \Bigg[&\mathrm{Li}_2\left(1-\frac{1}{u_i}\right) + \frac{1}{2}\log\left(\frac{u_{i+2}u_{i-2}}{u_{i+3}u_i u_{i-3}}\right)\log u_i \\ &+ \log s_{i,i+1} \log\left(\frac{s_{i,i+1}s_{i+3,i+4}}{s_{i+1,i+2}s_{i+2,i+3}}\right) + \frac{3}{2}\zeta_2 \Bigg]. \end{aligned} \tag{F.12}$$

In this form, we have conveniently isolated all of the three-particle invariants in the first two terms.

Now we would like to factor out the three-particle invariants from $F_7^{(1)}(0)$ because this removes their dependence from $M_7^{(1)}$ as well. We define the function

$$Y_7 = -\sum_{i=1}^{7} \left[\mathrm{Li}_2\left(1-\frac{1}{u_i}\right) + \frac{1}{2}\log\left(\frac{u_{i+2}u_{i-2}}{u_{i+3}u_i u_{i-3}}\right)\log u_i \right] \tag{F.13}$$

so that adding the term Y_7 removes the three-particle invariants from $M_7^{(1)}$:

$$\begin{aligned} \hat{M}_7^{(1)}(\epsilon) \;&\equiv\; M_7^{(1)}(\epsilon) + Y_7 \\ &=\; \sum_{i=1}^{7} \left[-\frac{1}{\epsilon^2}\left(\frac{\mu^2}{-s_{i,i+1}}\right)^{\epsilon} + \log s_{i,i+1} \log\left(\frac{s_{i,i+1}\, s_{i+3,i+4}}{s_{i+1,i+2}\, s_{i+2,i+3}}\right) + \frac{3}{2}\zeta_2 \right]. \end{aligned} \tag{F.14}$$

The BDS-like ansatz is defined to be the BDS ansatz with $M_7^{(1)}$ replaced by with $\hat{M}_7^{(1)}$, which does not depend on any three-particle invariant:

$$A_7^{\text{BDS-like}} = A_7^{\text{MHV}(0)} \exp\left[\sum_{L=1}^{\infty} a^L \left(f^{(L)}(\epsilon)\frac{1}{2}\left(M_7^{(1)}(L\epsilon) + Y_7 \right) + C^{(L)} \right) \right], \tag{F.15}$$

Factoring out the BDS ansatz explicitly, we have

$$A_7^{\text{BDS-like}} = A_7^{\text{BDS}} \exp\left[\sum_{L=1}^{\infty} \frac{a^L}{2}\left(f^{(L)}(\epsilon) Y_7\right)\right]. \tag{F.16}$$

Recall that in the BDS ansatz formulation, the limit $\epsilon \to 0$ is taken. Since Y_7 is independent of ϵ, we can set $\epsilon \to 0$ in eq. (F.2) and rewrite the BDS-like ansatz as simply

$$A_7^{\text{BDS-like}} = A_7^{\text{BDS}} \exp\left[\frac{Y_7}{4} \sum_{L=1}^{\infty} a^L \Gamma_{\text{cusp}}^{(L)}\right], \tag{F.17}$$

where we have used the definition (F.3). After introducing $\Gamma_{\text{cusp}} = \sum_{L=1}^{\infty} a^L \Gamma_{\text{cusp}}^{(L)}$, defined in eq. (4.24), we finally arrive at a simple representation of the BDS-like ansatz as a function of the BDS ansatz, the cusp anomalous dimension Γ_{cusp}, and Y_7,

$$A_7^{\text{BDS-like}} = A_7^{\text{BDS}} \exp\left[\frac{\Gamma_{\text{cusp}}}{4} Y_7\right]. \tag{F.18}$$

This result can be generalized to any n for which a suitable BDS-like ansatz exists, see eq. (4.21).

Bibliography

[1] S. J. Parke and T. R. Taylor, "Gluonic Two Goes to Four," *Nucl. Phys.*, vol. B269, pp. 410–420, 1986.

[2] S. J. Parke and T. R. Taylor, "An Amplitude for n Gluon Scattering," *Phys. Rev. Lett.*, vol. 56, p. 2459, 1986.

[3] Z. Bern, L. J. Dixon, D. C. Dunbar, and D. A. Kosower, "One loop n point gauge theory amplitudes, unitarity and collinear limits," *Nucl.Phys.*, vol. B425, pp. 217–260, 1994.

[4] Z. Bern, L. J. Dixon, and D. A. Kosower, "One loop amplitudes for e+ e- to four partons," *Nucl. Phys.*, vol. B513, pp. 3–86, 1998.

[5] R. Britto, F. Cachazo, and B. Feng, "New recursion relations for tree amplitudes of gluons," *Nucl. Phys.*, vol. B715, pp. 499–522, 2005.

[6] R. Britto, F. Cachazo, B. Feng, and E. Witten, "Direct proof of tree-level recursion relation in Yang-Mills theory," *Phys. Rev. Lett.*, vol. 94, p. 181602, 2005.

[7] N. Arkani-Hamed, J. L. Bourjaily, F. Cachazo, S. Caron-Huot, and J. Trnka, "The All-Loop Integrand For Scattering Amplitudes in Planar N=4 SYM," *JHEP*, vol. 1101, p. 041, 2011.

[8] H. Kawai, D. C. Lewellen, and S. H. H. Tye, "A Relation Between Tree Amplitudes of Closed and Open Strings," *Nucl. Phys.*, vol. B269, pp. 1–23, 1986.

[9] Z. Bern, J. J. M. Carrasco, and H. Johansson, "New Relations for Gauge-Theory Amplitudes," *Phys. Rev.*, vol. D78, p. 085011, 2008.

[10] S. He and O. Schlotterer, "New Relations for Gauge-Theory and Gravity Amplitudes at Loop Level," *Phys. Rev. Lett.*, vol. 118, no. 16, p. 161601, 2017.

[11] N. Arkani-Hamed, J. L. Bourjaily, F. Cachazo, A. B. Goncharov, A. Postnikov, *et al.*, "Scattering Amplitudes and the Positive Grassmannian," 2012.

[12] N. Arkani-Hamed, F. Cachazo, C. Cheung, and J. Kaplan, "A Duality For The S Matrix," *JHEP*, vol. 03, p. 020, 2010.

[13] N. Arkani-Hamed and J. Trnka, "The Amplituhedron," *JHEP*, vol. 1410, p. 30, 2014.

[14] N. Arkani-Hamed and J. Trnka, "Into the Amplituhedron," *JHEP*, vol. 12, p. 182, 2014.

[15] L. Brink, J. H. Schwarz, and J. Scherk, "Supersymmetric Yang-Mills Theories," *Nucl. Phys.*, vol. B121, pp. 77–92, 1977.

[16] F. Gliozzi, J. Scherk, and D. I. Olive, "Supersymmetry, Supergravity Theories and the Dual Spinor Model," *Nucl. Phys.*, vol. B122, pp. 253–290, 1977.

[17] H. Elvang, D. Z. Freedman, and M. Kiermaier, "SUSY Ward identities, Superamplitudes, and Counterterms," *J. Phys.*, vol. A44, p. 454009, 2011.

[18] N. Beisert, C. Ahn, L. F. Alday, Z. Bajnok, J. M. Drummond, *et al.*, "Review of AdS/CFT Integrability: An Overview," *Lett.Math.Phys.*, vol. 99, pp. 3–32, 2012.

[19] L. F. Alday and J. M. Maldacena, "Gluon scattering amplitudes at strong coupling," *JHEP*, vol. 0706, p. 064, 2007.

[20] J. Drummond, G. Korchemsky, and E. Sokatchev, "Conformal properties of four-gluon planar amplitudes and Wilson loops," *Nucl.Phys.*, vol. B795, pp. 385–408, 2008.

[21] A. Brandhuber, P. Heslop, and G. Travaglini, "MHV amplitudes in $\mathcal{N} = 4$ super Yang-Mills and Wilson loops," *Nucl.Phys.*, vol. B794, pp. 231–243, 2008.

[22] J. Drummond, J. Henn, G. Korchemsky, and E. Sokatchev, "On planar gluon amplitudes/Wilson loops duality," *Nucl.Phys.*, vol. B795, pp. 52–68, 2008.

[23] J. Drummond, J. Henn, G. Korchemsky, and E. Sokatchev, "Conformal Ward identities for Wilson loops and a test of the duality with gluon amplitudes," *Nucl.Phys.*, vol. B826, pp. 337–364, 2010.

[24] L. F. Alday and R. Roiban, "Scattering Amplitudes, Wilson Loops and the String/Gauge Theory Correspondence," *Phys.Rept.*, vol. 468, pp. 153–211, 2008.

[25] T. Adamo, M. Bullimore, L. Mason, and D. Skinner, "Scattering Amplitudes and Wilson Loops in Twistor Space," *J.Phys.*, vol. A44, p. 454008, 2011.

[26] J. M. Drummond, J. Henn, V. A. Smirnov, and E. Sokatchev, "Magic identities for conformal four-point integrals," *JHEP*, vol. 01, p. 064, 2007.

[27] Z. Bern, M. Czakon, L. J. Dixon, D. A. Kosower, and V. A. Smirnov, "The Four-Loop Planar Amplitude and Cusp Anomalous Dimension in Maximally Supersymmetric Yang-Mills Theory," *Phys.Rev.*, vol. D75, p. 085010, 2007.

[28] Z. Bern, J. Carrasco, H. Johansson, and D. Kosower, "Maximally supersymmetric planar Yang-Mills amplitudes at five loops," *Phys.Rev.*, vol. D76, p. 125020, 2007.

[29] J. M. Drummond, J. Henn, G. P. Korchemsky, and E. Sokatchev, "Dual superconformal symmetry of scattering amplitudes in N=4 super-Yang-Mills theory," *Nucl. Phys.*, vol. B828, pp. 317–374, 2010.

[30] J. Drummond and L. Ferro, "Yangians, Grassmannians and T-duality," *JHEP*, vol. 1007, p. 027, 2010.

[31] Z. Bern, L. J. Dixon, and V. A. Smirnov, "Iteration of planar amplitudes in maximally supersymmetric Yang-Mills theory at three loops and beyond," *Phys. Rev.*, vol. D72, p. 085001, 2005.

[32] L. J. Dixon, J. M. Drummond, and J. M. Henn, "Bootstrapping the three-loop hexagon," *JHEP*, vol. 1111, p. 023, 2011.

[33] L. J. Dixon, J. M. Drummond, and J. M. Henn, "Analytic result for the two-loop six-point NMHV amplitude in $\mathcal{N} = 4$ super Yang-Mills theory," *JHEP*, vol. 1201, p. 024, 2012.

[34] L. J. Dixon, J. M. Drummond, M. von Hippel, and J. Pennington, "Hexagon functions and the three-loop remainder function," *JHEP*, vol. 1312, p. 049, 2013.

[35] L. J. Dixon, J. M. Drummond, C. Duhr, and J. Pennington, "The four-loop remainder function and multi-Regge behavior at NNLLA in planar $\mathcal{N} = 4$ super-Yang-Mills theory," *JHEP*, vol. 1406, p. 116, 2014.

[36] L. J. Dixon, J. M. Drummond, C. Duhr, M. von Hippel, and J. Pennington, "Bootstrapping six-gluon scattering in planar $\mathcal{N} = 4$ super-Yang-Mills theory," *PoS*, vol. LL2014, p. 077, 2014.

[37] L. J. Dixon and M. von Hippel, "Bootstrapping an NMHV amplitude through three loops," *JHEP*, vol. 1410, p. 65, 2014.

[38] L. J. Dixon, M. von Hippel, and A. J. McLeod, "The four-loop six-gluon NMHV ratio function," *JHEP*, vol. 01, p. 053, 2016.

[39] J. Golden, A. B. Goncharov, M. Spradlin, C. Vergu, and A. Volovich, "Motivic Amplitudes and Cluster Coordinates," *JHEP*, vol. 1401, p. 091, 2014.

[40] J. Golden and M. Spradlin, "A Cluster Bootstrap for Two-Loop MHV Amplitudes," *JHEP*, vol. 02, p. 002, 2015.

[41] J. M. Drummond, G. Papathanasiou, and M. Spradlin, "A Symbol of Uniqueness: The Cluster Bootstrap for the 3-Loop MHV Heptagon," *JHEP*, vol. 03, p. 072, 2015.

[42] A. B. Goncharov, M. Spradlin, C. Vergu, and A. Volovich, "Classical Polylogarithms for Amplitudes and Wilson Loops," *Phys.Rev.Lett.*, vol. 105, p. 151605, 2010.

[43] C. Duhr, "Hopf algebras, coproducts and symbols: an application to Higgs boson amplitudes," *JHEP*, vol. 1208, p. 043, 2012.

[44] L. F. Alday, D. Gaiotto, J. Maldacena, A. Sever, and P. Vieira, "An Operator Product Expansion for Polygonal null Wilson Loops," *JHEP*, vol. 1104, p. 088, 2011.

[45] D. Gaiotto, J. Maldacena, A. Sever, and P. Vieira, "Bootstrapping Null Polygon Wilson Loops," *JHEP*, vol. 1103, p. 092, 2011.

[46] D. Gaiotto, J. Maldacena, A. Sever, and P. Vieira, "Pulling the straps of polygons," *JHEP*, vol. 1112, p. 011, 2011.

[47] A. Sever, P. Vieira, and T. Wang, "OPE for Super Loops," *JHEP*, vol. 1111, p. 051, 2011.

[48] B. Basso, A. Sever, and P. Vieira, "Spacetime and Flux Tube S-Matrices at Finite Coupling for $\mathcal{N} = 4$ Supersymmetric Yang-Mills Theory," *Phys.Rev.Lett.*, vol. 111, no. 9, p. 091602, 2013.

[49] B. Basso, A. Sever, and P. Vieira, "Space-time S-matrix and Flux tube S-matrix II. Extracting and Matching Data," *JHEP*, vol. 1401, p. 008, 2014.

[50] B. Basso, A. Sever, and P. Vieira, "Space-time S-matrix and Flux-tube S-matrix III. The two-particle contributions," *JHEP*, vol. 1408, p. 085, 2014.

[51] B. Basso, A. Sever, and P. Vieira, "Space-time S-matrix and Flux-tube S-matrix IV. Gluons and Fusion," *JHEP*, vol. 1409, p. 149, 2014.

[52] A. Belitsky, S. Derkachov, and A. N. Manashov, "Quantum mechanics of null polygonal Wilson loops," *Nucl.Phys.*, vol. B882, pp. 303–351, 2014.

[53] A. V. Belitsky, "Nonsinglet pentagons and NMHV amplitudes," *Nucl. Phys.*, vol. B896, pp. 493–554, 2015.

[54] A. V. Belitsky, "Fermionic pentagons and NMHV hexagon," *Nucl. Phys.*, vol. B894, pp. 108–135, 2015.

[55] B. Basso, J. Caetano, L. Cordova, A. Sever, and P. Vieira, "OPE for all Helicity Amplitudes," 2014.

[56] B. Basso, J. Caetano, L. Cordova, A. Sever, and P. Vieira, "OPE for all Helicity Amplitudes II. Form Factors and Data Analysis," *JHEP*, vol. 12, p. 088, 2015.

[57] B. Basso, A. Sever, and P. Vieira, "Hexagonal Wilson loops in planar $\mathcal{N} = 4$ SYM theory at finite coupling," *J. Phys.*, vol. A49, no. 41, p. 41LT01, 2016.

[58] J. Bartels, L. Lipatov, and A. Sabio Vera, "BFKL Pomeron, Reggeized gluons and Bern-Dixon-Smirnov amplitudes," *Phys.Rev.*, vol. D80, p. 045002, 2009.

[59] J. Bartels, L. Lipatov, and A. Sabio Vera, "$\mathcal{N} = 4$ supersymmetric Yang Mills scattering amplitudes at high energies: The Regge cut contribution," *Eur.Phys.J.*, vol. C65, pp. 587–605, 2010.

[60] V. Fadin and L. Lipatov, "BFKL equation for the adjoint representation of the gauge group in the next-to-leading approximation at $\mathcal{N} = 4$ SUSY," *Phys.Lett.*, vol. B706, pp. 470–476, 2012.

[61] L. Lipatov, A. Prygarin, and H. J. Schnitzer, "The Multi-Regge limit of NMHV Amplitudes in $\mathcal{N} = 4$ SYM Theory," *JHEP*, vol. 1301, p. 068, 2013.

[62] B. Basso, S. Caron-Huot, and A. Sever, "Adjoint BFKL at finite coupling: a short-cut from the collinear limit," *JHEP*, vol. 01, p. 027, 2015.

[63] M. Bullimore and D. Skinner, "Descent Equations for Superamplitudes," 2011.

[64] S. Caron-Huot and S. He, "Jumpstarting the All-Loop S-Matrix of Planar $\mathcal{N} = 4$ Super Yang-Mills," *JHEP*, vol. 1207, p. 174, 2012.

[65] O. Steinmann, "Über den Zusammenhang zwischen den Wightmanfunktionen und der retardierten Kommutatoren," *Helv. Physica Acta*, vol. 33, p. 257, 1960.

[66] O. Steinmann, "Wightman-Funktionen und retardierten Kommutatoren. II," *Helv. Physica Acta*, vol. 33, p. 347, 1960.

[67] K. E. Cahill and H. P. Stapp, "Optical Theorems and Steinmann Relations," *Annals Phys.*, vol. 90, p. 438, 1975.

[68] S. Caron-Huot, L. J. Dixon, A. McLeod, and M. von Hippel, "Bootstrapping a Five-Loop Amplitude Using Steinmann Relations," *Phys. Rev. Lett.*, vol. 117, no. 24, p. 241601, 2016.

[69] N. Arkani-Hamed, A. Hodges, and J. Trnka, "Positive Amplitudes In The Amplituhedron," *JHEP*, vol. 08, p. 030, 2015.

[70] L. J. Dixon, M. von Hippel, A. J. McLeod, and J. Trnka, "Multi-loop positivity of the planar $\mathcal{N} = 4$ SYM six-point amplitude," *JHEP*, vol. 02, p. 112, 2017.

[71] L. J. Dixon, J. Drummond, T. Harrington, A. J. McLeod, G. Papathanasiou, and M. Spradlin, "Heptagons from the Steinmann Cluster Bootstrap," *JHEP*, vol. 02, p. 137, 2017.

[72] S. Mandelstam, "Light-cone superspace and the finiteness of the N=4 model," *AIP Conf. Proc.*, vol. 116, pp. 99–108, 1984.

[73] L. Brink, O. Lindgren, and B. E. W. Nilsson, "The Ultraviolet Finiteness of the N=4 Yang-Mills Theory," *Phys. Lett.*, vol. B123, pp. 323–328, 1983.

[74] P. S. Howe, K. S. Stelle, and P. K. Townsend, "Miraculous Ultraviolet Cancellations in Supersymmetry Made Manifest," *Nucl. Phys.*, vol. B236, pp. 125–166, 1984.

[75] Z. Bern, L. Dixon, D. Kosower, R. Roiban, M. Spradlin, *et al.*, "The Two-Loop Six-Gluon MHV Amplitude in Maximally Supersymmetric Yang-Mills Theory," *Phys.Rev.*, vol. D78, p. 045007, 2008.

[76] J. Drummond, J. Henn, G. Korchemsky, and E. Sokatchev, "Hexagon Wilson loop = six-gluon MHV amplitude," *Nucl.Phys.*, vol. B815, pp. 142–173, 2009.

[77] V. P. Nair, "A Current Algebra for Some Gauge Theory Amplitudes," *Phys. Lett.*, vol. B214, pp. 215–218, 1988.

[78] G. Georgiou, E. N. Glover, and V. V. Khoze, "Non-MHV tree amplitudes in gauge theory," *JHEP*, vol. 0407, p. 048, 2004.

[79] M. Bianchi, H. Elvang, and D. Z. Freedman, "Generating Tree Amplitudes in N=4 SYM and N = 8 SG," *JHEP*, vol. 09, p. 063, 2008.

[80] N. Arkani-Hamed, F. Cachazo, and J. Kaplan, "What is the Simplest Quantum Field Theory?," *JHEP*, vol. 1009, p. 016, 2010.

[81] A. Hodges, "Eliminating spurious poles from gauge-theoretic amplitudes," *JHEP*, vol. 1305, p. 135, 2013.

[82] L. Mason and D. Skinner, "Dual Superconformal Invariance, Momentum Twistors and Grassmannians," *JHEP*, vol. 0911, p. 045, 2009.

[83] J. J. M. Carrasco and H. Johansson, "Generic multiloop methods and application to N=4 super-Yang-Mills," *J.Phys.*, vol. A44, p. 454004, 2011.

[84] J. L. Bourjaily, A. DiRe, A. Shaikh, M. Spradlin, and A. Volovich, "The Soft-Collinear Bootstrap: N=4 Yang-Mills Amplitudes at Six and Seven Loops," *JHEP*, vol. 1203, p. 032, 2012.

[85] A. E. Lipstein and L. Mason, "From the holomorphic Wilson loop to 'd log' loop-integrands for super-Yang-Mills amplitudes," *JHEP*, vol. 05, p. 106, 2013.

[86] A. E. Lipstein and L. Mason, "From d logs to dilogs the super Yang-Mills MHV amplitude revisited," *JHEP*, vol. 01, p. 169, 2014.

[87] K.-T. Chen, "Iterated path integrals," *Bull. Amer. Math. Soc.*, vol. 83, no. 5, pp. 831–879, 1977.

[88] V. Del Duca, C. Duhr, and V. A. Smirnov, "An Analytic Result for the Two-Loop Hexagon Wilson Loop in $\mathcal{N} = 4$ SYM," *JHEP*, vol. 1003, p. 099, 2010.

[89] V. Del Duca, C. Duhr, and V. A. Smirnov, "The Two-Loop Hexagon Wilson Loop in $\mathcal{N} = 4$ SYM," *JHEP*, vol. 1005, p. 084, 2010.

[90] F. C. Brown, "Multiple zeta values and periods of moduli spaces $\overline{\mathfrak{M}}_{0,n}(\mathbb{R})$," *Annales Sci.Ecole Norm.Sup.*, vol. 42, p. 371, 2009.

[91] A. B. Goncharov, "A simple construction of Grassmannian polylogarithms," *Adv. Math.*, vol. 241, pp. 79–102, 2013.

[92] C. Duhr, H. Gangl, and J. R. Rhodes, "From polygons and symbols to polylogarithmic functions," *JHEP*, vol. 1210, p. 075, 2012.

[93] A. Goncharov, "Multiple polylogarithms and mixed Tate motives," 2001.

[94] A. B. Goncharov, "Galois symmetries of fundamental groupoids and noncommutative geometry," *Duke Math. J.*, vol. 128, pp. 209–284, 06 2005.

[95] F. Brown, "On the decomposition of motivic multiple zeta values," 2011.

[96] F. Brown, "Mixed Tate motives over $\mathbb{Z}$," *Ann. of Math. (2)*, vol. 175, no. 2, pp. 949–976, 2012.

[97] D. Parker, A. Scherlis, M. Spradlin, and A. Volovich, "Hedgehog Bases for A_n Cluster Polylogarithms and An Application to Six-Point Amplitudes," *JHEP*, vol. 11, p. 136, 2015.

[98] S. Caron-Huot and S. He, private communication.

[99] A. V. Belitsky, "Descent equation for superloop and cyclicity of OPE," *Nucl. Phys.*, vol. B913, pp. 815–833, 2016.

[100] A. V. Belitsky, "Towards NMHV amplitudes at strong coupling," *Nucl. Phys.*, vol. B911, pp. 517–562, 2016.

[101] L. Lipatov and A. Prygarin, "Mandelstam cuts and light-like Wilson loops in $\mathcal{N} = 4$ SUSY," *Phys.Rev.*, vol. D83, p. 045020, 2011.

[102] L. Lipatov and A. Prygarin, "BFKL approach and six-particle MHV amplitude in $\mathcal{N} = 4$ super Yang-Mills," *Phys.Rev.*, vol. D83, p. 125001, 2011.

[103] J. Bartels, L. Lipatov, and A. Prygarin, "MHV Amplitude for 3→3 Gluon Scattering in Regge Limit," *Phys.Lett.*, vol. B705, pp. 507–512, 2011.

[104] J. Bartels, L. Lipatov, and A. Prygarin, "Collinear and Regge behavior of 2 -> 4 MHV amplitude in N = 4 super Yang-Mills theory," 2011.

[105] L. J. Dixon, C. Duhr, and J. Pennington, "Single-valued harmonic polylogarithms and the multi-Regge limit," *JHEP*, vol. 1210, p. 074, 2012.

[106] J. Pennington, "The six-point remainder function to all loop orders in the multi-Regge limit," *JHEP*, vol. 1301, p. 059, 2013.

[107] S. Caron-Huot, "When does the gluon reggeize?," 2013.

[108] Y. Hatsuda, "Wilson loop OPE, analytic continuation and multi-Regge limit," *JHEP*, vol. 1410, p. 38, 2014.

[109] J. M. Drummond and G. Papathanasiou, "Hexagon OPE Resummation and Multi-Regge Kinematics," *JHEP*, vol. 02, p. 185, 2016.

[110] `http://www.slac.stanford.edu/~lance/V4/`.

[111] J. Drummond, J. Henn, G. Korchemsky, and E. Sokatchev, "Generalized unitarity for N=4 super-amplitudes," *Nucl.Phys.*, vol. B869, pp. 452–492, 2013.

[112] H. Elvang and Y.-t. Huang, "Scattering Amplitudes," 2013.

[113] L. F. Alday, D. Gaiotto, and J. Maldacena, "Thermodynamic Bubble Ansatz," *JHEP*, vol. 09, p. 032, 2011.

[114] N. Beisert, B. Eden, and M. Staudacher, "Transcendentality and Crossing," *J. Stat. Mech.*, vol. 0701, p. P01021, 2007.

[115] E. Remiddi and J. Vermaseren, "Harmonic polylogarithms," *Int.J.Mod.Phys.*, vol. A15, pp. 725–754, 2000.

[116] A. V. Belitsky, private communication.

[117] F. C. Brown, "Single-valued multiple polylogarithms in one variable," *C. R. Acad. Sci. Paris, Ser. I*, vol. 338, no. 7, pp. 527–532, 2004.

[118] L. Mason and D. Skinner, "The Complete Planar S-matrix of $\mathcal{N} = 4$ SYM as a Wilson Loop in Twistor Space," *JHEP*, vol. 1012, p. 018, 2010.

[119] S. Caron-Huot, "Notes on the scattering amplitude / Wilson loop duality," *JHEP*, vol. 1107, p. 058, 2011.

[120] B. Basso, "Exciting the GKP string at any coupling," *Nucl.Phys.*, vol. B857, pp. 254–334, 2012.

[121] G. Papathanasiou, "Hexagon Wilson Loop OPE and Harmonic Polylogarithms," *JHEP*, vol. 1311, p. 150, 2013.

[122] G. Papathanasiou, "Evaluating the six-point remainder function near the collinear limit," *Int.J.Mod.Phys.*, vol. A29, no. 27, p. 1450154, 2014.

[123] Z. Bern and G. Chalmers, "Factorization in one loop gauge theory," *Nucl.Phys.*, vol. B447, pp. 465–518, 1995.

[124] B. Basso, A. Sever and P. Vieira, in progress. Talk at *Amplitudes 2015*, `http://amp15.itp.phys.ethz.ch/talks/Sever.pdf`.

[125] C. W. Bauer, A. Frink, and R. Kreckel, "Introduction to the GiNaC framework for symbolic computation within the C++ programming language," *J. Symb. Comput.*, vol. 33, p. 1, 2000.

[126] J. Vollinga and S. Weinzierl, "Numerical evaluation of multiple polylogarithms," *Comput. Phys. Commun.*, vol. 167, p. 177, 2005.

[127] J. Ablinger, J. Blumlein, and C. Schneider, "Harmonic Sums and Polylogarithms Generated by Cyclotomic Polynomials," *J.Math.Phys.*, vol. 52, p. 102301, 2011.

[128] T. Gehrmann and E. Remiddi, "Two loop master integrals for gamma* —¿ 3 jets: The Planar topologies," *Nucl.Phys.*, vol. B601, pp. 248–286, 2001.

[129] N. Arkani-Hamed, S. Caron-Huot and J. Trnka, private communication.

[130] R. E. Cutkosky, "Singularities and discontinuities of Feynman amplitudes," *J. Math. Phys.*, vol. 1, pp. 429–433, 1960.

[131] L. J. Dixon, J. M. Drummond, and J. M. Henn, "The one-loop six-dimensional hexagon integral and its relation to MHV amplitudes in N=4 SYM," *JHEP*, vol. 1106, p. 100, 2011.

[132] V. Del Duca, C. Duhr, and V. A. Smirnov, "The massless hexagon integral in D = 6 dimensions," *Phys.Lett.*, vol. B703, pp. 363–365, 2011.

[133] S. Weinzierl, "Does one need the O(epsilon)- and O(epsilonˆ2)-terms of one-loop amplitudes in an NNLO calculation ?," *Phys. Rev.*, vol. D84, p. 074007, 2011.

[134] `http://www.slac.stanford.edu/~lance/Steinmann/`.

[135] G. Papathanasiou, private communication.

[136] Y. Bai and S. He, "The Amplituhedron from Momentum Twistor Diagrams," *JHEP*, vol. 02, p. 065, 2015.

[137] S. Franco, D. Galloni, A. Mariotti, and J. Trnka, "Anatomy of the Amplituhedron," *JHEP*, vol. 03, p. 128, 2015.

[138] Y. Bai, S. He, and T. Lam, "The Amplituhedron and the One-loop Grassmannian Measure," *JHEP*, vol. 01, p. 112, 2016.

[139] L. Ferro, T. Lukowski, A. Orta, and M. Parisi, "Towards the Amplituhedron Volume," *JHEP*, vol. 03, p. 014, 2016.

[140] D. Galloni, "Positivity Sectors and the Amplituhedron," 2016.

[141] S. N. Karp and L. K. Williams, "The m=1 amplituhedron and cyclic hyperplane arrangements," 2016.

[142] S. Laporta and E. Remiddi, "Analytic treatment of the two loop equal mass sunrise graph," *Nucl. Phys.*, vol. B704, pp. 349–386, 2005.

[143] S. Mller-Stach, S. Weinzierl, and R. Zayadeh, "A Second-Order Differential Equation for the Two-Loop Sunrise Graph with Arbitrary Masses," *Commun. Num. Theor. Phys.*, vol. 6, pp. 203–222, 2012.

[144] S. Caron-Huot and K. J. Larsen, "Uniqueness of two-loop master contours," *JHEP*, vol. 10, p. 026, 2012.

[145] D. Correa, J. Henn, J. Maldacena, and A. Sever, "An exact formula for the radiation of a moving quark in N=4 super Yang Mills," *JHEP*, vol. 06, p. 048, 2012.

[146] J. M. Henn and T. Huber, "The four-loop cusp anomalous dimension in $\mathcal{N} = 4$ super Yang-Mills and analytic integration techniques for Wilson line integrals," *JHEP*, vol. 09, p. 147, 2013.

[147] D. Maitre, "HPL, a mathematica implementation of the harmonic polylogarithms," *Comput.Phys.Commun.*, vol. 174, pp. 222–240, 2006.

[148] J. M. Henn and T. Huber, "Systematics of the cusp anomalous dimension," *JHEP*, vol. 11, p. 058, 2012.

[149] J. Blumlein, D. J. Broadhurst, and J. A. M. Vermaseren, "The Multiple Zeta Value Data Mine," *Comput. Phys. Commun.*, vol. 181, pp. 582–625, 2010.

[150] R. J. Eden, P. V. Landshoff, D. I. Olive, and J. C. Polkinghorne, *The Analytic S-Matrix*. Cambridge University Press, 1966.

[151] Z. Bern, L. J. Dixon, and D. A. Kosower, "On-shell recurrence relations for one-loop QCD amplitudes," *Phys. Rev.*, vol. D71, p. 105013, 2005.

[152] Z. Bern, L. J. Dixon, and D. A. Kosower, "Bootstrapping multi-parton loop amplitudes in QCD," *Phys. Rev.*, vol. D73, p. 065013, 2006.

[153] C. F. Berger, Z. Bern, L. J. Dixon, D. Forde, and D. A. Kosower, "Bootstrapping One-Loop QCD Amplitudes with General Helicities," *Phys. Rev.*, vol. D74, p. 036009, 2006.

[154] D. C. Dunbar and W. B. Perkins, "Two-loop five-point all plus helicity Yang-Mills amplitude," *Phys. Rev.*, vol. D93, no. 8, p. 085029, 2016.

[155] D. C. Dunbar, G. R. Jehu, and W. B. Perkins, "The two-loop n-point all-plus helicity amplitude," *Phys. Rev.*, vol. D93, no. 12, p. 125006, 2016.

[156] D. C. Dunbar, G. R. Jehu, and W. B. Perkins, "Two-loop six gluon all plus helicity amplitude," *Phys. Rev. Lett.*, vol. 117, no. 6, p. 061602, 2016.

[157] L. F. Alday and J. Maldacena, "Comments on gluon scattering amplitudes via AdS/CFT," *JHEP*, vol. 0711, p. 068, 2007.

[158] J. Drummond, J. Henn, G. Korchemsky, and E. Sokatchev, "The hexagon Wilson loop and the BDS ansatz for the six-gluon amplitude," *Phys.Lett.*, vol. B662, pp. 456–460, 2008.

[159] D. A. Kosower, R. Roiban, and C. Vergu, "The Six-Point NMHV amplitude in Maximally Supersymmetric Yang-Mills Theory," *Phys. Rev.*, vol. D83, p. 065018, 2011.

[160] V. V. Fock and A. B. Goncharov, "Cluster ensembles, quantization and the dilogarithm," *Ann. Sci. Éc. Norm. Supér. (4)*, vol. 42, no. 6, pp. 865–930, 2009.

[161] M. Gekhtman, M. Shapiro, and A. Vainshtein, "Cluster algebras and Poisson geometry," *Mosc. Math. J.*, vol. 3, no. 3, p. 899, 2003.

[162] A. Sever and P. Vieira, "Multichannel Conformal Blocks for Polygon Wilson Loops," *JHEP*, vol. 1201, p. 070, 2012.

[163] A. V. Belitsky, "On factorization of multiparticle pentagons," *Nucl. Phys.*, vol. B897, pp. 346–373, 2015.

[164] A. V. Belitsky, "Matrix pentagons," 2016.

[165] L. Córdova, "Hexagon POPE: effective particles and tree level resummation," *JHEP*, vol. 01, p. 051, 2017.

[166] H. T. Lam and M. von Hippel, "Resumming the POPE at One Loop," *JHEP*, vol. 12, p. 011, 2016.

[167] T. Dennen, I. Prlina, M. Spradlin, S. Stanojevic, and A. Volovich, "Landau Singularities from the Amplituhedron,"

[168] L. Dixon, J. Drummond, T. Harrington, A. McLeod, G. Papathanasiou, and M. Spradlin. to appear.

[169] J. Bartels, A. Kormilitzin, L. Lipatov, and A. Prygarin, "BFKL approach and $2 \to 5$ maximally helicity violating amplitude in $\mathcal{N} = 4$ super-Yang-Mills theory," *Phys.Rev.*, vol. D86, p. 065026, 2012.

[170] J. Bartels, A. Kormilitzin, and L. Lipatov, "Analytic structure of the $n = 7$ scattering amplitude in $\mathcal{N} = 4$ SYM theory at multi-Regge kinematics: Conformal Regge pole contribution," *Phys.Rev.*, vol. D89, p. 065002, 2014.

[171] J. Bartels, A. Kormilitzin, and L. N. Lipatov, "Analytic structure of the $n = 7$ scattering amplitude in $\mathcal{N} = 4$ theory in multi-Regge kinematics: Conformal Regge cut contribution," *Phys. Rev.*, vol. D91, no. 4, p. 045005, 2015.

[172] T. Bargheer, "Systematics of the Multi-Regge Three-Loop Symbol," 2016.

[173] J. Broedel, M. Sprenger, and A. Torres Orjuela, "Towards single-valued polylogarithms in two variables for the seven-point remainder function in multi-Regge-kinematics," *Nucl. Phys.*, vol. B915, pp. 394–413, 2017.

[174] V. Del Duca, S. Druc, J. Drummond, C. Duhr, F. Dulat, R. Marzucca, G. Papathanasiou, and B. Verbeek, "Multi-Regge kinematics and the moduli space of Riemann spheres with marked points," *JHEP*, vol. 08, p. 152, 2016.

[175] G. Georgiou, "Null Wilson loops with a self-crossing and the Wilson loop/amplitude conjecture," *JHEP*, vol. 09, p. 021, 2009.

[176] L. J. Dixon and I. Esterlis, "All orders results for self-crossing Wilson loops mimicking double parton scattering," *JHEP*, vol. 07, p. 116, 2016. [Erratum: JHEP08,131(2016)].

[177] `https://goo.gl/vKCtoX`.

[178] L. Magnea and G. F. Sterman, "Analytic continuation of the Sudakov form-factor in QCD," *Phys. Rev.*, vol. D42, pp. 4222–4227, 1990.

[179] S. Catani, "The Singular behavior of QCD amplitudes at two loop order," *Phys. Lett.*, vol. B427, pp. 161–171, 1998.

[180] G. F. Sterman and M. E. Tejeda-Yeomans, "Multiloop amplitudes and resummation," *Phys. Lett.*, vol. B552, pp. 48–56, 2003.

[181] S. Caron-Huot, "Superconformal symmetry and two-loop amplitudes in planar $\mathcal{N} = 4$ super Yang-Mills," *JHEP*, vol. 1112, p. 066, 2011.

[182] J. Golden and M. Spradlin, "The differential of all two-loop MHV amplitudes in $\mathcal{N} = 4$ Yang-Mills theory," *JHEP*, vol. 1309, p. 111, 2013.

[183] J. Golden and M. Spradlin, "An analytic result for the two-loop seven-point MHV amplitude in $\mathcal{N} = 4$ SYM," *JHEP*, vol. 1408, p. 154, 2014.

[184] J. M. Drummond, "Review of AdS/CFT Integrability, Chapter V.2: Dual Superconformal Symmetry," *Lett. Math. Phys.*, vol. 99, pp. 481–505, 2012.

[185] N. Arkani-Hamed, F. Cachazo, and C. Cheung, "The Grassmannian Origin Of Dual Superconformal Invariance," *JHEP*, vol. 03, p. 036, 2010.

[186] N. Arkani-Hamed, J. L. Bourjaily, F. Cachazo, and J. Trnka, "Local Integrals for Planar Scattering Amplitudes," *JHEP*, vol. 06, p. 125, 2012.

[187] F. A. Berends and W. T. Giele, "Recursive Calculations for Processes with n Gluons," *Nucl. Phys.*, vol. B306, pp. 759–808, 1988.

[188] G. Yang, "A simple collinear limit of scattering amplitudes at strong coupling," *JHEP*, vol. 03, p. 087, 2011.

[189] G. Yang, "Scattering amplitudes at strong coupling for 4K gluons," *JHEP*, vol. 12, p. 082, 2010.

[190] J. Golden, M. F. Paulos, M. Spradlin, and A. Volovich, "Cluster Polylogarithms for Scattering Amplitudes," *J. Phys.*, vol. A47, no. 47, p. 474005, 2014.

[191] A. Prygarin, M. Spradlin, C. Vergu, and A. Volovich, "All Two-Loop MHV Amplitudes in Multi-Regge Kinematics From Applied Symbology," *Phys.Rev.*, vol. D85, p. 085019, 2012.

[192] R. C. Brower, H. Nastase, H. J. Schnitzer, and C.-I. Tan, "Analyticity for Multi-Regge Limits of the Bern-Dixon-Smirnov Amplitudes," *Nucl. Phys.*, vol. B822, pp. 301–347, 2009.

[193] R. C. Brower, H. Nastase, H. J. Schnitzer, and C.-I. Tan, "Implications of multi-Regge limits for the Bern-Dixon-Smirnov conjecture," *Nucl. Phys.*, vol. B814, pp. 293–326, 2009.

[194] S. Caron-Huot, private communication.

[195] M. T. Grisaru, H. N. Pendleton, and P. van Nieuwenhuizen, "Supergravity and the S Matrix," *Phys. Rev.*, vol. D15, p. 996, 1977.

[196] M. T. Grisaru and H. N. Pendleton, "Some Properties of Scattering Amplitudes in Supersymmetric Theories," *Nucl. Phys.*, vol. B124, pp. 81–92, 1977.

[197] B. Basso, A. Sever and P. Vieira, private communication.

[198] A. Sever. Talk at *Amplitudes 2015*, `http://amp15.itp.phys.ethz.ch/talks/Sever.pdf`.

[199] T. Dennen, M. Spradlin, and A. Volovich, "Landau Singularities and Symbology: One- and Two-loop MHV Amplitudes in SYM Theory," *JHEP*, vol. 03, p. 069, 2016.